

ISSN 1512-1127

საქართველოს გეოფიზიკური საზოგადოების  
ჟურნალი

მყარი დედამიწის, ატმოსფეროს, ოკეანისა და კოსმოსური პლაზმის  
ფიზიკა

*ტომი 23, № 1*

**JOURNAL  
OF THE GEORGIAN GEOPHYSICAL SOCIETY**

*Physics of Solid Earth, Atmosphere, Ocean and Space Plasma*

*Vol. 23, № 1*

**Tbilisi**

**2020**

ISSN 1512-1127

საქართველოს გეოფიზიკური საზოგადოების  
ჟურნალი

მყარი დედამიწის, ატმოსფეროს, ოკეანისა და კოსმოსური პლაზმის  
ფიზიკა

*ტომი 23, № 1*

**JOURNAL  
OF THE GEORGIAN GEOPHYSICAL SOCIETY**

*Physics of Solid Earth, Atmosphere, Ocean and Space Plasma*

*Vol. 23, № 1*

**Tbilisi  
2020**

საქართველოს გეოფიზიკური საზოგადოების ჟურნალი  
მყარი დედამიწის, ატმოსფეროს, ოკეანისა და კოსმოსური პლაზმის ფიზიკა  
მთავარი რედაქტორი: თ. ჭელიძე

**სარედაქციო კოლეგია**

მ. ალანია, ა. ამირანაშვილი (მდივანი), თ. ბიბილაშვილი (აშშ), ე. ბოლოპოულოსი (საბერძნეთი), გ. ჩაგელიშვილი, თ. ჭელიძე, ლ. დარახველიძე, დ. დემეტრაშვილი, კ. ევტაქსიასი (საბერძნეთი), ვ. ერემეევი (უკრაინა), ნ. ლლონტი, ა. გოგიჩაიშვილი (მექსიკა), ი. გეგენი (საფრანგეთი), ა. გველესიანი (მთ. რედაქტორის მოადგილე), თ. გვენცაძე, ზ. კერესელიძე, ო. ხარშილადე, ზ. ხვედელიძე, ჯ. ქირია, თ. ქირია, გ. კოროტაევი (უკრაინა), თ. მაჭარაშვილი, გ. მეტრეველი, ი. მურუსიძე, თ. ოგუზი (თურქეთი), ვ. სტაროსტენკო (უკრაინა), რ. ტამსალუ (ესტონეთი), კ. თავართქილაძე, ნ. ვარამაშვილი, ვ. ზალესნი (რუსეთი), ი. ჩშაუ (გერმანია).

**ჟურნალის შინაარსი:**

ჟურნალი მოიცავს მყარი დედამიწის, ატმოსფეროს, ოკეანისა და კოსმოსური პლაზმის ფიზიკის ყველა მიმართულებას. ჟურნალში ქვეყნდება: კვლევითი წერილები, მიმოხილვები, მოკლე ინფორმაციები, დისკუსიები, წიგნების მიმოხილვები, განცხადებები, კონფერენციების მოხსენებები.

**JOURNAL OF THE GEORGIAN GEOPHYSICAL SOCIETY**

*Physics of Solid Earth, Atmosphere, Ocean and Space Plasma*

**Editor-in-chief: T. Chelidze**

**Editorial board:**

М. Alania, A. Amiranashvili (secretary), T. Bibilashvili (USA), E. Bolopoulos (Greece), G. Chagelishvili, T. Chelidze, L. Darakhvelidze, D. Demetrashvili, K. Eftaxias (Greece), V. N. Eremeev (Ukraine), N. Ghlonti, A. Gogichashvili (Mexico), Y. Gueguen (France), A. Gvelesiani (Vice-Editor), T. Gventsadze, Z. Kereselidze, O. Kharshiladze, Z. Khvedelidze, J. Kiria, T. Kiria, G. K. Korotaev (Ukraine), T. Matcharashvili, G. Metreveli, I. Murusidze, T. Oguz (Turkey), V. Starostenko (Ukraine), R. Tamsalu (Estonia), K. Tavartkiladze, N. Varamashvili, V. B. Zalesny (Russia), J. Zschau (Germany).

**Scope of the Journal:**

The Journal is devoted to all branches of the Physics of Solid Earth, Atmosphere, Ocean and Space Plasma. Types of contributions are: research papers, reviews, short communications, discussions, book reviews, announcements, conference reports.

**ЖУРНАЛ ГРУЗИНСКОГО ГЕОФИЗИЧЕСКОГО ОБЩЕСТВА**

**Физика Твёрдой Земли, Атмосферы, Океана и Космической Плазмы**

**Главный редактор: Т. Челидзе**

**Редакционная коллегия:**

М. Алания, А. Амиранашвили (секретарь), Т. Бибилашвили (США), Е. Боллопуос (Греция), Г. Чагелишвили, Т.Л. Челидзе, Л. Дарахвелидзе, Д. Деметрашвили, К. Эфтаксиас (Греция), В. Н. Еремеев (Украина), Н. Глонти, А. Гогичайшвили (Мексика), И. Геген (Франция), А.И. Гвелесиани (зам. гл. редактора), Т. Гвенцадзе, З. Кереселидзе, О. Харшиладзе, З. Хведелидзе, Дж. Кирия, Т. Кирия, Г. К. Коротаев (Украина), Т. Мачарашвили, Г. Метревели, И. Мурусидзе, Т. Огуз (Турция), В. Старостенко (Украина), Р. Тамсалу (Эстония), К. Таварткиладзе, Н. Варамашвили, В. Б. Залесный (Россия), И. Чшау (Германия).

**Содержание журнала:**

Журнал Грузинского геофизического общества охватывает все направления физики твердой Земли, Атмосферы, Океана и Космической Плазмы. В журнале публикуются научные статьи, обзоры, краткие информации, дискуссии, обзоры книг, объявления, доклады конференций.

**მისამართი:**

საქართველო, 0160, თბილისი, ალექსიძის ქ. 1, მ. ნოდიას სახ. გეოფიზიკის ინსტიტუტი  
ტელ.: 233-28-67; ფაქსი; (995 32 2332867); ელ. ფოსტა: [tamaz.chelidze@gmail.com](mailto:tamaz.chelidze@gmail.com);  
[avtandilamiranashvili@gmail.com](mailto:avtandilamiranashvili@gmail.com);  
[geophysics.journal@tsu.ge](mailto:geophysics.journal@tsu.ge)

**გამოქვეყნების განრიგი და ხელმოწერა:**

გამოიცემა წელიწადში ორჯერ. მყარი ვერსიის წლიური ხელმოწერის ფასია: უცხოელი ხელმომწერისათვის - 30 დოლარი, საქართველოში - 10 ლარი. ხელმოწერის მოთხოვნა უნდა გაიგზავნოს რედაქციის მისამართით. შესაძლებელია უფასო ონლაინ წვდომა:  
<http://openjournals.gela.org.ge/index.php/GGS>

ქურნალი ინდექსირებულია Google Scholar-ში:  
<https://scholar.google.com/citations?hl=en&user=pdG-bMAAAAAAJ>

**Address:**

M. Nodia Institute of Geophysics, 1 Alexidze Str., 0160 Tbilisi, Georgia  
Tel.: 233-28-67; Fax: (99532) 2332867; e-mail: [tamaz.chelidze@gmail.com](mailto:tamaz.chelidze@gmail.com);  
[avtandilamiranashvili@gmail.com](mailto:avtandilamiranashvili@gmail.com);  
[geophysics.journal@tsu.ge](mailto:geophysics.journal@tsu.ge)

**Publication schedule and subscription information:**

The journal is issued twice a year. The subscription price for print version is 30 \$ in year. Subscription orders should be sent to editor's address. Free online access is possible:  
<http://openjournals.gela.org.ge/index.php/GGS>

The journal is indexed in the Google Scholar:  
<https://scholar.google.com/citations?hl=en&user=pdG-bMAAAAAAJ>

**Адрес:**

Грузия, 0171, Тбилиси, ул. Алексидзе, 1. Институт геофизики им. М. З. Нодиа  
Тел: 233-28-67; 294-35-91; Fax: (99532)2332867; e-mail: [tamaz.chelidze@gmail.com](mailto:tamaz.chelidze@gmail.com);  
[avtandilamiranashvili@gmail.com](mailto:avtandilamiranashvili@gmail.com);  
[geophysics.journal@tsu.ge](mailto:geophysics.journal@tsu.ge)

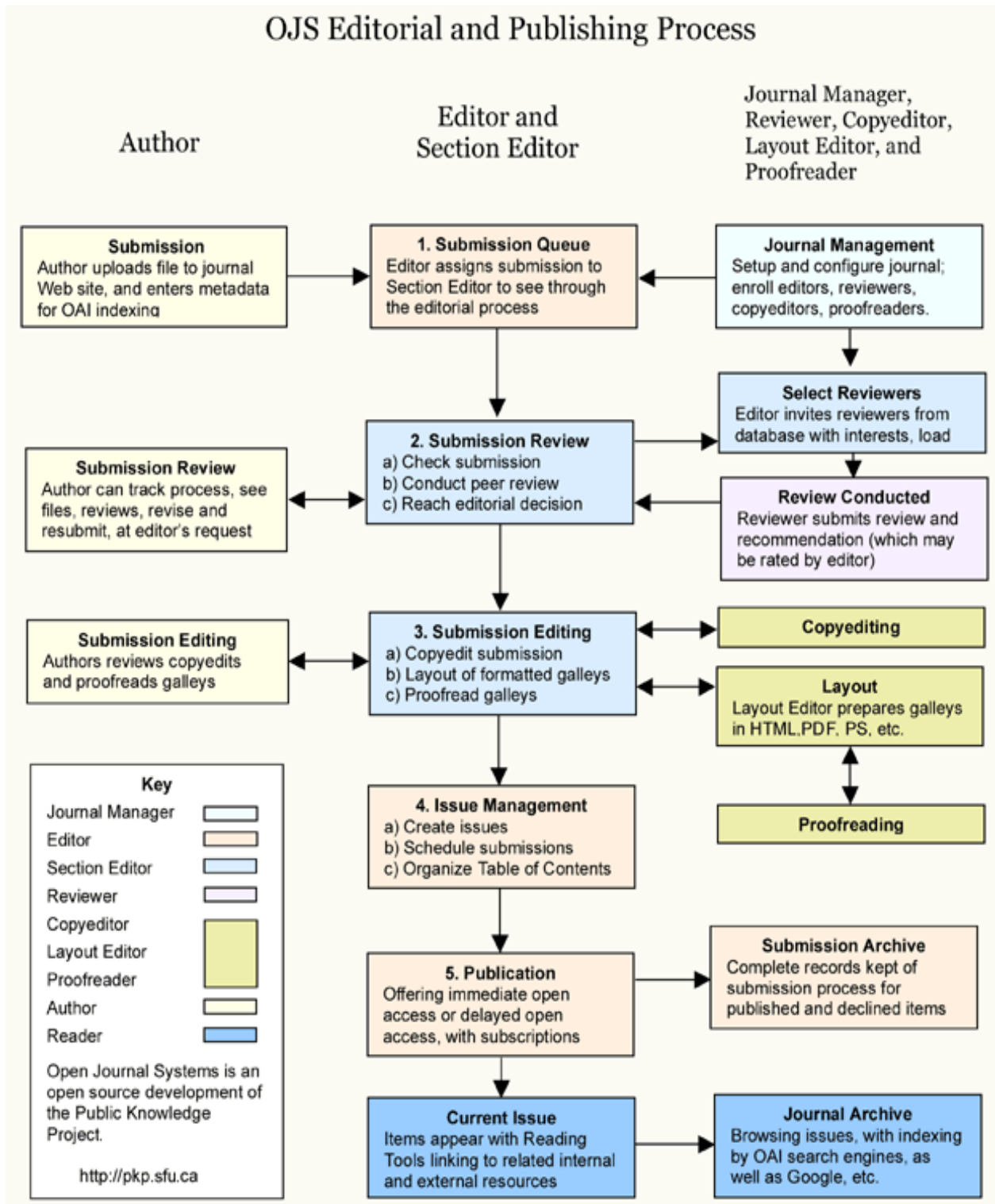
**Порядок издания и условия подписки:**

Журнал издается дважды в год. Годовая подписная цена для печатной версии - 30 долларов США. Заявка о подписке высылается в адрес редакции. Имеется бесплатный онлайн доступ  
<http://openjournals.gela.org.ge/index.php/GGS>

Журнал индексируется в Google Scholar:  
<https://scholar.google.com/citations?hl=en&user=pdG-bMAAAAAAJ>

This journal uses Open Journal Systems 2.4.8.3, which is open source journal management and publishing software developed, supported, and freely distributed by the Public Knowledge Project under the GNU General Public License.

(<http://openjournals.gela.org.ge/index.php?journal=GGS&page=about&op=aboutThisPublishingSystem>)



# **Models for Area Seismic Source Definition and Parameterization for Georgia and the Surrounding Region**

**Otar Sh. Varazanashvili, Nino S. Tsereteli**

*M. Nodia Institute of Geophysics, Iv. Javakhishvili Tbilisi State University, Georgia*  
*e-mail: otar.varazanashvili@tsu.ge*

## **ABSTRACT**

*Models of area seismic source (ASSs) are the basic and most important inputs required for Probabilistic Seismic Hazard Analysis (PSHA), because on them mainly depends the reliability of the final results of seismic hazard assessment. Determinations of these models include the delineation of ASSs and their parameterization. In practical applications, when clear procedures for constructing ASSs do not exist, this leads to large variations in the computed hazard.*

*In the Caucasus, where active faults are clearly defined and parameterized, and seismicity is relatively well documented, a method of ASS delineation is used, which was developed by us. The procedure for constructing ASSs is based on the delineation, along the active fault, of an area with a certain width. The width of the ASS is dependent from fault plane dip and width, from the thickness of seismically active layers and from geometrical sizes earthquake source. ASSs asymmetry relative to the axial line of the fault is a characteristic feature of these construction. On the basis of these method, ASSs were delineated for Georgia and the surrounding region.*

*Each ASS is expressed by a set of parameters that will represent the basic input for seismic hazard assessment.  $M_{max}$  assessments were implemented on the basis of three seismological and two geological methods. The magnitude-frequency distribution  $b$  parameter was calculated for 16 generalized tectonic units, for which seismic statistics were quite complete, and the  $a$  parameter was determined for each ASS. A study of the depth distribution of earthquakes showed that seismicity in this region is mainly shallow.*

**Keywords:** *Georgia, seismic source, seismic hazard, active faults, magnitude-frequency distribution, earthquake depth.*

## **1 Introduction**

The development of seismogenic source models is one of the first steps in the implementation of Probabilistic Seismic Hazard Analysis (PSHA).

In practice, PSHA studies use mainly three types of seismogenic source model: 1 – point source, where seismicity is concentrated in a small area at very long distance from the site; 2 – line source, where seismicity is related to a active faults; 3 — area seismic source, where seismicity is related to localized active geological structures or where the historical seismicity is assumed to be uniformly distributed. Theoretically, each seismogenic source should be associated with an individual fault or its segment. However, in actual practice, due to lack of data about all the faults and dispersion of the epicenters of historical earthquakes, area seismic sources (ASS) are preferentially used, which cover one or more active faults and have homogeneous characteristics of seismicity (Gupta, [8]).

It is worth noting that in practical applications, when clear procedures for constructing ASS do not exist, this leads to large variations in the computed hazard and to unreliable results. Therefore, in the absence of formal and consistent procedures for the development and parameterization ASS, the problem of their delineation is often a controversial one in the practice of PSHA (Weatherill and Burton, [16]).

ASS models should be based on the definition of seismotectonic laws (models), which in turn are based on the three-dimensional comparison of real geometric dimensions of geological (e.g. faults) and

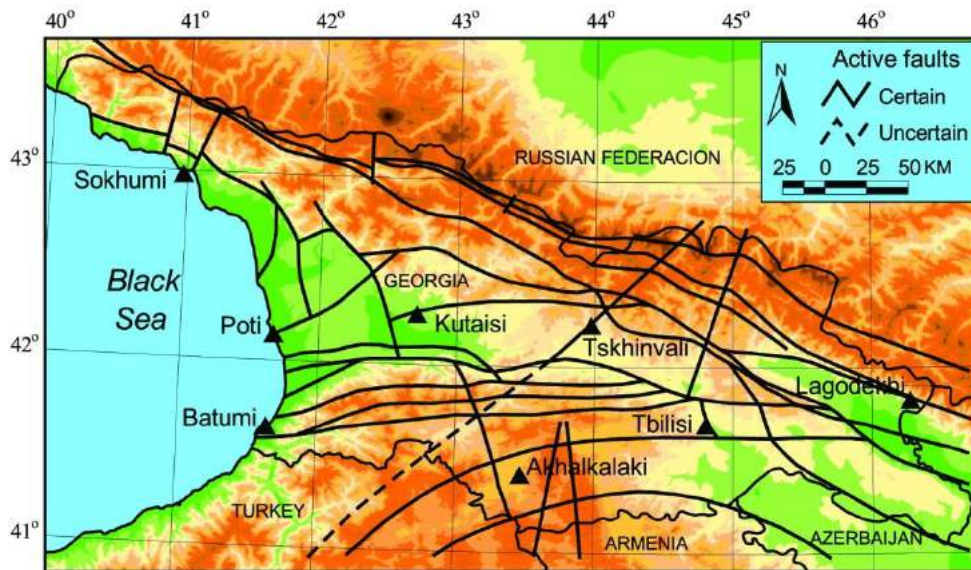
seismological (e.g. earthquake sources) objects. However, there are differences in the approaches by which basic seismotectonic schemes are constructed.

The main seismotectonic concept, used in this study, is based on the crustal divisions into separate blocks, under conditions of continuous crustal deformation caused by endogenous processes. Relative mutual displacement of blocks leads to the accumulation of potential energy in some transition zones of interblock. These accumulated energy can be released during the earthquakes. So it is necessary to reveal special distribution of such transition zones and related earthquakes for delineation of ASS. Therefore, to solve this problem is required to have data of active faults for investigated area.

## 2 Tectonic and seismotectonic background

Since the delineation of active faults depends partly on the subjective judgment by experts, various schemes of active faults can be obtained by different authors. In our study, we used only those schemes for active faults in Georgia (see Figs. 1a-b) that were published in peer-reviewed journals. These publications are Caputo et al., [4] and Adamia et al., [1]. The active fault scheme presented in the latter was further improved by the authors taking into account the latest results obtained in the framework of the EMME project (Danciu et al., [5]).

(a)



(b)

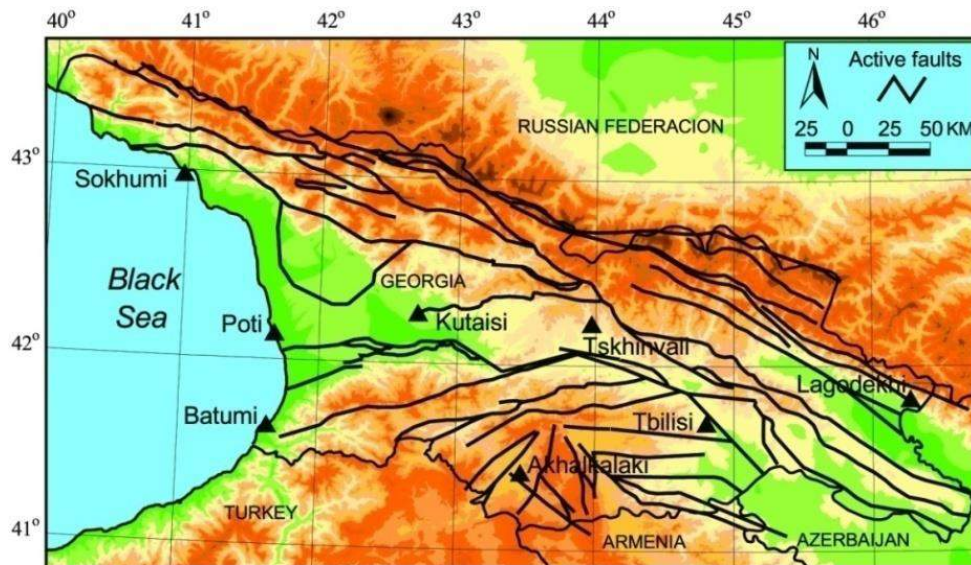


Fig. 1. Different tectonic maps for Georgia reporting only active faults: (a) the faults are from Caputo et al. [4] and (b) the faults are from Adamia et al. [1].

In order to assess the seismic hazard of the whole territory of Georgia by means of the PSHA method, it is also necessary to consider ASSs within at least 100 km from the borders of Georgia, considering the fact that seismicity increases to the south (Turkey, Armenia, Iran) and east (Azerbaijan) from Georgia, and that it rapidly decreases to the west (Black Sea) and north (Northern Caucasus, Russian Federation) (Fig. 3). Therefore, for Georgia, two different maps reporting the active faults (see Fig. 2a-b) and a seismotectonic map were compiled (Fig. 3). Information about active faults of the study area and associated parameters as well as about seismicity was derived from the mega-database, developed by the EMME project.

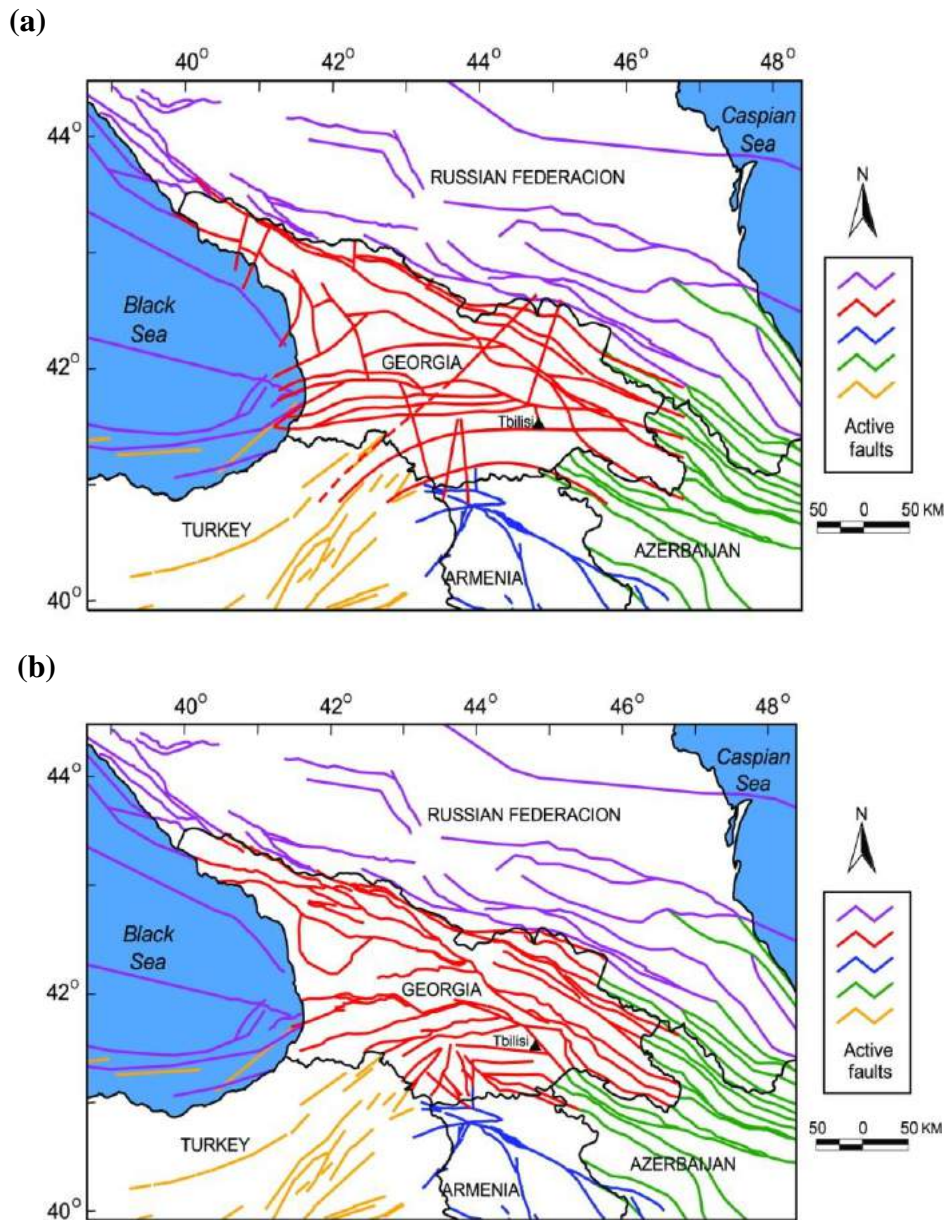


Fig. 2. Tectonic map of the investigated region reporting only active faults: (a) the faults are from Caputo et al. [4] and from Danciu et al., [5]; (b) the faults are from Adamia et al., [1] and from Danciu et al., [5]. In the legend, active faults are highlighted in different colors according to data from different countries, provided in the mega-database of the EMME project (see Danciu et al., [5]).

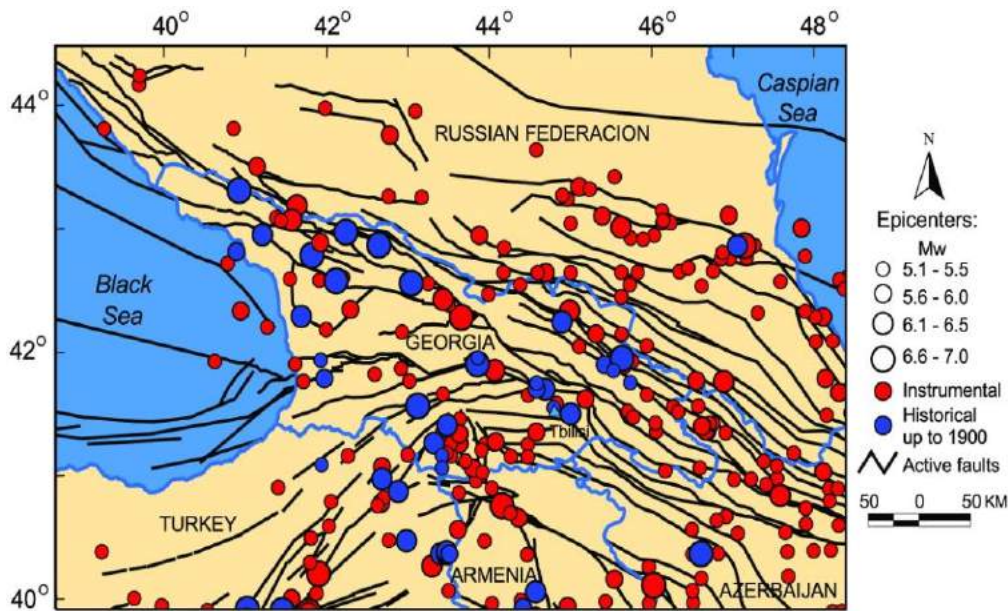


Fig. 3. Seismotectonic map: active faults, from Adamia et al. [1] and from Danciu et al. [5] and seismicity with  $M_w > 5$  for Georgia and the regions around it (Zare et al., [19]; Varazanashvili et al., [15]).

### 3 Methodology for ASSs delineation and its application

Area seismic source models used in this study are defined according to the following principles: a ASS is defined as a seismically homogenous area, in which every point is assumed to have the same probability of being the epicenter of a future earthquake; the seismic potential (e.g.,  $M_{max}$ ) of any ASS has to be distinctly different from the other adjacent ASS; when compiling a map of ASS, zones of high seismic potential overlap with the zones with lower potential.

ASS models consider two basic geometric elements: firstly – a linear zone, representing the projection of the three-dimensional active fault, which reflects the structural seismicity; secondly - a geographical polygon, that delineate an area with quasi-homogeneous geological characteristics and are characterized by diffuse seismicity. The latter is located between the zones of the first type and is a background area.

The Caucasus is a region where active faults are well defined and parameterized, and seismicity is relatively well documented, so the source zones are fairly obvious. Therefore, in the present study, a method of ASS delineation is used, which was developed by us and includes formal and consistent procedures.

As shown in Figure 4, a proper procedure for ASS delineation requires the following information:

- The geometric parameters (length, width, depth) of the considered active fault and its segments.
- The dip of the fault plane, location of branching faults, width of the cataclastic zone. The thickness of the seismically-active layer.

In addition, the relationship of individual, moderate and strong earthquakes with the considered, active fault is based on the following factors related to earthquake sources:

- Data on the geometric size of the earthquake sources, position of the hypocenter (epicenter coordinates, depth).
- Data on the orientation of the scattering area of foreshocks and aftershocks, data on the direction of higher isoseismals.
- Data on the location of the dislocation and landslides caused by the earthquake.

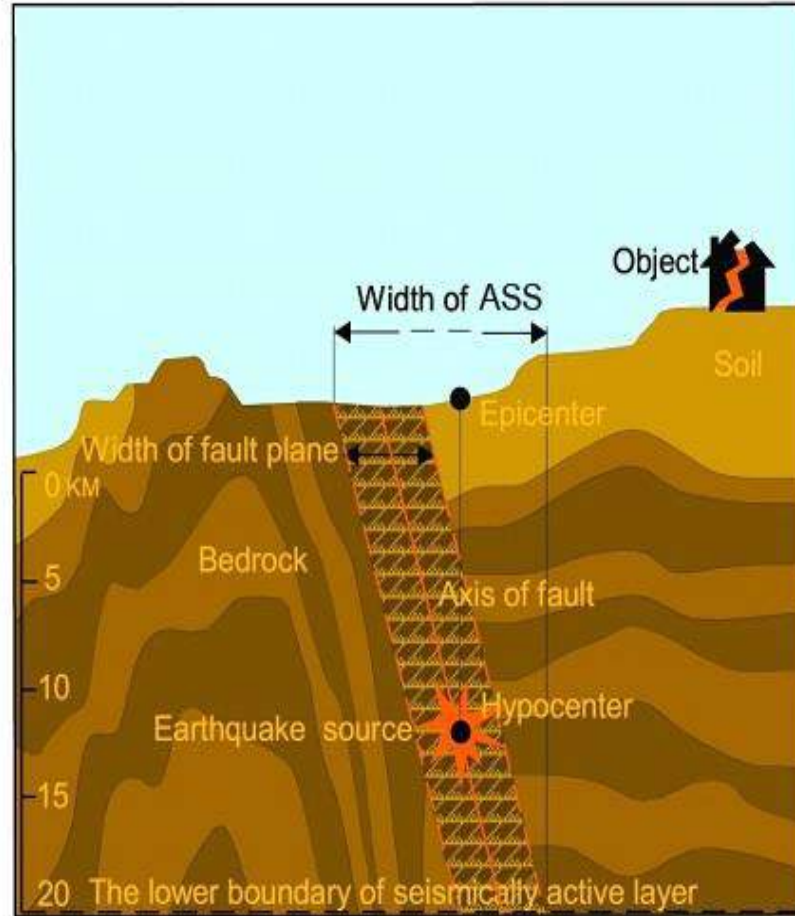


Fig. 4. Scheme illustrating the procedure for determining the width of the ASS, i.e. the width of the projection of the three-dimensional fault on the Earth's surface.

The procedure for constructing a ASS is based on the delineation, along the active fault, of an area with a certain width. In this case, the width of the ASS is crucial in the creating a model ASSs for the study region. In turn, the width of the ASS is dependent on fault width, the dip of the fault plane, the thickness of the seismically active layer, the geometrical size of the source of the maximum possible earthquake (Fig. 4). The ASS asymmetry relative to the axial line of the dipping fault is a characteristic feature of this construction.

To illustrate the application of this procedure for ASS delineation, Figure 5 shows the location of the epicenter of the 2011 Sairme earthquake, in south-western Georgia, with  $M_w=5.6$ ,  $h=21$  km, and  $I_o=7$  (MSK) (Varazanashvili et al., [15]) in relation to active faults and the ASSs, which clearly demonstrates the reliability of the procedure used for constructing the ASS along the fault. On the map of Figure 5, ASSs with the maximum possible magnitude  $M_{max}=6$  are shown in blue, whereas the ASSs with  $M_{max}=5$  are in light blue colour.

Only by using the above procedure, it is possible to identify the connection of the focus of the Sairme earthquake with the ASS, located along the western segment of the Surami active fault. Given the dip-direction and the dip angle of the fault and the distance from the epicenter to the projection of the fault axis on the surface, the resulting depth of the hypocenter is 20 km, that practically coincides with instrumental depth ( $h=21$  km) and once again testifies to the correctness of the geometric reconstruction.

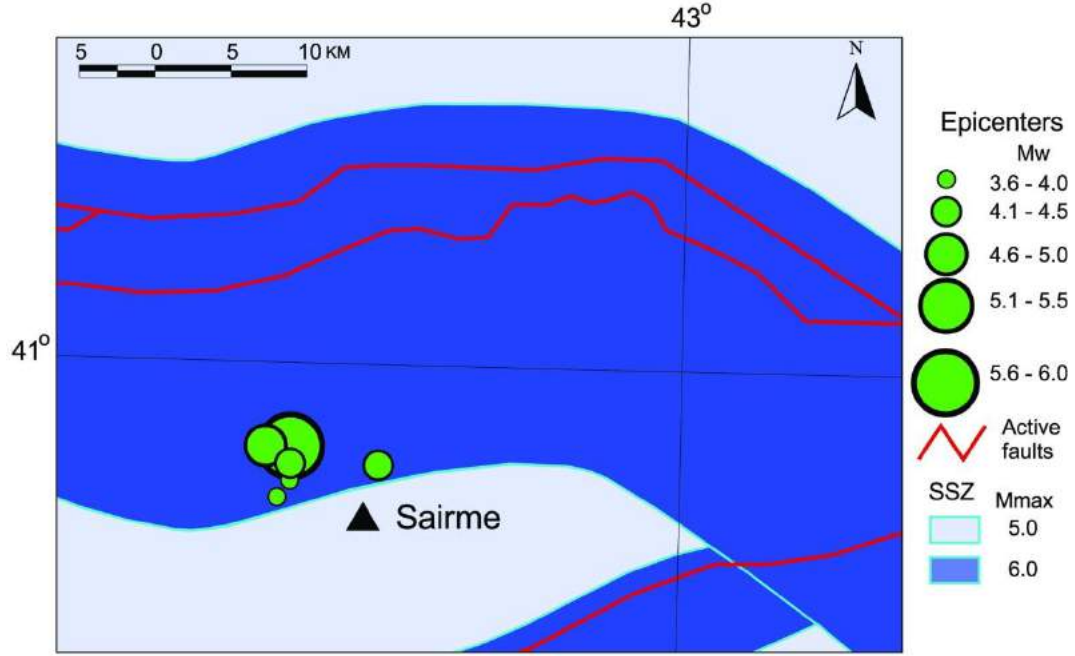


Fig. 5. The location of the Sairme earthquake epicenter, 2011 in south-western Georgia, in relation to active faults and ASSs.

The geometrical parameters (length and penetration depth) of active faults were derived from the corresponding database of active faults, developed in the framework of the EMME project and from correlation dependence (for the width of the fault) based on Aleshin et al., [3], which is best suited to the conditions of Georgia and the regions around it:

$$\text{Log}S=0.77\text{lg}L-1.20 \quad (1)$$

where  $S$  – the width of the fault, and  $L$  – the length of the fault. From the same database were collected also the data about the dip angle of the fault plane.

The thickness of seismically active layer in this study were set at 14 major tectonic units allocated in Georgia and around it. For this was used the distribution of the number of earthquakes by depth in each selected tectonic unit (see Section 4.3).

Geometrical sizes of the earthquake sources of various magnitudes in Georgia were determined by correlation dependencies from the work of Ulomov, [14]:

$$\text{Log}L_M=0.60M-2.50 \quad \text{with } M \geq 6.5 \quad (2)$$

$$\text{Log}W_M=0.15M-0.42 \quad \text{with } M \geq 6.5 \quad (3)$$

$$\text{Log}L_M'=0.24M-0.16 \quad \text{with } M < 6.5 \quad (4)$$

where  $L_M$  and  $W_M$  are the length and width of the projection of earthquake volume sources (ellipsoid) on the Earth's surface, and  $L_M'$  – diameter spherical sources.

Orientation in space sources of moderate and strong earthquakes has been established on the basis of a joint analysis of the respective information specified above. These materials have been collected from the seismic database, created at the M. Nodia Institute of Geophysics of TSU.

The procedure for constructing a ASS corresponding to a given active fault, as indicated above, is based on the delineation, along the fault, of an area with a certain width. The width of the area, in turn, depends on the dip angle of the fault plane, the width of fault dynamic impact zone (the position of branching faults, the width of the fractured zone and the thickness of the seismoactive layer) (see Fig. 4). Depending on which map of active faults (see Fig. 2) we took as the basis for constructing ASSs, model 1 and model 2 were obtained for the ASSs in the study area.

Thus, based on the above described method, two ASSs models were obtained for the study area (Fig. 6a-b).

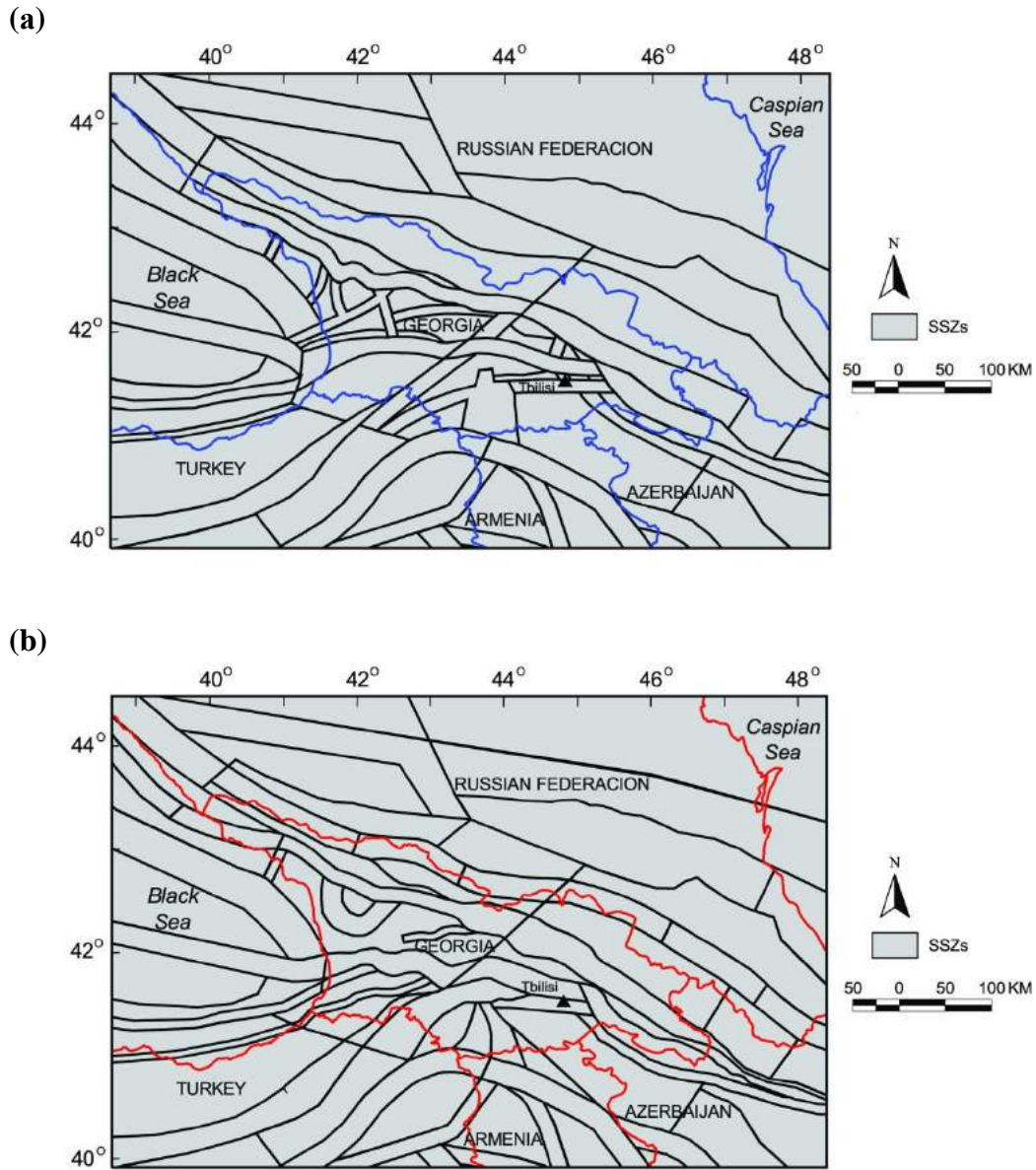


Fig. 6. ASSs models for Georgia and the regions around it: (a) based on Model 1. (b) based on Model 2.

#### 4 Parameterization of ASSs

For each ASS, a model must be selected, which is expressed by a set of parameters that represent the basic input for the seismic hazard assessment.

In ASS model, the following parameters are considered:

- i. The maximum magnitude.
- ii. parameters of the magnitude-frequency distribution of the earthquakes.
- iii. The parameters of earthquake depth distribution.

The values of some ASSs parameters in this study area were set only in large, isolated tectonic units, in and around Georgia, according to Adamia et al., [2]. Then, these tectonic units were generalized (see, for example, Fig. 7), so that each ASS fell into some sort of Generalized Tectonic Unit (GTU). Many boundaries between GTUs are reflected in the structure of seismicity, as dividing lines between zones with different rates of seismicity.

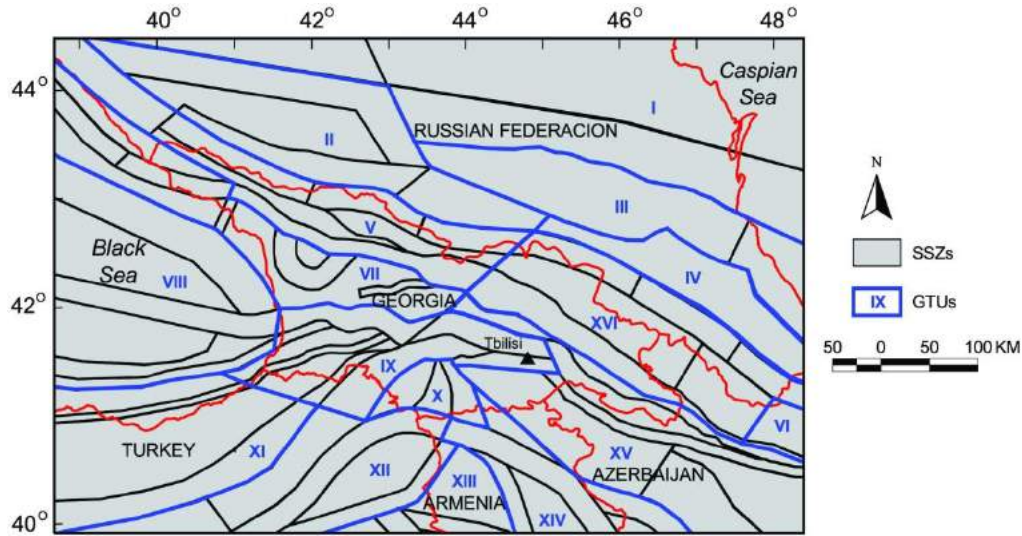


Fig. 7. Generalized tectonic units (GTUs) and ASSs (according to Adamia et al., [2]).

#### 4.1 Maximum magnitude ( $M_{max}$ )

In the PSHA, the assessment of the expected maximum earthquake magnitude ( $M_{max}$ ) for each ASS is required. Such assessment is conducted by using multiple methods for the estimation of  $M_{max}$ . In Georgia and the areas around it, for the purpose of hazard assessment, five methods to estimate  $M_{max}$  (within individual ASS) were used. Of these, three are of seismological and two of geological nature.

The seismological methods use historical and instrumental records of seismicity and, in particular, the assessment of the magnitudes of the largest earthquakes observed within each ASS ( $M_{obs}$ ), plus an increment to determine  $M_{max}$ . Also,  $M_{max}$  is assigned by extrapolation of the magnitude-frequency dependence of earthquakes in each ASS to the specified recurrence period value (e.g., 2475 years). The geological methods adopted for determining  $M_{max}$  in the ASS, are focused on the use of the geographical extent of the active faults and their individual segments, as it is expected that they control the  $M_{max}$  in each ASS (Wells and Coppersmith, [18]; Shebalin et al., [11]; Wheeler, [19]).

Below, the basic concepts of the five used methods are described in more detail. In particular, the first method for evaluating the  $M_{max}$  is based on the definition of the largest observed magnitude in a ASS ( $M_{obs}$ ). This method is relatively simple and can be applied anywhere in the investigated region. However, it provides in many area only a lower bound on  $M_{max}$  and it is suitable only for ASS, where large historical earthquakes were observed (Wheeler, [19]).

According to the second method, the  $M_{max}$  is equal to  $M_{obs}$  plus an increment. Like in the case of the first method, it is a straightforward one and can be applied anywhere in the given region, especially in zones where  $M_{obs}$  is small. For the investigated region, the increment is equal to 0.5 magnitude unit. The average accuracy of determining the magnitude for the entire observation period (up to 2019) is equal to  $\Delta M = \pm 0.5$ .

The third method for  $M_{max}$  assessment uses a magnitude-frequency extrapolation of observed records. The magnitude-frequency equation can help determine the magnitude for a given recurrence period. The question is what return period should be considered in any given ASS, to estimate  $M_{max}$ . Experience of

seismic hazard assessment for Georgia and surrounding areas showed that the seismic hazard maps with a 1% ( $T \leq 4750$  years return period of events) and 2% ( $T \leq 2475$  years) probability of exceedance within 50 years differ very little from each other, i.e. after  $T=2475$  years there is a saturation value of seismic hazard. The maps with a 2% probability of exceedance cover almost all the observed maximum earthquakes recorded over the 2000 years of historical observations. Therefore, the 2475-year return period can be taken for the purpose of  $M_{\max}$  assessment in this region.

In the fourth method,  $M_{\max}$  is estimated considering the maximum length ( $L_{\max}$ ) of an active fault (or fault system), which falls into a given ASS. In particular, the  $M_{\max}$  can be estimated by the maximum length  $L_{\max}$  of an active fault, provided that 10% of the fault's length falls into the ASS. This method uses a nomogram  $M_{\max}(L_{\max})$ -dependence from Shebalin et al., [11], which takes into account the level of development of active fault systems in the ASS (single faults, weak fault system or developed fault system) and various seismotectonic situations in the ASS (active, moderately active or weakly active).

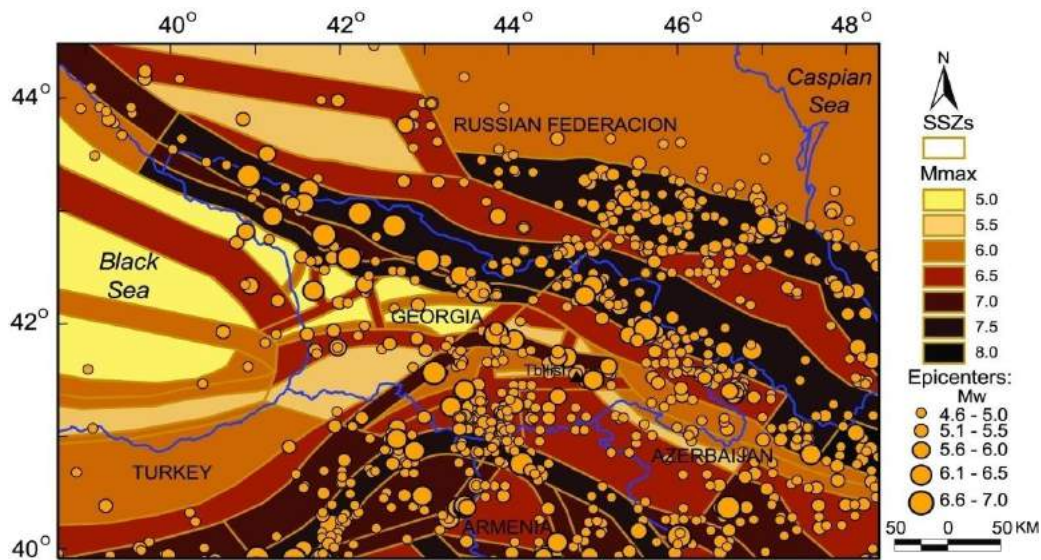
The fifth method evaluates the  $M_{\max}$  by taking into account the size of active fault segments and fault systems. The key point of this method is the fact that earthquakes typically occur due to the rupture of individual fault segments. Thus, carrying out the segmentation of a fault, the determination of the size of individual segments provides a basis for assessing the maximum length of a future rupture and, consequently, the expected maximum magnitude (DePolo et al., [6]; Wells and Coppersmith, [18]; Pizzi and Paladini, [10]). For the calculation of the  $M_{\max}$  in the investigated region, we used the regression equation of subsurface rupture length ( $L$ ) on moment magnitude ( $M_w$ ), and in particular the formula (Wells and Coppersmith, [18]):

$$M_w = 4.38 + 1.49 \log(L), \quad (5)$$

which is best suited to the seismotectonic conditions of Georgia and its surrounding areas. Since in the four methods for determining  $M_{\max}$  use magnitude in terms of surface waves ( $M_s$ ), for conversion from  $M_s$  to  $M_w$  have been used the formula provided by Zare et al., [20]).

The final values of the  $M_{\max}$  in terms of moment magnitude ( $M_w$ ) were estimated in the investigated region by averaging individual values obtained through the above described methods. Analysis of the results showed that the used geological methods relatively overstate the estimated value of  $M_{\max}$ , and seismological methods, on the contrary, relatively understate. Fig. 8a,b show maps of the investigated region, differentiated by average values of the  $M_{\max}$ , obtained using the above methods. These maps are the basis for the calculation of the new Georgian seismic hazard maps for different probabilities of exceedance in 50 years.

(a)



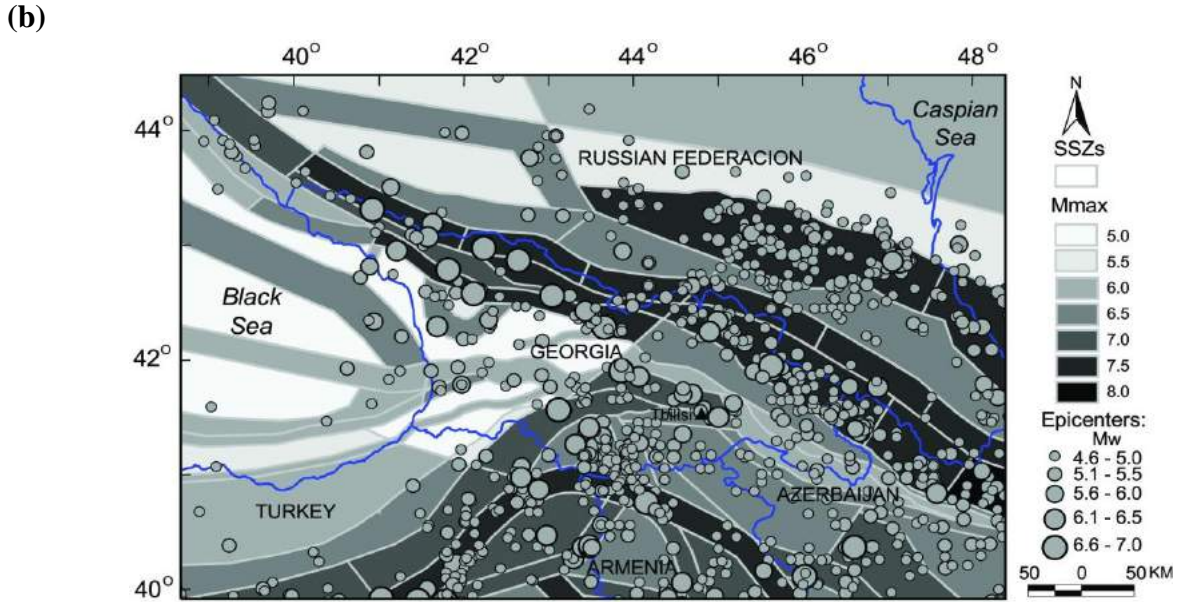


Fig. 8. ASSs maps of the investigated region, differentiated by  $M_{\max}$ : (a) for ASSs Model 1. (b) for ASSs Model 2.

#### 4.2 Recurrence of earthquakes

The next main step in the probabilistic seismic hazard assessment is the definition of recurrence law for each ASS. Recurrence law may be determined from Gutenberg-Richter frequency-magnitude distributions  $\text{Log}_{10}N(M) = a - b \cdot M$  and in particular by its parameters:  $b$  - the slope of magnitude-frequency occurrence curve (bGR);  $a$  - level of the corresponding graphics (aGR). The values of parameters  $a$  and  $b$  vary depending on the sizes of temporal and spatial window., parameter  $a$  is associated with the level of seismicity rate in a specific area, whereas parameter  $b$  determines the ratio of numbers of larger to smaller earthquakes and it is also associated with the seismic stress (see, for example, Pailoplee and Choowong, [9]).

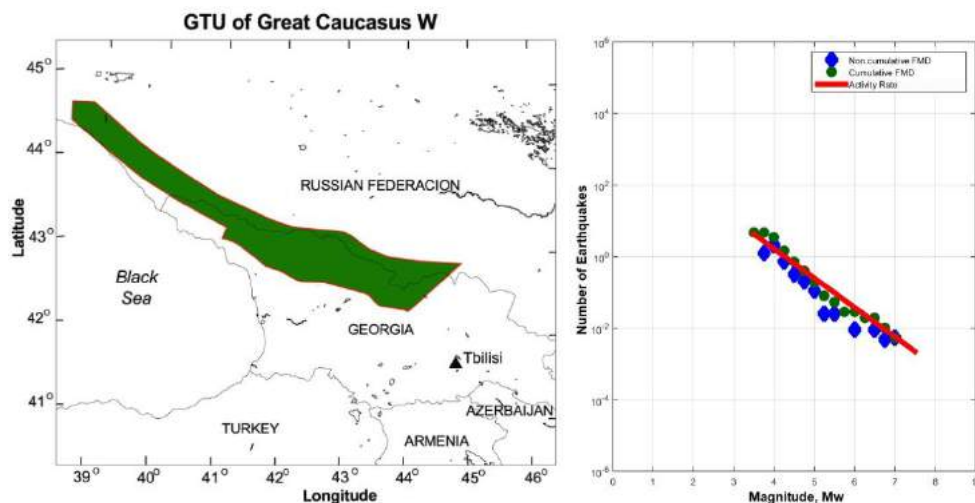
Therefore, to characterize a ASS in the investigated region, it is required to solve the problem of the determination of  $a$  and  $b$  values.

The primary data source for determining  $a$  and  $b$  values is a new instrumental earthquakes catalogue for Georgia over the 1900-2018 period, with  $M_w \geq 4.0$  events, as well as the earthquake catalogue for the Middle East region, from the EMME project (Zare et al., [20]) for the 1900-2006 period, with  $M_w \geq 4.0$  events; this was integrated by data on earthquakes for the 2007-2018 time interval from catalogues from neighboring countries. Parameters  $a$  and  $b$  of earthquake recurrence law are estimated for independent events (declustered earthquake catalogue) and completeness intervals for area sources using declustered catalogue by the Gardner and Knopoff, [7].

First in the study area, parameter  $b$  was calculated through the maximum likelihood (MLE) procedure of Weichert, ([17], for the 16 GTUs in which the data of earthquakes were sufficient for reliable determination of this parameter. The  $b$ -value obtained for each GTU is generalized for all ASS falling into given GTU. Then, recurrence parameters  $a$  and  $b$  were independently estimated for ASSs with number of earthquakes more than 10 with the same MLE. For ASSs with smaller number of earthquakes (less than 10 events), the  $b$  value was adopted from corresponding GTUs and the corresponding activity rate,  $a$ , was estimated by the distribution of the total number of events in the GTU to the smaller ASS.

Fig. 9a, b show examples of recurrence curves for GTUs: Western Greater Caucasus and Adjara-Trialeti zone.

(a)



(b)

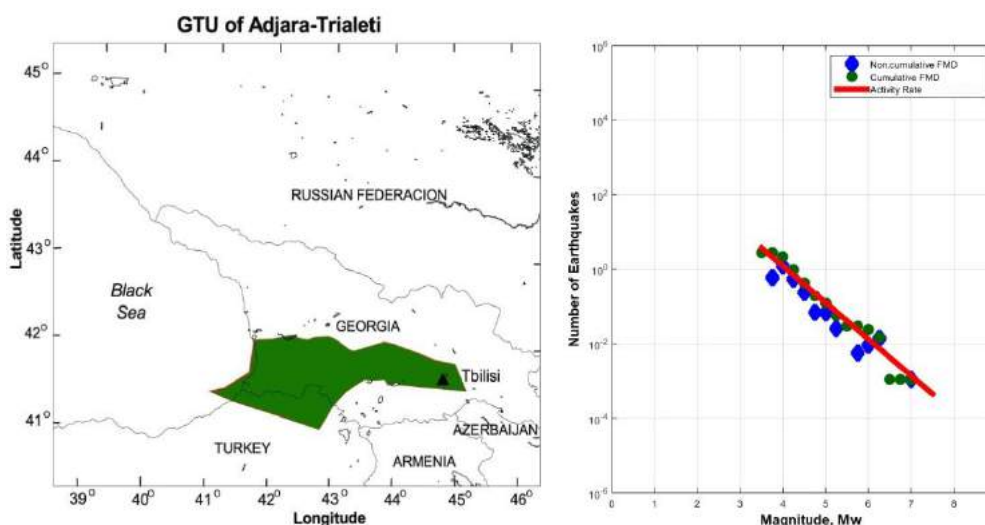


Fig. 9. Gutenberg-Richter magnitude-frequency distribution for GTUs: (a) Western Greater Caucasus; (b) Adjara-Trialeti zone.

### 4.3 Earthquakes depth distribution

Studying the distribution of earthquakes depths within the crust or upper mantle, gives us important information about the Earth's structure and the tectonic setting where the earthquakes are occurring, i.e. is an important indicator of seismicity type. In the continental crust, seismicity is usually concentrated in the upper crust and the lower crust is much less active.

This section discusses the depth distribution of the seismicity in 14 GTUs of the investigated extensive region around Georgia. The number of earthquake sources in the investigated region shows statistically a high degree of dependence on the depth location in the crust. Most of the earthquakes are located in the sedimentary and granite layers, while the deeper layers (Basalt and upper mantle) show relatively less seismic activity.

In particular, Figures 10a, b provide the distribution of earthquake depths according to the 1900-2018 data for the GTUs of the Greater Caucasus and Adjara-Trialeti zone. An analysis of these distributions shows that, in both cases, about 95% of earthquakes occur at depths of  $\leq 20$  km, which means that the thickness of the main seismically-active layer is 20 km. About 4% of earthquakes occurred at depths of 21 to 40 km, and

the remaining 1% occurred at depths >40 km. As regards all the 14 GTUs, an average of about 85% of the total number of earthquakes occurred in the 1- to-20-km depth range. The weaker earthquakes ( $M_w < 5.5$ ) took place in sedimentary units, whereas the stronger ones ( $M_w \geq 5.5$ ) occurred in granite units. About 10% of earthquakes occurred at depths of 21 to 40 km, and the remaining 5% occurred between depths of 41 to 160 km (Tibaldi, et al., [12]).

Thus, it is clear that most of the seismicity in this extensive region is shallow, and this conclusion is particularly important with respect to the choice of ground-motion models to be used in seismic hazard calculations.

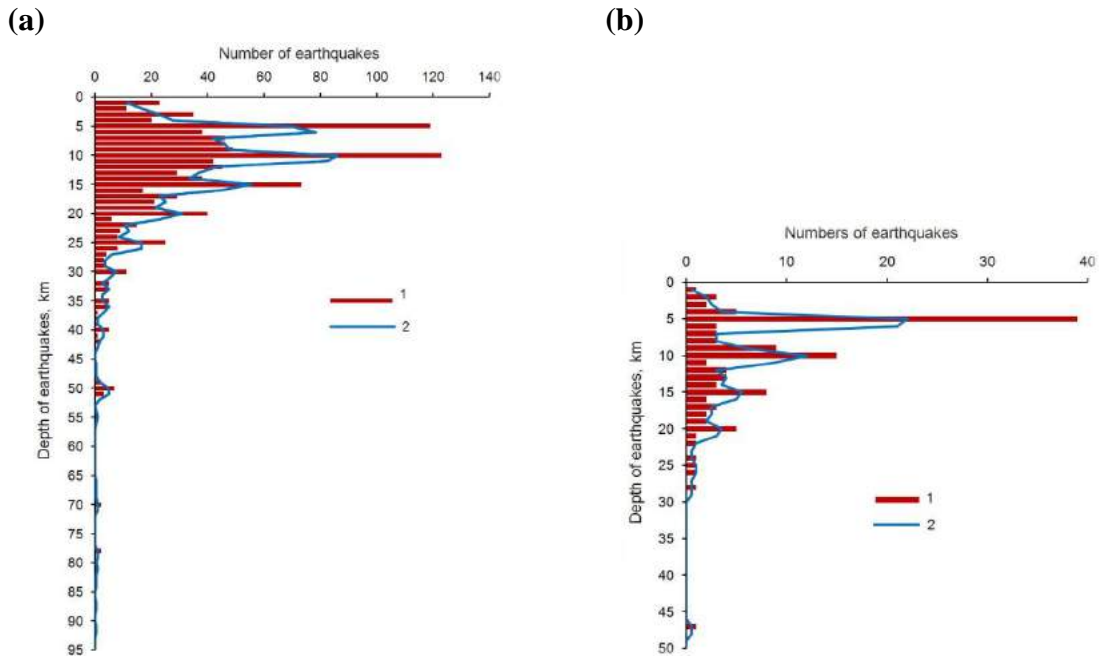


Fig. 10. Number of earthquakes (Tsereteli et al., [13]) with different depths (km) for GTUs: (a) Greater Caucasus; (b) Adjara-Trialeti zone. 1 – Distribution of the number of earthquakes according to depth (from 1900 to 2018); 2 – Moving averaging curve.

## 5 Final remarks

The delineation and parameterization of ASSs are among the first steps in the implementation of a PSHA. In practice, area seismic sources are preferentially used, which cover one or more active faults and have homogeneous characteristics of seismicity. In practical applications, in the absence of formal and consistent procedures the issue of ASSs delineation is often a controversial one in the field of PSHA. The main seismotectonic concepts for the definition of ASSs are based on the subdivision of the crust into separate blocks.

In identifying of potential ASS is necessary to clarify the spatial location of active faults and earthquake sources. For Georgia, the used tectonic maps are the ones (see Fig. 1a, b) that were published in high-rank, peer-reviewed journals: Caputo et al., [4] and Adamia, et al., [1]. For the extensive area around Georgia, other tectonic maps were used, derived from the mega-database, developed by EMME the project.

A method for ASS delineation in Georgia has been developed, based on the definition, along the active fault, of an area with a certain width. In turn, the width of the ASS is dependent on fault width, the dip angle of the fault plane, the thickness of the seismically active layer, and the geometrical parameters of the earthquake source. This was illustrated by way of an example from the 2011 Sairme earthquake epicenter, in south-western Georgia.

Finally, on the basis of this methodology, ASSs models were obtained for the whole study area.

Five methods were used to estimate  $M_{max}$  within individual ASSs. Two map versions for the studied region were constructed, differentiated in agreement with the averaged values of  $M_{max}$ .

As regards the ASSs, also the earthquake recurrence law was established from the Gutenberg-Richter magnitude-frequency distribution, and its  $a$  and  $b$  parameters were determined. Based on the completed instrumental catalogue of earthquakes for Georgia and surrounding regions for the 1900-2018 period, and by the maximum likelihood (MLE) procedure of Weichert, [17], parameter  $b$  was determined for 16 GTUs. Then, parameter  $b$  and  $a$  was calculated for each ASS.

The distribution of the depth of earthquakes was studied for 14 GTUs in Georgia and its surrounding areas. Our analysis of the obtained distributions has enabled us to document that most of the seismicity of this region is at shallow crustal levels.

The above results were used to come up with the new Georgian seismic hazard maps, for different exceedance probabilities in 50 years.

## References

- [1] Adamia Sh., Mumladze N., Sadradze N., Tsereteli E., Tsereteli N., Varazanashvili O. Late Cenozoic tectonics and geodynamics of Georgia (SW Caucasus). *Georgian International Journal of Science and Technology*, vol. 1(1), 2008, 77-107.
- [2] Adamia Sh., Zakariadze G., Chkhotua T., Sadradze N., Tsereteli N., Chabukiani A., Gvencadze A. Geology of the Caucasus: a review. *Turkish Journal of Earth Science*, vol. 20(5), 2011, 489-544.
- [3] Aleshin A. S., Barkhatov I. I., Nesmeyanov S. A., Sevostyanov V. V., Fedorov S. A., Shmidt G. A. *Tectonicheskie razlomi na uchastkakh seismicheskogo microraionirovania*. Moscow: Pub. House Nauka, 1982.
- [4] Caputo M., Gamkrelidze I., Malvezzi V., Sgrigna V., Shengelaia G., Zilpimiani, D. Geostructural basis and geophysical investigations for the seismic hazard assessment and prediction in the Caucasus. *Il Nuovo Cimento*, 23C(2), 2000, 191-215.
- [5] Danciu L., Şeşetyan K., Demircioglu M., Gülen L., Zare M., Basili R., Elias A., Adamia Sh., Tsereteli N., Yalçın H., Utkucu M., Asif Khan M., Sayab M., Hessami Kh., Rovida A. N., Stucchi M., Burg J. P., Karakhanian A., Babayan H., Avanesyan M., Mammadli T., Al-Qaryouti M., Kalafat D., Varazanashvili O., Erdik M., Giardini D. The 2014 Earthquake Model of the Middle East: seismogenic sources. *Bulletin of Earthquake Engineering*, vol. 16(8), 2018, 3465–3496.
- [6] DePolo C. M., Clark D. G., Slemmons D. B., Ramelli A. R. Historical surface faulting in the Basin and Range province, western North America: implications for fault segmentation. *Journal of Structural Geology*, vol.13(2), 1991, 123-136.
- [7] Gardner J.K., Knopoff L. Is the sequence of earthquakes in southern California, with aftershocks removed, Poissonian? *Bull. Seismol. Soc. Am.*, 1974, 64(5),1363–1367.
- [8] Gupta I. D. Probabilistic seismic hazard analysis method for mapping of spectral amplitudes and other design-specific quantities to estimate the earthquake effects on man-made structures. *ISSET Journal of Earthquake Technology*, vol. 44(1), 2007, 127–167.
- [9] Pailoplee S., Choowong M. Earthquake frequency-magnitude distribution and fractal dimension in mainland Southeast Asia. *Earth, Planets and Space*, vol. 66(8), 2014, 1-10.
- [10] Pizzi A., Galadini F. Pre-existing cross-structures and active fault segmentation in the northern-central Apennines (Italy). *Tectonophysics*, vol. 476(1-2), 2009, 304–319.
- [11] Shebalin N. V., Trifonov V. G., Kozhurin A. I., Ulomov V. I., Tatevossian R. E., Ioffe A. I. A unified seismotectonic zonation of Northern Eurasia. *Journal of Earthquake Prediction Research*, v. 8, 2000, 8-31.
- [12] Tibaldi A., Tsereteli N., Varazanashvili O., Babayev G., Barth A., Bonali F. L., Russo E., Kadirov F., Yetirmishli G., Kazimova S., Mumladze T. Active stress field and fault kinematics of the Greater Caucasus. *Journal of Asian Earth Sciences*, 2019, <https://doi.org/10.1016/j.jseaes.2019.104108>
- [13] Tsereteli N., Varazanashvili O., Kupradze M., Kvavadze N., Gogoladze Z. Seismic catalog for Georgia. *Journal of Georgian Geophysical Society* 16a, 2016, 62-69.
- [14] Ulomov V. I. Focal zones of earthquakes modeled in terms of the lattice regularization. *Izvestiya, Physics of the Solid Earth*, vol. 34(9), 1998, 717–733.
- [15] Varazanashvili O., Tsereteli N., Bonali F. L., Arabidze V., Russo E., Mariotto F. P., Gogoladze Z., Tibaldi A., Kvavadze N., Oppizzi P. GeoInt: the first macroseismic intensity database for the Republic of Georgia. *Journal of Seismology*, 22(3), 2018, 625-667.

- [16] Weatherill G., Burton P. W. Delineation of shallow seismic source zones using K-means cluster analysis, with application to the Aegean region. *Geophysical Journal International*, vol. 176(2), 2009, 565-588.
- [17] Weichert D.H. Estimation of the earthquake recurrence parameters for unequal observation periods for different magnitudes. *Bull. Seismol. Soc. Am.* 70(4), 1980, 1337-1346.
- [18] Wells D. L., Coppersmith K. J. New empirical relationships among magnitude, rupture length, rupture width, rupture area, and surface displacement. *Bulletin of the Seismological Society of America*, vol. 84(4), 1994, 974-1002.
- [19] Wheeler R. L. Methods of  $M_{max}$  Estimation East of the Rocky Mountains. U.S. Geological Survey Open-File Report 2009-1018, 2009, 44 p.
- [20] Zare M., Amini H., Yazdi P., Sesetyan K., Demircioglu M.B., Kalafat D., Erdik M., Giardini D., Khan M.A., Tsereteli N. Recent developments of the Middle East catalog. *Journal of Seismology*, 18(4), 2014, 749-772.

## სეისმური კერების არეების მოდელების აგება და პარამეტრიზაცია საქართველოსა და გარემომცველი რეგიონისთვის

ო. ვარაზანაშვილი, ნ. წერეთელი

### რეზიუმე

სეისმური კერების არეების (სკა) მოდელების განვითარება წარმოადგენს პირველ ნაბიჯს ალბათური სეისმური საშიშროების ანალიზის (ასსა) განხორციელებაში, რადგან სეისმური საშიშროების შეფასების საბოლოო შედეგების სანდოობა ძირითადად მათზეა დამოკიდებული. ამ მოდელების განსაზღვრა მოიცავს სეისმური კერების არეების (სკა) გამოყოფას და მათ პარამეტრიზაციას. უნდა აღინიშნოს, რომ პრაქტიკულ საქმიანობაში, როდესაც არარსებობს სკა-ს აგების მკაფიო პროცედურები, ამას მივყავართ დიდ ცვლილებებთან საშიშროების გამოთვლაში და არასანდო რეზულტატებთან.

კავკასიაში, სადაც აქტიური რღვევები მკაფიოდ არის განსაზღვრული და პარამეტრიზირებული, ხოლო სეისმურობა შედარებით კარგად - დოკუმენტირებული, გამოიყენება სკა-ს გამოყოფის ჩვენ მიერ განვითარებული მეთოდი. სკა-ს აგების პროცედურა ეფუძნება აქტიური რღვევის გასწვრივ გარკვეული სიგანის ფართობების გამოყოფას. სკა-ს სიგანე დამოკიდებულია რღვევის სიგანის მონაცემზე, რღვევის სიბრტყის დახრაზე, სეისმურად აქტიური ფენის სიმძლავრეზე, მიწისძვრის კერის გეომეტრიულ ზომებზე. სკა-ს ასიმეტრია რღვევის ღერძულა ხაზის მიმართ წარმოადგენს ასეთი აგებების დამახასიათებელ ნიშანს. ამ მეთოდის საფუძველზე, სკა გამოიყო საქართველოსა და მისი გარემომცველი რეგიონისათვის.

ყოველი სკა გამოხატულია პარამეტრების ნაკრებით, რომელიც განსაზღვრავს შემავალ საზაზისო მონაცემს სეისმური საშიშროების შეფასებისთვის.  $M_{max}$ -ის შეფასება ხდებოდა სამი სეისმოლოგიური და ორი გეოლოგიური მეთოდის საფუძველზე.

მაგნიტუდურ-სიხშირული განაწილების  $b$  პარამეტრი გამოთვლილი იქნა 16 განზოგადოებული ტექტონიკური ერთეულისთვის, სადაც სეისმური სტატისტიკა იყო საკმარისად სრული, ხოლო პარამეტრი  $a$  განისაზღვრა ყოველი სკა-თვის. მიწისძვრების სიღრმეების განაწილების შესწავლამ გვიჩვენა, რომ სეისმურობა ამ რეგიონში ძირითადად არ არის ღრმა.

# Модели определения и параметризации зон сейсмических очагов для Грузии и окружающего региона

О.Ш. Варазанашвили, Н.С. Церетели

## Резюме

Развитие моделей зон сейсмических очагов (ЗСО) является первым шагом в осуществлении анализа вероятностной сейсмической опасности (АВСО), так как от них в основном зависит достоверность окончательных результатов оценки сейсмической опасности. Определение этих моделей включает разграничение ЗСО и их параметризацию. Следует отметить, что в практических приложениях, когда не существуют четкие процедуры построения ЗСО, это приводит к большим изменениям в вычислении опасности и к неправдоподобным результатам.

На Кавказе, где активные разломы четко определены и параметризованы, а сейсмичность относительно хорошо документирована, используется, разработанный нами метод разграничения ЗСО. Процедура построения ЗСО основана на выделении вдоль активного разлома площади определенной ширины. Ширина ЗСО зависит от данных о ширине разлома, наклона плоскости разлома, мощности сейсмоактивного слоя, геометрических размеров очага землетрясения. Асимметрия ЗСО относительно осевой линии разлома является характерной чертой этих построений. На основе этого метода были выделены ЗСО для Грузии и окружающего региона.

Каждая ЗСО выражается набором параметров, которые будут представлять собой базовые данные для оценки сейсмической опасности. Оценки  $M_{\max}$  проводились на основе трех сейсмологических и двух геологических методов.

Параметр  $b$  распределения амплитудно-частотных характеристик был рассчитан для 16 обобщенных тектонических единиц, для которых сейсмическая статистика была достаточно полной, а параметр  $a$  был определен для каждой ЗСО. Изучение глубинного распределения землетрясений показало, что сейсмичность в этом регионе в основном неглубокая.

# **General Relativity Theory and Earthquakes**

**Bakhram Nurtaev**

*Institute of Helioclimatology, Germany  
nurtaev@gmx.net*

## **ABSTRACT**

*Earthquakes are caused by movements within the Earth's crust and uppermost mantle. Earthquakes epicenters occur mostly along tectonic plate boundaries. Solar energy drives the major processes that happen at the earth's surface, like the water cycle, wind, ocean currents, weathering, erosion, sediments transports and growth of plants. This huge mass transfer in combination with earth's rotation and gravitational effect disturbs the equilibrium of continental plates.*

*In this paper, we propose a statistical approach to compute the influence of solar energy on earthquakes. Also we estimate the relationship of aa- geomagnetic indices from solar energy. The results show that increase of solar activity leads to the growth of number of earthquake events. Finally, we discuss how general relativity theory interacts as a complex system with earthquakes.*

**Key words:** *significant earthquakes; general relativity; solar irradiance; earth rotation; aa-indices.*

## **1.Introduction**

The goal of this research is to develop a physics-based model of the earthquakes. Earthquake releases enormous amounts of energy. To release a huge amount of energy it is necessary to apply a force equal the same energy. This can be triggered by two forces, either energy of sun or internal processes within the Earth.

The absorbed sunlight drives photosynthesis, fuels evaporation, melts snow and ice, and warms the Earth system. The sun provides 99.97% of the energy required for all physical processes that take place on the earth, 0,025% - geothermal energy, Taylor (2005). The Sun doesn't heat the Earth evenly. Because the Earth is a sphere, the Sun heats equatorial regions more than polar regions. The atmosphere and ocean work non-stop to even out solar heating imbalances through evaporation of surface water, convection, rainfall, winds, and ocean circulation. This coupled atmosphere and ocean circulation is known as Earth's heat engine.

Between the end of the 17th century and the end of the 20th centuries, the Total Solar Irradiance has increased by 1.25 W/m<sup>2</sup>, or about 0.09%, Krivova et al (2010). The slight upward trend since then has led us to conclude that the Sun has played a significant role in earthquakes increase.

In comparison, only about 0.06 W/m<sup>2</sup> come as heat radiation from inside the Earth. This is more than 2000 times less than the power of the Sun, (Kleidon, 2012).

Mass-energy equivalence is the famous concept in physics represented mathematically by  $E=mc^2$ , which states that mass and energy are one and the same (Knight, 2008).

Additionally, the equation suggests that energy and mass are interchangeable with each other. In other words, energy can be converted to mass and mass to energy.

In accordance with our hypothesis, earthquakes release huge amounts of energy through the stored solar radiation. The objectives of study are verification of the relationship of earthquakes with solar energy.

## **2. Method**

Over the period of last 300 years have been observed increasing of solar irradiance and significant earthquakes events (Fig.1)

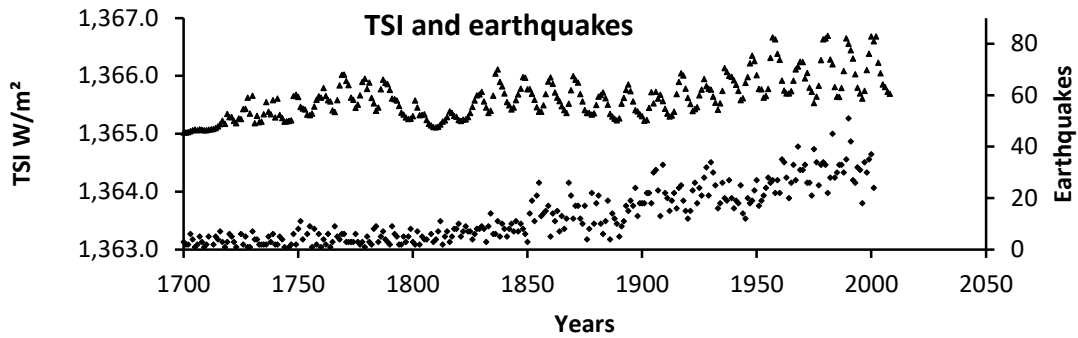


Fig. 1. Solar irradiance and earthquakes over the period 1700-2000.

Annual amount of total significant earthquakes data, in mathematical sense, represents a set of natural numbers and can be described as:

$$EQ = \{eq_0, eq_1, eq_2, eq_i, \dots\}; \quad (1)$$

-where  $eq_0, eq_i$  –averaged yearly number of earthquakes.

In accordance with our concept that earthquakes cause from stored solar energy and notion of sets (mathematic), every member of earthquakes “EQ” set is also a member of set solar activity presented as Total Solar Irradiance “TSI” (Nurtaev,2019), then “EQ” is said to be a subset of “TSI” (Fig. 1).

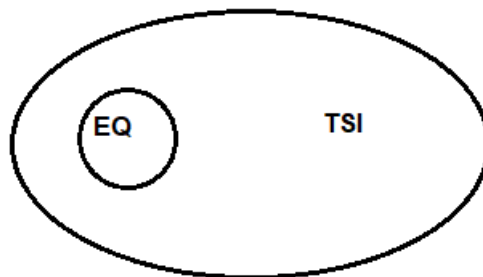


Fig. 2. Earthquakes (EQ) are subsets of solar activity,  $EQ \subset TSI$ .

$$TSI = \{tsi_0, tsi_1, tsi_2, tsi_3, tsi_i, \dots\}; \quad (2)$$

-where  $tsi_1, tsi_2, \dots, tsi_i$  - measured Total Solar Irradiance in  $W/m^2$ .

Each value of  $tsi_i$  predetermines the corresponding value of earthquake  $EQ_i$ . The conversion of earthquakes series into numerical sets allows working with them as with mathematical objects.

For discovery of relationship a set of data points plotted on an x and y axis to represent two sets of variables is created. An independent variable “tsi” is plotted along the horizontal axis. The observed number of earthquakes or dependent variable EQ is plotted along the vertical axis.

In accordance with concept of mass- energy equivalence and sets theory (Figure 2) –every change of sun output- “tsi”, leads to change of subset earthquakes “EQ”. This means, that every change in average annual solar energy leads to a change of earthquakes amount.

We tested a relationship between amount of earthquakes and solar energy “tsi” over the period 1700-2000. The generally positive relationship between the two variables can be easily discernible from the cloud formed by 300 points (Fig. 3).

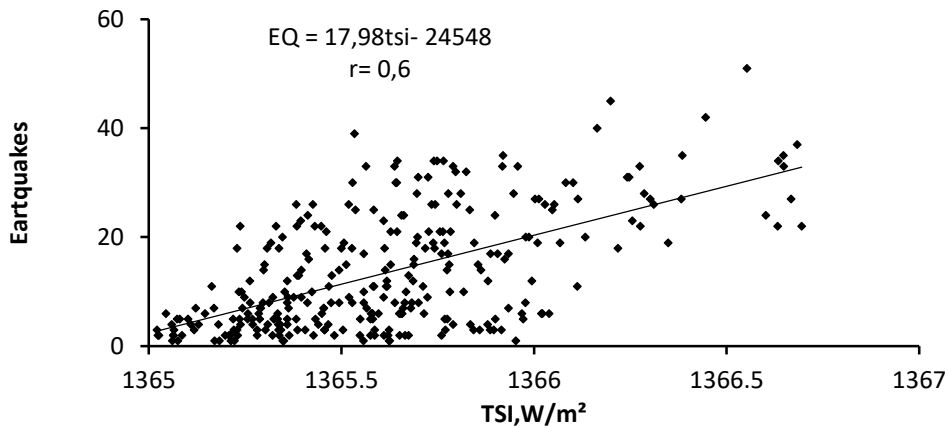


Fig. 3. Dependence of earthquakes from solar energy.

To enhance the trend in the graph, we used an global attractor ( Nurtaev, 2018,2019), expressed in the length of the solar cycle.

Observation period for meteorological objects was divided on 11 years solar cycles time intervals for earthquakes and solar irradiance. It was calculated for every such interval averaged Total Solar Irradiance and earthquakes events, Nurtaev (2015):

$$TSI = \frac{1}{n} \sum_{i=0}^n tsi_i; \quad (3)$$

$$EQ = \frac{1}{n} \sum_{i=0}^n EQ_i; \quad (4)$$

where TSI– averaged Total Solar Irradiance for one solar cycle with length  $n = 11$  years; EQ – averaged earthquake events for one solar cycle,  $i$  - solar cycles.

This averaging allows avoiding a cyclic variability of Total Solar Irradiance as well earthquakes and leads to uniform sampling both parameters in the same time interval. Solar minima and maxima are the two extremes of the Sun's 11-year activity cycle. Averaging over 11 years as a rule gives a smoothing effect and reveals a earthquakes trend at centennial timescales, these are three centuries in our study, Fig.4.

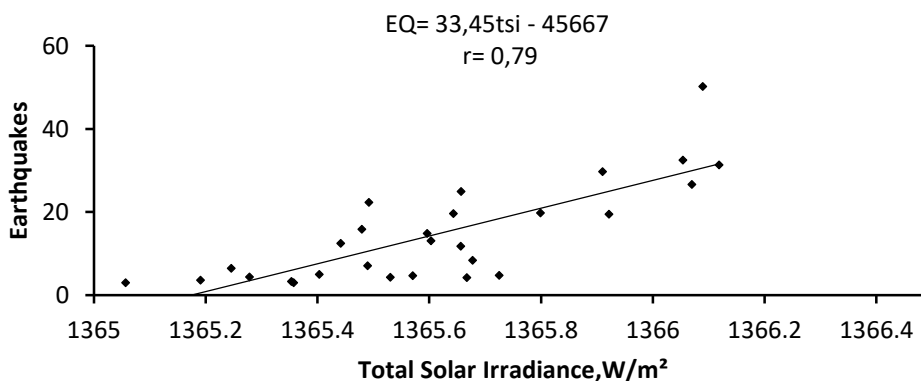


Fig. 4. World Quakes and Total Solar Irradiance over the period 1700-2008.

Electromagnetic waves of solar heat energy also change the magnetic field of the earth, Fig.5.

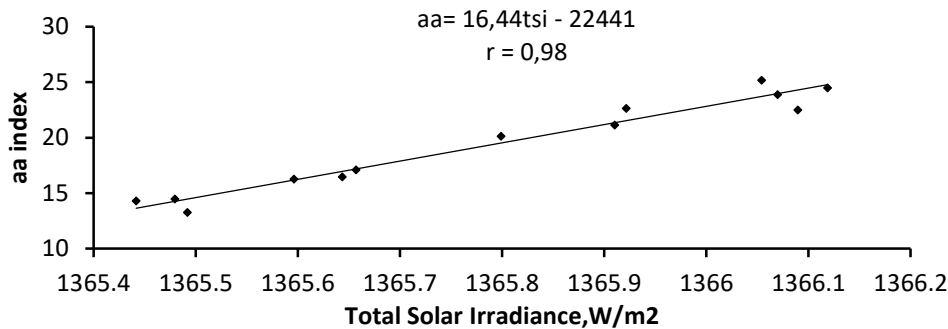


Fig. 5. Dependence of aa- geomagnetic indices from TSI over the period 1878-1996.

Relationship of earthquakes from aa-index over the period of instrumental observation 1867-1996 shows also good correlation:

$$EQ = 1,15aa + 0,55; r = 0,75 \quad (5)$$

### 3. Discussion

The sun radiates energy uniformly in all directions and the Earth intercepts and receives part of this energy during rotation around the sun. The source of almost all the energy on Earth is the sun. Changes in the Earth's system atmosphere, hydrosphere, biosphere and lithosphere (sedimentary rocks) depend on continuous stream of particles flowing outward from the Sun.

Sun loses about 5.5 million tones of mass every second or about 174 trillion tones of mass every year.

A huge amount of energy- mass transfer from the Sun causes consequences for earth's crust and movable continental plates. The energy mass transfer is transmitted by way of the mass energy transfer, direct pressure (solar sail), and magnetic field.

#### 3.1 Mass energy transfer and gravity forces.

The Sun loses about 5,5 million tons of mass every second to energy (Lang, 2006). Part of this energy reaches the Earth. A total of 173, 000 terawatts (trillions of watts of solar energy) strikes the Earth continuously. That's more than 10,000 times the world's total energy use.

In accordance with the Einstein equation  $E=mc^2$ , this amount of energy is equivalent to billion ton of mass, entering in the earth's atmosphere. Geothermal energy provides 50 terawatts, the gravitation of the moon and the sun-5 terawatts, (Kleidon .2016).

The solar energy leads to weathering of mother rocks, river sediments transport and redistribution of sediments in different parts of continental plates. For example, just world-wide rivers sediment contributes about  $7 \times 10^9$  tons of suspended sediment to the ocean yearly, John at al (1983). About 70% of this total is derived from southern Asia and the larger islands in the Pacific and Indian Oceans, where sediment yields are much greater than for other.

This huge amount of mass-energy transfer upsets of plate tectonics equilibrium and increase them inertial mass. Mass and energy are closely related. Due to mass-energy equivalence , every object that has mass also has an equivalent amount of energy and any additional energy acquired by the object above that rest energy will increase the object's total mass just as it increases its total energy. For example, after heating an object, its increase in energy could be measured as a small increase in mass, with a sensitive enough scale.

The Sun transfers in each second and amount of 1367 J (Wagemann,1994) on each square meter of the Earth's diameter. This value calls the "solar constant".

$$E_0 = 1367 \frac{W}{m^2} = 1367 \frac{J}{m^2 s} = 1367 \frac{kg}{s^3} \quad (6)$$

The annual mean solar irradiance is known as the solar constant and is  $1367 \pm 2 \text{ W / m}^2$ .

This amount of energy, in accordance with energy-mass concept equals to 12,5 kg/sec of mass, entering in earth's atmosphere.

The total photoautotrophic (green plants and photosynthetic bacteria are generally using energy from light are photoautotroph) for the Earth is about 104.9 billion tones C/yr. This translates to about 426 gC/m<sup>2</sup>/yr land production, and 140 gC/m<sup>2</sup>/yr for the oceans, (Field et al, 1998). There are 42, 6 kg/m<sup>2</sup> and 14 kg/m<sup>2</sup> relatively in the 100 years.

Taking into account earth rotation speed -1,675 kilometers per hour at the equator and square of continental plates it is the enormous load for earth crust.

Gravity change also deforming the Earth and cause earthquakes. Einstein envisioned gravity as a bending of space-time by mass. The geodetic effect is the warping of space and time by the gravitational field of a massive body (in this case, Earth).

GRACE detected a migration pattern of gravity changes due to deep and crustal processes a few months prior to the 2011 Tohoku (Japan) earthquake (Panet et al.2018).

The force of gravity acts to move the particles along the sloping surface on which they are resting.

### 3.2. Direct pressure (solar sail).

Einstein's equation  $E = mc^2$  shows that energy and mass are interchangeable. This equation gives the amount of energy equivalent to a certain mass and is a result derived from Einstein's theory of relativity. The radiation pressure of sunlight on earth is equivalent to that exerted by about a thousandth of a gram on an area of one square meter. Taking into account Earth's surface area- 510 072 000 km<sup>2</sup>, the total pressure acts on the surface of the earth with force of many billions kg/force in year. So a quasi-stationary stream (current) of photons should to perturb equilibrium of the Earth's tectonic plates. A sudden increase in the solar wind velocity directly correlates with maximum in the number of earthquakes, Odintsov et al (2007). Mass/energy simply moves from one place to another. The amount of energy remains constant and energy is neither created nor destroyed.

Dr. Sten Odenwald (NASA) presented calculation of direct mass of solar light in second.

Direct pressure of light: "the ratio of the total mass per second, to that intercepted by the earth is 1.9 kilograms/sec", Total mass falling direct on earth: 59 754 240 kg/year.

### 3.3. Magnetic field of earth.

The continuous stream of solar particles (solar wind) pushes Earth's magnetic field. As a result, the geomagnetic field, acting as an electromagnetic barrier, is compressed in the direction towards the Sun and is stretched into a (tail) in the direction away from the Sun. Fluctuations in its speed, density, direction, and entrained magnetic field strongly affect Earth's local space environment.

The interaction between the solar wind and Earth's magnetic field, and the influence of the underlying atmosphere and ionosphere, creates various regions of fields and currents inside the magnetosphere such as the plasmasphere, the ring current, and radiation belts.

## 4. Conclusion

Mass-energy equivalence is the famous concept in physics represented mathematically by  $E=mc^2$ , which states that mass and energy are one and the same. The Sun bathes the Earth with enormous amount of surface energy. This energy is converted into forces that change earth's surface by way of weathering, sediment transfer and biological production.

These processes are enhanced by relativistic effect of inertial rotation of the Earth.

The presented results derive from cosmological, geological, physics and biological studies.

It has been indicated statistically significant influence of solar irradiance on earthquakes.

We show how quantum of energy during period of long time can affects on the earth crust and finally on earthquakes. Constant tiny change of solar irradiance is accumulated over many years in huge amount of mass. Redistribution of sediments also has a significant impact on plates.

Earthquakes physics demands an ubiquitous knowledge. This knowledge includes a comparison of the methods and results also of relativity theory. General relativity is intended to explain unity of physics. For this it is necessary bringing all our physical, geological and biological knowledge by a single deductive logical system.

### **Conflicts of interest.**

The authors declare that there are no conflicts of interest.

### **Acknowledgments.**

We would like to express our deepest appreciation to all those who provided following open sources: NOAA National Centers for Environmental Information (NCEI), Earthquakes data.

Royal Netherlands Meteorological Institute KNMI, these have invested their full effort for accumulation of many years Databases, Total Solar Irradiance data.

### **References**

- [1] Kleidon A. Was leistet die Erde? Thermodynamik des Erdsystems. 2012. <https://doi.org/10.1002/piuz.201201294>
- [2] Knight R. D. "Relativity" in Physics for Scientists and Engineers: A Strategic Approach, 3rd ed. San Francisco, U.S.A.: Pearson Addison-Wesley, ch.37, sec. 10, 2008, pp.1172-1176.
- [3] Krivova N. A., Vieira L. E. A., Solanki S. K. Reconstruction of solar spectral irradiance since the Maunder Minimum. Journal of Geophysical Research (Space Physics), 115, A12112, 2010, 11 p.
- [4] Nurtaev B. Big data processing in hydrology. East European Scientific Journal, N 6 (46), 2019, pp.41-45.
- [5] Nurtaev B. Observation and Measurement of Solar Activity for Study of Climate Trends. Int. Journal of Science and Engineering Investigations. vol. 7, issue 81, 2018, pp.64-68.
- [6] Nurtaev B. Effect of solar forces on earthquakes. Int. Scientific Conference „Natural Disasters in Georgia: Monitoring, Prevention, Mitigation“, Proceedings, Tbilisi, Georgia, December 12-14, 2019, pp. 43-44.
- [7] Field C.B, Behrenfeld M.J, Randerson J.T, Falkowski P. Primary production of the biosphere: integrating terrestrial and oceanic components. Science. **281** (5374), 1998, pp. 237–240. Bibcode:1998Sci...281..237F. doi:10.1126/science.281.5374.237. PMID 9657713.
- [8] John D., Milliman, Robert H. World-Wide Delivery of River Sediment to the Oceans. Meade Source: The Journal of Geology, Vol. 91, No. 1, 1983, pp. 1-21.
- [9] Odintsov S.D., Ivanov-Kholodnyi G.S., Georgieva K. Bull. Russ. Acad. Sci. Phys. 71: 593, 2007. <https://doi.org/10.3103/S1062873807040466>
- [10] Odenwald S. (NASA) 2020. <https://image.gsfc.nasa.gov/poetry/ask/a11325.html>
- [11] Taylor F. W. Elementary Climate Physics. Oxford University Press, Oxford, 2005, p. 232.
- [12] Wagemann H-G, Eschrich H. Grundlagen der photovoltaischen. Energiewandlung (= Teubner Studienbücher Physik). Teubner, Stuttgart, ISBN 3-519-03218-X, 1994.
- [13] NOAA National Centers for Environmental Information (NCEI). <https://www.ngdc.noaa.gov/>
- [14] Royal Netherlands Meteorological Institute KNMI, <https://www.knmi.nl>

# ფარდობითობის ზოგადი თეორია და მიწისძვრები

ბ. ნურტაევი

## რეზიუმე

მიწისძვრები გამოწვეულია მოძრაობებით დედამიწის ქერქში და ყველაზე ზედა მანტიის საზღვრებში. მიწისძვრის ეპიცენტრები ძირითადად ტექტონიკური ფილების საზღვრების გასწვრივ არის განლაგებული. მზის ენერგია აკონტროლებს დედამიწის ზედაპირზე არსებულ ძირითად პროცესებს, როგორცაა წყლის ციკლი, ქარი, ოკეანის დინებები, გამოფიტვა, ეროზია, ნალექების გადატანა და მცენარეთა ზრდა. მასების ეს უზარმაზარი გადატანა, დედამიწის ბრუნვასთან და გრავიტაციულ ეფექტთან ერთად, არღვევს კონტინენტური ფილების წონასწორობას.

ამ სტატიაში ჩვენ გთავაზობთ სტატისტიკურ მიდგომას, რათა გამოვთვალოთ მზის ენერგიის გავლენა მიწისძვრებზე. ჩვენ ასევე ვახდენთ  $aa$  - გეომაგნიტური ინდექსების კავშირის შეფასებას მზის ენერგიასთან.

შედეგები აჩვენებს, რომ მზის აქტივობის ზრდა იწვევს მიწისძვრათა რაოდენობის ზრდას. დაბოლოს, ჩვენ განვიხილავთ, თუ როგორ ურთიერთქმედებს ფარდობითობის ზოგადი თეორია, როგორც მიწისძვრათა რთული სისტემა.

# Общая теория относительности и землетрясения

Б. Нуртаев

## Резюме

Землетрясения вызваны движениями в пределах земной коры и самой верхней мантии. Эпицентры землетрясений расположены в основном вдоль границ тектонических плит. Солнечная энергия управляет основными процессами, которые происходят на поверхности Земли, такими как круговорот воды, ветер, океанические течения, выветривание, эрозия, перенос осадков и рост растений. Этот огромный перенос массы в сочетании с вращением Земли и гравитационным эффектом нарушает равновесие континентальных плит.

В этой статье мы предлагаем статистический подход для расчета влияния солнечной энергии на землетрясения. Также мы оцениваем связь  $aa$  - геомагнитных индексов с солнечной энергией.

Результаты показывают, что увеличение солнечной активности приводит к росту числа землетрясений. Наконец, мы обсуждаем, как общая теория относительности взаимодействует как сложная система с землетрясениями.

# Formation of Sporadic E (Es) Layer by Homogeneous Horizontal Wind

**Giorgi T. Dalakishvili, Goderdzi G. Didebulidze, Maya M. Todua**

*Abastumani Astrophysical Observatory of Ilia State University, Kakutsa Cholokashvili ave. 3/5, Tbilisi 0162, Georgia.*

## ABSTRACT

*Theoretically and by corresponding numerical simulations it is shown that the formation and localization of sporadic E (Es) layer at its mainly observable mid-latitude lower thermosphere heights can be determined by homogeneous horizontal wind velocity direction and value. In the suggested theory, differently from 'windshear' theory, the wind direction and value, in addition to geomagnetic field and vertically changing ion-neutral collision frequency, determine the minimal negative value of the divergence of heavy metallic ions drift velocity, which in turn causes ion convergence into Es type horizontal thin layer. Here, in the upper heights of the lower thermosphere, the Es layer peak density and thickness are also controlled by ion ambipolar diffusion.*

*In the lower thermosphere of the northern hemisphere, the Es layer caused by horizontal homogeneous wind can be located at height regions where (1) the ions vertical drift velocity is zero and its divergence is negative (east-northward wind), (2) the ions drift downward (northward and westward wind), which occurs more frequently, or (3) the ions drift upward (eastward wind) and their negative divergences vanish and (4) in the case of dominance of southward wind the divergence of ion drift velocity is positive, consequently ion density divergence occurs and Es type layer formation is not expectable. The Es layer density increase and its vertical motion to its expectable location are faster for greater values of the horizontal wind velocity. The possibility of development of the suggested theory for vertically inhomogeneous wind is noted.*

**Key words:** *sporadic e (es) layer, homogeneous horizontal wind*

## 1. Introduction

The knowledge of physical mechanisms of sporadic E (Es) layer formation could give a possibility to predict its possible location, which is very important for modern radio communications. The search for physical mechanisms of Es layer formation had started in early 1960-ies [1,2]. The 'windshear' theory is considered to be the main one explaining of sporadic E formation [3,4]. According to this theory, in the lower thermosphere the eastward wind at lower heights changes to the westward one at upper heights or southward wind to northward which causes the accumulation of the heavy metallic ions into the horizontal thin layer in the regions close to wind polarisation changes [5]. The observations show that the Es layers do not always form in the regions of changes of horizontal wind polarisation [6,7,8], which shows the necessity of modification of this theory.

In the presented study, the formation of sporadic E by horizontal homogeneous wind in its main observable region of 95-150km is shown using theoretical and corresponding numerical methods. According to the suggested theory the ion vertical drift velocity, caused by horizontal wind in the lower thermosphere, already has minimal negative or/and maximal positive values in its divergence, which is determined by geomagnetic field, vertically changing ion-neutral collision frequency, and also direction and value of wind velocity. In the framework of this theory, in the lower thermosphere, for the known dominant ions distribution and wind field the formation and possible location of the Es layer can be predicted.

In this case, the east-northward wind can form Es type layers at about middle height of these regions where ions drift velocity is zero and its divergence is negative. Relatively frequent formation of Es layer and its location at the bottom side of the lower thermosphere, where ions downward drift velocity and its negative divergence vanishes, occur during dominance of northward and westward components of wind velocity. For the upper heights of the lower thermosphere (about 135-150km) Es layer formation occurs during dominance of eastward wind where ions upward drift and their negative divergence vanishes. Here the Es layer density also is controlled by ions ambipolar diffusion. The Es type layer formation is faster for greater horizontal wind velocity. According to the suggested theory, an ion/electron divergence also occurs in case of dominance of southward component of the horizontal wind, where ions upward drift velocity divergence is positive.

Considering the influence of horizontal wind direction and values on the ion /electron behavior and taking into account their ambipolar diffusion, it is important to create a realistic model of sporadic E formation and predict its possible location [9]. The presented mechanism does not exclude the additional effect of influence of wind shear caused by tidal motion [10] or atmospheric waves and instabilities, as well as wind and electric field directions on the Es formation and behavior [11,12,13,14,15], which can be developed by suggested theory.

## 2. Theory of sporadic E formation under the influence of homogeneous horizontal wind

The horizontal wind influences on ion vertical drift velocity via combined action of the Lorentz forcing and ion-neutral collision. The dependence of ions motion on the meridional  $V_x$  and zonal  $V_y$  components of background horizontal wind velocity of neutral particles  $\mathbf{v}(V_x, V_y, 0)$ , taking into account their ambipolar diffusion, can be described by the equation of ions vertical drift velocity  $w_i$  [14,16,17]:

$$w_i = -C_x(z)V_x - C_y(z)V_y - D_a(z) \frac{1}{N_i} \frac{\partial N_i}{\partial z}, \quad (1)$$

where

$$C_x(z) = \frac{1}{1 + \kappa^2(z)} \sin I \cos I, \quad (2)$$

$$C_y(z) = \frac{\kappa(z)}{1 + \kappa^2(z)} \cos I, \quad (3)$$

$$D_a(z) = \frac{\kappa^2(z) + \sin^2 I}{1 + \kappa^2(z)} \frac{2kT}{M_i v_{in}(z)}, \quad (4)$$

Here  $\kappa(z) = v_{in}(z)/\omega_i$ ,  $v_{in}(z)$  is ion-neutral collision frequency,  $\omega_i = eB/M$  is the ion gyrofrequency ( $\omega_i = 80s^{-1}$ ),  $\mathbf{B}(B \cos I, 0, -B \sin I)$  is the Earth's magnetic field vector,  $I$  is the magnetic dip angle,  $M_i$  is the ion mass,  $D_a(z)$  is ambipolar diffusion coefficient,  $T = (T_e + T_i)/2$  is mean plasma temperature,  $T_e$  and  $T_i$  are ions and electrons temperatures, respectively,  $k_B$  is Boltzmann constant. We take a right-handed set of coordinates  $(x, y, z)$  with  $x$  directed to the magnetic north,  $y$  to the west and  $z$  vertically upwards. The  $C_x(z)$  and  $C_y(z)$  coefficients determine an influence of the meridional ( $V_x = V \cos \varphi$ ) and zonal ( $V_y = V \sin \varphi$ ) components of horizontal wind velocity  $\mathbf{V}$  on ions vertical drift velocity. These coefficients significantly change in the lower thermosphere in the region between 100 km and 140 km height. This change is mainly caused by  $v_{in}(z)$ , which is determined by vertical distribution of neutral particle densities ([N2], [O2] and [O]) which are dominant in this region [18]:

$$v_{in}(z) = (2.62[N_2](z) + 2.61[O_2](z) + 1.43[O](z)) \cdot 10^{-10} s^{-1} \quad (5)$$

To investigate the behavior of height profile of electron density  $N_e(z, t)$ , assuming quasi-neutrality  $N_e = N_i$ , we use continuity equation, taking into account the presence of background horizontal wind with meridional  $V_x = V \cos \varphi$  and zonal  $V_y = V \sin \varphi$  components ( $V = |\mathbf{V}|$ ), in the expressions of ions vertical drift velocity, equations (1)-(4), which has the following form:

$$\frac{\partial N_i}{\partial t} = C'(z)VN_i + C(z)V \frac{\partial N_i}{\partial z} + C(z)N_i \frac{\partial V}{\partial z} + \frac{\partial}{\partial z} [D_a(z) \frac{\partial N_i}{\partial z}], \quad (6)$$

where

$$C(z, \varphi) \equiv C_x(z) \cos \varphi + C_y(z) \sin \varphi = \frac{\cos \varphi \sin I + \kappa(z) \sin \varphi}{1 + \kappa^2(z)} \cos I, \quad (7)$$

$$C'(z, \varphi) \equiv \cos \varphi \frac{\partial C_x}{\partial z} + \sin \varphi \frac{\partial C_y}{\partial z} = \frac{\sin \varphi - 2\kappa(z) \cos \varphi \sin I - \kappa^2(z) \sin \varphi}{[1 + \kappa^2(z)]^2} \cos I \frac{\partial \kappa}{\partial z}, \quad (8)$$

$\varphi = \angle \mathbf{x}\hat{\mathbf{V}}$  ( $0 \leq \varphi < 360^\circ$ ) is angle between horizontal wind and  $x$  axes direction -wind orientation angle. Equation (6) shows that the behavior of the  $N_e(z, t)$  in the lower thermosphere is determined by vertical changes in vertical flux of ion/electron ( $\partial(N_e w_i)/\partial z$ ), where it can be influenced by an ambipolar diffusion ( $\propto D_a$ ), horizontal background wind value ( $V = |\mathbf{V}|$ ) and shear ( $\frac{\partial V}{\partial z}$ ), as well as by the height profile of the  $C(z, \varphi)$  and  $C'(z, \varphi)$  coefficients, equations (7) and (8). The latter coefficients are important in the current investigation. In turn, the height profile of the  $C(z, \varphi)$  and  $C'(z, \varphi)$  coefficients, equations (7) and (8), are determined by the background horizontal wind direction ( $\varphi$ ), geomagnetic field ( $\mathbf{B}$ ), ion-neutrals collision frequency  $\nu_{in}(z)$  and its vertical changes ( $\frac{\partial \kappa}{\partial z} \propto \frac{\partial \nu_{in}}{\partial z}$ ), see equations (2), (3), (7) and (8).

Equation (1) shows that when vertical drift velocity caused by horizontal wind exceeds their diffusive displacement characteristic velocity  $CV \gg \frac{D_a}{N_e} \frac{\partial N_e}{\partial z}$ , then their vertical flux

$N_i w_i \approx -N_i VC(z)$  is proportional to ion vertical drift factor  $C(z)$ . In this case, in a certain region of the lower thermosphere, where  $\partial w_i/\partial z \approx -VC'(z) - C(z) \frac{\partial V}{\partial z} > 0$ , the ion/electron density can be increased ( $\frac{\partial N_e}{\partial t} > 0$ ) and where  $\partial w_i/\partial z \approx -VC'(z) - C(z) \frac{\partial V}{\partial z} < 0$ , it can be decreased (equation (6)). The windshear theory does not take into account the influence of  $C'$  factor on vertical changes in ions drift velocity (equation (8)) and, thus on sporadic E formation. According to this theory, when  $-C(z) \frac{\partial V}{\partial z} > 0$ , in the region where horizontal wind velocity ( $\mathbf{V}$ ) changes its polarisation, and where  $w_i \approx -C(z)V = 0$ , the ion/electron may converge into a thin layer and form the Es layer. Here, the condition  $-C(z) \frac{\partial V}{\partial z} > 0$  depends on the wind shear and it can be met for any direction. In the present consideration, an increase in the ion/electron density ( $\frac{\partial N_e}{\partial t} \propto -\frac{\partial w_i}{\partial z} \approx C'(z)V > 0$ ) is possible under the influence of the particular direction

of the homogeneous horizontal wind ( $\frac{\partial V}{\partial z} = 0, \frac{\partial w_i}{\partial z} \approx -C'(z)V$ ), when  $C' > 0$ . In this case in the region where the factor  $C'$  is maximal, the vertical change of ions drift velocity is minimal ( $\partial w_i / \partial z$ ) min  $< 0$ , so their convergence into a thin layer and formation Es is also possible.

In the case of homogeneous horizontal wind the  $C'$  factor determines both increase (e.g.,  $C' > 0$ ) and decrease (e.g.,  $C' < 0$ ) tendencies of ion/electron density, so it will be referred as an ion convergence/divergence factor. The points  $z = z_c$  or  $z = z_d$ , where  $C'$  is maximal,  $C'(z = z_c) = C'_{\max} > 0$  ( $(\partial w_i / \partial z)$  min  $< 0$ ), and minimal  $C'(z = z_d) = C'_{\min} < 0$

( $(\partial w_i / \partial z)$  max  $> 0$ ), determine the regions with maximal tendency of ion/electron density convergence or their divergence and will be referred as ion convergence driving point (ICDP)  $z = z_c$  and ion divergence driving point (IDDP)  $z = z_d$ .

Let us note that when wind's direction changes to opposite ( $\mathbf{V} \rightarrow -\mathbf{V}$ ),  $C'(z)$  also changes the sign i.e.  $C'(z, \varphi) \rightarrow -C'(z, \varphi + 180^\circ)$ , see equation (8), therefore the ICDP  $z_c$  and IDDP  $z_d$  also exchange places -  $z_c(\varphi) = z_d(\varphi + 180^\circ)$ .

The approximated analytic solution of equation (6),

$$N_e(z, t) \approx N_{om} \exp \left\{ \left[ -\frac{2D_a}{H_{ic}^2} + C'(z)V \right] (t - t_o) - \left( \frac{z - [z_{om} - C(z)V(t - t_o)]}{H_{ic}} \right)^2 \right\}, \quad (9)$$

shows the possibility of sporadic E formation in the case of presence of homogeneous horizontal wind, with behavior significantly determined by ions vertical drift factor  $C$  and their convergence/divergence  $C'$  factors. This solution is valid for small time of  $t - t_o \ll H_{ic}^2 / 2D_a$  and heights  $(z - z_{om}) \ll H_{ic}$ . The equation (9) at the initial time of  $t = t_o$  correspond to the ion/electron Gaussian type distribution layer with maximal density  $N_{om}$  (peak density) at corresponding  $z = z_{om}$  height (peak height), which in the case of absence of wind ( $C, C' = 0$ ) decreases due to ambipolar diffusion  $\propto N_{om} \exp[-\frac{2D_a}{H_{ic}^2}(t - t_o)]$ .  $H_{ic}$  is characteristic scale

height of ions, which at some initial time  $t = t_o$  determines ion/electron main layer thickness ( $2H_{ic}$ ) and height region  $z - z_{om} = \pm H_{ic}$ , where their density decreases e-times. Despite the fact that  $N_e(z, t)$  described by equation (9) does not take into account the time dependence of parameters  $N_{om}$  and  $H_{ic}$ , which will be considered in numerical simulations in the next chapter, it still describes a tendency of sporadic E formation under the influence of homogeneous horizontal wind taking into account ions vertical drift and their ambipolar diffusion.

The  $N_e(z, t)$  of equation (9) shows that, when

$$C'_{\max} V > \frac{2D_a}{H_{ic}^2} \quad (10)$$

then its increase ( $N_e / N_{om} > 1$ ) is possible. In this case when  $C = 0$ , then at ICDP  $z_c$  the maximal increase in electron density occurs (developing convergence instability), equation (9), and the Es type high density narrow layer formation is possible around this point. Such convergence instability, continuing increase in electron density and decrease in its thickness around  $z_c$  in case of  $C = 0$  should be balanced by their

ambipolar diffusive displacement ( $\propto \frac{2D_a}{H_{ic}^2}$ ), which increases with decrease of this layer thickness.

According to equation (9), the development of ion/electron convergence processes (  $\frac{\partial N_e}{\partial t} \propto C'(z)V > 0$  or  $C' > 0$  ), are also possible during the downward ( $VC > 0$  or  $C > 0$ ) or upward ( $VC < 0$  or  $C < 0$ ) drift of peak height  $z_m = z_{om} - VC(t - t_o)$  by velocity  $VC$ . These processes should be faster for greater values of the horizontal wind velocity  $V$ . So, for various directions of the horizontal homogeneous wind, the height profiles of the factors  $C(z)$  and  $C'(z)$  determine the regions, where, under its influence, the ion/electron convergence into dense thin layer and correspondingly sporadic E formation is possible. The  $C(z)$  and  $C'(z)$  factors also determine the regions of ion/electron density divergence ( $C' < 0$ ). For example, when  $C=0$  and  $-C'_{\min}V \gg \frac{2D_a}{H_{ic}^2}$ , then maximal decrease of the ion/electron density will occur in the IDDP  $z_d$  ( $C'_{\min} < 0$ ).

Figure 1 depicts (a) the ions vertical drift  $C(z, \varphi)$  and (b) convergence/divergence  $C'(z, \varphi)$  factors height profiles for various horizontal wind ( $\mathbf{V}$ ) direction angle  $\varphi = \angle \mathbf{x}\hat{\mathbf{V}}$  ( $0 \leq \varphi < 360^\circ$ ) at north hemisphere mid-latitude regions ( $45^\circ \pm 2^\circ$  N,  $45^\circ \pm 2^\circ$  E) with geomagnetic declination  $I = 6I^\circ \pm 2^\circ$ . Blue and yellow lines correspond to the heights where ions vertical drift factor  $C=0$  at their divergence region ( $C' < 0$ ) for wind direction angles  $\varphi_{b,W-S} = 90^\circ + \arctan g(\kappa/\sin I)$  and at their convergence region ( $C' > 0$ ) for  $\varphi_{b,E-N} = 270^\circ + \arctan g(\kappa/\sin I)$ , respectively. The arrows express the ions drift velocity direction at given height and horizontal wind direction angle  $\varphi$  determined by drift factor  $C(z, \varphi)$ , equation (7). The lower height arrows correspond to the height regions with comparatively smaller values of ion drift velocity ( $C \approx 0.02C_{\max}$ ).  $z = h - h_o$  is the difference between an actual and some initial height  $h_o$ . Here and hereafter for simplicity  $z = h$  ( $h_o = 0$ ).

Figure 1 shows that, in the height region of the Es layers formation (100-140 km), the ion convergence/divergence factor  $C'(z, \varphi)$  always exists and has maximal positive ( $C' > 0$ ) or/and minimal negative ( $C' < 0$ ) values. Therefore, in the framework of proposed mechanism, the convergence ( $N_{em}/N_{om} > 1$ ) or divergence ( $N_{em}/N_{om} < 1$ ) of ion/electron density under the influence of horizontal wind could occur.

In the upper atmosphere, at  $z > 140 - 145 \text{ km}$  and  $z < 95 - 100 \text{ km}$  the ion vertical drift factor  $C(z)$  changes slightly ( $C \rightarrow \text{constant}$ ), and the ions convergence/divergence factor  $C'$  vanishes ( $C' \rightarrow 0$ ). Therefore, according to the proposed mechanism, formation of Es layer under the influence of the homogeneous wind ( $\frac{\partial V}{\partial z} = 0$ ) horizontal components ( $V_x, V_y \neq 0$ ) are less expected.

Figure 1b shows that, in case of northward wind ( $\varphi = 0^\circ$ ), the ICDP  $z_{cN}$  ( $C'(z = z_{cN}) = C'_{\max} > 0$ ) and, in case of southward wind ( $\varphi = 180^\circ$ ), the IDDP  $z_{dS}$  ( $C'(z = z_{dS}) = C'_{\min} < 0$ ) are at about 121km height. For non-meridional directions of wind both - the ICDP  $z_c$  and IDDP  $z_d$  exist. During westward ( $\varphi = 90^\circ$ ) and eastward ( $\varphi = 270^\circ$ ) winds,  $z_{cW} = z_{dE} \approx 116 \text{ km}$  and  $z_{cE} = z_{dW} \approx 131 \text{ km}$ .

Here and hereafter the lower thermosphere parameters in equations (1-6) are used in accordance with NRLMMSISE-00 model [19].  $z_{c,d}, z_m = h_m, H_{ic}$  and normalized electron density  $N_e/N_{om}$  will be given with 0.5km, 0.05km and 0.05 accuracy, respectively.

If we assume that neutral particles in the lower thermosphere have barometric distribution, then  $v_{in}, \kappa \propto \exp(-z/H)$ , and from equation (8) the maximal value of  $C'(z, \varphi = 0) = C'_x(z)$

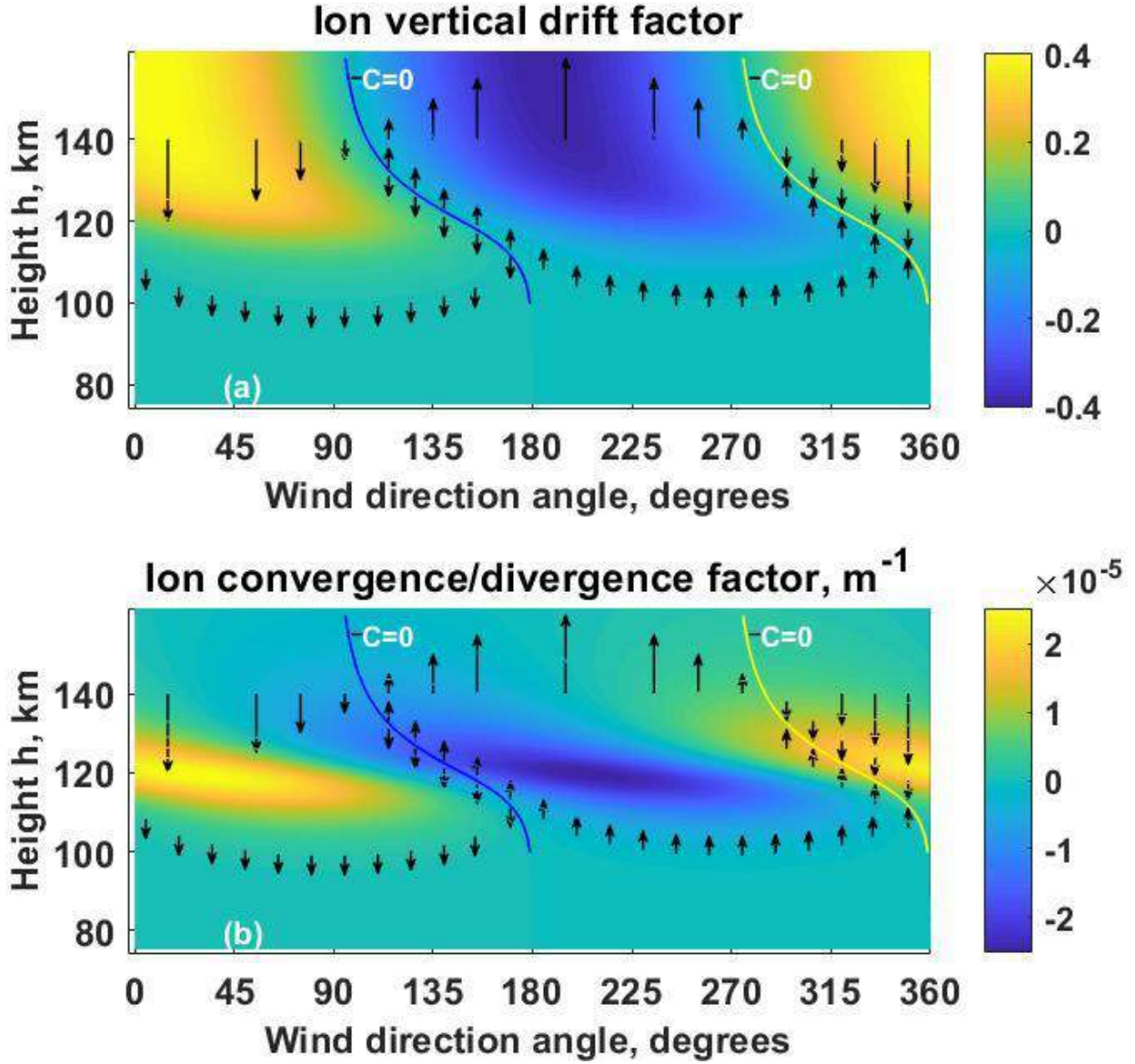


**Figure 1.** (a) The ion vertical drift  $C(z, \varphi)$  and (b) convergence/divergence  $C'(z, \varphi)$  factors height profiles for various horizontal wind ( $\mathbf{V}$ ) direction angle  $\varphi = \angle \mathbf{x}\hat{\mathbf{V}}$  ( $0 \leq \varphi < 360^\circ$ ) at north hemisphere mid-latitude regions ( $45^\circ \pm 2^\circ$  N,  $45^\circ \pm 2^\circ$  E) with geomagnetic declination  $I = 61^\circ \pm 2^\circ$ . Blue and yellow lines correspond to the heights where ions vertical drift factor  $C=0$  at their divergence region ( $C' < 0$ ) for wind direction angles  $\varphi_{b,W-S} = 90^\circ + \arctan g(\kappa/\sin I)$  and at their convergence region ( $C' > 0$ ) for  $\varphi_{b,E-N} = 270^\circ + \arctan g(\kappa/\sin I)$ , respectively. The arrows express the ion drift velocity direction at given height and horizontal wind direction angle  $\varphi$  determined by drift factor  $C(z, \varphi)$ , equation (7). The lower height arrows correspond to the height regions with expectably, comparatively smaller values of ion drift velocity ( $C \approx 0.02C_{\max}$ ).

can be obtained:

$$C'_{x\max}(\varphi = 0) = \frac{1}{2H} \sin I \cos I, \quad (11)$$

which corresponds to  $\kappa = 1$  ( $v_{in} = \Omega_i$ ).  $H$  is the atmospheric scale. So, for the northward wind the ICDP  $z_{cN}$  corresponds to the height where  $v_{in} = \Omega_i$  and for heavy metallic ions (Fe+) it is located at about

$z_{cN} \approx 12 \text{ km}$ . In case of southward wind ( $\varphi = 180^\circ$ )  $C'_{x\min}(\varphi = 180^\circ) = -C'_{x\max} = -(1/2H)\sin I \cos I$  and the IDDP  $z_{dS} = z_{cN} \approx 12 \text{ km}$ . For the mid-latitude regions ( $\sin I \cos I \neq 0$ ), in case of presence of the meridional wind ( $\varphi = 0$  or  $\varphi = 180^\circ$ ) the ICDP  $z_{cN}$  ( $(\partial w_i / \partial z) \min < 0$ ) and IDDP  $z_{dS}$  already exist (Figure 1b) and they vanish at equatorial ( $I \rightarrow 0$ ) and polar ( $I \rightarrow 90^\circ$ ) regions.

For the barometric atmosphere, in case of westward wind  $C'(z, \varphi = 90^\circ) = C'_v(z)$ , eastward wind  $C'(z, \varphi = 270^\circ) = -C'_v(z)$ , the ICDP  $z_c(\varphi = 90^\circ) \equiv z_{cW}$  and  $z_c(\varphi = 270^\circ) \equiv z_{cE}$  are located at about  $0.9H$  ( $z_{cW} - z_{cN} = -0.5H \ln(3 + \sqrt{8})$ ) below and above ( $z_{cE} - z_{cN} = -0.5H \ln(3 - \sqrt{8})$ ) the point  $z_{cN,dE} \approx 12 \text{ km}$ , where:

$$C'_{v\max} = \frac{1}{4H} \cos I. \quad (12)$$

In this case, the IDDP  $z_d(\varphi = 90^\circ) \equiv z_{dW}$  and  $z_d(\varphi = 270^\circ) \equiv z_{dE}$  are located at about  $0.9H$  above and below  $z_{cN,dS} \approx 12 \text{ km}$ , where  $C'_{y\min} = -(1/4H) \cos I$ .

Figure 1 shows that in case of meridional ( $\varphi = 0$  or  $\varphi = 180^\circ$ ) and zonal winds ( $\varphi = 90^\circ$  or  $\varphi = 270^\circ$ ), the location of convergence/divergence points and the values of  $C'$  at these points are close to those estimated for barometric atmosphere by equations (11) and (12), for the atmospheric scale heights  $H=8-10\text{km}$ . So, for northward wind there is only the ICDP ( $C'>0$ ), while for southward wind - the IDDP ( $C'<0$ ). Thus, according to equation (9), the development of electron convergence or divergence processes at  $z_{cN} = z_{dS} \approx 12 \text{ km}$  are only expectable. For westward and eastward winds there are both convergence and divergence points and, correspondingly, the electron density behavior, equation (9), is determined by convergence and divergence processes developed in this region. For any other directions of the horizontal wind,  $C$  and  $C'$  factors are determined by their sums for meridional and zonal winds ( $C_x(z) \cos \varphi$ ,  $C'_x(z) \cos \varphi$ ,  $C_y(z) \sin \varphi$  and  $C'_y(z) \sin \varphi$ ), equations (7) and (8), the ICDP and IDDP locations are different.

Figure 1 shows that depending on wind direction ( $\varphi$ ) the ICDP  $z_c$  ( $C'(z = z_c) = C'_{\max} > 0$ ) and IDDP  $z_d$  ( $C'(z = z_d) = C'_{\min} < 0$ ) can be located between 100km and 140km heights. In these regions of height the ion vertical drift factor  $C(z)$  is different ( $C=0$ ,  $C>0$ ,  $C<0$ ). Therefore, according to equation (9), various scenarios of electron/ion convergence into a thin layer and formation of sporadic E can be developed.

We consider the possible scenario of Es type layer formation ( $C'>0$ ) when ion vertical drift caused by horizontal wind: (1)  $VC=0$ , (2)  $VC>0$  is downward, (3)  $VC<0$  is upward, and also when (4) ion divergence occurs ( $C'<0$ ).

(1) The condition of  $VC(z = z_b) = 0$  ( $C=0$ ) occurs at midlatitude lower thermosphere during east-northward and west-southward winds.  $z = z_b$  is height where ion upstream and downstream flux caused by horizontal wind is balanced and  $w_i(z = z_b) = 0$  (see Figure 1 and equation (1)). In case of smaller influence of ion

ambipolar diffusion on its vertical motion,  $|CV| \gg \left| \frac{D_a}{N_e} \frac{\partial N_e}{\partial z} \right|$ , the value of  $w_i(z = z_b) \approx 0$ , equation (1). In

the considered midlatitude region the ions vertical drift balance points exist at 100-140km for the east-northward  $285^\circ < \varphi < 360^\circ$  and its opposite west-southward  $105^\circ < \varphi < 180^\circ$  winds, equations (1) and (7). Here  $C(z = 140\text{km}, \varphi \approx 105^\circ; 285^\circ) = 0$ .

For east-northward wind the condition of  $C(z = z_b) = 0$  ( $-C_x V \cos \varphi - C_y V \sin \varphi = 0$ ) occurs in the ion convergence ( $C' > 0$ ) region (see Figure 1), where the ion upward drift  $-C_y V \sin \varphi > 0$  ( $z < z_b$ ), caused by horizontal wind velocity east component ( $U_y = V \sin \varphi < 0$ ), is balanced by their downward drift  $-C_x V \cos \varphi < 0$  ( $z > z_b$ ), caused by the northward component ( $U_x = V \cos \varphi > 0$ ). In this case the horizontal wind direction angle is  $\varphi = 270^\circ + \arctan g(C_y / C_x) \equiv \varphi_{bE-N}$ . When  $\varphi_{bE-W} = 307^\circ$ , ICDP  $z_c \approx 127 \text{ km}$  and  $w_i(z = z_b) = 0$  ( $z_c \approx z_b$ ). In this case, from equation (9) the convergence layer and correspondingly, sporadic E formation are expected at height  $z_c = z_b$ .

When ion vertical drift velocity  $VC(z = z_c) = 0$ , then according to equation (9), in the ICDP  $z_c$ , region ion convergence into a thin layer (convergence instability), caused by horizontal wind, can be balanced by their ambipolar diffusion and  $C'V = \frac{2D_a}{H_{ic}^2}$ . In this case the formation of sporadic E type thin layer with minimal thickness  $H_{ic} = 1-3 \text{ km}$  at 120-130km heights is possible for the horizontal wind velocity about 50-150m/s or greater ( $H_{ic} \propto 1/\sqrt{V}$ ). In case of small changes in the total electron content (TEC) in lower thermosphere, the Es type layer peak density  $N_{em} / N_{om}$  ( $N_{em} \propto 1/H_{ic}$ ) can be increased by order of magnitude (for  $H_{ic}(t = t_o) = 10 \text{ km}$ ).

During west-southward wind the condition of  $C(z = z_b) = 0$  occurs in ion divergence ( $C' < 0$ ) region (see Figure 1), where the ions upward drift velocity  $-C_y V \sin \varphi > 0$  ( $z > z_b$ ), caused by the wind velocity west component  $U_y = V \sin \varphi > 0$ , is equal to their downward drift  $-C_x V \cos \varphi > 0$  ( $z < z_b$ ), caused by the wind southward component  $U_x = V \cos \varphi < 0$ . In this case wind direction angle is  $\varphi_b = 90^\circ + \arctan g(C_y / C_x) \equiv \varphi_{bW-S}$ . For the horizontal wind west-east direction with  $\varphi = 127^\circ$  at the IDDP  $z_d(\varphi = 127^\circ) \approx 127 \text{ km}$  and  $C(z = z_d) = 0$ . In this case, different from wind opposite east-north direction  $\varphi = 307^\circ$  ( $z_c(\varphi = 307^\circ) \approx 127 \text{ km}$ ), at the height of about 127km the ion/electron density divergence occurs, equation (9), and their upstream and downstream flow from this region increases. When ICDP is  $z_c \approx 112 \text{ km}$  the electron convergence in the thin dense layer is possible during the downstream flow ( $C > 0$ ), shown by equation (10), and the formed Es type layer can be localized below ICDP regions with  $C'(z)V \rightarrow +0$ ,  $C(z)V \rightarrow +0$ , ( $w_i \rightarrow -0$ ). Here  $+0$  and  $-0$  denote negligibly small positive and negative values, respectively. The condition  $C' \rightarrow 0$ ,  $C \rightarrow 0$  means that, for given direction of the wind, the values of  $(C'/C'_{\max}) \ll 1$ ,  $C \ll 1$  are decreased.

The ion/electron wind induced upstream flow ( $z > 127 \text{ km}$ ) from region with  $C(z = z_d) = 0$  (see Figure 1) makes their diffusive displacement to the upper height quicker than in case of absence of wind.

(2) The ion downward drift ( $VC > 0$ ) at ICDP, caused by horizontal wind ( $VC_x \cos \varphi + VC_y \sin \varphi > 0$ ), in addition to its west-southward direction, also occurs for northward ( $\varphi = 0$ ), north-west and westward winds (see Figure 1). In these cases the ion convergence into a thin layer and correspondingly sporadic E formation, descending towards lower regions identified by  $C'(z)V \rightarrow +0$ ,  $C(z)V \rightarrow +0$ , are expected. For different directions of horizontal wind, when  $307^\circ < \varphi < 360^\circ$  ( $270^\circ + \arctan g(\kappa(z = z_{cb}) / \sin I) < \varphi < 360^\circ$ ,  $z_{cb} \equiv z_c = z_b$ ), the ICDP  $z_c$  is located above the point where  $C = 0$  ( $z_c > z_b$ ) and correspondingly the convergence layer should descent and locate at  $z_b$  height region, equation (9).

(3) When  $285^\circ < \varphi < 307^\circ$  ( $285^\circ < \varphi < 270^\circ + \arctan g(\kappa(z = z_{cb})/\sin I)$ ), then ICDPs are located below the region with  $C=0$  ( $127\text{km} < z < 140\text{km}$ ) and the convergence layer should have a tendency of upwelling to this region ( $w_i = 0$ ). Here for  $\varphi = 285^\circ$  the condition  $C=0$  occurs at about 140km, where ion diffusive displacement for  $H_{ic} < 5\text{km}$  exceeds their convergence caused by wind with velocities 50-150m/s and formation of high density ( $N_{em}/N_{om} > 1$ ) thin ( $H_{ic} < 5\text{km}$ ) layer during ions upward flux ( $C < 0$ ) is expectable to about 140 km. For horizontal wind direction  $260^\circ < \varphi < 285^\circ$ , the region with condition  $C=0$  located at  $z > 140\text{km}$ , where  $C'(z)V \rightarrow +0$ ,  $C(z)V \rightarrow -0$  for 140-150km heights, the formation of convergence layer with smaller density is expected, compared to the wind direction with  $285^\circ < \varphi < 307^\circ$ . Note, that in these cases ( $CV < 0$ ), with increase of wind velocity, significant increase in the convergence layer is not expected, therefore the increase of upward drift of this layer to the region with  $C'(z)V \rightarrow +0$ ,  $C(z)V \rightarrow -0$  ( $w_i \rightarrow +0$ ) occurs.

(4) During southward wind ( $\varphi = 180^\circ$ ) the divergence factor  $C' < 0$ , equation (7), and in the region of heights 100-140km divergence processes of electron density are expected, equation (9). If the influence of southward component of wind velocity  $V \cos \varphi < 0$  on ions upward drift is dominant, ( $90^\circ + \arctan g(\kappa(z)/\sin I) < \varphi < 270^\circ$  i.e.  $(-VC_x \cos \varphi - VC_y \sin \varphi > 0)$ ), then formation of their high density convergence layer ( $N_{em}/N_{om} > 1$ ) is less expected. Here it is important to note, that the development of above mentioned ion convergence or/and divergence processes also depend on its initial layer location with respect to the points  $z_c$ ,  $z_d$  and  $z_b$ .

The winds with directions  $\varphi = 105^\circ, 127^\circ, 285^\circ, 307^\circ$ , for which  $C(\varphi = 105^\circ, 285^\circ; z \approx 140\text{km}) = 0$  and  $C(\varphi = 127^\circ, 307^\circ; z \approx 127\text{km}) = 0$ , correspond to the considered regions ( $45^\circ \pm 2^\circ$  N,  $45^\circ \pm 2^\circ$  E;  $I = 61^\circ \pm 2^\circ$ ) and can be estimated similarly by equations (2, 3) and (7) for the other midlatitude regions.

The details of the above described possibility of the electron density height profile behavior  $N_e(z, t)$  under the influence of horizontal homogeneous wind, Es type dense thin layer formation for its relatively main directions and the development of divergence processes will be shown using numerical solution of equation (6) [20, 21, 22].

### 3. Results and discussion

By numerical solution of equation (6) we will demonstrate the normalized electron density height profile  $N_e(h, t)/N_{om}$  behavior at lower thermosphere 90-150km height regions. For predominantly main directions of the horizontal wind for which we theoretically show a possibility of Es layer formation (equation (9)) at fixed height (with  $C=0$ ), its downward and upward motions to the region with  $C=0$  or those where ion convergence positive factor ( $C' > 0$ ) vanishes. Considering wind direction for which ions drift factor  $C(z = z_{c,d}) = 0$  and additional eight directions (north, north-west, ..., east-north), their influence on development of ion/electron divergence processes (when  $C' < 0$ ) is also seen.

At the first step, when  $C(z = z_{c,d}) = 0$ , we show that the influence of homogeneous horizontal wind on  $N_e(h, t)/N_{om}$  behavior and Es layer formation is important at  $V=50\text{m/s}$ . In this case we assume relatively wide layer of heavy metallic ions at initial time  $H_{ic}(t = t_o) = 16\text{km}$  when small changes in electron/ion density are expected due to their ambipolar diffusion at the absence of wind. For the lower thermosphere with dominant Fe+ ions the values of  $H_{ic} = 8 - 16\text{km}$ , which is used in suggested simulations, is close to the value of  $k(T_i + T_e)/Mg$  [19]. Note, that for some midlatitude lower thermosphere regions

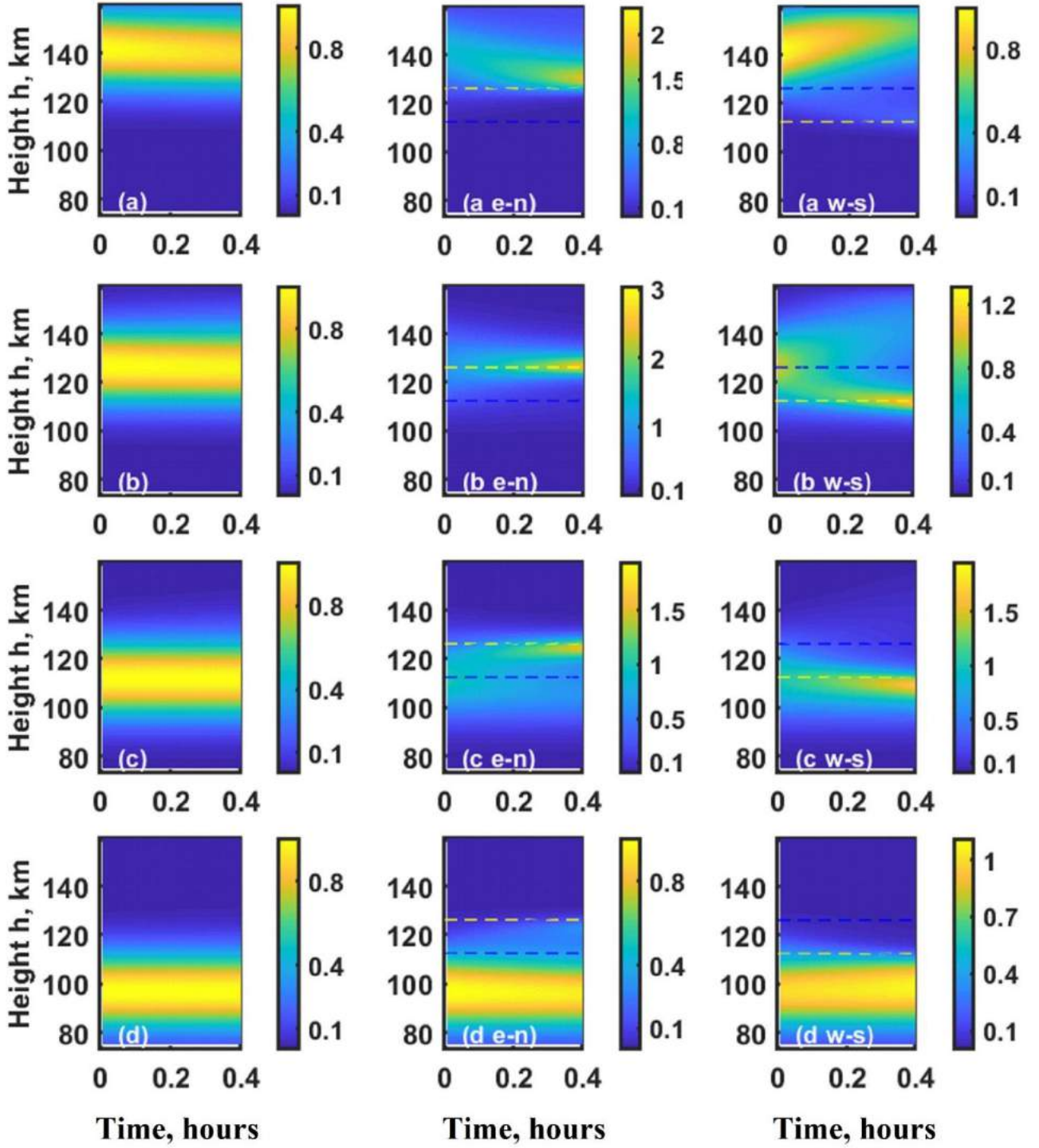
the horizontal wind velocity of about 50m/s corresponds to the maximal values of mean seasonal meridional and zonal winds, because its high value is 100m/s or even higher [ 23,24,25].

Figure 2 presents the behavior of the normalized height profile of electron density  $N_e(h,t)/N_{om}$  in the mid-latitude lower thermosphere in case of absence of wind ( $\mathbf{V}=0$ ) for its initial distribution peak height (**(a)**  $z_{om}=142km$ , **(b)**  $z_{om}=127km$ , **(c)**  $z_{om}=112km$  and **(d)**  $z_{om}=97km$ , and during presence of horizontal wind with  $V=50m/s$  directed (**(a n-w)**, **(b n-w)**, **(c n-w)**, **(d n-w)** to east-northward ( $\varphi=307^\circ$ ,  $z_{cE-N}=z_b$ ) and **(a w-s)**, **(b w-s)**, **(c w-s)**, **(d w-s)** to west-southward ( $\varphi=127^\circ$ ,  $z_{dW-S}=z_b$ ), respectively.

Figure 2 shows the possibility of electron convergence into a dense thin layer,  $N_{em}/N_{om} > 1$  and  $H_{ic}(t > t_o) < H_{ic}(t = t_o)$ , (Figures 2a e-n, 2b e-n, 2c e-n, 2b w-e and 2c w-e ). It also shows that their density divergence ( $N_{em}/N_{om} < 1$ ) dominates (Figure 2a w-s) and development of these processes is negligible (Figures 2d e-n and 2d w-s ) under the influence of horizontal homogeneous wind, for various locations of the initial electron density  $N_e(z,t=t_o)$  peak height ( $z_{om}=142km$ ,  $z_{om}=127km$ ,  $z_{om}=112km$  and  $z_{om}=97km$ - Figures 2a-2d) at 90-150km height regions of the lower thermosphere. Here we demonstrate the electron convergence/divergence processes under the influence of the east-north directed  $\varphi=307^\circ$  wind (middle panels),  $C(\varphi=307^\circ, z=z_c \approx 127km)=0$  and  $z_d \approx 112km$  (see Figure 1), as well as its opposite west-south directed wind  $\varphi=127^\circ$  (right panels),  $C(\varphi=127^\circ, z=z_d \approx 127km)=0$  and  $z_c \approx 112km$  (see Figure 1). In case of absence of wind ( $\mathbf{V}=0$ ), for  $t-t_o < 0.4h$ , changes in electron density  $N_e(z,t)/N_{om}$  are smaller due to ambipolar diffusion of ions (Figures 2b, 2c and 2d), while they are noticeable (Figure 2a) only at upper location of its layer ( $z_{om}=142km$ ). When  $z_{om}=z_c=z_b \approx 127km$  (where  $C=0, C' > 0$  and  $w_i=0$ ), electrons converge into higher density ( $N_{em}/N_{om} > 1$ ) thin layer (convergence instability), under the influence of east-north directed  $\varphi=307^\circ$  wind, occurring at  $z \approx 127km$  (Figure 2b e-n), which is expected from equation (9). When peak height of the initial electron density  $z_{om}$  is located above 127 km ( $z_{om}=142km$ ), where  $C(z > 127km) < 0$ , their convergence layer descends to  $z_c=z_b \approx 127km$  ( $C=0$ ). When  $z_{om}$  is located at IDDP  $z_d \approx 112km$  (Figure 2c), then the electron convergence layer for  $z > 112km$  moves upward ( $C < 0$ ) to the height region of  $z_c=z_b \approx 127km$ . However, when  $z_{om}$  is located below  $z_d \approx 112km$  ( $z_{om}=97km$ , Figure 2d), then their downward flux from divergence region and smaller values in ion ambipolar diffusion do not change its density significantly (Figure 2d e-n).

Divergence and convergence processes developed during the west-south directed wind,  $\varphi=127^\circ$  at the IDDP  $z_d(\varphi=127^\circ)=z_c(\varphi=307^\circ) \approx 127km$  ( $C=0$  and  $C' < 0$ ) and ICDP  $z_c(\varphi=127^\circ)=z_d(\varphi=307^\circ) \approx 112km$  ( $C > 0$  and  $C' > 0$ ) (see Figure 1) influence electron density behavior (Figure 2, right panels). In this case when  $z_{om} > 127km$  ( $z_{om}=142km$  -Figure 2a), the electron upstream flow is dominant,  $C(\varphi=127^\circ, z > 127km) < 0$  (see Figure 1), and its density decreases ( $N_{em}/N_{om} < 1$ , Figure 2a w-s). When  $z_{om}=127km$  (Figure 2b), a part of electron density initial layer ( $z > 127km$ ) vanishes by their upstream flow,  $C(\varphi=127^\circ, z > 127km) < 0$ , and ion ambipolar diffusion increases, but downward moving electrons for height of  $z < 127km$  is converged ( $N_{em}/N_{om} > 1$ ) at  $z_c \approx 112km$  and below (Figure 2b w-s). The development of electron convergence into thin dense layer ( $N_{em}/N_{om} > 1$ ), which probably move downward ( $C > 0$ ) to the region with  $C \rightarrow +0, C' \rightarrow +0$ , is more noticeable ( $N_{em}/N_{om} > 1.5$ ) for  $z_{om}=112km$ . The development of electrons convergence at  $z_c \approx 112km$  for its initial layer lower location of  $z_{om}=97km$  is less noticeable ( $N_{em}/N_{om} \approx 1$ ) in this case of  $V=50m/s$ .

## Electron density $N_e(h, t)/N_{om}$



**Figure 2.** The behavior of the normalized height profile of electron density  $N_e(h, t)/N_{om}$  in the mid-latitude lower thermosphere in case of absence of wind ( $V=0$ ) for its initial distribution peak height (a)  $z_{om} = 142\text{km}$ , (b)  $z_{om} = 127\text{km}$ , (c)  $z_{om} = 112\text{km}$  and (d)  $z_{om} = 97\text{km}$ , and during presence of horizontal wind with  $V=50\text{m/s}$  directed (a n-w), (b n-w), (c n-w), (d n-w) to east-northward ( $\varphi = 307^\circ$ ,  $z_{cE-N} = z_b$ ) and (a w-s), (b w-s), (c w-s), (d w-s) to west-southward ( $\varphi = 127^\circ$ ,  $z_{dW-S} = z_b$ ), respectively. Yellow and blue dashed lines correspond to the heights of ICDDPs:  $z_{cE-N}(\varphi = 307^\circ) \approx 127\text{km}$  and  $z_{cW-S}(\varphi = 127^\circ) \approx 112\text{km}$  and IDDDPs:  $z_{dE-N}(\varphi = 307^\circ) \approx 112\text{km}$  and  $z_{dW-S}(\varphi = 127^\circ) \approx 127\text{km}$ , respectively.

Figure 2 also shows the possibility of Es type layer formation and development of divergence processes of electrons density as well as in the lower thermosphere, under the influence of considered horizontal wind ( $V=50\text{m/s}$ ) for  $t-t_o < 0.4h$ , which agrees with its behavior described by equation (9). Relatively quick formation ( $\frac{\partial N_e}{\partial t} \propto C'V$ ) of high density Es type layer, its vertical motion ( $\frac{\partial z_m}{\partial t} \propto -CVa$ ) and tendency to saturation in its location, where  $C=0$  and  $C'>0$  or  $VC \rightarrow 0, VC' \rightarrow +0$ , should be more noticeable for greater values of the horizontal wind velocity.

We will consider electron density  $N_e(z,t)$  behavior for eight main directions of the horizontal wind ( $\mathbf{V}$ ): north ( $\varphi = 0^\circ, z_c \approx 121\text{km}$ ) north-west ( $\varphi = 45^\circ, z_c \approx 118\text{km}, z_d \approx 140\text{km}$ ), west ( $\varphi = 90^\circ, z_c \approx 116\text{km}, z_d \approx 131\text{km}$ ), west-south ( $\varphi = 135^\circ, z_c \approx 112\text{km}, z_d \approx 126\text{km}$ ), south ( $\varphi = 180^\circ, z_d \approx 121\text{km}$ ), south-east ( $\varphi = 225^\circ, z_c \approx 140\text{km}, z_d \approx 118\text{km}$ ), east ( $\varphi = 270^\circ, z_d \approx 116\text{km}, z_c \approx 131\text{km}$ ) and east-north ( $\varphi = 315^\circ, z_c \approx 126\text{km}, z_d \approx 112\text{km}$ ). For brevity the initial peak height of electron density is assumed at  $z_{om}=120\text{km}$ . For this case the most characteristics of the Es type layer formation and also its motion/localization to regions with  $C=0$  and  $C'>0$  or  $VC \rightarrow 0, VC' \rightarrow +0$ , should be revealed. In order to have more profound diffusive effect in formation of sporadic E, relatively narrow initial electron density layer with  $H_{ic} = 8\text{km}$  will be considered.

Figure 3 presents the behavior of the normalized electron density height profile  $N_e(h,t)/N_{om}$  in the mid-latitude lower thermosphere in case of horizontal wind with  $V=100\text{ m/s}$  directed to (**n**) north -  $\varphi=0^\circ$ , (**n-w**) north-west -  $\varphi=45^\circ$ , (**w**) west -  $\varphi=90^\circ$ , (**w-s**) west-south -  $\varphi=135^\circ$ , (**s**) south -  $\varphi=180^\circ$ , (**s-e**) south-east -  $\varphi=225^\circ$ , (**e**), east -  $\varphi=270^\circ$ , (**e-n**) east-north -  $\varphi=315^\circ$ . The ion distribution characteristic scale at initial time, equation (9), is  $H_{ic}(t=t_o) = 8\text{km}$ . Here for the Es type layers the peak densities (at  $z = z_m$  or  $h = h_m$ ) and thicknesses at  $t-t_o=1.5h$  are:  $N_e(z_m \approx 108\text{km}, \varphi = 0^\circ)/N_{om} \approx 5, H_{ic} \approx 1.58\text{km}$ ;  $N_e(z_m \approx 99\text{km}, \varphi = 45^\circ)/N_{om} \approx 6.2, H_{ic} \approx 1.26\text{km}$ ;  $N_e(z_m \approx 98\text{km}, \varphi = 90^\circ)/N_{om} \approx 6.5, H_{ic} \approx 1.25\text{km}$ ;  $N_e(z_m \approx 100\text{km}, \varphi = 135^\circ)/N_{om} \approx 3.7, H_{ic} \approx 1.6\text{km}$ ;  $N_e(z_m \approx 137\text{km}, t-t_o = 0.7h, \varphi = 270^\circ)/N_{om} = 1.2, H_{ic} = 5.6\text{km}$ ;  $N_e(z_m \approx 124\text{km}, \varphi = 315^\circ)/N_{om} \approx 4.3, H_{ic} \approx 1.5\text{km}$ .

Figure 3 shows that the formation of Es type dense ( $N_{me}(z, t-t_o = 1.5h)/N_{om} \approx 1.2-6.5$ ) thin ( $H_{ic} \approx 1.2-5.6\text{km}$ ) layer occurs under the influence of horizontal wind with velocity  $100\text{m/s}$  for its north (panel n), north-west (panel n-w), west (panel w), west-south (panel w-s) and east-north (panel e-n) directions. In cases of wind directions with  $\varphi = 0^\circ, \varphi = 45^\circ, \varphi = 90^\circ$  and  $\varphi = 135^\circ$ , the Es type layer descend ( $C>0$ ) to the regions with  $VC \rightarrow +0, VC' \rightarrow +0$  (Figure 1), where  $z_m(\varphi = 0^\circ) \approx 108\text{km}$ ,  $z_m(\varphi = 45^\circ) \approx 99\text{km}$ ,  $z_m(\varphi = 90^\circ) \approx 98\text{km}$  and  $z_m(\varphi = 135^\circ) \approx 100\text{km}$  (Figures 3n, 3n-w, 3w and 3w-s), while for east-north directed ( $\varphi = 315^\circ$ ) wind it is formed at

### Electron density $N_e(h, t)/N_{om}$

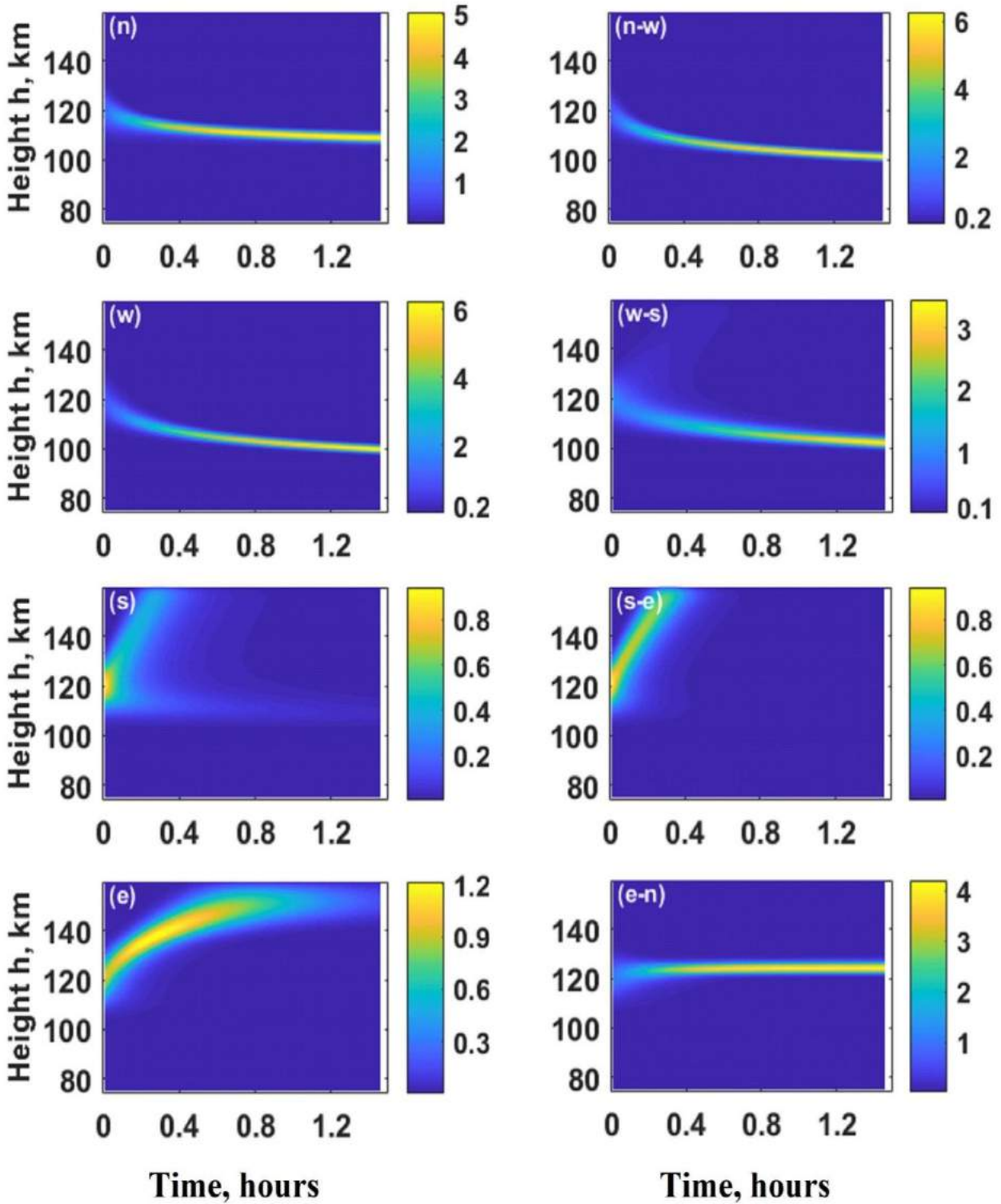


**Figure 3.** The behavior of the normalized electron density height profile  $N_e(h, t) / N_{om}$  in the mid-latitude lower thermosphere in case of horizontal wind with  $V=100$  m/s directed to **(n)** north -  $\varphi=0^\circ$ , **(n-w)** north-west -  $\varphi=45^\circ$ , **(w)** west -  $\varphi=90^\circ$ , **(w-s)** west-south -  $\varphi=135^\circ$ , **(s)** south -  $\varphi=180^\circ$ , **(s-e)** south-east -  $\varphi=225^\circ$ , **(e)**, east -  $\varphi=270^\circ$ , **(e-n)** east-north -  $\varphi=315^\circ$ .

$z_b(\varphi = 315^\circ) = z_m \approx 124km$ ,  $C(z = z_b) = 0$ . Here the lower location of the peak heights of Es type layer corresponds to the regions with  $C \rightarrow +0$  ( $w_i \rightarrow -0$ ),  $C' \rightarrow +0$  which occur at the lowest heights for westward wind (see Figure 1).

During the east-northward wind  $\varphi = 315^\circ$  the upward motion of Es type layer is also noticeable to its location at  $z_b \approx 124km$  (Figure 3e-n) for  $t-t_o < 1h$  (similar to the one shown in Figure 2c e-n). In this case the ion characteristic scale  $H_{ic}(t-t_o = 1h) \approx 1.3km$  corresponds to the minimal thickness of the Es layer, which is balanced by ambipolar diffusion of ions at  $z_b \approx 124km$  region, with about  $H_{ic} = (2D_a / VC')^{1/2}$ .

Figure 3e shows that during eastward wind ( $\varphi = 270^\circ$ ) with velocity  $V=100m/s$  the ions/electrons drift upward ( $CV < 0$ ) and the convergence layer ( $N_e(z = z_m, t-t_o = 0.7h, \varphi = 270^\circ) / N_{om} = 1.2, H_{ic} = 5.6km$ ) formed in upper heights ( $z_m \approx 137km$ ) is comparatively wider than the one in cases of other directions of wind noted above (Figures 3n, 3n-w, 3w and 3w-s) where their drift was downward ( $CV > 0$ ). The formed convergence layer for time of  $t-t_o > 0.8h$  vanishes ( $C' \rightarrow +0$ ,  $C \rightarrow -0$ ) to about 150km heights. In this case a decrease in  $C'$  at the upper heights is also accompanied with an increase of ambipolar diffusion displacement rate, which causes the convergence layer with  $H_{ic} \approx 5.6km$  to vanish at  $z > 137km$  ( $H_{ic} = (2D_a / VC')^{1/2}$ ). The formation of the Es type layer and its localization to the height regions with  $C=0$  ( $w_i = 0$ ) and  $C' > 0$ , or  $VC' \rightarrow +0$  and  $VC(z) \rightarrow 0$  ( $w_i \rightarrow 0$ ) are expectable relatively faster at greater horizontal wind velocity ( $V$ ).

Figure 4 presents the behavior of the normalized electron density height profile  $N_e(h,t) / N_{om}$  in the mid-latitude lower thermosphere in case of horizontal wind with  $V=150$  m/s directed to (n) north -  $\varphi=0$ , (n-w) north-west -  $\varphi=45^\circ$ , (w) west -  $\varphi=90^\circ$ , (w-s) west-south -  $\varphi=135^\circ$ , (s) south -  $\varphi=180^\circ$ , (s-e) south-east -  $\varphi=225^\circ$ , (e), east -  $\varphi=270^\circ$ , (e-n) east-north -  $\varphi=315^\circ$ . Here for the Es type layers the peak densities and thicknesses at  $t-t_o=1.5h$  are:

$$N_e(z_m \approx 108km, \varphi = 0) / N_{om} = 5.7, H_{ic} = 1.4km;$$

$$N_e(z_m \approx 97km, \varphi = 45^\circ) / N_{om} \approx 6.8, H_{ic} \approx 1.18km; \quad N_e(z_m \approx 95km, \varphi = 90^\circ) / N_{om} \approx 6.8, H_{ic} \approx 1.18km;$$

$$N_e(z_m \approx 98km, \varphi = 135^\circ) / N_{om} \approx 4.1, H_{ic} \approx 1.4km;$$

$$N_{em}(z_m = 143km, \varphi = 270^\circ) / N_{om} \approx 1.3, H_{ic} \approx 5.2km; \quad N_e(z = z_m, \varphi = 315^\circ) / N_{om} = 5.3, H_{ic} \approx 1.26km.$$

Figure 4 shows that the formation of Es type layer under the influence of horizontal wind with  $V=150m/s$  occurs similarly but faster for its north (Figure 4n), north-west (Figure 4n-w), west (Figure 4w), west-south (Figure 4w-s) and east-north (Figure 4e-n) directions, than for wind velocity  $V=100m/s$  (Figure 3). The rates of formation and descend to the regions with  $VC(z) \rightarrow +0, VC' \rightarrow +0$  [ $z_m(\varphi = 0) \approx 108km$ ,  $z_m(\varphi = 45^\circ) \approx 97km$ ,  $z_m(\varphi = 90^\circ) \approx 95km$  and

## Electron density $N_e(h, t)/N_{om}$

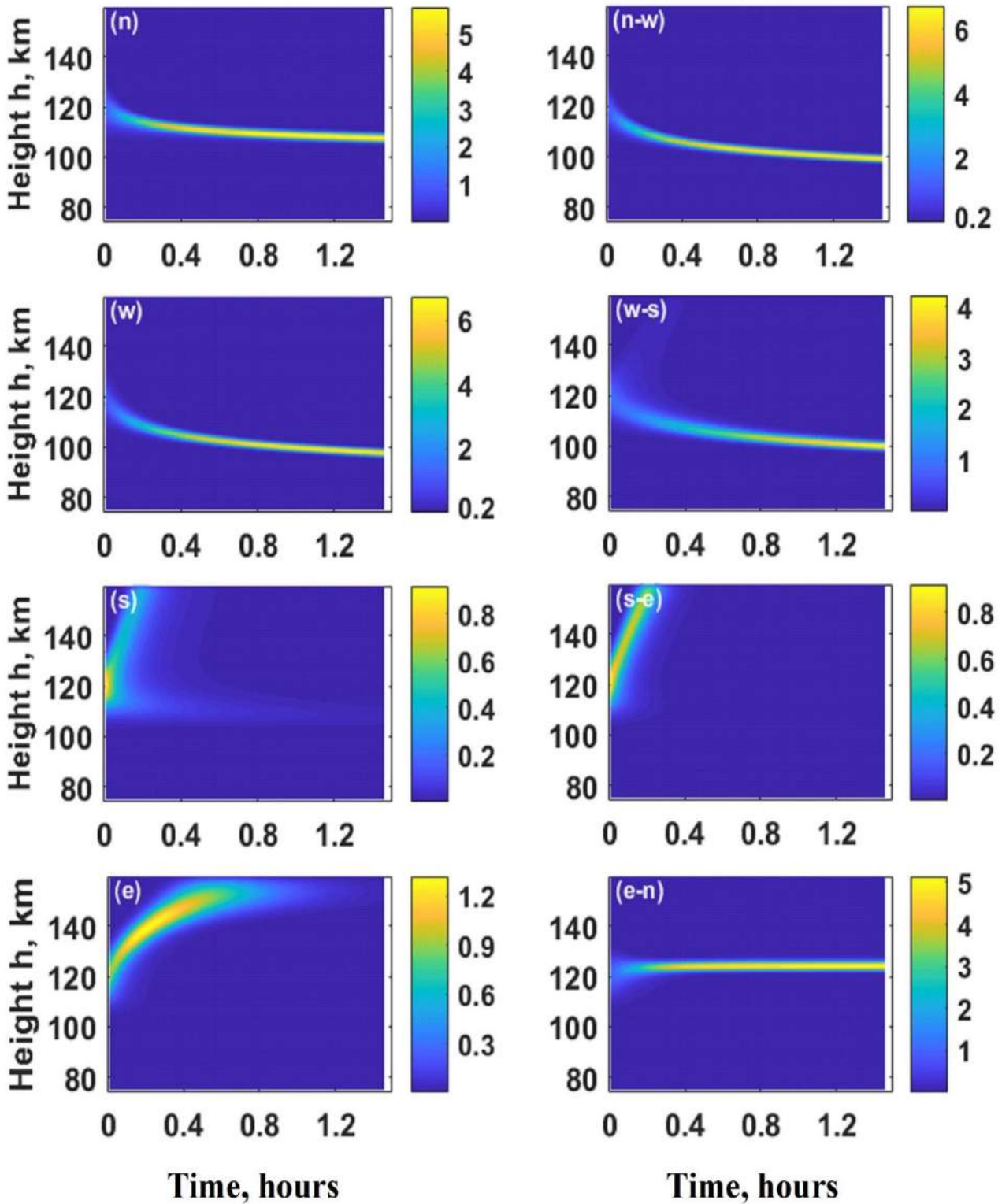


**Figure 4.** Same as Figure 3 but for the horizontal wind velocity  $V=150\text{ m/s}$  are applied. than those for the same directions of the wind velocity  $V=100\text{ m/s}$  (see Figure 3 ). In these cases 1.5-time increase rate in electron densities is accompanied by about 1.5-time decrease in time of their descent to their final location to the regions with  $VC(z) \rightarrow +0$ ,  $VC' \rightarrow +0$ , where changes in their relatively small increased peak density and descent (than that of the for  $V=100\text{ m/s}$ ) vanish.

$z_m(\varphi=135^\circ) \approx 98km$ ] of comparatively high density ( $N_{me}(z, t-t_o=1.5h)/N_{om} \approx 1.3-6.8$ ) and thin Es layers ( $H_{ic} \approx 0.9-5.2km$ ) are about 1.5 times greater ( $\frac{\partial N_e}{\partial t} \propto C'V$ ,  $\frac{\partial z_m}{\partial t} \propto -CV$ ).

Note that small increase in Es type layer density in these locations at the bottom of the lower thermosphere can also be balanced or reduced by its decrease due to ion/electron recombination  $\propto N_e^2$  [16, 26]. The latter can be included in equation (6) and correspondingly in the suggested theoretical model simulations.

Relatively big increase in the peak electron density occurs during increase in the east-north directed ( $\varphi=315^\circ$ ) wind (Figure 4e-n). In this case 1.5-time increase in the wind velocity causes about 1.5 times quicker localization of the convergence layer to the region  $z_b \approx 124km, C(z \approx 124km, \varphi=315^\circ)=0$ , where its peak density increases (about  $\propto \sqrt{V}$ ) and corresponding thickness (about  $H_{ic} \propto 1/\sqrt{V}$ ) is smaller (Figure 3e-n and Figure 4e-n). For the greater values in opposite west-south directed ( $\varphi=135^\circ$ ) wind velocity  $V=150m/s$ , the electrons downstream flow is more noticeable ( $C>0$ ) from IDDP  $z_d(\varphi=135^\circ) \approx 126km$ , which converges into Es type layer below ICDP  $z_c(\varphi=135^\circ) \approx 112km$ , at height  $z_m(\varphi=135^\circ) = 98km$  where  $VC(z) \rightarrow +0$  ( $w_i \rightarrow -0$ ),  $VC' \rightarrow +0$ .

Figure 4e shows that increase in the eastward wind velocity up to 150m/s correspondingly increases the charge particles vertical flow and high ambipolar diffusion in the upper heights gives less value in ion/electron convergence layer density  $N_{em}(z_m \approx 143km, \varphi=270^\circ)/N_{om} \approx 1.3$  ( $H_{ic} \approx 5.2km$ ) with  $z_m(\varphi=270^\circ) \approx 139km$  formed in relatively short time ( $\propto 1/V$ ), than in the case of smaller  $V=100m/s$  (Figure 3e). In this case the time of electron convergence layer existence is also shorter than that for smaller horizontal wind velocity (Figure 3). During greater horizontal wind velocity the electron convergence rate ( $C'V>0$ ) and their vertical drift ( $CV<0$ ) to the upper regions where  $C'V < 2D_a/H_{ic}^2$ , equation (9),  $C' \rightarrow 0$  and  $C \rightarrow -0$  causes relatively quick damping of its convergence layer than during  $V=100m/s$  (Figure 3e).

In case of wind direction  $270^\circ < \varphi < 285^\circ$  the ion/electron convergence layer formation above 140 km with  $H_{ic} \approx (2D_a/C'V)^{0.5}$  is similar to the one demonstrated on Figure 4e. The Es type layer formation and localization at height about 115-140km, where  $C=0$ , occur similarly to those shown in Figure 4 E-N during the other east-west directed wind (e.g., for wind direction with  $\varphi=285^\circ$ ,  $\varphi=325^\circ$  and  $\varphi=345^\circ$ , is demonstrated on Figure S1). In this high region, in addition to wind velocity, the Es layer peak density also increases with decrease ( $\propto 1/\sqrt{D_a}$ ) in ion ambipolar diffusion coefficients.

Figures 4s and 4s-e also show that the divergence of ion/electron from  $z_d(\varphi=180^\circ) \approx 121km$  and  $z_c(\varphi=255^\circ) \approx 140km$  regions happens faster under the influence of greater winds ( $V=150m/s$ ) directed to south and south-east, than in case of its relatively smaller value of  $V=100m/s$ . In the presented simulation, the structural data of the lower thermosphere are used from NRLMSISE-00 model, for midlatitude  $45^\circ \pm 2^\circ N$ ,  $45^\circ \pm 2^\circ E$  and  $I=6I^\circ \pm 2^\circ$  regions in spring of 1998, between Solar maximum and minimum phases. Similarly, the results are extendable for other mid-latitude regions of the northern or southern hemispheres, for various directions and values of the horizontal wind.

So, we have shown theoretically and correspondingly numerically, that in the main observable heights of about 95-150km [4, 5] of the mid-latitude lower thermosphere the formation of sporadic E is possible during homogeneous horizontal wind. Besides Es layer formation in this region, its other observable features are also revealed.

The formation of Es type layer is expected more frequently during dominance of northward or westward components of the wind velocity ( $C>0$ ) at heights below 120 km (Figures 3 and 4), which is the observed phenomenon [5]. The descent of the Es type layer, which is an observable phenomenon [3, 4, 5],

occurs in most cases of its formation under the influence of horizontal homogeneous wind, equation (9), (Figures 3n-3w-s and Figures 4n-4w-s). In these cases an increase in the electron density in the regions of 95km-110km also can cause higher loss rate of the molecular ion (e.g., NO+) [26], and the long-lived metallic ions become dominant, which is also observed [27, 28]. In the framework of suggested theory seasonal variations in Es layers occurrence are expectable [3, 5, 8, 29] determined by ion/electron density changes, as well as its regional peculiarities caused by geomagnetic declination changes and wind field variations for given midlatitude regions.

Note that for higher wind velocities, which are observable mostly at 100km-120km heights [24], they should have some vertical components [30], which also influences ion vertical drift velocity [16, 17]. In this case, in addition to northward or/and westward wind component, its downward component can cause ions additional downward flux and correspondingly Es layer shift to the bottom of the lower thermosphere at 90-100km height regions, which can be developed in the framework of the suggested theory. Since the Es layers could be formed by zonal or northward component of wind velocity, they could be observed more frequently at mid-latitudes, than in equatorial ( $I \approx 0$ ) and polar ( $I \approx 90^\circ$ ) regions (3-5).

So, according to the presented theoretical mechanism, many observational properties of the mid-latitude Es layer formation and location can be determined by horizontal wind direction and value. This mechanism does not exclude the additional influence of wind with vertical ( $\partial V/\partial z \neq 0$ ) or horizontal shear on ion convergence and formation of sporadic E [17, 31, 32, 33]. In the lower thermosphere the horizontal wind velocity  $\mathbf{V}$  can be determined by the sum  $\mathbf{V} = \mathbf{V}_0 + \mathbf{V}_w(\mathbf{z}, \mathbf{t})$ , where  $\mathbf{V}_0$  is homogeneous velocity and  $\mathbf{V}_w(\mathbf{z}, \mathbf{t})$  is varying perturbation caused by atmospheric waves, tidal motion or shear instability [5, 15, 17]. Here atmospheric waves or tidal wind, in addition to background horizontal wind ( $\mathbf{V}_0$ ), could also lead the ion/electron additional convergence (when  $C \partial V/\partial z = C \partial V_n/\partial z > 0$ ) or divergence (when  $C \partial V/\partial z = C \partial V_n/\partial z < 0$ ) in the regions of polarization changes of perturbed velocity  $\mathbf{V}_w(\mathbf{z}, \mathbf{t})$ . Wave induced convergence/divergence processes of charge particles could amplify or weaken the ones caused by background horizontal wind ( $\mathbf{V}_0$ ). Such wave induced convergence of charged particles ( $\propto C \frac{\partial V_w}{\partial z}$ ), equation (6), for vertical wavelength about 20-60km and with amplitude of about 50-100m/s, could be of the same order as the convergence caused by homogeneous horizontal wind ( $\propto C V_0$ ) with velocity 50-150m/s at the ICDP (Figure 1). Depending on the wavelength and amplitude of perturbed wind velocity, the additional convergence of ions at height regions, where it changes the polarization, and formation of multi-layered sporadic E are also possible [17]. In these cases, it is also important to take into account the influence of neutrals wind velocity direction and vertical changes of ions drift velocity, like the one in the presented theoretical model for homogeneous wind, and makes more predictable the behavior of ion/electron density in the lower thermosphere, thus the formation of sporadic E, its dynamics and location region [9, 10].

#### 4. Conclusions

Theoretically and by corresponding numerical simulations it has been shown that the formation and localization of sporadic E (Es) layer in its mainly observable mid-latitude lower thermosphere heights of about 95-150km can be determined by homogeneous horizontal wind velocity direction and value. In this theory, differently from 'windshear' theory, the wind direction and value, in addition to geomagnetic field and vertically changing ion-neutral collision frequency, determine the minimal negative value of the heavy metallic ions (Fe+) drift velocity divergence, which in turn causes ion convergence into Es type horizontal thin layer. In the upper heights of the lower thermosphere, the Es layer peak density and thickness, in addition to the wind direction and values, are also controlled by ambipolar diffusion. Here, the decrease of the ambipolar diffusion coefficient produces increase of the Es layer density caused by horizontal wind.

It has been shown that in the lower thermosphere of the northern hemisphere, the Es layer caused by horizontal homogeneous wind can be located at height regions where (1) the ions vertical drift velocity is zero and its divergence is negative (east-northward wind), (2) the ions drift downward (northward and westward wind), which occurs more frequently, or (3) the ions drift upward (eastward wind), and their

negative divergences vanish, and (4) in the case of dominance of southward wind the divergence of ion drift velocity is positive consequently ion density divergence occurs and Es type layer formation is not expectable. These ion/electron convergence/divergence processes faster for greater values in the horizontal homogeneous wind. In this case the speed of Es layer vertical motion to its expectable location is also faster for greater values of the horizontal wind velocity.

The importance and possibility of development of the suggested theory of sporadic E layer formation in case of horizontal wind with vertical shear has been noted.

**Acknowledgements:** This study is supported by Georgian Shota Rustaveli National Science Foundation Grant no. FR17-357.

## References

- [1] Whitehead J. D. J. *Atmos. Terr. Phys.*, 1960, v.51, pp. 20-49 .
- [2] Axford W. I. J. *Geophys. Res.*, 1963, v.68, pp. 769-779.
- [3] Whitehead J. D. J. *Atmos. Terr. Phys.*, 1989, v.51, pp. 401-424.
- [4] Mathews J.D. J. *Atmos. Sol.-Terr. Phys.*, 1998, v.60, pp. 413-435.
- [5] Haldoupis C. *Space Sci. Rev.*, 2012, v.168, pp. 441–461, DOI 10.1007/s11214-011-9786-8.
- [6] Bishop R. L., et al. *J. Geophys. Res.*, 2005, v.110, (A04309 ), doi:10.1029/2004JA010686.
- [7] Yeh W.-H., J.-Y. Liu, C.-Y. Huang and S.-P. Chen. *J. Geophys.Res. Atmos.*, 2014, v.119, pp. 4568–4579, doi:10.1002/2013JD020798
- [8] Liu, Y. et al. *Adv. Space Res.*, 2018, v.62, pp. 426–439, doi.org/10.1016/j.asr.2018.04.026.
- [9] Didebulidze G.G., Dalakishvili G., Todua M. AGU Fall meeting 2019, SA21B-3100.
- [10] Dalakishvili G., Didebulidze G.G., Todua M. *LPMR2019\_Abstractbook*, 2019, pp. 10.
- [11] Nygrén, T., Jalonen L., Oksman J., Turunen T. *J. Atmos. Terr. Phys.*, 1984, v.46(4), pp. 373-381.
- [12] Haldoupis C., Pancheva D. *J. Geophys. Res.*, 2002, v.107, doi:10.1029/2001JA000212.
- [13] Didebulidze G.G., Lomidze L. *Ann. Geophys.* 2008, v.26, pp. 1741-1749..
- [14] Didebulidze G. G., Lomidze L.N., *Phys. Lett. A*, 2010, v.374, pp. 952-959, doi:10.1016/j.physleta.2009.12.026.
- [15] Hysell D. L., Munk J., McCarrick M. *Geophys.Res. Lett.*, 2014, v.41, pp. 6987–6993, doi:10.1002/2014GL061691.
- [16] Yokoyama T., Yamamoto M., Fukao S. *J. Geophys. Res.*, 2003, v.108(A2), 1054, doi:10.1029/2002JA009513.
- [17] Didebulidze G.G., Dalakishvili G., Lomidze L., Matiashvili G. *J. Atmos. Sol.-Terr. Phys.*, 2015, v.136, pp. 163-173, <http://dx.doi.org/10.1016/j.jastp.2015.09.012>
- [18] Banks P.M., Kockarts G. *Aeronomy*. 1973, Part A, Academic, New York.
- [19] Picone J. M., Hedin A.E., Drob D.P., Aikin A.C. *J. Geophys. Res.*, 2002, v.107(A12), 1468, doi.org/10.1029/2002JA009430.
- [20] Du Fort E. C., Frankel S. P. *MTAC*. 1953, v.7, pp. 135-152.
- [21] Lanser D., Verwer G. J. *J. Com.Appl. Math.*, 1999, v.111, pp. 201-216.
- [22] Hundsdorfer W., and G. J., pp. 325-417, Springer-Verlag Berlin Heidelberg.
- [23] Portnyagin Y. I., Solovjova T. V. *Ann. Geophys.*, 2000, v.18, pp. 300-315, doi:10.1029/2002JA009513.
- [24] Larsen M.F. *J. Geophys. Res.*, 2002, v.107 (A8), 1215, doi:10.1029/2001JA000218.
- [25] Drob D. P., et al. *J. Geophys. Res.*, 2008, v.113, A12304, doi:10.1029/2008JA013668.
- [26] Lin Y.C., Chu Y.H. *J. Geophys. Res. Space Phys.*, 2017, v.122, pp. 2505–2529, doi:10.1002/2016JA022855.
- [27] Kopp E. *J. Geophys. Res.*, 1997, v.102 (A5), pp. 9667-9674.
- [28] Roddy P. A., et al. *J. Geophys. Res.*, 2007, v.112, A06312, doi:10.1029/2006JA011713.
- [29] Pietrella M., Pezzopane M., Bianchi C. *Adv. Space Res.*, 2014, v.54, pp. 150–160.
- [30] Hysell D. L., Larsen M. F., Sulzer M. P. *J. Geophys.Res. Space Phys.*, 2014, v. 119, pp. 2345–2358, doi:10.1002/2013JA019621.
- [31] Chimonas G. *J. Geophys. Res.* 1971, v.76, pp. 4578-4586.
- [32] Shalimov S., Haldoupis C., Voiculescu M., Schlegel K. *J. Geophys. Res.*, 1999, v.104, 28207.
- [33] Shalimov S., Haldoupis C. *Ann. Geophys.*, 2002, v. 20, pp. 1193–1201.

# სპორადული E (Es) ფენის ფორმირება ერთგვაროვანი ჰორიზონტალური ქარის მიერ

გ. დალაქიშვილი, გ. დიდებუღიძე, მ. თოდუა

## რეზიუმე

თეორიული და შესაბამისი რიცხვითი გამოთვლებით ნაჩვენებია, რომ დედამიწის საშუალო განედების ატმოსფეროს ქვედა თერმოსფეროში სპორადული E (Es) ფენის ფორმირება და ლოკალიზაცია შესაძლებელია განსაზღვროს ერთგვაროვანი ქარის სიჩქარის მიმართულებით და სიდიდით. "ქარის წანაცვლების" (windshear theory) თეორიისაგან განსხვავებით, შემოთავაზებულ თეორიაში ქარის სიდიდე და მიმართულება, გეომანტურ ველთან და სიმაღლის მიხედვით ცვლად იონ-ნეიტრალების დაჯახების სიხშირესთან ერთად, განსაზღვრავს მძიმე მეტალური იონების (Fe<sup>+</sup>) დრეიფის სიჩქარის დივერგენციის მინიმალურ უარყოფითი მნიშვნელობას, რომელიც, თავის მხრივ, იწვევს იონების მაღალი სიმკვრივის Es ტიპის ვიწრო ფენად კონვერგენციას. ქვედა თერმოსფეროს ზედა სიმაღლეებისთვის Es ფენის პიკის სიმაღლე ასევე კონტროლდება იონების ამბიპოლარული დიფუზიით.

ჩრდილოეთის ნახევარსფეროს ქვედა თერმოსფეროში ჰორიზონტალური ერთგვაროვანი ქარით გამოწვეული Es ფენა შესაძლებელია ლოკალიზდეს რეგიონებში სადაც (1) იონების დრეიფის სიჩქარე ნულია და მისი დივერგენცია უარყოფითია (აღმოსავლეთ-ჩრდილოეთის ქარი), (2) იონები დრეიფობენ ქვემოთ (ჩრდილოეთის და დასავლეთის ქარი), რომელიც უფრო ხშირია, ან (3) იონები დრეიფობენ ზემოთ და მათი უარყოფითი დივერგენცია ქრება და (4) სამხრეთის ქარის დომინირებისას იონების დრეიფის სიჩქარის დივერგენცია დადებითია, შესაბამისად, ადგილი აქვს მათი სიმკვრივის დივერგენციას და Es ტიპის ფენის ფორმირება არაა მოსალოდნელი. ქარის სიჩქარის დიდი მნიშვნელობებისთვის უფრო სწრაფია Es ფენის ფორმირება და ლოკაცია რეგიონებში, სადაც დრეიფის სიჩქარე ნულია ან ქრება. შენიშნულია შემოთავაზებული თეორიის გამოყენება ვერტიკალურად არაერთგვაროვანი ქარისთვის.

## Формирование спорадического E (Es) слоя под воздействием однородного горизонтального ветра

Г.Т. Далакишвили, Г.Г. Дидебулидзе, М.М. Тодуа

### Резюме

Теоретически, а также соответствующим численным моделированием показано, что образование и локализация спорадического E (Es) слоя в среднширотной нижней термосфере Земли (где они в основном наблюдаемы) возможно определить с помощью величины и направления горизонтального ветра. В предложенной теории, в отличие от теории "ветрового сдвига" (windshear theory), в дополнении к геомагнитному полю и вертикально меняющейся частоте столкновения ионов с нейтральными частицами, направление и величина горизонтального ветра определяют минимальное отрицательное значение дивергенции скорости дрейфа тяжелых металлических ионов (Fe<sup>+</sup>), что, в свою очередь, вызывает их конвергенцию в горизонтальный узкий и плотный Es слой. В этом случае, в верхних высотах низкой термосферы высота максимальной плотности Es слоя также контролируется амбиполярной диффузией.

В нижней термосфере северного полушария, Es слой, возникший под воздействием однородного горизонтального ветра, локализуется в регионах, где (1) скорость вертикального дрейфа ионов равна нулю (восточно-северный ветер), (2) ионы дрейфуют ниже (северный и западный ветры), что бывает более часто, или (3) ионы дрейфуют вверх (восточный ветер) и их отрицательная дивергенция исчезает и (4) в случае превосходства южного ветра, дивергенция дрейфа скорости положительна и формирование Es слоя не ожидается. Формирование Es слоя и его локализация в ожидаемом регионе происходит быстрее для больших скоростей ветра. Отмечена возможность применения предлагаемой теории для вертикального неоднородного ветра.

## Numerical Modelling of Dust Propagation in the Atmosphere of Tbilisi City: The Case of Background Eastern Gentle Breeze

<sup>1</sup>Vepkhia G. Kukhalashvili, <sup>2</sup>George I. Kordzakhia, <sup>2</sup>Natia G. Gigauri,  
<sup>1,2</sup>Aleksandre A. Surmava, <sup>2</sup>Liana N. Intskirveli

<sup>1</sup>M. Nodia Institute of Geophysics at the Iv. Javakishvili Tbilisi State University,  
1, M. Aleksidze Str., 0160, Tbilisi, Georgia, e-mail: aasurmava@yahoo.com

<sup>2</sup>Institute of Hydrometeorology at the Georgian Technical University, 150-a D. Agmashenebeli Ave,  
0112 Tbilisi, Georgia, E-mail: intskirvelebi2@yahoo.com

### ABSTRACT

Dust propagation at the territory of Tbilisi is studied using the 3D regional model of atmospheric processes evolution and integration of the equation of contaminant transfer-diffusion. The dust pollution process that takes place in case of background eastern gentle breeze is numerically modeled. It is obtained that micro-scale dust propagation substantially depends on the terrain of city and its surrounding territories, on the magnitude and direction of background wind velocity. Dust dispersed in Tbilisi is mainly concentrated in the lower 600 m thick atmospheric boundary layer. At 2 m height over a ground maximum concentration 1.0-1.5 maximum allowable concentration (MAC = 0.5 mg/m<sup>3</sup>) is formed in the time interval from 12 a.m. to 9 p.m. in the central and southern parts of the city as well as at relatively low-lying territories. Peculiarities of dust vertical distribution and time variation are studied.

**Keywords:** Numerical modeling, pollution source, diffusion, dust propagation, wind.

### Introduction.

The research goal is to study via numerical modeling Tbilisi atmospheric air pollution by dust in case of background eastern gentle wind. Dust propagation at Tbilisi city territory is simulated using the 3D regional model of evolution of atmospheric processes in the Caucasus and integration of the equation of admixtures transfer-diffusion [1, 2]. Motor transport is a source of dust pollution. It is assumed that the quantity of dust dispersed in the atmosphere linearly depends on traffic intensity. The magnitude of background eastern gentle breeze at 100 m height from earth surface (upper boundary of surface layer of atmosphere) equals to 5 m/sec and linearly increases up to 23 m/sec at 9 km altitude above sea level. Time and space variation of meteorological fields that are necessary for modeling are calculated by the numerical model described in [1, 2]. Meteorological situation corresponds to dry weather of June, when relative atmospheric humidity is 50%. Calculations are made along parallel and meridian with 300 and 400 m horizontal steps. Vertical step in the free atmosphere varies in time and equals 300 m in average. In 100 m thick surface layer of the atmosphere a vertical step varies from 2 to 15 m. Tbilisi city having complex terrain is disposed in the center of modeling area.

### Modeling results

Spatial distribution of dust concentration and wind velocity obtained via calculation at 2, 100 and 600 m height over a ground at t = 0, 3 and 6 h of the first day is shown in Fig. 1. Concentration is given in units of maximum allowable concentration (MAC = 0.5 mg/m<sup>3</sup>). It is seen from Fig. 1 that at 2 m height from underlying surface the maximum value of dust concentration, 0.5-0.7 MAC is obtained in the south-western part of the city, at low-lying territory of Ponichala in the shape of a narrow and long band, and in the Tbilisi Sea surroundings. At the rest territory a concentration value is within a limit of 0.001-0.3 MPC. The area of maximum pollution extends with height increase. At 100 m height concentration of 0.5-0.7 MPC is formed in three parts of the city. Above the surface layer of atmosphere dust concentration is getting smaller. Its value is within 0.1-0.3 MAC at 600 m height over a ground.

Starting with  $t = 0$  h city air pollution gradually decreases and becomes minimal at 6.00 a.m. At this time a concentration value varies within a range of 0.001-0.3 MAC in the city and its surrounding territories.

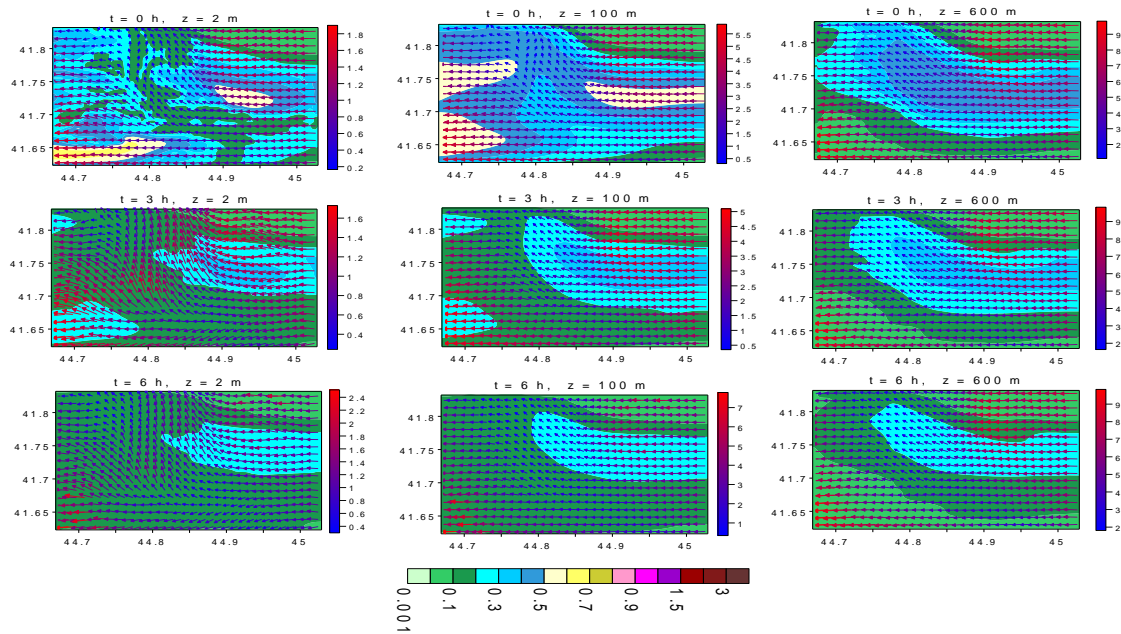


Fig. 1. Wind velocity (m/sec) and dust concentration (MAC) distribution, when  $t = 0, 3$  and  $6$  h at  $2, 100$  and  $600$  m height over a ground

After  $t = 6.00$  h, along with vehicular traffic intensity growth the dust pollution of city atmosphere starts to increase in the vicinity of pollution sources – along the city mains and nearby (Fig. 2). When  $t = 9$  h dust concentration at  $z = 2$  m height is especially high in the mains crossing areas and low-lying territories. Vake, Saburtalo, Gldani, TEMKA and Ortachala are among these districts. Concentration values reach 1 MAC in these areas.

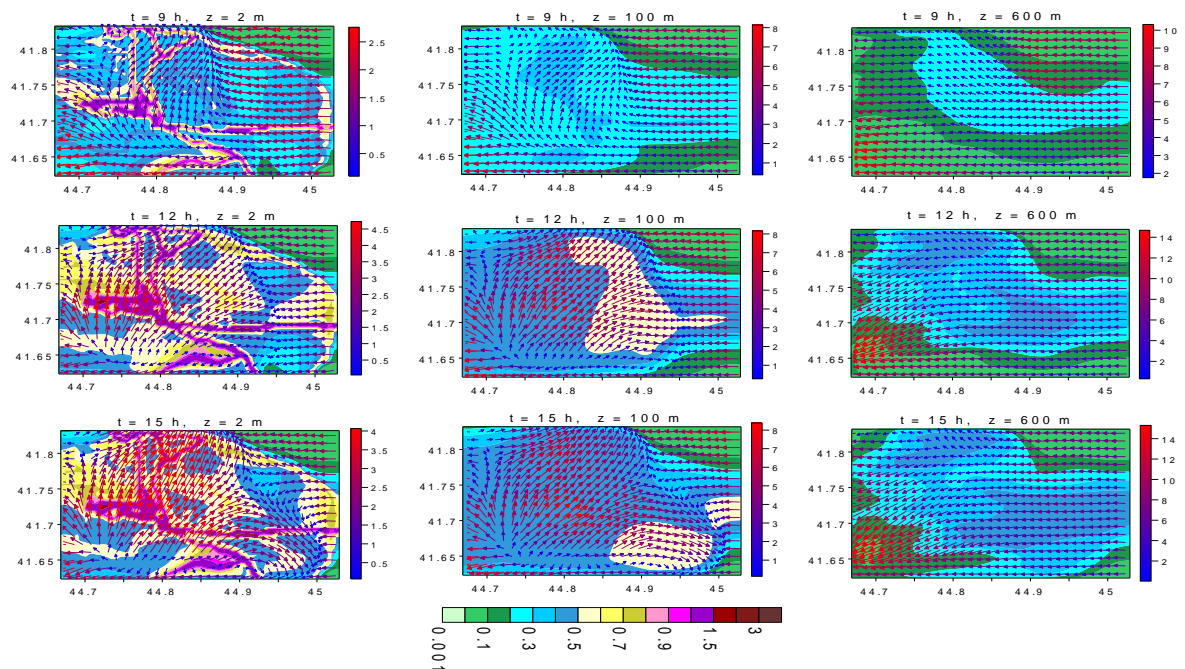


Fig. 2. Wind velocity (m/sec) and dust concentration (MAC) distribution, when  $t = 9, 12$  and  $15$  h at  $2, 100$  and  $600$  m height over a ground

Maximum dust pollution level is obtained in the time period from  $t = 12.00$  H to  $21.00$  h. Heavy pollution zones include the center of city, Vake, Saburtalo and Ortachala. Concentration varies within a limit of 1.0-1.5 MAC at these territories. In the urban parts distanced from city mains, dust concentration varies within a range of 0.5-0.7 MAC. As for recreational and unsettled territories, where we have no dust pollution sources, pollution occurs according to the mechanism of advective and diffusive transfer. As a result, a ground level concentration varies from 0.3 to 0.5 MAC.

At  $t = 9.00$  h an intense vertical convective transfer of the dust begins, due to which a dust originated near the ground starts to propagate towards upper layers, and when  $t = 12.00$  h, dust concentration reaches 0.7 MAC at 100 m height.

From  $t = 18.00$  to  $21.00$ h there takes place a slight increase of dust concentration and change of size and location of heavily polluted areas at 2 m height. This change is caused by wind velocity daily evolution in the surface layer of atmosphere (Fig. 3). The area of high concentration zone is increased in the center of southern part of the city, at the territories adjacent to Ponichala, and in the vicinity of Rustavi and Marneuli highways. Concentration is decreased in the central and northern parts close to Georgian Military Road and Gldani main.

In the time period from  $t = 15.00$  to  $21.00$ h a vertical turbulent and convective diffusion of the dust becomes especially high. As a result, concentration magnitude reaches 0.9-1.2 MAC at 100 m height above the major part of the city. At 600 m height a concentration reaches 0.6 MAC. After  $t = 21.00$  h a sharp decrease of concentration takes place. When  $t = 24.00$  h, a spatial distribution of concentration is similar to distribution obtained early in the day.

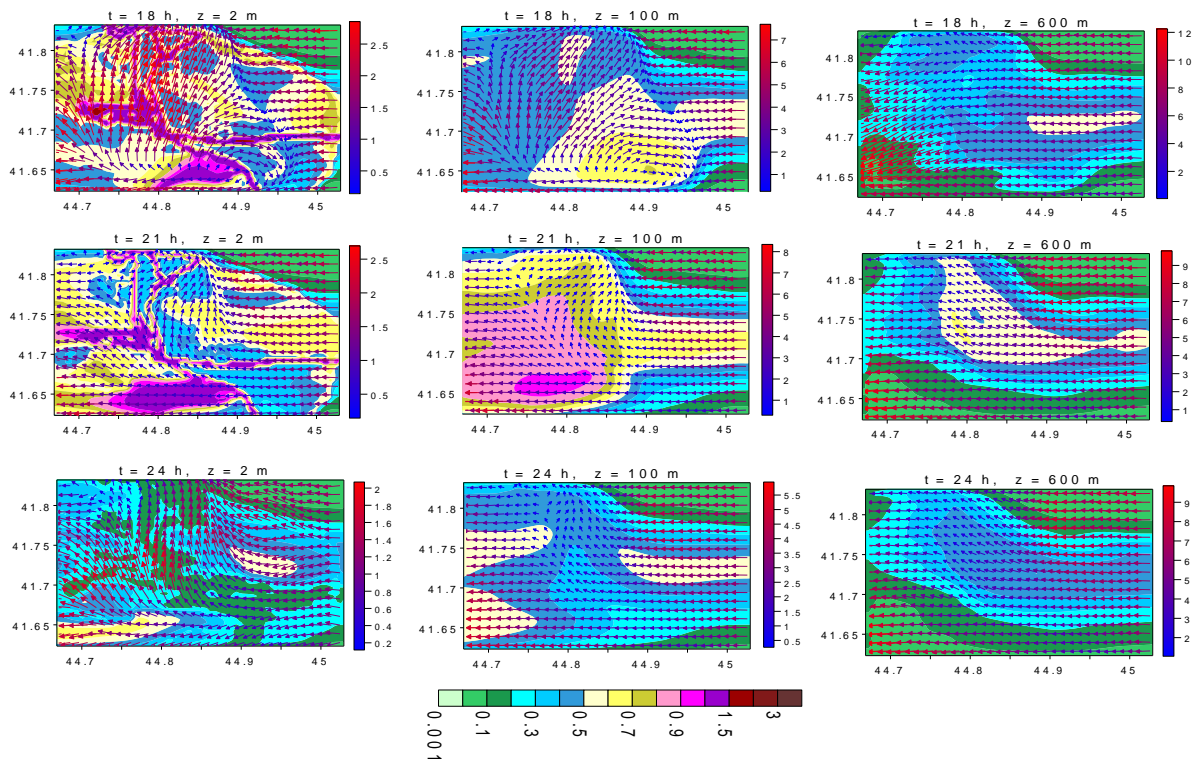


Fig. 3. Wind velocity (m/sec) and dust concentration (MAC) distribution, when  $t = 18, 21$  and  $24$  h at 2, 100 and 600 m height over a ground

In Fig. 4 there is shown a vertical distribution of dust concentration in three vertical sections drawn along the parallel in the surface layer of atmosphere, latitudes of which are  $41.69^\circ$  N,  $41.72^\circ$  N,  $41.77^\circ$  N. It is seen from the Figure that the vertical distribution of concentration varies during a day in all three sections. From  $t = 0.00$  to  $6.00$  h a dust concentration reduction takes place in the ground-level layer. This decrease is caused by termination of dust pollution process and dust transfer from modeling area to the outside.

The process of dust vertical diffusion that is caused by diurnal convective motion of heated air existing near a ground, becomes intense. Air flow catches dust particles. Transfer occurs by means of separate convective cells having different sizes and shape due to orography. As a consequence we have a situation, during which the dust concentration transferred to the upper 50 m area of surface layer of atmosphere exceeds the dust concentration remained in the lower 50 m area.

From  $t=6.00$  to  $12.00$  h, the quantity of dispersed dust increases along with vehicular traffic intensification and, respectively, atmosphere pollution in the lower part of the surface layer nearby traffic arteries is getting higher.

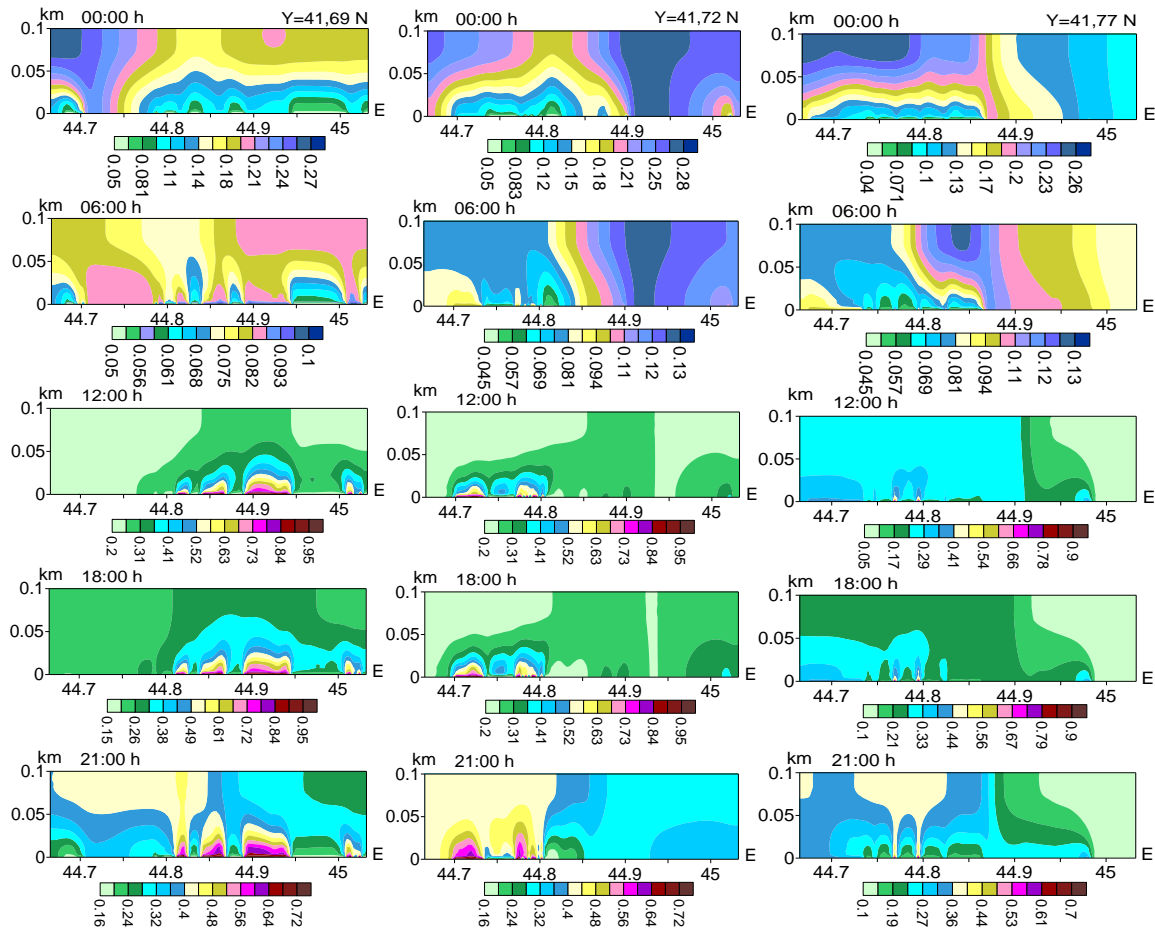


Fig. 4. Dust concentration vertical distribution (MPC) in three vertical sections ( $41.69^{\circ}$  N,  $41.72^{\circ}$  N,  $41.77^{\circ}$  N) drawn along the parallel in the surface layer of atmosphere

By  $t = 12$  h a dust cloud similar to a ground-level wide thermal is formed in the lower part of atmospheric boundary layer, in some areas of the city. This cloud gradually increases in size and creates high concentration areas. From this period the concentration in 50 m thick lower layer of the atmosphere exceeds the concentration existing in upper 50 m layer. The areas maximally polluted according both geometrical dimension and concentration, create in  $t=18.00-21.00$  h time interval. After  $t = 21.00$  h, due to vertical advective and diffusive transfer, dust concentration starts to decrease nearby earth surface and to increase in its upper part.

### Conclusion

The kinematics of dust change created by motor transport at Tbilisi territory and daily pattern of its spatial distribution are studied in case of background eastern gentle breeze. Via analysis of wind velocity and concentration fields it is obtained that spatial distribution of heavily polluted areas depends on city mains disposition, and local circulation systems formed under dynamic impact of terrain and diurnal change of thermal regime on the underlying surface. Maximum concentration 1.0-1.5 MAC is formed in  $t = 12.00-$

21.00 h time interval in the central, southern and relatively low-lying territories of the city. At 600 m height from earth surface a maximum value of concentration reaches 0.7 MAC, when  $t = 21.00$  h.

**Acknowledgment.** The study is carried out under financial support of Shota Rustaveli National Science Foundation of Georgia [FR-18-3667].

## References

- [1] Surmava A., Intskirveli L., Kukhalashvili V., Gigauri N.. Numerical Investigation of Meso- and Microscale Diffusion of Tbilisi Dust. Annals of Agrarian Science, 18, No. 3, 2020 (In print).  
[2] Gigauri N.G., Gverdsiteli L.V., Surmava A.A., Intskirveli L.N. Numerical Simulation of Industrial Dust Distribution in the Territory of Zestafoni, Georgia. WIT Transaction on Ecology and Environment, 230, 2018, pp. 119-128. Doi:10.2495/AIR1180111.

## ქ.თბილისის ატმოსფეროში მტვრის გავრცელების რიცხვითი მოდელირება: აღმოსავლეთის ფონური საშუალო სიჩქარის ქარის შემთხვევა

ვ. კუხალაშვილი, გ. კორძახია, ნ. გიგაური, ა. სურმავა, ლ. ინჭკირველი

### რეზიუმე

ატმოსფერული პროცესების ევოლუციის 3D რეგიონალური მოდელისა და მინარევების გადატანა-დიფუზიის განტოლების ერთობლივი ინტეგრირებით შესწავლილია მტვრის გავრცელება ქ.თბილისის ტერიტორიაზე. რიცხვობრივად მოდელირდება დამტვერიანების პროცესი, რომელიც მიმდინარეობს ფონური აღმოსავლეთის საშუალო სიჩქარის ქარის დროს. მიღებულია, რომ მტვრის მიკრომასშტაბური გავრცელება მნიშვნელოვნად არის დამოკიდებული ქალაქისა და მიმდებარე ტერიტორიის რელიეფზე, ფონური ქარის სიჩქარის სიდიდეზე და მიმართულებაზე. ქ.თბილისში გაფრქვეული მტვერი ძირითადად კონცენტრირებულია ატმოსფეროს სასაზღვრო ფენის ქვედა 600 მ ფენაში. მიწის ზედაპირიდან 2 მ სიმაღლეზე მაქსიმალური კონცენტრაცია 1.0-1.5 ზდკ ფორმირდება 12.00 – 21.00 საათის ინტერვალში ქალაქის ცენტრალურ და სამხრეთ ნაწილებში და შედარებით ჩაღმავებულ ტერიტორიებზე. გამოკვლეულია მტვრის ვერტიკალური განაწილების და დროში ცვლილების თავისებურებები.

## ЧИСЛЕННОЕ МОДЕЛИРОВАНИЕ РАСПРОСТРАНЕНИЯ ПЫЛИ В АТМОСФЕРЕ г.ТБИЛИСИ: СЛУЧАЙ ФОНОВОГО ВОСТОЧНОГО СРЕДНЕГО ВЕТРА

В.Г. Кухалашвили, Г.И. Кордзахиа, А.А. Сурмава, Н.Г. Гигаури, Л.Н. Инцкирвели

### Резюме

С помощью региональной модели атмосферных процессов на Кавказе и уравнения переноса-диффузии примесей изучено распространение пыли на территории г.Тбилиси. Численно моделируется процесс запыленности воздуха выбросами автотранспорта протекающий при средней скорости восточного фонового ветра. Было получено, что микро масштабное распределение пыли существенно зависит от рельефа города и его окрестностей, а также направления и величины скорости ветра. Пыль, рассеянная в г. Тбилиси, в основном сконцентрировано в нижней, 600-метровой зоне пограничного слоя атмосферы. На высоте 2 метра с поверхности земли концентрация 1.0-1.5 ПДК формируется во второй половине дня от 12.00 до 21.00 часа в центральной и южной частях города. Изучены особенности изменения во времени вертикального распределения пыли в приземном слое атмосферы г. Тбилиси.

## Numerical Modelling of Dust Propagation in the Atmosphere of Tbilisi City: The Case of Background Eastern Fresh Breeze

<sup>1</sup>Vepkhia G. Kukhalashvili, <sup>2</sup>Natia G. Gigauri, <sup>1,2</sup>Aleksandre A. Surmava,  
<sup>1</sup>Demuri I. Demetrashvili, <sup>2</sup>Liana N. Intskirveli

<sup>1</sup>M. Nodia Institute of Geophysics at the Iv. Javakhishvili Tbilisi State University, Tbilisi, Georgia.

1, M. Aleksidze Str., 0160, Tbilisi, Georgia, e-mail: aasurmava@yahoo.com

<sup>2</sup>Institute of Hydrometeorology at the Georgian Technical University, 150-a D.Agmashenebeli Ave, 0112  
Tbilisi, Georgia, E-mail: intskirvelebi2@yahoo.com

### ABSTRACT

Dust propagation at Tbilisi city territory in case of strong background eastern winds is studied using the 3D regional model of atmospheric processes evolution and integration of the equation of admixtures transfer-diffusion. It is shown that dust propagation substantially depends on both the terrain of city and surrounding territories and on the magnitude and direction of background wind velocity. It is obtained that dust propagation process in case of strong background wind is characterized by time variation and spatial distribution peculiarities. High pollution zones as well as the reasons of their time variation and dust accumulation are determined. It is established that a high pollution level (1.2-2.0 MAC) is obtained in the time interval from 3 p.m. to 9 p.m. in the up to 50 m thick lower part of surface layer of the atmosphere.

**Keywords:** numerical modeling, Tbilisi dust pollution, diffusion, strong wind.

### Introduction

The represented article is a continuation of studies started in [1] and dust pollution of Tbilisi city having complex terrain is studied in it via numerical modeling in case of strong background eastern wind. The magnitude of background eastern wind at 100 m height from earth surface (the upper boundary of the surface layer of atmosphere) equals to 10 m/sec and linearly increases up to 28.6 m/sec at 9 km altitude above sea level. It is assumed that the dust quantity dispersed in the atmosphere linearly depends on the traffic intensity. Time and space change of meteorological fields necessary for modeling is calculated according to numerical model described in [2, 3]. Meteorological situation corresponds to dry weather of June, when relative atmospheric humidity is 50%. Calculations are made along parallel and meridian with 300 and 400 m horizontal steps. Vertical step in the free atmosphere varies in time and equals 300 m in average. In 100 m thick surface layer of the atmosphere a vertical step varies from 2 to 15 m. Tbilisi city with a complex terrain is disposed in the center of modeling area.

### Modeling results

In Fig. 1 there is shown a spatial distribution of dust concentration and wind velocity at 2, 100 and 600 m height over a ground at  $t = 0, 3$  and 6 hours of the first day obtained via calculations. Dust content is given in units of one-off maximum allowable concentration (MAC = 0.5 mg/m<sup>3</sup>). It is seen from Fig. 1 that at 2 m height from underlying surfaces a dust concentration value is less than 0.1 MAC. In the interval of time from

0.00 a.m. to 6.00 a.m. there is no dust emission in the city atmosphere. Wind takes a dust away from city territory, and the atmosphere self-purification process occurs, that's why dust concentration is getting smaller and by 6.00 a.m. its value in the surface layer of atmosphere is of order of  $10^{-7}$ - $10^{-6}$  MAC. In this time period dust distribution is featured by the fact that a concentration value at 600 m height is higher than that obtained at 2 and 100 m height.

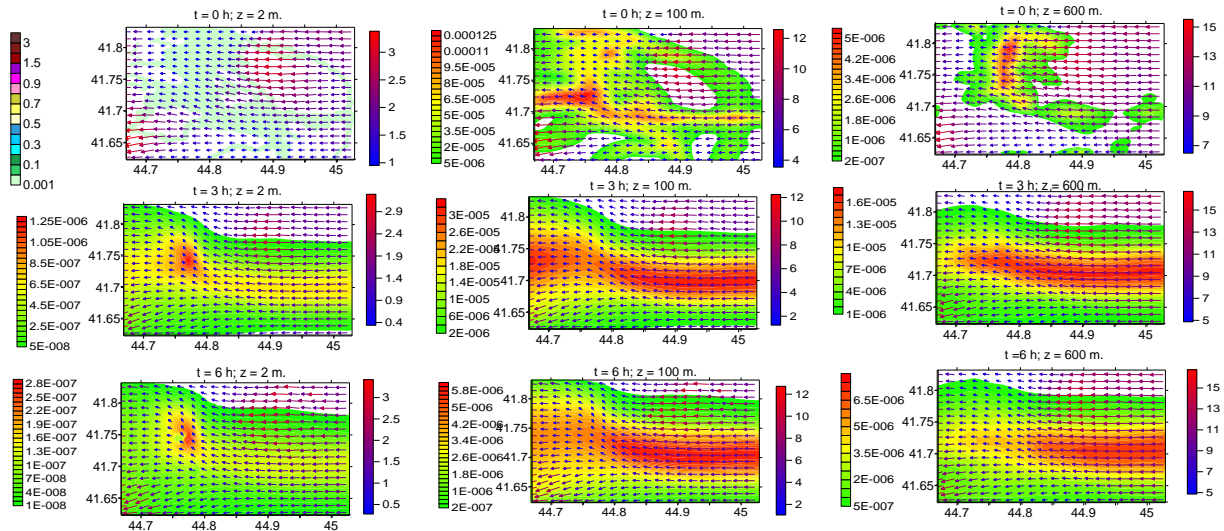


Fig. 1. Wind velocity (m/sec) and dust concentration (MAC) distribution, when  $t = 0, 3$  and  $6$  h at  $2, 100$  and  $600$  m height over a ground

Starting with 6.00 a.m., the dust pollution level of the atmosphere in city streets is getting higher (Fig. 2). Concentration increase is associated with beginning of intense vehicular traffic. As a result, by  $t = 9.00$  h we get a state when dust is propagated throughout a city. Large magnitudes of concentration are obtained at Gldani and Temka mains, their crossing areas, Guramishvili Avenue, Saburtalo and Vake mains, Heroes Square, and at separate sections of Gorgasali Avenue and Kakheti Highway. Concentration is within 0.8-1.0 MAC at mentioned territories. Despite the fact that the vehicle traffic intensity at Georgian Military Road, Tsereteli Avenue, and both sides of Mtkvari river embankment is roughly the same as at city mains with high pollution level, the concentration in their vicinity is relatively less and varies within limits of 0.5-0.8 MAC. The mentioned effect is obtained due to orography and thermal impact of underlying surface. In particular, along the Mtkvari river gorge, during the mentioned time interval, wind velocity direction changes by 90-180 grades and air stream convergence zone forms. The counter air flow brings along an originated dust and increases its concentration in Gldani, Temka and Nadzaladevi districts. In Vake and Saburtalo districts a dust brought by eastern flow, at high altitudes meets resistance of Mama Daviti ridge, cannot overcome it and increases dust pollution level in the mentioned districts. Dust horizontal distribution is such that dust concentrations are approximately within a limit of 0.3-0.5 MAC at 2-5 km distance from heavy pollution areas, while at more distances concentrations drop to 0.1-0.001 MPC. It should be noted that in morning hours dust pollution occurs mainly in the 50 m thick lower part of surface layer of the atmosphere. As for higher altitudes, concentrations are small there and are within a range of 0.1-0.3 MAC. From  $t = 9$  to 21 h the quantity of dust dispersed in the atmosphere, doesn't change. At the same time, this time interval can be divided into two periods according to concentration changes:

First, from  $t = 9$  to 18h, when concentration changes insignificantly; Second, from  $t = 18$  to 21 h, when dust pollution level increases in the central and western parts of the city and reduces in the eastern part (Fig. 2 and Fig. 3). In these periods dust concentration in high pollution zones reaches 1.5-2 MPC at 2 m height.

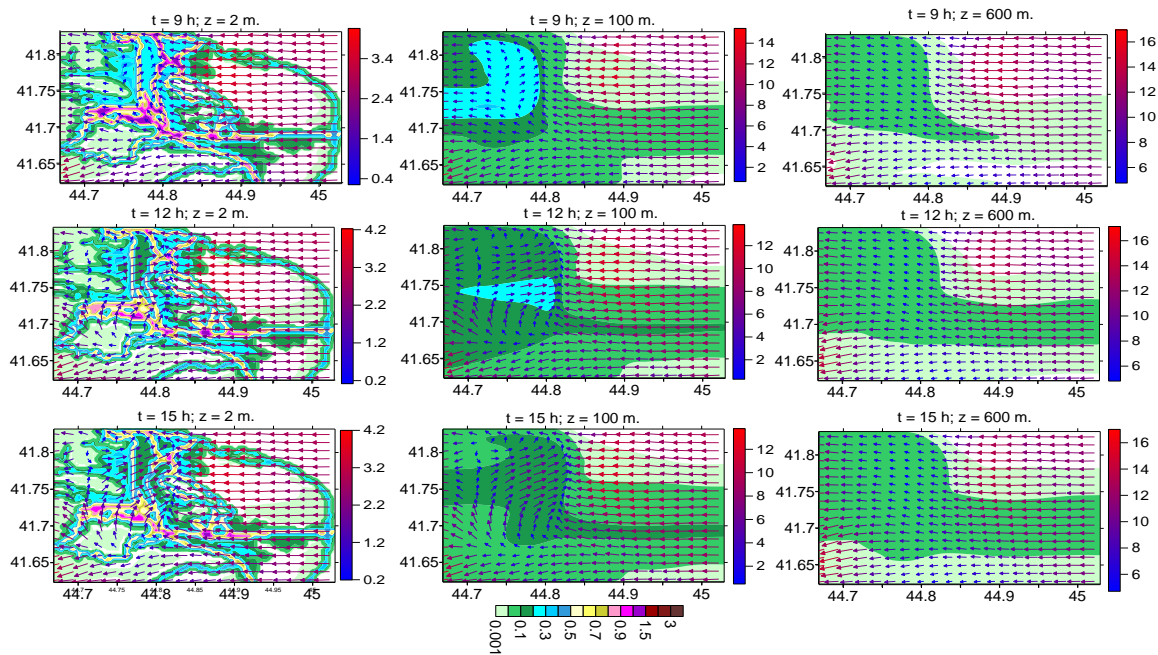


Fig. 2. Wind velocity (m/sec) and dust concentration (MAC) distribution, when  $t = 9, 12$  and  $15$  h at  $2, 100$  and  $600$  m height over a ground

In both periods, dust pollution pattern changes depend on diurnal variation of wind velocity. During the first period there takes place increase of western wind in the western part of the region and convergence band shift to the east by  $1.5-2.0$  km distance. Starting with  $t = 16$  h there takes place western wind weakening in the surface layer of atmosphere, convergence band breakup and eastern wind formation in the western part of the region. As a result, accumulation of local dust and dust taken by advection, and respectively its concentration increase occurs to the west of city, nearby the Mama Daviti piedmont slopes.

Two mutually opposite processes of dust pollution take place in the upper part of surface layer of the atmosphere and in the atmospheric boundary layer. At  $100$  m height over a ground from  $t = 9$  to  $15$  h dust concentration reduces and afterwards, from  $15$  to  $18$  h it increases. The mentioned effect is obtained in the atmospheric boundary layer at  $600$  m height, as well, though with less obviousness.

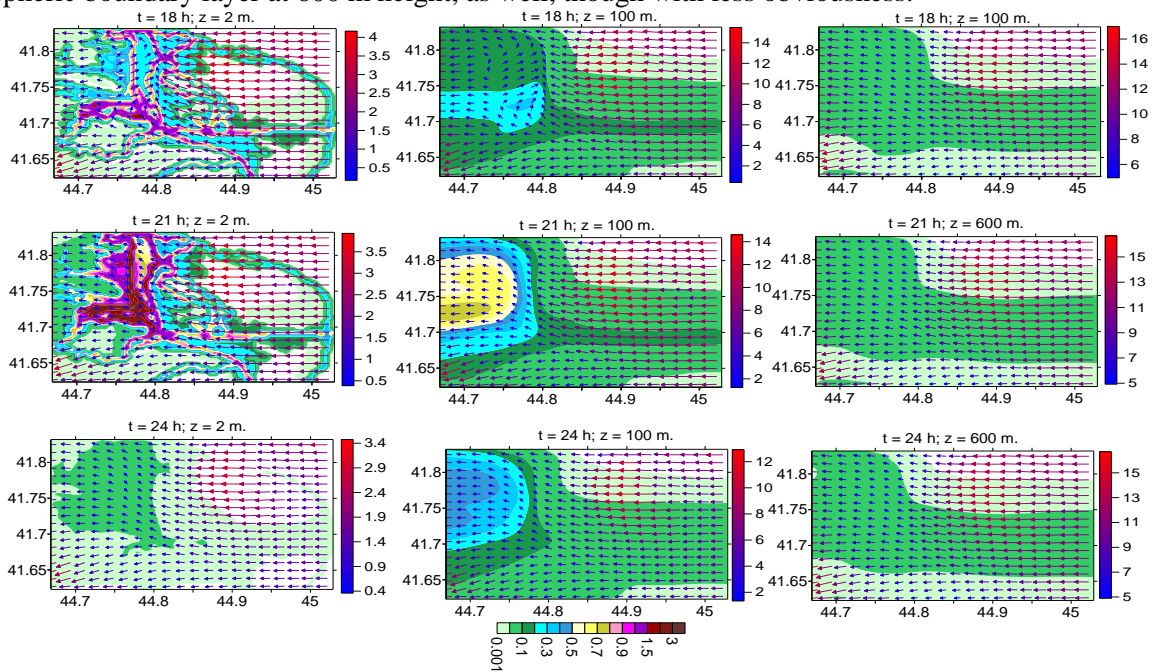


Fig. 3. Wind velocity (m/sec) and dust concentration (MPC) distribution, when  $t = 18, 21$  and  $24$  h at  $2, 100$  and  $600$  m height over a ground

From  $t = 21$  to  $24$  h a sharp decrease of vehicular traffic intensity takes place. As a consequence, the quantity and concentration of dispersed dust at 2 m height reduces. At this time, the wind velocity and vertical turbulence are high in the lower part of a surface layer that causes powerful vertical diffusion and advective transfer of near-the-ground dust. So, we get a steady state, when maximum dust concentration at 100 m height (0.7 MAC) exceeds the concentrations that are obtained at 2 and 600 m heights (0.1 MAC).

Dust vertical distribution for different moments is shown in Fig. 4. Concentration isozones in 3 cross-sections drawn along the parallels in the surface layer of atmosphere are depicted there. It is seen from Fig. 4 that from the beginning of a day in this period  $0 \text{ h} < t < 6 \text{ h}$  dust concentration in the lower part of surface layer of the atmosphere is less than above it. After  $t = 6 \text{ h}$ , with intensification of vehicular traffic, the high pollution areas shaped like convection clouds are formed in the near-the-ground surroundings of dust pollution sources. Starting with this moment, dust concentration in the lower 50 m thick part of surface layer substantially exceeds concentration values obtained above it. Afterwards, there takes place intensification of abovementioned dust pollution processes, which reaches its maximum by  $t = 21 \text{ h}$ . After  $t = 21 \text{ h}$  a self-purification process – dust pollution reduction occurs. Self-purification process lasts until 6.00 a.m.. Then, this process repeats on a quasi-periodic basis.

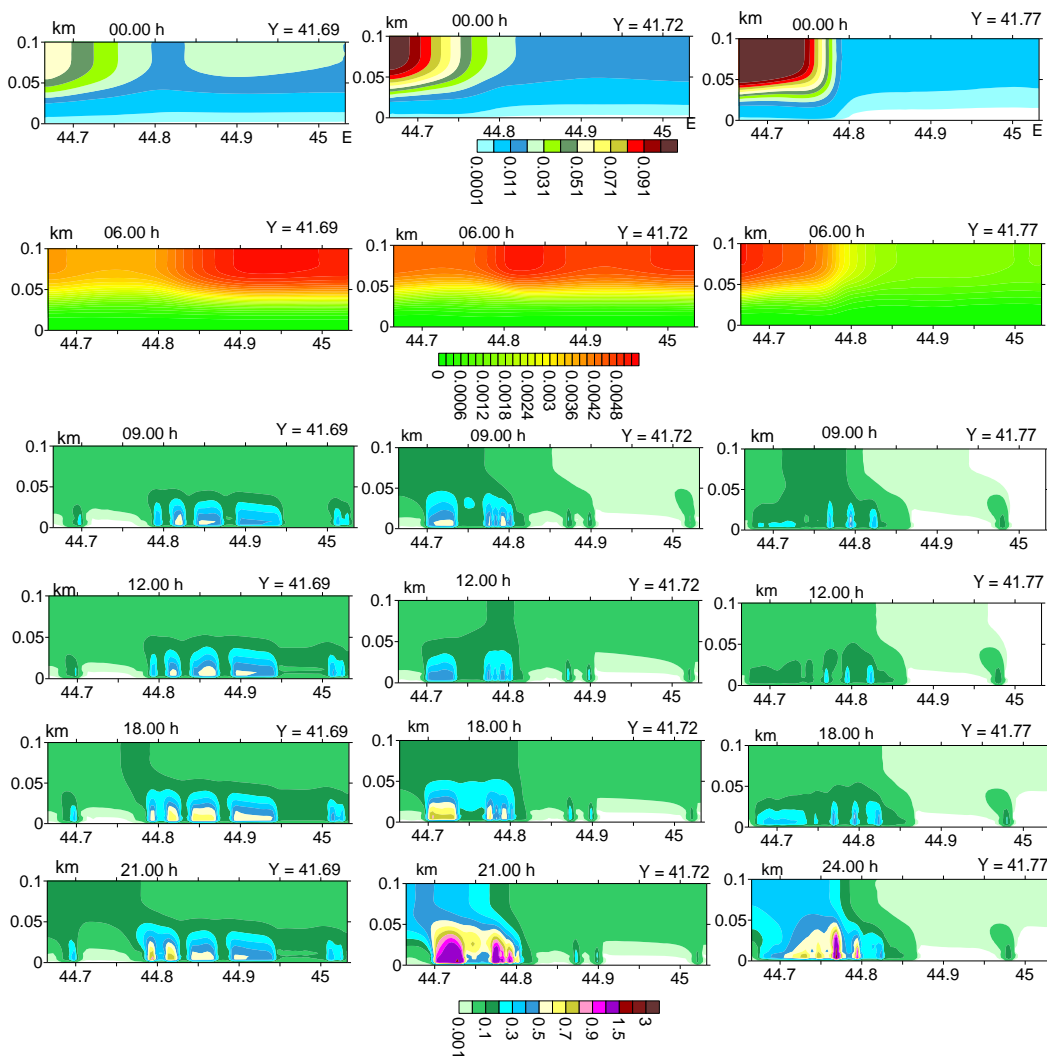


Fig. 4. Dust concentration vertical distribution (MPC) in three vertical sections ( $41,69^{\circ}\text{N}$ ,  $41,72^{\circ}\text{N}$ ,  $41,77^{\circ}\text{N}$ ) drawn along the parallel in the surface layer of atmosphere

## Conclusion.

The kinematics of dust concentration change created by motor transport at the territory of Tbilisi and diurnal pattern of its spatial distribution in case of strong background eastern wind are studied. Via analysis of wind velocity and concentration fields it is obtained that spatial distribution of heavily polluted areas depends on city mains disposition, and local circulation systems formed under dynamic impact of terrain and diurnal change of thermal regime at the underlying surface. Maximum concentration 1.5-2.0 MPC is obtained in time interval of  $t = 15-21$  h in the central and western parts of the city. At 600 m height from earth surface a maximum value of concentration reaches 0.7 MAC, when  $t = 21$ h.

Results obtained through modeling of time and spatial changes of dust concentration qualitatively correctly describe the true picture. From a quantitative viewpoint, modeling results are close to average characteristic data of observations [3].

**Acknowledgment.** The study was carried out under financial support of Shota Rustaveli National Science Foundation of Georgia [FR-18-3667].

## References

- [1] Kukhalashvili V.G., Kordzakhia G.I., Gigauri N.G., Surmava A.A., Intskirveli L.N. Numerical Modelling of Dust Propagation in the Atmosphere of Tbilisi City: The Case of Background Eastern Gentle Breeze. Journal of the Georgian Geophysical Society, ISSN: 1512-1127, Physics of Solid Earth, Atmosphere, Ocean and Space Plasma, v. 23(1), 2020, pp. 46 -50.
- [2] Surmava A., Intskirveli L., Kukhalashvili V., Gigauri N.. Numerical Investigation of Meso- and Microscale Diffusion of Tbilisi Dust. Annals of Agrarian Science, 18, No. 3, 2020 (In print).
- [3] Gigauri N.G., Gverdtseteli L.V., Surmava A.A., Intskirveli L.N. Numerical Simulation of Industrial Dust Distribution in the Territory of Zestafoni, Georgia. WIT Transaction on Ecology and Environment, 230, 2018, pp. 119-128. Doi:10.2495/AIR1180111.

## ქ. თბილისის ატმოსფეროში მტვრის გავრცელების რიცხვითი მოდელირება: ფონური აღმოსავლეთის ძლიერი ქარის შემთხვევა

ვ. კუხალაშვილი, ნ. გიგაური, ა. სურმავა, დ. დემეტრაშვილი,  
ლ. ინჭკირველი

### რეზიუმე

ატმოსფერული პროცესების ევოლუციის 3D რეგიონალური მოდელისა და მინარევების გადატანა-დიფუზიის განტოლების ერთობლივი ინტეგრირებით შესწავლილია მტვრის გავრცელება ქ.თბილისის ტერიტორიაზე ფონური აღმოსავლეთის ძლიერი ქარის დროს. მიღებულია, რომ მტვრის გავრცელების პროცესი ძლიერი ფონური ქარის შემთხვევაში ხასიათდება დროში ცვლილების და სივრცული განაწილების თავისებურებებით. ქარის სიჩქარისა და კონცენტრაციის ველების ანალიზით დადგენილია, რომ ძლიერ დამტვერიანებული არეების სივრცული განაწილება დამოკიდებულია ავტომაგისტრალების მდებარეობაზე, რელიეფის დინამიკური ზემოქმედების და ქვეფენილ ზედაპირზე თერმიული რეჟიმის დღეღამური ცვლილებით ფორმირებულ ლოკალურ ცირკულაციურ სისტემებზე. მაქსიმალური კონცენტრაცია 1.5 – 2.0 ზდკ ფორმირდება 15.00 – 21.00 საათის ინტერვალში ატმოსფეროს ქვედა 50 მეტრამდე ფენაში ქალაქის ცენტრალურ და დასავლეთ ნაწილებში. მიწის ზედაპირიდან 600 მეტრის სიმაღლეზე კონცენტრაციის მაქსიმალური მნიშვნელობა 21.00 საათზე აღწევს 0.7 ზდკ-ს.

# **ЧИСЛЕННОЕ МОДЕЛИРОВАНИЕ РАСПРОСТРАНЕНИЯ ПЫЛИ В АТМОСФЕРЕ г.ТБИЛИСИ: СЛУЧАЙ ВОСТОЧНОГО СИЛЬНОГО ФОНОВОГО ВЕТРА**

**В.Г. Кухалашвили, Н.Г. Гигаури, А.А. Сурмава,  
Д.И. Деметрашили, Л.Н. Инцкирвели**

## **Резюме**

С помощью региональной модели атмосферных процессов на Кавказе и уравнения переноса-диффузии примеси в атмосфере, изучено распространение пыли на территории г. Тбилиси при сильном фоновом ветре. Анализ полей скорости ветра и концентрации пыли показал, что пространственное распределение областей высоких концентрации зависит от расположения автомагистралей, динамического воздействия рельефа и локальных циркуляционных процессов, сформированных изменением суточного термического режима на подстилающей поверхности. В нижней приземной 50-метровой зоне центральной и западных частях города максимальные концентрации 1.5-2.0 ПДК формируются во временном интервале от 15 до 21 часа. На высоте 600 м от поверхности земли максимальная концентрация 0.7 ПДК достигается к 21 часу.

## Pandemic of Coronavirus COVID-19 and Air Pollution in Tbilisi in Spring 2020

<sup>1</sup>Avtandil G. Amiranashvili, <sup>1</sup>Darejan D. Kirkitadze, <sup>1,2</sup>Eliso N. Kekenadze

<sup>1</sup>Mikheil Nodia Institute of Geophysics of Ivane Javakhishvili Tbilisi State University, Tbilisi, Georgia  
1, M. Alexidze Str., 0160, Tbilisi, Georgia  
avtandilamiranashvili@gmail.com

<sup>2</sup>Military Scientific-Technical Center "DELTA"

### ABSTRACT

*At the end of 2019, a novel coronavirus COVID-19 emerged in Wuhan, China and later spread throughout the world, including Georgia. To control the rapid dispersion of the virus, Georgia, as another countries has imposed national lockdown policies to praxise social distancing, restriction of automobile traffic, industrial enterprises, etc. This has led to reduced human activities and hence primary air pollutant emissions, which caused improvement of air quality.*

*In this work data about influence of these limitation in Georgia in connection with the pandemic of COVID-19 to the decrease of the level of air pollution in Tbilisi during spring 2020 compared to the same period in 2017-2019.*

*The data of Georgian National Environmental Agency about the daily mean values of dust concentration (atmospheric particulate matter - PM<sub>2.5</sub> and PM<sub>10</sub>), NO<sub>2</sub>, CO and O<sub>3</sub> and also data of the satellite monitoring of the aerosol optical thickness of atmosphere are used. In particular, there has been a significant increase in ozone in the air and a significant decrease in other atmospheric pollutants.*

**Key words:** Pandemic of Coronavirus COVID-19, air pollution.

### 1. Introduction

At the M. Nodia Institute of Geophysics for many decades has been conducting research on atmospheric aerosols (including radioactive ones) [1-7] and ozone [3-5, 8, 9]. Some experimental and theoretical studies of the structure of atmospheric aerosols, their optical properties, distribution in the atmosphere, etc. are presented in [5, 10-20]. Data about experimental laboratory studies of the processes of washing out aerosols and ozone, their ice-forming properties, etc. are presented in [2, 5, 21].

Particular attention is paid to full-scale studies of ozone, mineral and secondary aerosols (stationary monitoring of ozone, solid particles and secondary aerosols in the surface atmosphere [2, 5, 8, 22-27], aircraft research of mineral aerosols and ozone in the lower troposphere [ 2, 7, 8, 28-30], mobile monitoring of aerosols and ozone in Tbilisi [5], data analysis of stationary ground-based remote and satellite monitoring of the aerosol optical depth of the atmosphere and ozone [4, 5, 31-42], radar monitoring of large dust formations in the atmosphere [43,44]).

In recent years, in Georgia, the Environmental Agency, in accordance with international standards [45], began monitoring particulate matter with a diameter of  $\leq 2.5 \mu\text{m}$  (PM<sub>2.5</sub>) and  $\leq 10 \mu\text{m}$  (PM<sub>10</sub>), and the gas pollution of the atmosphere: SO<sub>2</sub>, NO<sub>2</sub>, CO, O<sub>3</sub>, [[http://air.gov.ge/reports\\_page](http://air.gov.ge/reports_page)].

The statistical characteristics of the weight concentrations of aerosols (particulate matter PM<sub>2.5</sub> and PM<sub>10</sub>) in three points of Tbilisi city (A. Kazbegi av., A. Tsereteli av. and Varketili) in 2017-2018 are represented in [46]. In particular, it is obtained that the greatest average annual values of PM<sub>2.5</sub> on the A. Tsereteli av. were observed (24.9  $\mu\text{g}/\text{m}^3$ , the range of the change: 0-440  $\mu\text{g}/\text{m}^3$ ), smallest - on A. Kazbegi av. (16.6  $\mu\text{g}/\text{m}^3$ , the range of the change: 0-494  $\mu\text{g}/\text{m}^3$ ). The greatest average annual values PM<sub>10</sub> also on A. Tsereteli av. were observed (57.2  $\mu\text{g}/\text{m}^3$ , the range of the change: 0-553  $\mu\text{g}/\text{m}^3$ ), smallest - in Varketili (37.4  $\mu\text{g}/\text{m}^3$ , the range of the change: 0-319  $\mu\text{g}/\text{m}^3$ ).

It is obtained, that the value of the linear correlation coefficient between the hourly values PM<sub>2.5</sub> and PM<sub>10</sub> on all points sufficiently high and changes from 0.77 to 0.89. The value of the correlation coefficient between the hourly values of PM<sub>2.5</sub> between the points changes from 0.64 to 0.73, and PM<sub>10</sub> - from 0.49 to 0.60.

The statistical characteristics of surface ozone concentration (SOC) in three same points of Tbilisi city (A. Kazbegi av., A. Tsereteli av. and Varketili) in 2017-2018 are represented in [47].

In particular, it is obtained that the greatest average annual values of SOC in Varketili were observed (53.9 µg/m<sup>3</sup>, the range of the change: 1-134 µg/m<sup>3</sup>), smallest – at the A. Tsereteli av. (21.6 µg/m<sup>3</sup>, the range of the change: 0-102 µg/m<sup>3</sup>). The value of the correlation coefficient between the eight hour values SOC between the points sufficiently high and changes from 0.74 to 0.91.

At the end 2019 - to first half 2020, in connection with the pandemia of coronavirus COVID-19 in many countries of world, including Georgia, were introduced the limitations in the work of some industrial objects, the cancellation of aviation communication, movement of truck transport, etc. Those indicated limitation brought to the decrease of the level of the air pollution in many countries of the world [48-53].

In the work [48] it is noted that responding to the ongoing novel coronavirus (agent of COVID-19) outbreak, China implemented “the largest quarantine in human history” in Wuhan on 23 January 2020. Similar quarantine measures were imposed on other Chinese cities within days. Human mobility and relevant production and consumption activities have since decreased significantly. As a likely side effect of this decrease, many regions have recorded significant reductions in air pollution. Authors employed daily air pollution data and Intracity Migration Index (IMI) data from Baidu between 1 January and 21 March 2020 for 44 cities in northern China to examine whether, how, and to what extent travel restrictions affected air quality. On the basis of this quantitative analysis, they reached the following conclusions: (1) The reduction of air pollution was strongly associated with travel restrictions during this pandemic—on average, the air quality index (AQI) decreased by 7.80%, and five air pollutants (i.e., SO<sub>2</sub>, PM<sub>2.5</sub>, PM<sub>10</sub>, NO<sub>2</sub>, and CO) decreased by 6.76%, 5.93%, 13.66%, 24.67%, and 4.58%, respectively. (2) Mechanism analysis illustrated that the lockdowns of 44 cities reduced human movements by 69.85%, and a reduction in the AQI, PM<sub>2.5</sub>, and CO was partially mediated by human mobility, and SO<sub>2</sub>, PM<sub>10</sub>, and NO<sub>2</sub> were completely mediated.

On another work [49] it is shown, that industrial emission reduction has played a significant role in the improvement of air quality in Yangtze River Delta Region of China. Concentrations of PM<sub>2.5</sub>, NO<sub>2</sub> and SO<sub>2</sub> decreased by 31.8%, 45.1% and 20.4% during the Level I period; and 33.2%, 27.2% and 7.6% during the Level II period compared with 2019. However, ozone did not show any reduction and increased greatly. Results of [49] also show that even during the lockdown, with primary emissions reduction of 15%–61%, the daily average PM<sub>2.5</sub> concentrations range between 15 and 79 µg·m<sup>-3</sup>, which shows that background and residual pollutions are still high. Source apportionment results indicate that the residual pollution of PM<sub>2.5</sub> comes from industry (32.2–61.1%), mobile (3.9–8.1%), dust (2.6–7.7%), residential sources (2.1–28.5%) in YRD and 14.0–28.6% contribution from long-range transport coming from northern China. This indicates that in spite of the extreme reductions in primary emissions, it cannot fully tackle the current air pollution.

The first COVID-19 case in Brazil was confirmed on February 25, 2020 [50]. On March 16, the state's governor declared public health emergency in the city of Rio de Janeiro and partial lockdown measures came into force a week later. The main goal of work [50] is to discuss the impact of the measures on the air quality of the city by comparing the particulate matter, carbon monoxide, nitrogen dioxide and ozone concentrations determined during the partial lockdown with values obtained in the same period of 2019 and also with the weeks prior to the virus outbreak. Concentrations varied with substantial differences among pollutants and also among the three studied monitoring stations. CO levels showed the most significant reductions (30.3–48.5%) since they were related to light-duty vehicular emissions. NO<sub>2</sub> also showed reductions while PM<sub>10</sub> levels were only reduced in the first lockdown week. In April, an increase in vehicular flux and movement of people was observed mainly as a consequence of the lack of consensus about the importance and need of social distancing and lockdown. Ozone concentrations increased probably due to the decrease in nitrogen oxides level. When comparing with the same period of 2019, NO<sub>2</sub> and CO median values were 24.1–32.9 and 37.0–43.6% lower.

In Almaty, a city-scale quarantine came into force on March 19, 2020, which was a week after the first COVID-19 case was registered in Kazakhstan [51]. In study [51] analyze the effect of the lockdown from March 19 to April 14, 2020 (27 days), on the concentrations of air pollutants in Almaty is conducted. Daily concentrations of PM<sub>2.5</sub>, NO<sub>2</sub>, SO<sub>2</sub>, CO, O<sub>3</sub>, and BTEX were compared between the periods before and during the lockdown. During the lockdown, the PM<sub>2.5</sub> concentration was reduced by 21% with spatial variations of 6–34% compared to the average on the same days in 2018–2019, and still, it exceeded WHO daily limit values for 18 days. There were also substantial reductions in CO and NO<sub>2</sub> concentrations by 49%

and 35%, respectively, but an increase in O<sub>3</sub> levels by 15% compared to the prior 17 days before the lockdown. The concentrations of benzene and toluene were 2–3 times higher than those during in the same seasons of 2015–2019. It is noted, that temporal reductions may not be directly attributed to the lockdown due to favorable meteorological variations during the period, but the spatial effects of the quarantine on the pollution levels are evidenced. The results demonstrate the impact of traffic on the complex nature of air pollution in Almaty, which is substantially contributed by various nontraffic related sources, mainly coal-fired combined heat and power plants and household heating systems, as well as possible small irregular sources such as garbage burning and bathhouses.

In the work [52] was a substantial reduction in many countries in the level of nitrogen dioxide (NO<sub>2</sub>: 0.00002 mol·m<sup>-2</sup>), a low reduction in CO (<0.03 mol·m<sup>-2</sup>), and a low - to moderate reduction in Aerosol Optical Thickness (AOT: ~0.1–0.2) in the major hotspots of COVID-19 out break during February–March 2020, which may be attributed to the mass lockdowns.

In the work [53] authors assessed air quality during the COVID-19 pandemic for fine particulate matter (PM<sub>2.5</sub>) and nitrogen dioxide (NO<sub>2</sub>) in the continental United States from January 8th-April 21st in 2017–2020. They considered pollution during the COVID-19 period (March 13–April 21st) and the pre-COVID-19 period (January 8th-March 12th) with 2020 representing ‘current’ data and 2017–2019 representing ‘historical’ data. County-level pollution concentrations were compared between historical versus current periods, and counties were stratified by institution of early or late non-essential business closures. Statistically significant NO<sub>2</sub> declines were observed during the current COVID-19 period compared to historical data: a 25.5% reduction with absolute decrease of 4.8 ppb. PM<sub>2.5</sub> also showed decreases during the COVID-19 period, and the reduction is statistically significant in urban counties and counties from states instituting early non-essential business closures.

In Georgia the following limitations were introduced: from March 21 to May 22, 2020 - state of emergency and curfew, from 17 to 27 April 2020 - complete ban of the movement of automobiles, from 28 April through 28 May 2020 - the permission of the movement of passenger automobiles, from 29 May 2020 - the permission of the movement of buses [<https://ren.tv/news/v-mire/687151-vlasti-gruzii-zapreshchaiut-dvizhenie-avtomobilei-iz-za-koronavirusa>, <https://www.ekhokavkaza.com/a/30578567.html>, <https://yandex.ru/turbo/s/vz.ru/news/2020/5/22/1040797.html>].

Data about influence of these limitations in Georgia in connection with the pandemic of coronavirus COVID-19 to the decrease of the level of air pollution in Tbilisi during spring 2020 compared to the same period in 2017-2019 are presented below.

## 2. Study area, material and methods

Study area – three locations of Tbilisi (A. Kazbegi av., A. Tsereteli av., Varketili). Coordinates of these locations of air pollution measurements points in [46,47] are presented.

The data of Georgian National Environmental Agency about the daily mean values of dust concentration (atmospheric particulate matter - PM<sub>2.5</sub> and PM<sub>10</sub>), NO<sub>2</sub>, CO and O<sub>3</sub> [[http://air.gov.ge/reports\\_page](http://air.gov.ge/reports_page)] that averaged on three indicated stations are used. Period of observation: January 1- May 31, 2017 - 2020.

Data of the satellite monitoring of the aerosol optical thickness of atmosphere (AOT) are used also [[https://neo.sci.gsfc.nasa.gov/view.php?datasetId=MODAL2\\_M\\_AER\\_OD](https://neo.sci.gsfc.nasa.gov/view.php?datasetId=MODAL2_M_AER_OD)]). Period of observation: April 2019, January 1 - June 1, 2020.

In the proposed work the analysis of data is carried out with the use of the standard statistical analysis methods of random events and methods of mathematical statistics for the non accidental time-series of observations [54, 55]. Missed data of time-series of observations were restored in the correspondence with the standard methods [54].

The following designations will be used below: Min – minimal values, Max - maximal values, St Dev - standard deviation, R<sup>2</sup> – coefficient of determination, K<sub>DW</sub> – Durbin-Watson Statistic, Res – residual component, Real - measured data, Calc – calculated data. The curve of trend is equation of the regression of the connection of the investigated parameter with the time at the significant value of the determination coefficient and such values of K<sub>DW</sub>, where the residual values are accidental. If the residual values are not accidental the connection of the investigated parameter with the time we will consider simply regression.

## 3. Results and discussion

Results in table 1-3 and fig. 1-16 are presented.

In table 1-2 statistical characteristics of PM<sub>2.5</sub>, PM<sub>10</sub>, NO<sub>2</sub>, CO and O<sub>3</sub> in air of Tbilisi in spring 2017-2020 are presented. In table 3 form of the equations of the regression of the time changeability of the daily values of five air pollutants in Tbilisi from 1 March through 31 May 2017-2020 are presented. In fig. 1,3,5,7 and 9 data about changeability of the measured values of five air pollutants in Tbilisi from 1 March through 31 May 2017-2020 are represented. In fig. 2,4,6,8 and 10 data about changeability of the calculated according to table 3 values of five air pollutants in Tbilisi from 1 March through 31 May 2017-2020 are represented.

Table 1. Statistical characteristics of PM<sub>2.5</sub> and PM<sub>10</sub> in air of Tbilisi in spring 2017-2020.

| Pollutant | PM <sub>2.5</sub> , (μg/m <sup>3</sup> ) |      |      |      | PM <sub>10</sub> , (μg/m <sup>3</sup> ) |      |      |       |
|-----------|--|------|------|------|---|------|------|-------|
|           | Year                                     | 2017 | 2018 | 2019 | 2020                                    | 2017 | 2018 | 2019  |
| Month     | March-May                                |      |      |      |   |      |      |       |
| Max       | 44.2                                     | 40.7 | 26.7 | 52.1 | 81.8                                    | 92.5 | 62.6 | 117.7 |
| Min       | 8.0                                      | 8.1  | 5.5  | 4.3  | 22.4                                    | 23.0 | 13.0 | 9.1   |
| Mean      | 16.7                                     | 17.8 | 14.5 | 14.9 | 38.7                                    | 41.1 | 31.8 | 31.9  |
| StDev     | 6.5                                      | 5.8  | 4.5  | 9.2  | 10.9                                    | 12.0 | 9.6  | 19.3  |
| Month     | March                                    |      |      |      |   |      |      |       |
| Max       | 44.2                                     | 40.7 | 26.7 | 52.1 | 81.8                                    | 92.5 | 51.5 | 117.7 |
| Min       | 11.2                                     | 8.1  | 6.9  | 6.6  | 26.6                                    | 23.0 | 13.1 | 12.1  |
| Mean      | 20.6                                     | 20.5 | 14.9 | 22.4 | 43.2                                    | 42.1 | 29.6 | 44.4  |
| StDev     | 8.4                                      | 8.3  | 5.8  | 12.0 | 14.1                                    | 17.6 | 9.7  | 27.0  |
| Month     | April                                    |      |      |      |   |      |      |       |
| Max       | 27.9                                     | 21.4 | 20.5 | 18.0 | 56.6                                    | 50.3 | 44.8 | 34.8  |
| Min       | 9.6                                      | 9.5  | 5.5  | 4.3  | 22.5                                    | 23.6 | 13.0 | 9.1   |
| Mean      | 15.8                                     | 17.0 | 14.0 | 11.0 | 36.7                                    | 36.7 | 29.6 | 22.1  |
| StDev     | 4.5                                      | 3.3  | 4.0  | 3.5  | 9.2                                     | 7.3  | 8.3  | 6.7   |
| Month     | May                                      |      |      |      |   |      |      |       |
| Max       | 21.5                                     | 20.7 | 22.6 | 19.1 | 52.6                                    | 52.2 | 62.6 | 50.9  |
| Min       | 8.0                                      | 9.0  | 7.2  | 5.7  | 22.4                                    | 27.9 | 14.3 | 13.0  |
| Mean      | 13.8                                     | 15.9 | 14.5 | 11.2 | 36.1                                    | 44.2 | 36.1 | 28.8  |
| StDev     | 3.8                                      | 3.2  | 3.6  | 3.7  | 7.2                                     | 6.9  | 9.5  | 9.4   |

Table 2. Statistical characteristics of NO<sub>2</sub>, CO and O<sub>3</sub> in air of Tbilisi in spring 2017-2020.

| Pollutant | NO <sub>2</sub> , (μg/m <sup>3</sup> ) |      |      |      | CO, (mg/m <sup>3</sup> ) |      |      |      | O <sub>3</sub> , (μg/m <sup>3</sup> ) |      |      |       |
|-----------|--|------|------|------|--------------------------|------|------|------|---------------------------------------|------|------|-------|
|           | Year                                   | 2017 | 2018 | 2019 | 2020                     | 2017 | 2018 | 2019 | 2020                                  | 2017 | 2018 | 2019  |
| Month     | March-May                              |      |      |      |                          |      |      |      |                                       |      |      |       |
| Max       | 77.3                                   | 53.9 | 53.0 | 32.5 | 2.0                      | 2.3  | 1.5  | 2.0  | 93.7                                  | 87.7 | 88.2 | 107.6 |
| Min       | 25.2                                   | 17.7 | 20.3 | 9.3  | 0.4                      | 0.6  | 0.5  | 0.3  | 37.3                                  | 22.4 | 32.0 | 21.1  |
| Mean      | 41.3                                   | 31.0 | 33.5 | 15.9 | 1.0                      | 1.0  | 0.9  | 0.7  | 69.5                                  | 62.0 | 62.7 | 76.3  |
| StDev     | 10.2                                   | 6.3  | 6.5  | 4.6  | 0.3                      | 0.3  | 0.2  | 0.3  | 12.1                                  | 14.1 | 11.6 | 14.8  |
| Month     | March                                  |      |      |      |                          |      |      |      |                                       |      |      |       |
| Max       | 67.8                                   | 41.0 | 53.0 | 32.5 | 2.0                      | 2.3  | 1.5  | 2.0  | 86.1                                  | 81.8 | 83.1 | 85.5  |
| Min       | 25.2                                   | 17.7 | 21.2 | 12.2 | 0.7                      | 0.6  | 0.5  | 0.4  | 40.8                                  | 22.4 | 32.0 | 21.1  |
| Mean      | 42.5                                   | 31.0 | 32.7 | 19.8 | 1.1                      | 1.2  | 0.9  | 0.9  | 67.5                                  | 52.8 | 60.0 | 64.9  |
| StDev     | 10.7                                   | 6.2  | 7.2  | 5.3  | 0.3                      | 0.4  | 0.3  | 0.4  | 10.0                                  | 15.2 | 10.8 | 12.1  |
| Month     | April                                  |      |      |      |                          |      |      |      |                                       |      |      |       |
| Max       | 77.3                                   | 38.6 | 52.3 | 16.6 | 1.7                      | 1.1  | 1.2  | 0.6  | 93.7                                  | 87.7 | 81.2 | 102.4 |
| Min       | 26.6                                   | 20.1 | 25.8 | 9.3  | 0.4                      | 0.6  | 0.6  | 0.3  | 42.9                                  | 53.7 | 35.5 | 58.3  |
| Mean      | 41.8                                   | 28.9 | 34.4 | 12.7 | 0.9                      | 0.8  | 0.8  | 0.5  | 74.0                                  | 70.2 | 61.1 | 82.9  |
| StDev     | 12.6                                   | 5.0  | 5.7  | 2.2  | 0.3                      | 0.2  | 0.2  | 0.1  | 12.6                                  | 8.6  | 13.5 | 11.5  |
| Month     | May                                    |      |      |      |                          |      |      |      |                                       |      |      |       |
| Max       | 50.1                                   | 53.9 | 46.9 | 22.5 | 1.4                      | 1.3  | 1.3  | 1.1  | 83.5                                  | 87.4 | 88.2 | 107.6 |
| Min       | 25.6                                   | 23.2 | 20.3 | 11.2 | 0.6                      | 0.6  | 0.5  | 0.4  | 37.3                                  | 34.7 | 54.8 | 40.8  |
| Mean      | 39.6                                   | 33.1 | 33.5 | 15.1 | 0.9                      | 0.9  | 0.8  | 0.6  | 67.2                                  | 63.3 | 67.1 | 81.4  |
| StDev     | 6.8                                    | 7.0  | 6.5  | 2.4  | 0.2                      | 0.2  | 0.2  | 0.2  | 12.6                                  | 11.9 | 9.2  | 13.6  |

As follows from tables 1-2 in 2020, compared with 2017-2019, the average monthly measured level of air pollution in Tbilisi changes as follows:

**PM2.5.**

- March-May: 2017 – decrease by 10.9% , 2018 – decrease by 16.4%, 2019 – slight increase on 3% ;
- March: 2017 – increase on 8.9% , 2018 – increase on 9.3% , 2019 – increase on 50.5%;
- April: 2017 – decrease by 30.7%, 2018 – decrease by 35.7%, 2019 decrease by 22%;
- May: 2017 – decrease by 18.4%, 2018 – decrease by 29.6%, 2019 – decrease by 22.4%

**PM10.**

- March-May: 2017 – decrease by 17.6%, 2018 – decrease by 22.4%, 2019 – virtually unchanged;
- March: 2017 – weak growth on 2.9%, 2018 - weak growth on 5.4%, 2019 – growth by 50.2%;
- April: 2017 – decrease by 39.8%, 2018 - decrease by 39.6% , 2019 - decrease by 25.4%;
- May: 2017 - decrease by 20.2%, 2018 - decrease by 34.9%, 2019 - decrease by 20.3%.

**NO<sub>2</sub>.** For all time periods, a decrease.

- March-May: 2017 – 61.5% , 2018 – 48.8%, 2019 – 52.6%;
- March: 2017 – 53.4%, 2018 – 36.2% , 2019 – 39.5%;
- April: 2017 – 69.6%, 2018 – 56.1%, 2019 – 63.1%;
- May: 2017 – 62.0%, 2018 – 54.5%, 2019 – 55.1%.

**CO.** For all time periods except March 2019, a decrease.

- March-May: 2017 – 29.3%, 2018 – 28.3%, 2019 – 19.4%;
- March: 2017 – 13.8%, 2018 – 19.9%, 2019 – slight increase on 5.8% ;
- April: 2017 – 49.4%, 2018 – 43.6%, 2019 – 45.6%;
- May: 2017 – 29.0%, 2018 – 26.1%, 2019 – 21.1%.

**O<sub>3</sub>.** For all time periods except March 2017, growth.

- March-May: 2017 – 9.8%, 2018 -23.1 % , 2019 -21.7 %;
- March: 2017 – slight decrease by 3.8%, 2018 – 23.0%, 2019 – 8.2%;
- April: 2017 – 12.1%, 2018 – 18.1%, 2019 – 35.8%;
- May: 2017 – 21.0%, 2018 – 28.5%, 2019 – 21.3%.

The time dependence of all measured components of air pollution in Tbilisi have fairly complicated behavior. For PM2.5, PM10, NO<sub>2</sub> and CO are satisfactorily described by the tenth order polynomial and for O<sub>3</sub> - by the fifth order polynomial (fig. 2,4,6,8,10, table 3).

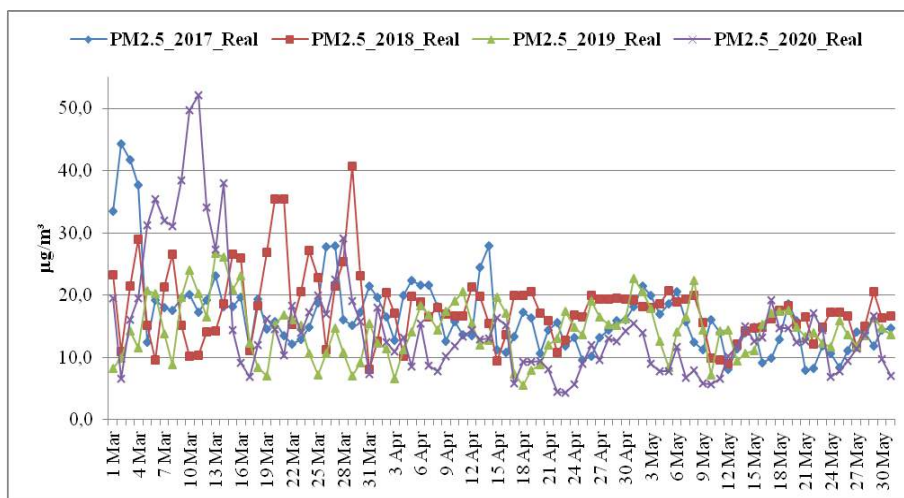


Fig. 1. Changeability of the measured values of PM2.5 in Tbilisi from 1 March through 31 May 2017-2020.

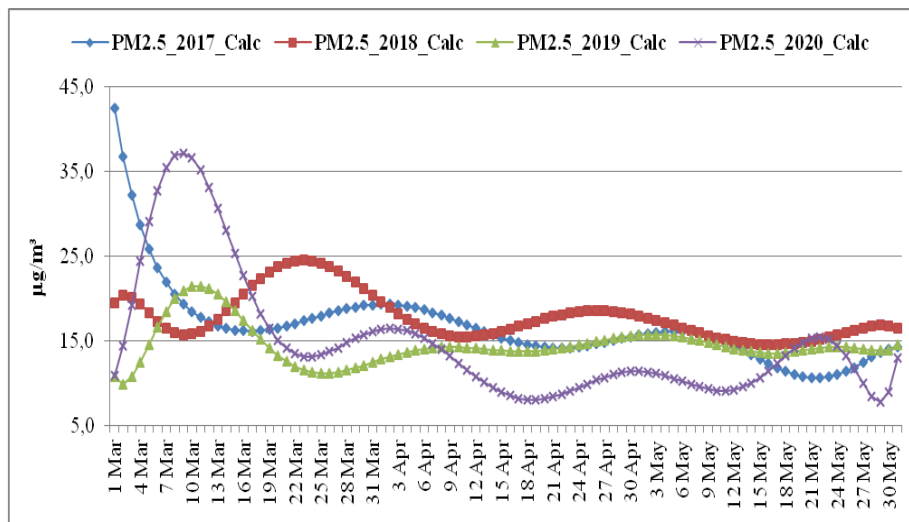


Fig. 2. Changeability of the calculated values of PM2.5 in Tbilisi from 1 March through 31 May 2017-2020.

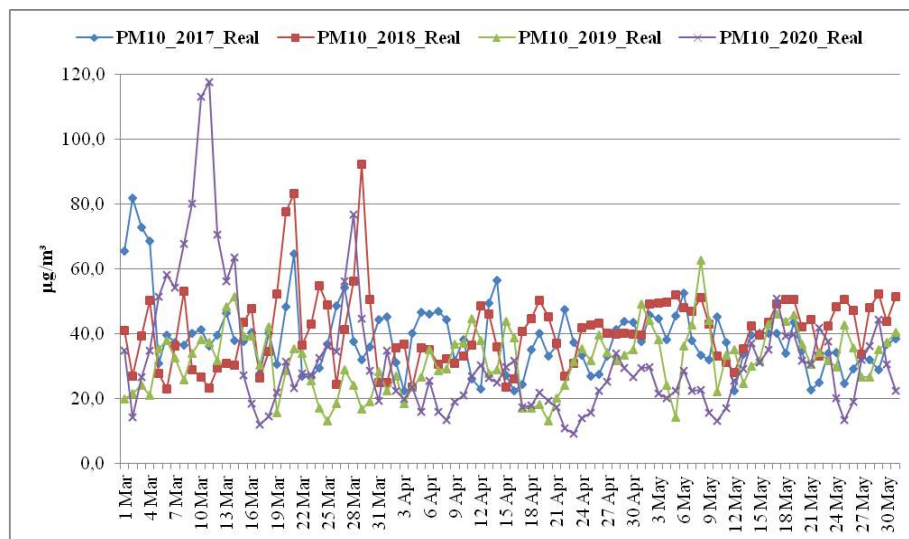


Fig. 3. Changeability of the measured values of PM10 in Tbilisi from 1 March through 31 May 2017-2020.

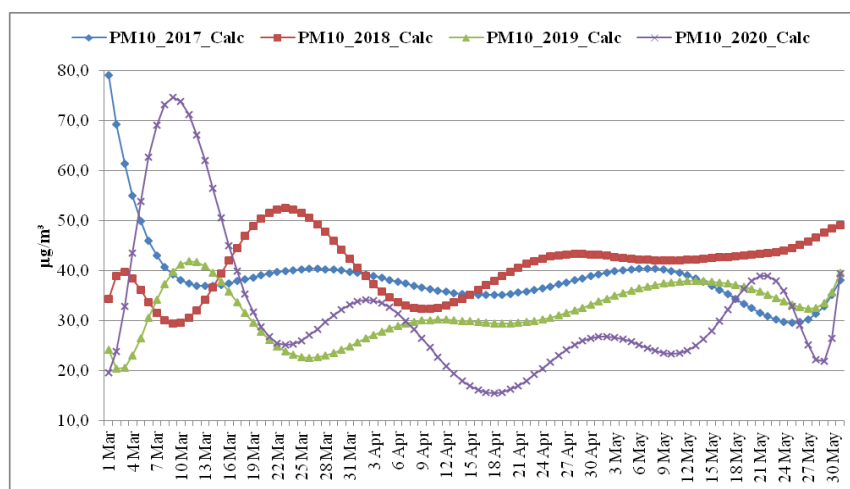


Fig. 4. Changeability of the calculated values of PM10 in Tbilisi from 1 March through 31 May 2017-2020.

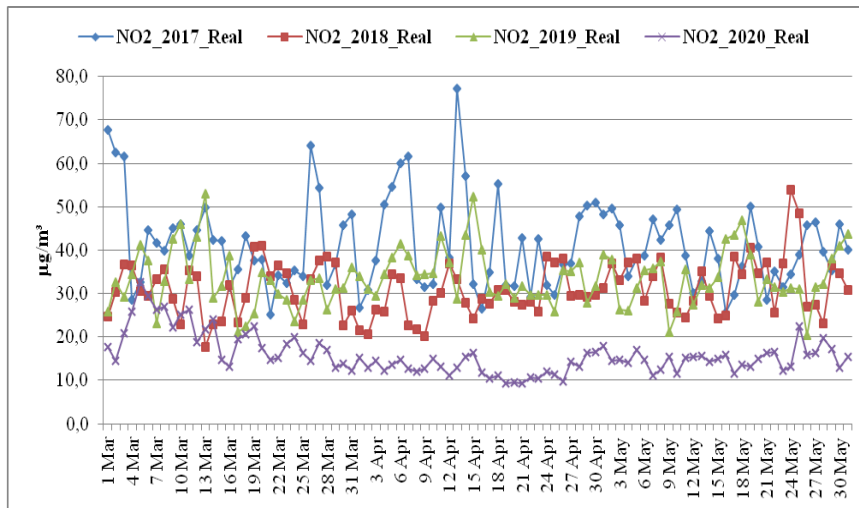


Fig. 5. Changeability of the measured values of NO<sub>2</sub> in Tbilisi from 1 March through 31 May 2017-2020.

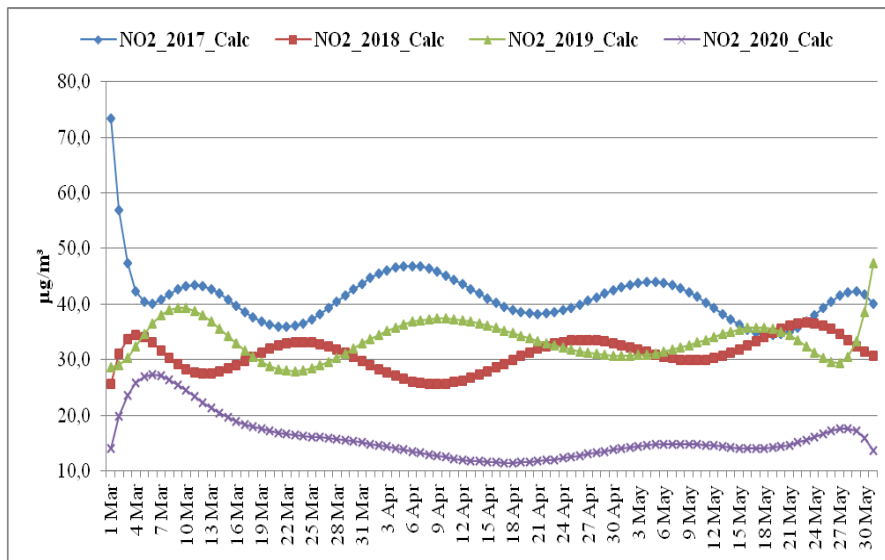


Fig. 6. Changeability of the calculated values of NO<sub>2</sub> in Tbilisi from 1 March through 31 May 2017-2020.

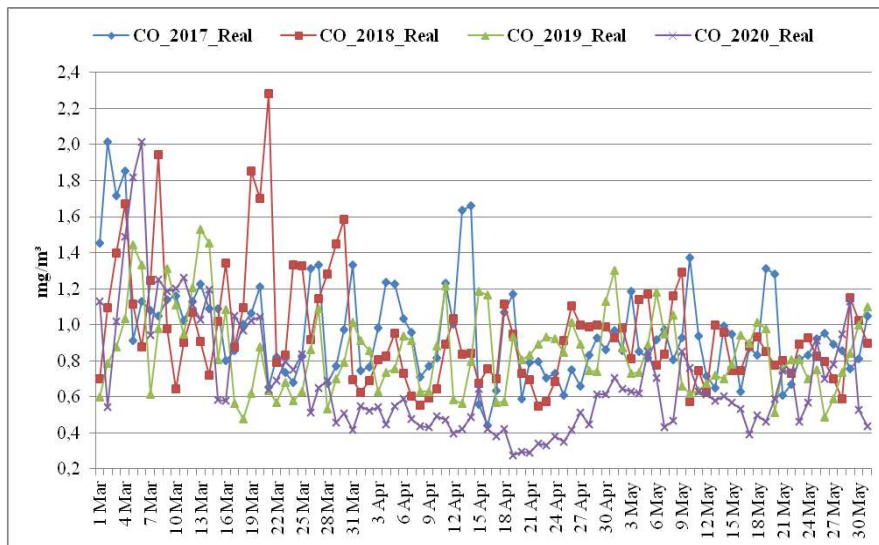


Fig. 7. Changeability of the measured values of CO in Tbilisi from 1 March through 31 May 2017-2020.

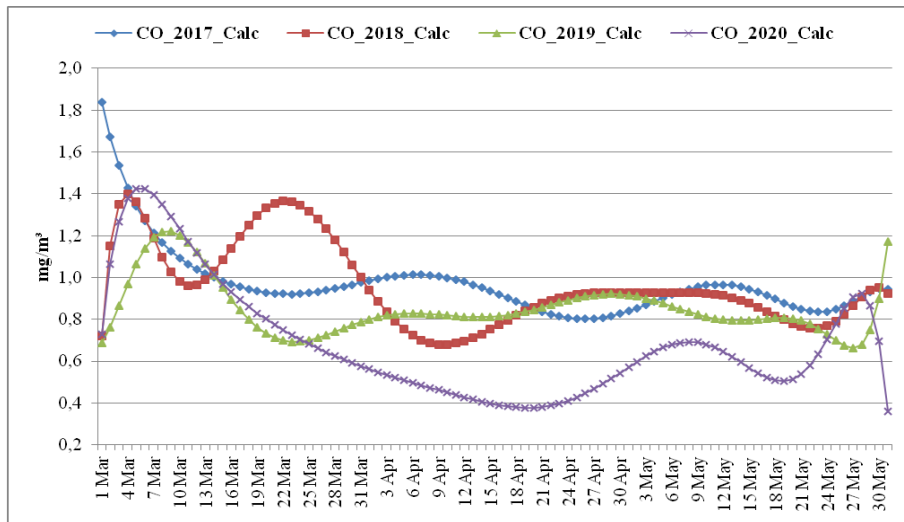


Fig. 8. Changeability of the calculated values of CO in Tbilisi from 1 March through 31 May 2017-2020.

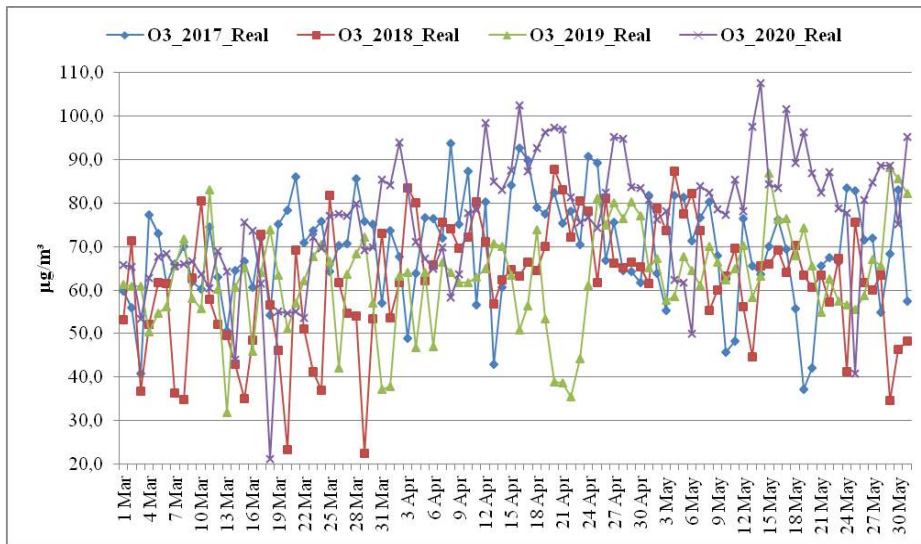


Fig. 9. Changeability of the measured values of O<sub>3</sub> in Tbilisi from 1 March through 31 May 2017-2020.

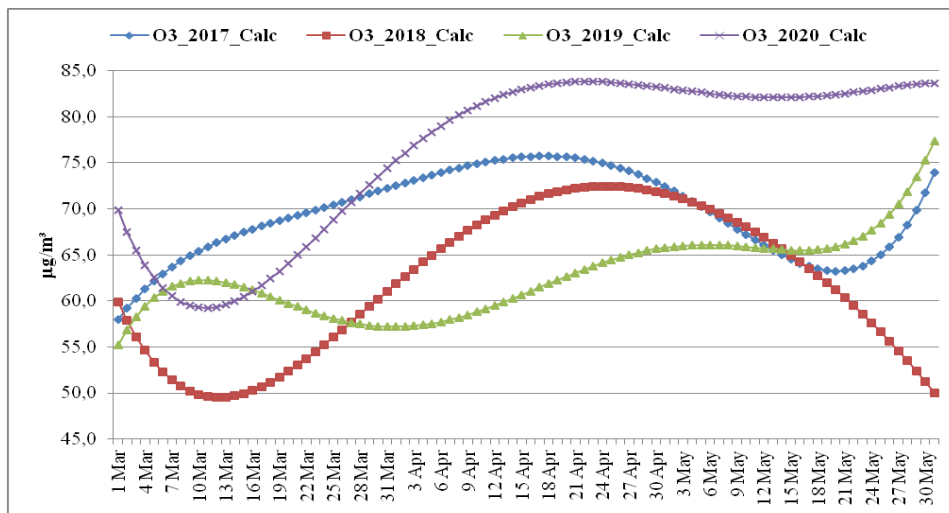


Fig. 10. Changeability of the calculated values of O<sub>3</sub> in Tbilisi from 1 March through 31 May 2017-2020.

Table 3. Form of the equations of the regression of the time changeability of the daily values of five air pollutants in Tbilisi from 1 March through 31 May 2017-2020. The level of significance of  $R^2$  is not worse than 0.001.

| Pollutant / Regression | PM2.5 / Tenth order polynomial           |                                       |                                       |                                       |
|------------------------|--|---------------------------------------|---------------------------------------|---------------------------------------|
| Year                   | 2017                                     | 2018                                  | 2019                                  | 2020                                  |
| $R^2$                  | 0.571                                    | 0.225                                 | 0.266                                 | 0.657                                 |
| $K_{DW}$               | 1.41                                     | 1.54                                  | 1.19                                  | 1.07                                  |
|                        | Positive autocorrelation of Res.         | The autocorrelation of Res. is absent | Positive autocorrelation of Res.      | Positive autocorrelation of Res.      |
| Pollutant / Regression | PM10 / Tenth order polynomial            |                                       |                                       |                                       |
| $R^2$                  | 0.412                                    | 0.228                                 | 0.307                                 | 0.535                                 |
| $K_{DW}$               | 1.58                                     | 1.37                                  | 1.23                                  | 0.75                                  |
|                        | The autocorrelation of Res. is absent    | Positive autocorrelation of Res.      | Positive autocorrelation of Res.      | Positive autocorrelation of Res.      |
| Pollutant / Regression | NO <sub>2</sub> / Tenth order polynomial |                                       |                                       |                                       |
| $R^2$                  | 0.240                                    | 0.207                                 | 0.271                                 | 0.732                                 |
| $K_{DW}$               | 1.58                                     | 1.40                                  | 1.60                                  | 1.74                                  |
|                        | The autocorrelation of Res. is absent    | Positive autocorrelation of Res.      | The autocorrelation of Res. is absent | The autocorrelation of Res. is absent |
| Pollutant / Regression | CO / Tenth order polynomial              |                                       |                                       |                                       |
| $R^2$                  | 0.352                                    | 0.370                                 | 0.306                                 | 0.734                                 |
| $K_{DW}$               | 1.63                                     | 1.63                                  | 1.61                                  | 1.92                                  |
|                        | The autocorrelation of Res. is absent    | The autocorrelation of Res. is absent | The autocorrelation of Res. is absent | The autocorrelation of Res. is absent |
| Pollutant / Regression | O <sub>3</sub> / Fifth order polynomial  |                                       |                                       |                                       |
| $R^2$                  | 0.148                                    | 0.323                                 | 0.140                                 | 0.358                                 |
| $K_{DW}$               | 1.60                                     | 1.77                                  | 1.19                                  | 1.17                                  |
|                        | The autocorrelation of Res. is absent    | The autocorrelation of Res. is absent | Positive autocorrelation of Res.      | Positive autocorrelation of Res.      |

In particular, during the period of a complete stop of automobile traffic in Georgia from April 17 to 27, 2020, compared with the same period of 2017-2019, the average measured and calculated level of air pollution in Tbilisi changed as follows (fig. 1-10):

**PM2.5.** Decrease.

Measured values: 2017 – 40.5%, 2018 – 54.3%, 2019 – 36.4%. Calculated values: 2017 – 37.5%, 2018 – 49.7%, 2019 – 36.8%.

**PM10.** Decrease.

Measured values: 2017 – 49.1%, 2018 – 56.9%, 2019 -32.2 %. Calculated values: 2017 – 47.9%, 2018 -54.1 %, 2019 – 35.7%.

**NO<sub>2</sub>.** Decrease.

Measured values: 2017 – 70.7%, 2018 – 65.4%, 2019 – 65.0%. Calculated values: 2017 – 69.2%, 2018 – 62.4%, 2019 – 63.6%.

**CO.** Decrease.

Measured values: 2017 – 53.1%, 2018 -55.8 %, 2019 -56.7 %. Calculated values: 2017 – 51.8%, 2018 – 54.1%, 2019 – 53.6%.

**O<sub>3</sub>.** Increase.

Measured values: 2017 – 9.3%, 2018 – 17.8%, 2019 – 49.8%. Calculated values: 2017 – 11.3%, 2018 – 16.0%, 2019 – 32.1%.

As is known, the comparison of ground-based observational data of the air pollution with satellite data is of significant interest. Previously similar studies we have carried out into [36-39]. The comparative analysis of satellite observations of the aerosol optical thickness of the atmosphere (AOT) with the data of ground-based measurements PM2.5 and PM10 in Tbilisi in the period of pandemic is given below.

From table 1 follows that in 2017-2019 the lowest content of PM2.5 and PM10 in Tbilisi was observed in 2019. Therefore, in this stage of studies we compared the average monthly data about AOT during April 2019 and 2020 years (fig. 11,12).

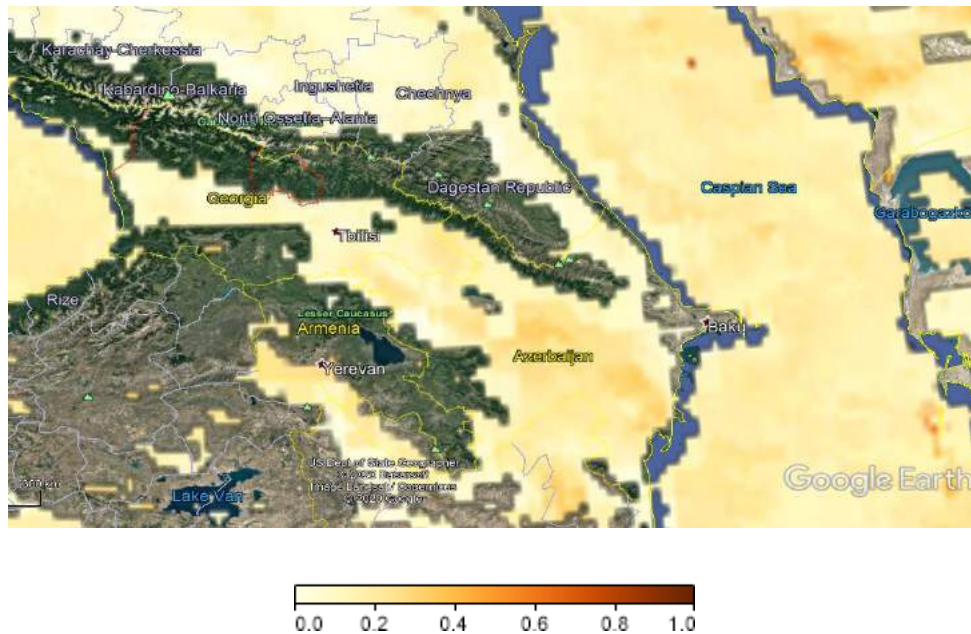


Fig. 11. Monthly mean values of AOT over the South Caucasus in April 2019.

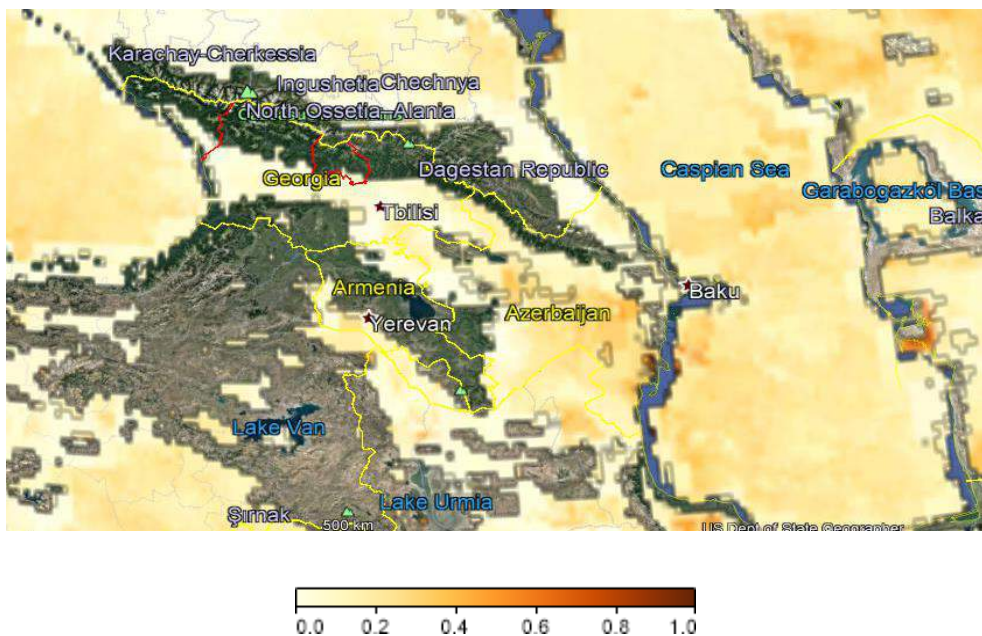


Fig. 12. Monthly mean values of AOT over the South Caucasus in April 2020.

As follows from these figures in April 2020 monthly mean values of AOT over Tbilisi is considerably lower than into 2019 (0.1 and 0.067 accordingly, decrease by 33%). Thus, the decrease of the level of the aerosol pollution of the atmosphere in Tbilisi in the period of pandemic as in [52] was fixed with satellite observations.

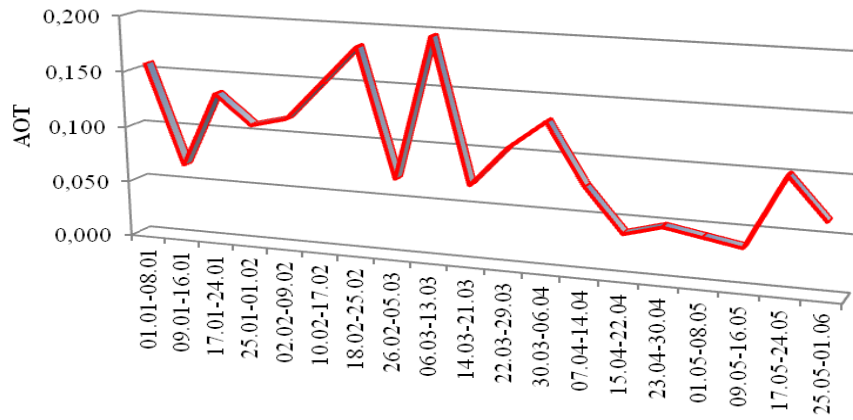


Fig. 13. Changeability of mean eight day values of AOT over Tbilisi from 1 January through 1 June 2020.

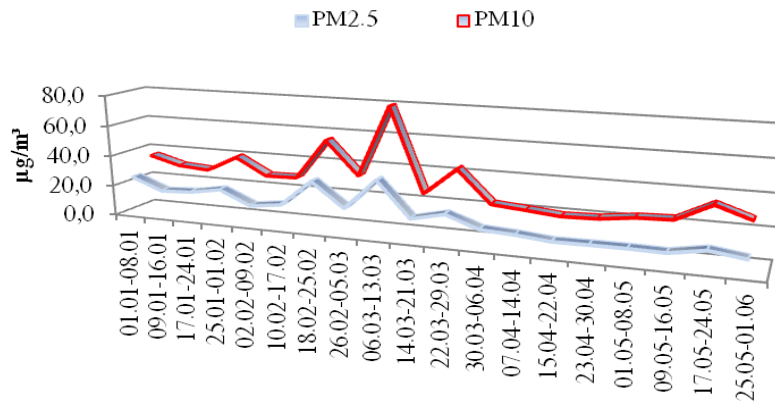


Fig. 14. Changeability of mean eight day values of PM2.5 and PM10 in Tbilisi from 1 January through 1 June 2020.

Let us finally estimate the correspondence of data of AOT satellite observations with the data of ground-based measurements of PM2.5 and PM10 in Tbilisi. In fig. 13 and 14 data about changeability of mean eight day values of AOT over Tbilisi and PM2.5 and PM10 in Tbilisi from 1 January through 1 June 2020 are presented. As follows from these figures in the time dependence of the indicated parameters of atmosphere it is observed similarity.

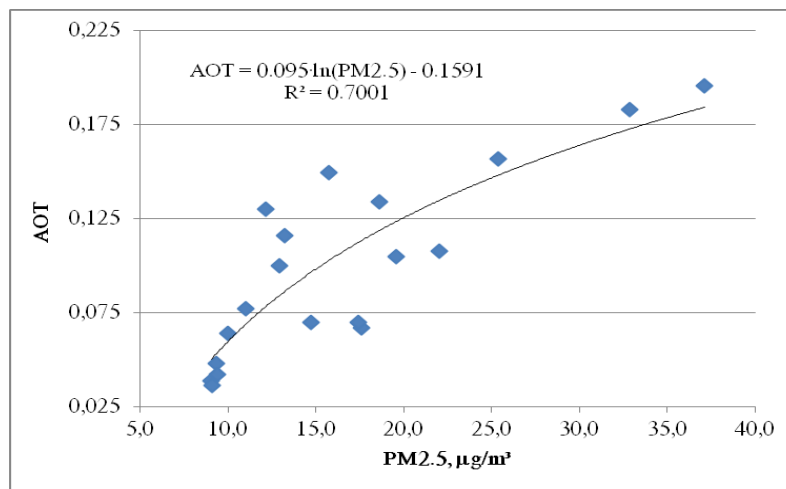


Fig. 15. Connection between mean eight day values of AOT and PM2.5 for Tbilisi from 1 January through 1 June 2020.

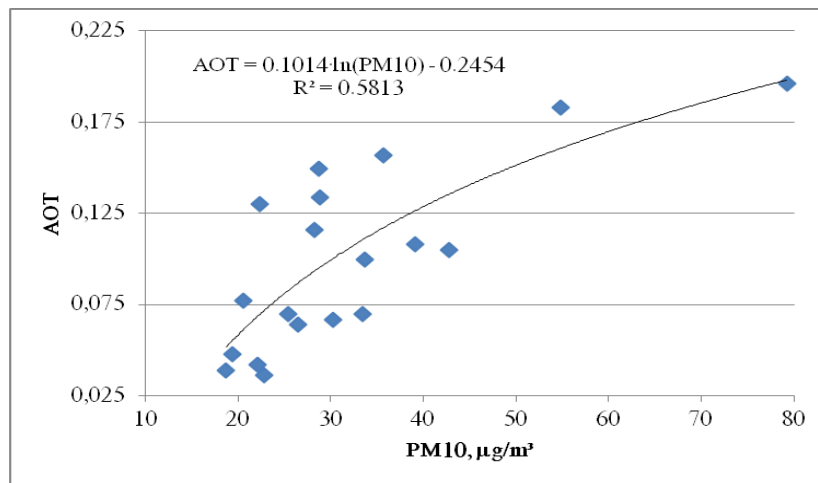


Fig. 16. Connection between mean eight day values of AOT and PM10 for Tbilisi from 1 January through 1 June 2020.

This is confirmed by fig. 15 and 16, in which curves of connection of mean eight day values of AOT with PM2.5 and PM10 for Tbilisi from 1 January through 1 June 2020 are presented. As follows from these figures the connection between AOT and PM2.5 and PM10 has logarithmic form and are sufficiently satisfactory ( $R^2 = 0.7$  and  $0.5813$  accordingly).

## Conclusion

In the near future we plan to continue analogous studies both for Tbilisi and other regions of Georgia, taking into account the new data about air pollution and different scales of averaging (hour, eight-hour, daily, eight day, monthly).

## Acknowledgments

We would like to express our deepest appreciation to all those who provided following open sources: Georgian National Environmental Agency, data about air pollution in Georgia; NASA, data of the satellite monitoring of the aerosol optical thickness of atmosphere.

## References

- [1] Kharchilava D.F., Lomaia O.V., Bukia G.N. The Conditions of Aerosols Formation and Accumulation in Cities. Proc. 3th Int. Aerosol Conf., Kyoto, Japan, Pergamon, vol. 2, 24-27 September, 1990, p. 986-989.
- [2] Amiranashvili A.G., Gzirishvili T.G. Aerosols and Ice Crystals in the Atmosphere. Tbilisi, Metsniereba, 1991, 113 p. (in Russian).
- [3] Amiranashvili A.G., Chikhladze V.A., Kharchilava J.F., Buachidze N.S., Intskirveli L.N. Variations of the Weight Concentrations of Dust, Nitrogen Oxides, Sulphur Dioxide and Ozone in the Surface Air in Tbilisi in 1981-2003, Proc. 16<sup>th</sup> International Conference on Nucleation&Atmospheric Aerosols, Kyoto, Japan, 26-30 July 2004, pp. 678-681.
- [4] Amiranashvili A.G., Amiranashvili V.A., Gzirishvili T.G., Kharchilava J.F., Tavartkiladze K.A. Modern Climate Change in Georgia. Radiatively Active Small Atmospheric Admixtures, Institute of Geophysics, Monograph, Trans. of M.Nodia Institute of Geophysics of Georgian Acad. of Sci., ISSN 1512-1135, vol. LIX, 2005, 128 p.
- [5] Amiranashvili A., Bliadze T., Chikhladze V. Photochemical smog in Tbilisi. Monograph, Trans. of Mikheil Nodia institute of Geophysics, ISSN 1512-1135, vol. 63, Tbilisi, 2012, 160 p., (in Georgian).
- [6] Kirkitadze D., Nikiforov G., Chankvetadze A., Chkhaidze G. Some Results of Studies of Atmospheric Aerosols in M. Nodia Institute of Geophysics in the Recent Three Decades. Trans. of Mikheil Nodia Institute of Geophysics, ISSN 1512-1135, vol. 66, Tbilisi, 2016, pp. 178-185, (in Russian).

- [7] Amiranashvili A. G. Boleslovas Styra. 105 Years from the Birthday. His Role in the Formation, Development and Modern Evolution of Nuclear Meteorology in Georgia. *Journal of Georgian Geophysical Society*, ISSN 1512-1127, Issue B. Physics of Atmosphere, Ocean and Space Plasma, Vol. 20 B, 2017, Tbilisi, 2017, pp. 73-87.
- [8] Kharchilava J., Amiranashvili A. Studies of Atmospheric Ozone Variations in Soviet Georgia. Results of Researches on the International Geophysical Projects, SGC, Moscow, 1998, 114 p. (in Russian).
- [9] Kharchilava J. Some Results of Investigations of Atmospheric Ozone in Georgia. *Trans. of M. Nodia Institute of Geophysics*, ISSN 1512-1135, vol. LXIX, 2018, pp. 211-219 (In Russian).
- [10] Gorchakov G.I., Emilenko A.S., Kartsivadze A.I., Metreveli D.M., Sidorov V.N. Variation of Submicron Aerosol Structure. *Proc. 9<sup>th</sup> Int. Conf. on Atmospheric Aerosols, Condensation and Ice Nuclei*, Budapest, Hungary, 3-8 September, vol.1, 1984, p. 159-163.
- [11] Amiranashvili V. Numerical Calculation of the Spectral Aerosol Optical Depth Using Data on Integral Irradiance of the Direct Solar Radiation. *Abstr. IUGG 99*, 19-30 July 1999, Birmingham UK, p. A.236.
- [12] Amiranashvili V. Modelling of Solar Radiation Transfer in the Atmosphere with Allowance to Aerosol Diffusion. *J. Aerosol Sci.*, Vol. 30, Suppl 1, Pergamon Press, 1999, p. S625-S626.
- [13] Tavartkiladze K, Shengelia I., Amiranashvili A., Amiranashvili V. The influence of relative humidity on the optical properties of atmospheric aerosols, *J. Aerosol Sci*, Pergamon, vol.30, Suppl.1, 1999, S639-S640.
- [14] Surmava A., Gigauri N., Gverdtsiteli L., Intskirveli L. Numerical Modeling of Zestafoni City Dust Distribution in Case of Background Western, Light Air, Gentle and Fresh Breezes. *Trans. of Mikheil Nodia Institute of Geophysics*, ISSN 1512-1135, vol. 69, Tbilisi, 2018, pp. 182-191, (in Georgian).
- [15] Surmava A. A. Numerical Modeling of Zestafoni City Dust Dispersion in case of Western Wind. *Journal of the Georgian Geophysical Society*, ISSN: 1512-1127, Physics of Solid Earth, Atmosphere, Ocean and Space Plasma, v. 21(2), Tbilisi, 2018, pp. 21-26.
- [16] Surmava A., Gigauri N., Kukhalashvili V., Intskirveli L., Mdivani S. Numerical Modeling of the Anthropogenic Dust Transfer by Means of Quasistatic and Non-Quasistatic Models. *International Scientific Conference "Natural Disasters in Georgia: Monitoring, Prevention, Mitigation"*. Proceedings, ISBN 978-9941-13-899-7, Publish House of Iv. Javakishvili Tbilisi State University, December 12-14, Tbilisi, 2019, pp. 134-137.
- [17] Surmava A., Intskirveli L., Kukhalashvili V., Gigauri N.. Numerical Investigation of Meso- and Microscale Diffusion of Tbilisi Dust. *Annals of Agrarian Science*, 18, No. 3, 2020 (In print).
- [18] Gigauri N.G., Gverdtsiteli L.V., Surmava A.A., Intskirveli L.N. Numerical Simulation of Industrial Dust Distribution in the Territory of Zestafoni, Georgia. *WIT Transaction on Ecology and Environment*, 230, 2018, pp. 119-128. Doi:10.2495/AIR1180111.
- [19] Kukhalashvili V.G., Kordzakhia G.I., Gigauri N.G., Surmava A.A., Intskirveli L.N. Numerical Modelling of Dust Propagation in the Atmosphere of Tbilisi City: The Case of Background Eastern Gentle Breeze. *Journal of the Georgian Geophysical Society*, ISSN: 1512-1127, Physics of Solid Earth, Atmosphere, Ocean and Space Plasma, v. 23(1), 2020, pp. 46-50.
- [20] Kukhalashvili V.G., Gigauri N.G., Surmava A.A., Demetrashvili D.I., Intskirveli L.N. Numerical Modelling of Dust Propagation in the Atmosphere of Tbilisi City: The Case of Background Eastern Fresh Breeze. *Journal of the Georgian Geophysical Society*, ISSN: 1512-1127, Physics of Solid Earth, Atmosphere, Ocean and Space Plasma, v. 23(1), 2020, pp. 51-56.
- [21] Gzirishvili T.G., Khorguani V.G. About Secondary Ice Crystal Production. *Proc. 10-th Int. Conf. Cloud Phys. Bad-Homburg, FRG*, 1988, p. 254-256.
- [22] Amiranashvili A., Bliadze T., Kirkitadze D., Nikiforov G., Nodia A., Kharchilava j., Chankvetadze A., Chikhladze V., Chochishvili K., Chkhaidze G.P. Some Preliminary Results of the Complex Monitoring of Surface Ozone Concentration (SOC), Intensity of Summary Solar Radiation and Sub-Micron Aerosols Content in Air in Tbilisi in 2009-2010. *Trans. of Mikheil Nodia Institute of Geophysics*, ISSN 1512-1135, vol. 62, Tbilisi, 2010, pp. 189-196, (in Russian).
- [23] Amiranashvili A., Chargazia Kh. Intra-Annual and Seasonal Variations of Sub-Micron Aerosols Concentration and their Connection with Radon Content in Surface Boundary Layer of Tbilisi City. *Bulletin of the Georgian National Academy of Sciences*, vol. 10, N 2, 2016, p. 72-78.
- [24] Bliadze T.G., Kirkitadze D.D., Tchankvetadze A. Sh., Chikhladze V.A. Comparative Analysis of Air Pollution in Tbilisi and Kutaisi. *International Scientific Conference „Modern Problems of Ecology“*, Proceedings, ISSN 1512-1976, v. 6, Kutaisi, Georgia, 21-22 September, 2018, pp. 157-160.

- [25] Kharchilava J., Kekenadze E., Chkhaidze G., Mchedlishvili K. Analysis of Weather Dependent Variations of Ozone Concentration in Near Earth Air in Hot Pollution Free and Pollution Pars of Tbilisi. Bulletin the Georgian Academy of sciences, 174, №3, 2006, pp. 427-430.
- [26] Kharchilava J., Kekenadze E., Bagashvili N. Investigation of Ozone Concentration Variability under Different Weather Conditions in the Ecologically Clean Surface Air as Exemplified by Ruispiri Village. Bulletin the Georgian Academy of sciences, 3, № 2, 2009, pp. 79-83.
- [27] Amiranashvili A., Kharchilava J., Chikhladze V. Statistical Characteristics of Surface Ozone Concentration in Ruispiri in 2006-2009. Journal of the Georgian Geophysical Society, Issue B. Physics of Atmosphere, Ocean and Space Plasma, ISSN 1512-1127, vol. 13B, Tbilisi, 2009, pp. 55-64.
- [28] Styra B., Amiranashvili A. Aerosol Distribution above Georgia Investigations. Institute of Physics of the Academy of Sciences of the Lithuanian SSR, Atmospheric Physics, ISSN 0135-1419, vol. 8, Vilnius, Mokslas, 1983, pp. 18-24, (in Russian).
- [29] Amiranashvili A.G., Gzirishvili T.G., Kartsivadze A.I., Nodia A.G. Aircraft investigations of the distribution of aerosols in the lower troposphere. Proc. 9<sup>th</sup> Int. Conf. on Atmospheric Aerosols, Condensation and Ice Nuclei, Budapest, Hungary, 3-8 September, vol.1, 1984, p. 148-153.
- [30] Amiranashvili A., Amiranashvili V., Chochishvili K., Kirkitadze D. The Distribution of Aerosols over the Georgian Territory in the Lower Troposphere, Journal of Georgian Geophysical Society, ISSN 1512-1127, Issue B. Physics of Atmosphere, Ocean and Space Plasma, Vol. 8 B, 2003, Tbilisi, 2004, pp. 70-76.
- [31] Amiranashvili A., Amiranashvili V., Tavartkiladze K. Dynamics of the Aerosol Pollution of the Atmosphere in Georgia in 1956-1990, J. Aerosol Sci, Pergamon, vol.30, Suppl.1, 1999, S667-S668.
- [32] Amiranashvili A.G., Amiranashvili V.A., Kirkitadze D.D., Tavartkiladze K.A. Some Results of Investigation of Variations of the Atmospheric Aerosol Optical Depth in Tbilisi, Proc. 16<sup>th</sup> Int. Conf. on Nucleation&Atmospheric Aerosols, Kyoto, Japan, 26-30 July 2004, pp. 416-419.
- [33] Amiranashvili A.G., Amiranashvili V.A., Kirkitadze D.D., Tavartkiladze K.A. Connection Between Atmospheric Aerosol Optical Depth and Aerosol Particle Number Concentration in the Air in Tbilisi, Proc. 17<sup>th</sup> Int. Conf. on Nucleation&Atmospheric Aerosols, Galway, Ireland, 13-18 August 2007, pp. 865-870.
- [34] Amiranashvili A.G., Amiranashvili V.A., Kirkitadze D.D., Tavartkiladze K.A. Weekly Distribution of the Aerosol Pollution of the Atmosphere in Tbilisi, Proc. 17<sup>th</sup> Int. Conf. on Nucleation&Atmospheric Aerosols, Galway, Ireland, 13-18 August 2007, pp. 756-760.
- [35] Amiranashvili A.G., Tavartkiladze K.A, Kirilenko A.A., Kortunova Z.V., Povolotskaya N.P., Senik I.A. Dynamics of the Aerosol Pollution of Atmosphere in Tbilisi and Koslovodsk. Trans. of the Institute of Hydrometeorology, Georgian Technical University, ISSN 1512-0902, 2013, vol. 119, pp. 212-215, (in Russian).
- [36] Stankevich S. A., Titarenko O., V., Amiranashvili A., G., Chargazia Kh., Z. Analysis of the Atmosphere Aerosol and Ozone Condition Over Tbilisi Using Satellite Data and Ground Truth Measurements. 14<sup>th</sup> Ukrainian Conference on Space Research, Uzhgorod, September, 8-12, 2014, Abstracts, Kyiv, 2014, p. 161.
- [37] Stankevich A.S., Titarenko O.V., Amiranashvili A.G., Chargazia Kh. Z. Determination of Distribution of Ozone Content in Lower Troposphere and Atmospheric Aerosol Optical Thickness over Territory of Georgia Using Satellite Data and Ground Truth Measurements. Journal of the Georgian Geophysical Society, Issue (B). Physics of Atmosphere, Ocean, and Space Plasma, ISSN: 1512-1127, v.17b, 2014, pp. 26-37.
- [38] Stankevich S., Titarenko O., Amiranashvili A., Chargazia Kh. Determination of Atmospheric Aerosol Optical Depth over Territory of Georgia during Different Regimes of Cloudiness Using the Satellite and Ground-Based Measurements Data. Bulletin of the Georgian National Academy of sciences, v. 9, No. 3, 2015, pp. 91-95.
- [39] Stankevich S., Titarenko O., Amiranashvili A., Chargazia Kh. Modeling of Ozone Content Distribution in Lower Troposphere over the Territory of Georgia Using the Data of Satellite and Ground Observations. Bulletin of the Georgian National Academy of sciences, vol. 9, No. 2, 2015, pp. 54-58.
- [40] Amiranashvili A., Amiranashvili V., Chikhladze V., Kharchilava J., Kartvelishvili L. The statistical analysis of average seasonal, semi-annual and annual values of surface ozone concentration in Tbilisi in 1984-2003. Journal of the Georgian Geophysical Society, Issue B. Physics of Atmosphere, Ocean and Space Plasma, ISSN 1512-1127, vol. 12B, Tbilisi, 2008, pp. 45-48.
- [41] Kharchilava J., Chikhladze V., Chargazia Kh. Changeability of Surface Ozone Concentration in Tbilisi in Last 30 year. International Conference “Applied Ecology: Problems, Innovations”, ICAE-2015. Proceedings, Tbilisi-Batumi, Georgia, ISBN 978-9941-0-7644-2, 7-10 May, 2015, Tbilisi, 2015, pp. 23-29.

- [42] Kekenadze E., Kharchilava J., Chkhaidze G., Senik I. Comparative Analysis of the Surface Ozone Concentration in Tbilisi and at Kislovodsk High Mountain Station. International Scientific Conference “Natural Disasters in Georgia: Monitoring, Prevention, Mitigation”. Proceedings, ISBN 978-9941-13-899-7, Publish Hous of Iv. Javakhishvili Tbilisi State University, December 12-14, Tbilisi, 2019, pp. 150-154
- [43] Amiranashvili A.G., Chikhladze V.A., Mitin M.N. Preliminary Results of the Analysis of Radar and Ground-Based Monitoring of Dust Formation in Atmosphere Above the Territory of Eastern Georgia on 27 July 2018. Journal of the Georgian Geophysical Society, ISSN: 1512-1127, Physics of Solid Earth, Atmosphere, Ocean and Space Plasma, v. 21(2), Tbilisi, 2018, pp. 61-69.
- [44] Berianidze N., Javakhishvili N. Mtchedlishvili A. About The Possibility of using the “METEOR 735CDP10” Radar for Monitoring Volcanic Formations, Dust Storms and Smoke from Large Fires in Atmosphere in South Caucasus. International Scientific Conference “Natural Disasters in Georgia: Monitoring, Prevention, Mitigation”. Proceedings, ISBN 978-9941-13-899-7, Publish Hous of Iv. Javakhishvili Tbilisi State University, December 12-14, Tbilisi, 2019, pp. 182-186.
- [45] WHO Air quality guidelines for particulate matter, ozone, nitrogen dioxide and sulfur dioxide. Global update 2005 Summary of risk assessment. World Health Organization, 2006, 22 p., [http://apps.who.int/iris/bitstream/handle/10665/69477/WHO\\_SDE\\_PHE\\_OEH\\_06.02\\_eng.pdf;jsessionid=48F380E7090ADBB4A166AC7A8610624A?sequence=1](http://apps.who.int/iris/bitstream/handle/10665/69477/WHO_SDE_PHE_OEH_06.02_eng.pdf;jsessionid=48F380E7090ADBB4A166AC7A8610624A?sequence=1)
- [46] Kirkitadze D.D. Statistical Characteristics of Aerosol Pollution of Atmosphere in Three Points of Tbilisi in 2017-2018. Journal of the Georgian Geophysical Society, ISSN: 1512-1127, Physics of Solid Earth, Atmosphere, Ocean and Space Plasma, v. 22(2), 2019, pp. 55–62.
- [47] Kekenadze E.N. Statistical Characteristics of Surface Ozone Concentration in Three Points of Tbilisi in 2017-2018. Journal of the Georgian Geophysical Society, ISSN: 1512-1127, Physics of Solid Earth, Atmosphere, Ocean and Space Plasma, v. 22(2), 2019, pp. 63–67.
- [48] Rui Bao, Acheng Zhang. Does Lockdown Reduce Air Pollution? Evidence from 44 Cities in Northern China. Science of the Total Environment, 731, 2020, 12 p., <https://doi.org/10.1016/j.scitotenv.2020.139052>
- [49] Li Li, Qing Li, Ling Huang, Qian Wang, Ansheng Zhu, Jian Xu, Ziyi Liu, Hongli Li, Lishu Shi, Rui Li, Majid Azari, Yangjun Wang, Xiaojuan Zhang, Zhiqiang Liu, Yonghui Zhu, Kun Zhang, Shuhui Xue, Maggie Chel Gee Ooi, Dongping Zhang, Andy Chan. Air Quality Changes During the COVID-19 Lockdown over the Yangtze River Delta Region: An Insight into the Impact of Human Activity Pattern Changes on Air Pollution Variation. Science of the Total Environment, 732, 2020, 11 p., <https://doi.org/10.1016/j.scitotenv.2020.139282>.
- [50] Guilherme Dantas, Bruno Siciliano, Bruno Boscaro França, Cleyton M. da Silva, Graciela Arbilla. The Impact of COVID-19 Partial Lockdown on the Air Quality of the City of Rio de Janeiro, Brazil. Science of the Total Environment, 729, 2020, 10 p. <https://doi.org/10.1016/j.scitotenv.2020.139085>
- [51] Kerimray A., Baimatova N., Ibragimova O.P., Bukenov B., Kenessov B, Plotitsyn P., Karaca F. Assessing Air Quality Changes in Large Cities During COVID-19 Lockdowns: The Impacts of Traffic-Free Urban Conditions in Almaty, Kazakhstan. Science of the Total Environment, 730, 2020, 8 p., <https://doi.org/10.1016/j.scitotenv.2020.139179>.
- [52] Lal P., Kumar A., Kumar S., Kumari S., Saikia P., Dayanandan A., Adhikari D., Khan M.L. The Dark Cloud with a Silver Lining: Assessing the Impact of the SARS COVID-19 Pandemic on the Global Environment. Science of the Total Environment, 732, 2020, 14 p., <https://doi.org/10.1016/j.scitotenv.2020.139297>.
- [53] Berman J.D., Ebisu K. Changes in U.S. Air Pollution During the COVID-19 Pandemic. Science of the Total Environment, 739, 2020, 4 p., <https://doi.org/10.1016/j.scitotenv.2020.139864>.
- [54] Kobisheva N., Narovlianski G. Climatological processing of the meteorological information, Leningrad, Gidrometeoizdat, 1978, 294 p., (in Russian).
- [55] Kendall M.G. Time-series, Moscow, 1981, 200 p., (in Russian).

# COVID-19 კორონავირუსის პანდემია და ჰაერის დაბინძურება თბილისში 2020 წლის გაზაფხულზე

ა. ამირანაშვილი, დ. კირკიტაძე, ე. კეკელიძე

## რეზიუმე

2019 წლის ბოლოს ჩინეთში, ქ. უხანში გაჩნდა კორონავირუსი COVID-19, ხოლო შემდეგ გავრცელდა მთელ მსოფლიოში და მათ შორის საქართველოშიც. ვირუსის გავრცელების სწრაფი გავრცელების კონტროლისთვის საქართველომ, ისევე როგორც სხვა ქვეყნებმა, შემოიღო შეზღუდვის ეროვნული პოლიტიკა, ჩათვალა საჭიროდ სოციალური დისტანცირება, საგზაო მოძრაობის შეზღუდვა, სამრეწველო წარმოების შეჩერება და სხვ. ამან გამოიწვია ადამიანთა საქმიანობის შემცირება, კერძოდ, ჰაერის პირველადი დამაბინძურებლების, გამონაბოლქვის შემცირება და ჰაერის ხარისხის გაუმჯობესება.

ნაშრომში მოცემულია მონაცემები საქართველოში პანდემია COVID-19 – თან დაკავშირებით შემოღებული შეზღუდვების გავლენის შესახებ თბილისში 2020 წლის გაზაფხულზე ჰაერის დაბინძურების დონის შემცირებაზე 2017 – 2019 წლების ანალოგიურ მონაცემებთან შედარებით.

ნაშრომში გამოყენებულია საქართველოში გარემოს დაცვის ეროვნული სააგენტოს მტვრის კონცენტრაციის მონაცემების საშუალო დღეღამური მნიშვნელობები (ატმოსფერული ნაწილაკები – PM<sub>2,5</sub> და PM<sub>10</sub>), NO<sub>2</sub>, CO და O<sub>3</sub>, ასევე ატმოსფეროს აეროზოლების ოპტიკური სისქის თანამგზავრული მონიტორინგის მონაცემები. კერძოდ, შეინიშნება ჰაერში ოზონის შემცველობის არსებითი მატება და ჰაერის სხვა დამაბინძურებლების მნიშვნელოვანი შემცირება.

## Пандемия коронавируса COVID-19 и загрязнение воздуха в Тбилиси весной 2020 года

А.Г. Амиранашвили, Д.Д. Киркитадзе, Э.Н. Кекенадзе

### Резюме

В конце 2019 года новый коронавирус COVID-19 появился в Ухане, Китай, а затем распространился по всему миру, включая Грузию. Чтобы контролировать быстрое распространение вируса, Грузия, как и другие страны, ввела национальную политику сдерживания, с тем чтобы учесть социальное дистанцирование, ограничение автомобильного движения, работы промышленных предприятий и т. д. Это привело к сокращению человеческой деятельности и, следовательно, к выбросам первичных загрязнителей воздуха, что вызвало улучшение качества воздуха.

В работе приводятся данные о влиянии этих ограничений в Грузии в связи с пандемией COVID-19 на снижение уровня загрязнения воздуха в Тбилиси весной 2020 года по сравнению с аналогичным периодом в 2017-2019 годах.

В работе использованы данные Национального агентства по охране окружающей среды Грузии о среднесуточных значениях концентрации пыли (атмосферные частицы - PM<sub>2,5</sub> и PM<sub>10</sub>), NO<sub>2</sub>, CO и O<sub>3</sub>, а также данные спутникового мониторинга аэрозольной оптической толщи атмосферы. В частности, отмечается существенный рост содержания озона в воздухе и значительное уменьшение остальных загрязнителей атмосферы.

## Statistical Characteristics of the Daily Max of Wind Speed in Kakheti in 2017-2019

<sup>1</sup>Avtandil G. Amiranashvili, <sup>1</sup>Victor A. Chikhladze,  
<sup>2,3</sup>Gvantsa D. Gvasalia, <sup>2</sup>Davit A. Loladze

<sup>1</sup>M. Nodia Institute of Geophysics of I. Javakishvili Tbilisi State University,  
e-mail:avtandilamiranashvili@gmail.com

<sup>2</sup>National Environmental Agency of Georgia

<sup>3</sup>State Military Scientific-Technical Center "DELTA"

### ABSTRACT

The statistical analysis of the daily maximum speed of wind ( $W$ ) for 13 points of Kakheti in the period from 1 January 2017 through 31 December of 2019 is represented.

In particular, the following results are obtained: mean monthly and seasonal (warm and cold half-years, year) values of  $W$  for all stations during entire period of observations are calculated; it is shown that the distributions of mean monthly values of  $W$  in the territory of Kakheti has the uneven nature and changes from 0.7 m/sec (Tsnori, November) to 9.5 m/sec (Sagarejo, June); the map of the distribution of mean annual values of  $W$  in the territory of Kakheti is given; repetition of daily values of  $W$  for all points of Kakheti in accordance with the Beaufort Wind Scale is studied; it is shown that the value of the linear correlation coefficient  $R$  between the stations in terms of all daily values of  $W$  on the average compose 0.45 and change from 0.15 to 0.83, for the cold half-year - 0.54 (it changes from 0.26 to 0.87), for the warm half-year - 0.36 (it changes from 0.03 to 0.78); the dependence of the linear correlation coefficient between the stations by values of  $W$  from the distance between them is studied (with an increase in the distance between the stations value of  $R$  diminishes in the correspondence with the power function); the dependence of  $W$  on the height of the stations arrangement on the average in the year, into the cold and warm half-years is studied.

**Key words:** Local climate, max wind speed.

### 1. Introduction

Wind is one of the most important climate-forming factors. Therefore in Georgia, as in other countries, to studies of the wind regime is paid special attention. Significant number of works is devoted to the climatology of wind, changeability of its regime [1-4]. Information about the wind regime is important for the development wind-power engineers, agrarian sector of economy [1,3], etc. High wind frequently it leads to the destruction of habitable and production units, the stoppage of the work of airports, the appearance of blizzards, the intensification of the negative consequences of other dangerous hydrometeorological phenomena (intensive precipitations, hail, etc.), human victims, etc. [5-9]. On wind speed depends the level of the air pollution [10-12]. Wind is also one of the most important bioclimatic factors. Therefore information about the wind regime is important for the development of health resort - tourism sector of economy [13-14] by the estimations of different simple and complex bioclimatic indices for the specific territories [15-20].

Since 2015 in Kakheti region of Georgia is restored the work of anti-hail service [21,22]. During the estimation of damage from the hail damages frequently is also necessary the information about other associated extreme meteorological elements, including wind speed [9]. In addition to this, the data about the regime of extreme wind are necessary for the optimum distribution of the points of action on clouds, etc. [22,23].

In connection with that indicated was set the task of investigating the regime of maximum daily wind speed in Kakheti, the special features of its distribution in the investigated territory, the comparison of the wind regime in the days with the hail with the non hail days, developments the possible connection between the data about the extreme wind on the earth's surface with the data of the radar measurements of the wind speed on 2-2.5 km [24]. In this stage of these studies is carried out the detailed statistical analysis of the

daily maximum wind speed for 13 points of Kakheti in the period from 1 January 2017 through 31 December of 2019, whose results are represented below.

## 2. Study area, material and methods

Study area – 13 locations of Kakheti region of Georgia. Coordinates of these locations of wind speed measurements points in table 1 are presented. Distance from these meteorological stations in table 2 are presented.

The data of Georgian National Environmental Agency about the daily max values of wind speed (W) on 13 indicated stations are used. Period of observation: January 1, 2017- December 31, 2019.

In the proposed work the analysis of data is carried out with the use of the standard statistical analysis methods [25]. Missed data of time-series of observations were restored in the correspondence with the standard methods [25].

The following designations will be used below: Mean – average values; Min – minimal values; Max - maximal values; Range – Max-Min; Median – median values; St Dev - standard deviation; Cv – coefficient of variation, %;  $R^2$  – coefficient of determination; R – coefficient of linear correlation; 99%\_L and 99%\_U - accordingly, 99% upper and lower levels of the confidence interval of average;  $\alpha$  - the level of significance. Cold period: October-March, warm period: April-September. The following rule of thumb for interpreting the size of a correlation coefficient is used [26] :  $0 \leq R < 0.3$  - Negligible correlation,  $0.3 \leq R < 0.5$  - Low correlation,  $0.5 \leq R < 0.7$  - Moderate correlation,  $0.7 \leq R < 0.9$  - High correlation,  $0.9 \leq R \leq 1.0$  - Very high correlation.

Table 1. Coordinates of 13 meteorological stations in Kakheti.

| Location              | Location (Abbrev.) | Long., E° | Lat, N° | Height (H), m (a.s.l.) |
|-----------------------|--------------------|-----------|---------|------------------------|
| Tsnori                | Tsn.               | 45.993    | 41.612  | 501                    |
| Kindzmarauli- Khareba | Kindz.             | 45.810    | 41.612  | 360                    |
| Telavi (Wine Cellar)  | Tel.               | 45.603    | 41.959  | 378                    |
| Saniore               | San.               | 45.489    | 42.051  | 550                    |
| Vachnadziani-Khareba  | Vachn.             | 45.657    | 41.867  | 496                    |
| Ruispiri              | Ruisp.             | 45.401    | 41.964  | 550                    |
| Dzveli Anaga          | Dz. An.            | 46.068    | 41.559  | 395                    |
| Bakurtsikhe           | Bakur.             | 45.935    | 41.733  | 236                    |
| Zemo Kedi             | Z. Kedi            | 46.381    | 41.421  | 681                    |
| Sagarejo              | Sagar.             | 45.368    | 41.650  | 580                    |
| Khornabuji            | Khorn.             | 46.181    | 41.513  | 251                    |
| Naendrovali           | Naendr.            | 46.068    | 41.760  | 230                    |
| Kistauri              | Kist.              | 45.269    | 42.005  | 519                    |

Table 2. Distance from 13 meteorological stations in Kakheti between itself (km).

|         | Tsn. | Kindz. | Tel. | San. | Vachn. | Ruisp. | Dz. An. | Bakur. | Z. Kedi | Sagar. | Khorn. | Naendr. | Kist. |
|---------|------|--------|------|------|--------|--------|---------|--------|---------|--------|--------|---------|-------|
| Tsn.    | 0    | 15     | 50   | 64   | 40     | 63     | 9       | 14     | 39      | 52     | 19     | 18      | 74    |
| Kindz.  | 15   | 0      | 42   | 56   | 31     | 52     | 22      | 17     | 52      | 37     | 33     | 27      | 63    |
| Tel.    | 50   | 42     | 0    | 14   | 11     | 17     | 59      | 37     | 88      | 40     | 69     | 44      | 28    |
| San.    | 64   | 56     | 14   | 0    | 25     | 12     | 73      | 51     | 102     | 46     | 83     | 58      | 19    |
| Vachn.  | 40   | 31     | 11   | 25   | 0      | 24     | 48      | 27     | 78      | 34     | 59     | 36      | 36    |
| Ruisp.  | 63   | 52     | 17   | 12   | 24     | 0      | 71      | 51     | 101     | 35     | 82     | 60      | 12    |
| Dz. An. | 9    | 22     | 59   | 73   | 48     | 71     | 0       | 22     | 30      | 59     | 11     | 22      | 83    |
| Bakur.  | 14   | 17     | 37   | 51   | 27     | 51     | 22      | 0      | 51      | 48     | 32     | 11      | 63    |
| Z. Kedi | 39   | 52     | 88   | 102  | 78     | 101    | 30      | 51     | 0       | 88     | 20     | 46      | 113   |
| Sagar.  | 52   | 37     | 40   | 46   | 34     | 35     | 59      | 48     | 88      | 0      | 69     | 59      | 40    |
| Khorn.  | 19   | 33     | 69   | 83   | 59     | 82     | 11      | 32     | 20      | 69     | 0      | 29      | 93    |
| Naendr. | 18   | 27     | 44   | 58   | 36     | 60     | 22      | 11     | 46      | 59     | 29     | 0       | 72    |
| Kist.   | 74   | 63     | 28   | 19   | 36     | 12     | 83      | 63     | 113     | 40     | 93     | 72      | 0     |

### 3. Results and discussion

Results in the fig. 1-8 and table 1-9 are presented.

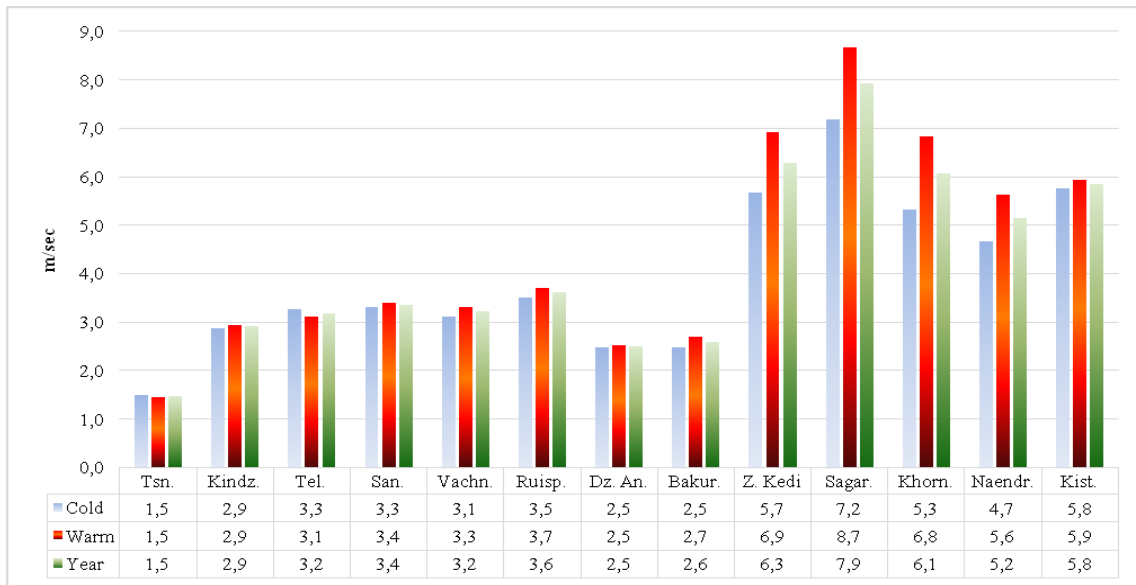


Fig. 1. Mean values of daily max of wind speed in Kakheti in 2017-2019 in three periods of year.

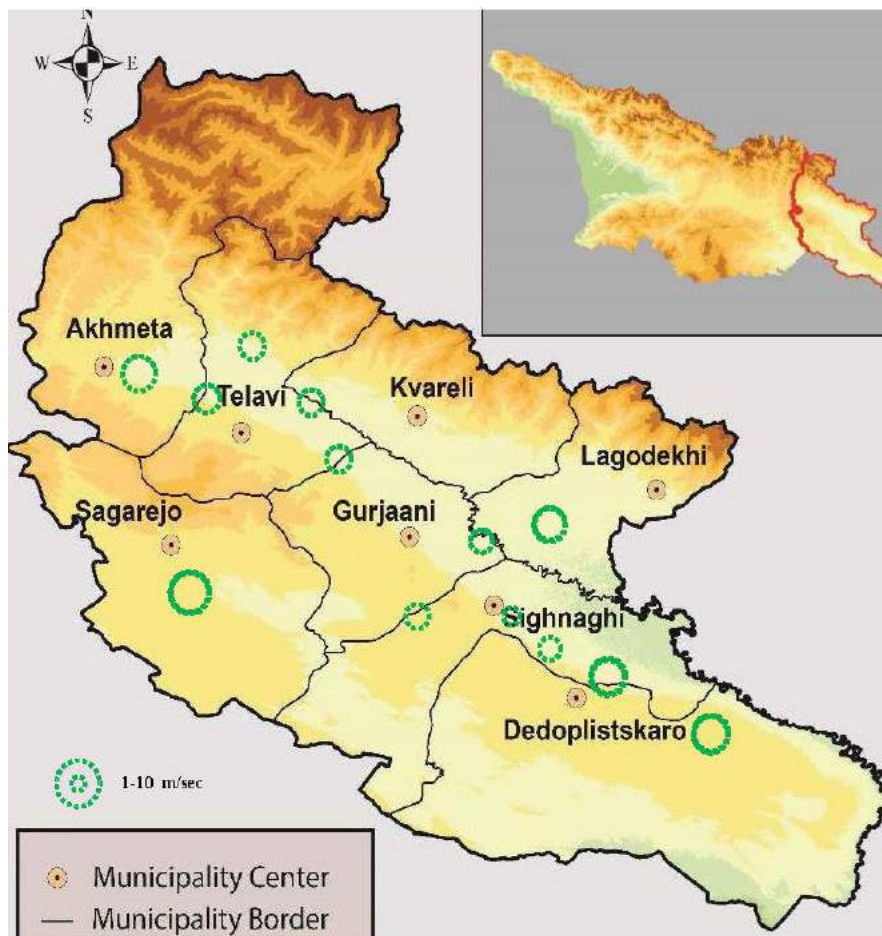


Fig. 2. Distribution of mean annual values of daily max of wind speed in Kakheti in 2017-2019.

As it follows from fig. 1, the smallest and greatest mean values of W in the year, into the cold and warm half-years in Kakheti change from 1.5 m/sec (Tsnori) to 7.9, 7.2 and 8.7 m/sec (Sagarejo). On the stations Tsnori, Kindzmarauli- Khareba, Telavi (Wine Cellar), Saniore, Vachnadziani-Khareba, Ruispiri, Dzveli Anaga, Bakurtsikhe and Kistauri the mean values of W during the three indicated periods of year either identical or differ little from each other.

At the stations Zemo Kedi, Sagarejo, Khornabuji and Naendrovali into the warm half-year mean values of W on 20.8-28.0 % are higher than into the cold and by 9.4-12.3 % higher than on the average in the year. It also follows from fig. 1 that the distribution of W values on the territory of Kakheti has heterogeneous nature. For the clarity fig. 2 gives the map of distribution of mean monthly values of W on the investigated territory.

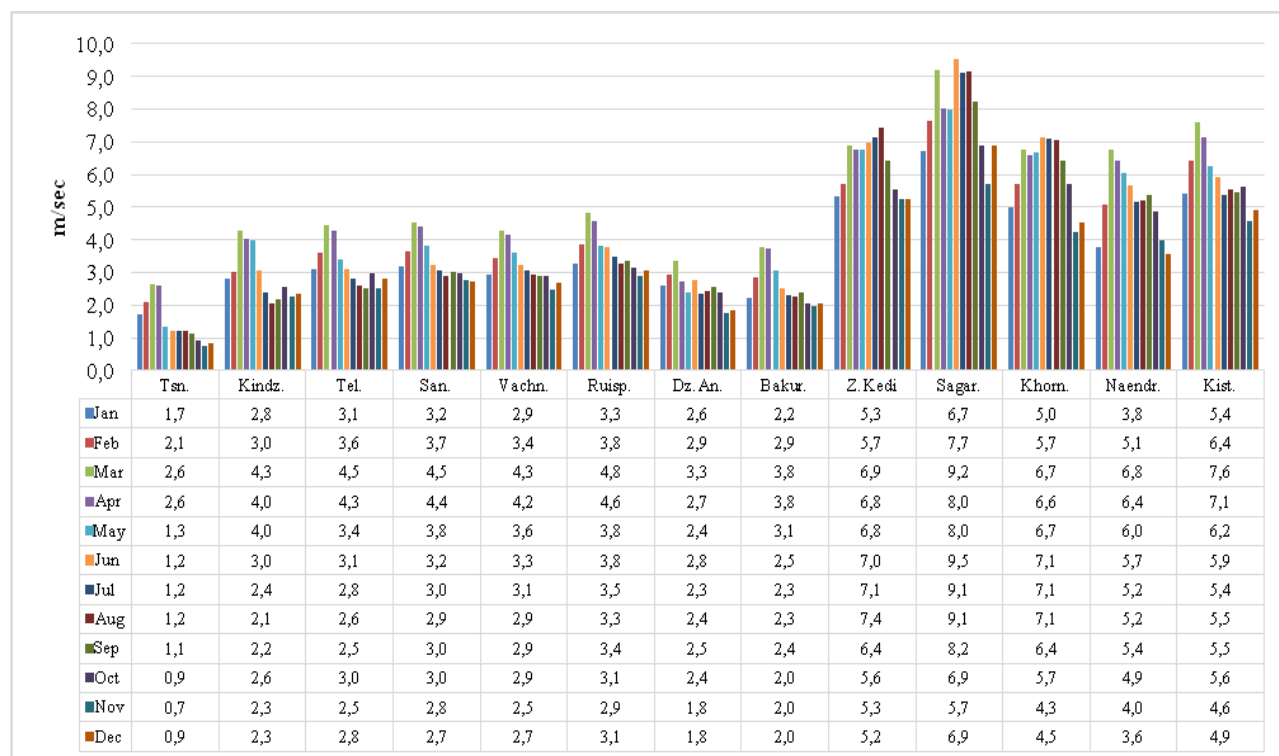


Fig. 3. Mean values of daily max of wind speed in Kakheti in 2017-2019 in different months of year.

Fig. 3 presents the data about mean monthly values of W on the Kakheti territory. As it follows from this figure, the intra-annual distribution of W values for all stations as a whole takes the single-modal form. The range of changes in the values of W for the separate stations is the following:

Tsn.: 0.7 m/sec (Nov) – 2.6 m/sec (Mar, Apr); Kindz.: 2.1 m/sec (Aug) – 4.3 m/sec (Mar); Tel.: 2.5 m/sec (Sep, Nov) – 4.5 m/sec (Mar); San.: 2.7 m/sec (Dec) – 4.5 m/sec (Mar); Vachn.: 2.5 m/sec (Nov) – 4.3 m/sec (Mar); Ruisp.: 2.9 m/sec (Nov) – 4.8 m/sec (Mar); Dz. An.: 1.8 m/sec (Nov, Dec) – 3.3 m/sec (Mar); Bakur.: 2.0 m/sec (Oct-Dec) – 3.8 m/sec (Mar-Apr); Z. Kedi: 5.2 m/sec (Dec) – 7.4 m/sec (Aug); Sagar.: 5.7 m/sec (Nov) – 9.5 m/sec (Jun); Khorn.: 4.3 m/sec (Nov) – 7.1 m/sec (Jun-Aug); Naendr.: 3.6 m/sec (Dec) – 6.8 m/sec (Mar); Kist.: 4.6 m/sec (Nov) – 7.6 m/sec (Mar).

In the season of anti-hail works (April- October) the range of changes in the values of W for the separate stations is following:

Tsn.: 0.9 m/sec (Oct) – 2.6 m/sec (Apr); Kindz.: 2.1 m/sec (Aug) – 4.0 m/sec (Apr, May); Tel.: 2.5 m/sec (Sep) – 4.3 m/sec (Apr); San.: 2.9 m/sec (Aug) – 4.4 m/sec (Apr); Vachn.: 2.9 m/sec (Aug-Oct) – 4.2 m/sec (Apr); Ruisp.: 3.1 m/sec (Oct) – 4.6 m/sec (Apr); Dz. An.: 2.3 m/sec (Jul) – 2.8 m/sec (Jun); Bakur.: 2.0 m/sec (Oct) – 3.8 m/sec (Apr); Z. Kedi: 5.6 m/sec (Oct) – 7.4 m/sec (Aug); Sagar.: 6.9 m/sec (Oct) – 9.5 m/sec (Jun); Khorn.: 5.7 m/sec (Oct) – 7.1 m/sec (Jun-Aug); Naendr.: 4.9 m/sec (Oct) – 6.4 m/sec (Apr); Kist.: 5.4 m/sec (Jul) – 7.1 m/sec (Apr).

Table 3 presents the data about statistical characteristics of daily max of wind speed in Kakheti in 2017-2019 in different months of year. The range of changes in the daily values of W for the separate stations is following: Tsn.: 0.0 m/sec (Feb, Apr, May, Jun) – 9.3 m/sec (Apr); Kindz.: 0.6 m/sec (Nov) – 12.5

m/sec (Apr); Tel.: 0.5 m/sec (Nov) – 10.3 m/sec (Mar); San.: 0.0 m/sec (Jan, Feb) – 13.4 m/sec (Apr); Vachn.: 0.6 m/sec (Jan) – 10.9 m/sec (Jan, Apr); Ruisp.: 0.0 m/sec (May, Oct) – 11.6 m/sec (Mar); Dz. An.: 0.0 m/sec (May, Jul, Aug, Dec) – 9.0 m/sec (Sep); Bakur.: 0.2 m/sec (Dec) – 11.0 m/sec (May); Z. Kedi: 1.6 m/sec (Feb) – 16.3 m/sec (Aug); Sagar.: 1.5 m/sec (Dec) – 31.2 m/sec (Jun); Khorn.: 1.7 m/sec (Feb) – 18.6 m/sec (Dec); Naendr.: 1.4 m/sec (Dec) – 20.8 m/sec (Oct); Kist.: 1.2 m/sec (Nov) – 22.1 m/sec (Jan).

Table 3. Statistical characteristics of daily max of wind speed in Kakheti in 2017-2019 in different months of year.

| Month | Param. | Location |        |      |      |        |        |         |        |         |        |        |         |
|-------|--------|----------|--------|------|------|--------|--------|---------|--------|---------|--------|--------|---------|
|       |        | Tsn.     | Kindz. | Tel. | San. | Vachn. | Ruisp. | Dz. An. | Bakur. | Z. Kedi | Sagar. | Khorn. | Naendr. |
| Jan   | min    | 0.4      | 0.9    | 0.6  | 0.0  | 0.6    | 1.4    | 0.1     | 0.6    | 2.6     | 2.1    | 2.2    | 1.5     |
| Jan   | max    | 5.0      | 7.5    | 9.5  | 9.8  | 10.9   | 8.3    | 8.4     | 7.1    | 12.6    | 18.8   | 15.1   | 11.4    |
| Jan   | 99%_L  | 1.4      | 2.4    | 2.7  | 2.8  | 2.6    | 2.9    | 2.1     | 1.9    | 4.9     | 5.8    | 4.4    | 3.3     |
| Jan   | 99%_U  | 2.0      | 3.2    | 3.5  | 3.6  | 3.3    | 3.6    | 3.0     | 2.5    | 5.8     | 7.7    | 5.6    | 4.2     |
| Feb   | min    | 0.0      | 1.0    | 1.3  | 0.0  | 1.4    | 1.4    | 1.1     | 0.5    | 1.6     | 2.2    | 1.7    | 2.4     |
| Feb   | max    | 7.7      | 8.5    | 8.1  | 7.1  | 8.4    | 8.9    | 6.7     | 6.5    | 14.2    | 21.0   | 17.2   | 14.6    |
| Feb   | 99%_L  | 1.7      | 2.5    | 3.2  | 3.3  | 3.0    | 3.3    | 2.5     | 2.5    | 5.0     | 6.3    | 4.8    | 4.4     |
| Feb   | 99%_U  | 2.5      | 3.5    | 4.0  | 4.1  | 3.9    | 4.4    | 3.3     | 3.2    | 6.4     | 9.0    | 6.6    | 5.7     |
| Mar   | min    | 0.8      | 1.1    | 1.6  | 2.3  | 2.0    | 2.0    | 1.5     | 1.4    | 4.0     | 3.1    | 2.6    | 3.0     |
| Mar   | max    | 7.1      | 12.3   | 10.3 | 9.0  | 9.5    | 11.6   | 8.4     | 9.8    | 14.8    | 19.4   | 14.7   | 16.2    |
| Mar   | 99%_L  | 2.3      | 3.6    | 4.0  | 4.1  | 3.8    | 4.2    | 3.0     | 3.4    | 6.3     | 8.2    | 6.0    | 6.0     |
| Mar   | 99%_U  | 3.0      | 4.9    | 4.9  | 5.0  | 4.7    | 5.4    | 3.7     | 4.2    | 7.5     | 10.2   | 7.5    | 7.6     |
| Apr   | min    | 0.0      | 1.5    | 1.9  | 2.4  | 2.6    | 2.0    | 1.1     | 1.1    | 3.7     | 3.9    | 3.4    | 2.9     |
| Apr   | max    | 9.3      | 12.5   | 10.1 | 13.4 | 10.9   | 11.3   | 6.8     | 10.4   | 15.3    | 17.9   | 15.0   | 18.5    |
| Apr   | 99%_L  | 2.1      | 3.3    | 3.8  | 4.0  | 3.8    | 4.0    | 2.4     | 3.3    | 6.1     | 7.1    | 6.0    | 5.6     |
| Apr   | 99%_U  | 3.1      | 4.7    | 4.7  | 4.9  | 4.6    | 5.1    | 3.1     | 4.2    | 7.4     | 9.0    | 7.2    | 7.2     |
| May   | min    | 0.0      | 1.6    | 1.2  | 1.9  | 2.0    | 0.0    | 0.0     | 1.2    | 3.9     | 3.6    | 3.2    | 2.4     |
| May   | max    | 7.1      | 9.9    | 8.9  | 7.0  | 10.4   | 7.6    | 5.6     | 11.0   | 13.5    | 18.3   | 13.5   | 15.0    |
| May   | 99%_L  | 0.9      | 3.5    | 3.1  | 3.5  | 3.3    | 3.4    | 2.1     | 2.7    | 6.2     | 7.1    | 6.0    | 5.3     |
| May   | 99%_U  | 1.8      | 4.5    | 3.7  | 4.2  | 3.9    | 4.3    | 2.7     | 3.5    | 7.4     | 8.8    | 7.3    | 6.8     |
| Jun   | min    | 0.0      | 1.3    | 1.3  | 1.8  | 1.7    | 2.0    | 1.4     | 0.8    | 4.3     | 3.2    | 4.1    | 2.5     |
| Jun   | max    | 2.6      | 8.9    | 8.2  | 6.8  | 8.3    | 7.8    | 6.8     | 6.1    | 13.3    | 31.2   | 16.8   | 14.7    |
| Jun   | 99%_L  | 1.1      | 2.6    | 2.7  | 2.9  | 2.9    | 3.4    | 2.4     | 2.2    | 6.5     | 8.2    | 6.6    | 5.0     |
| Jun   | 99%_U  | 1.4      | 3.5    | 3.5  | 3.5  | 3.6    | 4.1    | 3.1     | 2.8    | 7.5     | 10.8   | 7.7    | 6.3     |
| Jul   | min    | 0.5      | 1.1    | 0.8  | 1.7  | 1.8    | 2.1    | 0.0     | 1.0    | 4.1     | 4.1    | 2.0    | 2.3     |
| Jul   | max    | 2.6      | 6.7    | 7.5  | 5.6  | 7.0    | 7.2    | 8.9     | 6.5    | 13.7    | 29.4   | 15.8   | 12.9    |
| Jul   | 99%_L  | 1.1      | 2.1    | 2.5  | 2.8  | 2.8    | 3.2    | 1.9     | 2.0    | 6.7     | 8.0    | 6.4    | 4.6     |
| Jul   | 99%_U  | 1.3      | 2.7    | 3.1  | 3.3  | 3.4    | 3.8    | 2.8     | 2.6    | 7.6     | 10.2   | 7.7    | 5.7     |
| Aug   | min    | 0.5      | 1.0    | 0.6  | 1.1  | 1.7    | 1.5    | 0.0     | 1.1    | 4.7     | 3.8    | 3.6    | 3.0     |
| Aug   | max    | 2.1      | 4.9    | 6.3  | 4.6  | 7.1    | 6.0    | 4.4     | 6.5    | 16.3    | 28.5   | 14.2   | 13.7    |
| Aug   | 99%_L  | 1.1      | 1.9    | 2.4  | 2.7  | 2.7    | 3.0    | 2.2     | 2.0    | 6.8     | 8.0    | 6.5    | 4.7     |
| Aug   | 99%_U  | 1.3      | 2.2    | 2.8  | 3.1  | 3.2    | 3.5    | 2.7     | 2.5    | 8.0     | 10.2   | 7.6    | 5.7     |
| Sep   | min    | 0.4      | 0.7    | 0.8  | 0.8  | 1.4    | 1.3    | 1.0     | 1.0    | 2.9     | 3.0    | 2.8    | 2.7     |
| Sep   | max    | 3.2      | 6.8    | 7.9  | 6.3  | 10.0   | 9.8    | 9.0     | 5.9    | 16.1    | 19.1   | 15.1   | 15.9    |
| Sep   | 99%_L  | 1.0      | 1.9    | 2.2  | 2.8  | 2.5    | 2.9    | 2.2     | 2.0    | 5.9     | 7.2    | 5.8    | 4.7     |
| Sep   | 99%_U  | 1.3      | 2.4    | 2.9  | 3.2  | 3.3    | 3.8    | 2.9     | 2.7    | 7.0     | 9.2    | 7.1    | 6.1     |
| Oct   | min    | 0.3      | 1.1    | 1.2  | 1.4  | 1.4    | 0.0    | 1.1     | 0.9    | 3.3     | 2.5    | 2.4    | 2.0     |
| Oct   | max    | 2.3      | 8.5    | 7.4  | 7.2  | 9.0    | 10.4   | 7.3     | 6.6    | 15.3    | 18.8   | 16.6   | 20.8    |
| Oct   | 99%_L  | 0.8      | 2.2    | 2.5  | 2.7  | 2.5    | 2.7    | 2.0     | 1.7    | 5.0     | 5.8    | 5.0    | 4.1     |
| Oct   | 99%_U  | 1.0      | 2.9    | 3.5  | 3.3  | 3.3    | 3.6    | 2.8     | 2.4    | 6.1     | 7.9    | 6.4    | 5.7     |
| Nov   | min    | 0.1      | 0.6    | 0.5  | 1.3  | 1.1    | 1.1    | 0.3     | 0.9    | 3.0     | 2.0    | 2.1    | 1.8     |
| Nov   | max    | 2.0      | 9.8    | 8.2  | 6.7  | 7.7    | 9.7    | 4.9     | 6.6    | 11.9    | 19.1   | 13.9   | 13.1    |
| Nov   | 99%_L  | 0.6      | 1.9    | 2.1  | 2.5  | 2.2    | 2.5    | 1.5     | 1.7    | 4.7     | 4.8    | 3.7    | 3.4     |
| Nov   | 99%_U  | 0.8      | 2.6    | 2.9  | 3.1  | 2.8    | 3.3    | 2.1     | 2.3    | 5.8     | 6.6    | 4.8    | 4.6     |
| Dec   | min    | 0.1      | 0.7    | 1.3  | 1.1  | 1.3    | 0.8    | 0.0     | 0.2    | 2.3     | 1.5    | 1.8    | 1.4     |
| Dec   | max    | 3.3      | 8.0    | 7.6  | 6.1  | 7.2    | 7.7    | 7.8     | 5.3    | 12.0    | 19.5   | 18.6   | 10.4    |
| Dec   | 99%_L  | 0.7      | 2.0    | 2.4  | 2.4  | 2.3    | 2.6    | 1.5     | 1.8    | 4.7     | 5.8    | 3.7    | 3.2     |
| Dec   | 99%_U  | 1.0      | 2.7    | 3.2  | 3.0  | 3.0    | 3.5    | 2.2     | 2.3    | 5.8     | 7.9    | 5.3    | 4.0     |

In the season of anti-hail works (April- October) the range of changes in the daily values of W for the separate stations is following: Tsn.: 0.0 m/sec (Apr-Jun) – 9.3 m/sec (Apr); Kindz.: 0.7 m/sec (Sep) –

12.5 m/sec (Apr); Tel.: 0.6 m/sec (Aug) – 10.1 m/sec (Apr); San.: 0.8 m/sec (Sep) – 13.4 m/sec (Apr); Vachn.: 1.4 m/sec (Sep) – 10.9 m/sec (Apr); Ruisp.: 0.0 m/sec (May, Oct) – 11.3 m/sec (Apr); Dz. An.: 0.0 m/sec (May, Jul, Aug) – 9.0 m/sec (Sep); Bakur.: 0.8 m/sec (Jun) – 11.0 m/sec (May); Z. Kedi: 2.9 m/sec (Sep) – 16.3 m/sec (Aug); Sagar.: 2.5 m/sec (Oct) – 31.2 m/sec (Jun); Khorn.: 2.0 m/sec (Jul) – 16.8 m/sec (Jun); Naendr.: 2.0 m/sec (Oct) – 20.8 m/sec (Oct); Kist.: 1.9 m/sec (Oct) – 15.2 m/sec (Apr).

Table 4. Repetition of daily max of wind speed in Kakheti in 2017-2019 according to Beaufort Wind Scale (BWS) in three periods of year.

| Location             | Season | Beaufort Wind Scale (Force) |           |           |           |           |            |            |            |            |            |            |            |
|----------------------|--------|-----------------------------|-----------|-----------|-----------|-----------|------------|------------|------------|------------|------------|------------|------------|
|                      |        | 0                           | 1         | 2         | 3         | 4         | 5          | 6          | 7          | 8          | 9          | 10         | 11         |
|                      |        | Wind Speed, m/sec           |           |           |           |           |            |            |            |            |            |            |            |
|                      |        | 0 - 0.2                     | 0.3 - 1.5 | 1.6 - 3.3 | 3.4 - 5.4 | 5.5 - 7.9 | 8.0 - 10.7 | 10.8- 13.8 | 13.9- 17.1 | 17.2- 20.7 | 20.8- 24.4 | 24.5- 28.4 | 28.5- 32.6 |
| Repetition, %        |        |                             |           |           |           |           |            |            |            |            |            |            |            |
| Tsnori               | Cold   | 1.6                         | 65.0      | 24.7      | 7.1       | 1.5       | 0.0        |            |            |            |            |            |            |
|                      | Warm   | 7.3                         | 67.9      | 18.0      | 4.6       | 2.0       | 0.2        |            |            |            |            |            |            |
|                      | Year   | 4.5                         | 66.5      | 21.4      | 5.8       | 1.7       | 0.1        |            |            |            |            |            |            |
| Kindzmarauli-Khareba | Cold   |                             | 13.7      | 60.8      | 14.7      | 8.2       | 2.2        | 0.4        |            |            |            |            |            |
|                      | Warm   |                             | 8.6       | 66.8      | 16.0      | 5.8       | 2.0        | 0.7        |            |            |            |            |            |
|                      | Year   |                             | 11.1      | 63.8      | 15.3      | 7.0       | 2.1        | 0.5        |            |            |            |            |            |
| Telavi (Wine Cellar) | Cold   |                             | 8.2       | 56.9      | 21.7      | 12.0      | 1.2        |            |            |            |            |            |            |
|                      | Warm   |                             | 5.8       | 61.4      | 25.1      | 6.7       | 0.9        |            |            |            |            |            |            |
|                      | Year   |                             | 7.0       | 59.2      | 23.5      | 9.3       | 1.0        |            |            |            |            |            |            |
| Saniore              | Cold   | 0.4                         | 3.3       | 52.0      | 36.3      | 7.3       | 0.7        | 0.0        |            |            |            |            |            |
|                      | Warm   | 0.0                         | 0.7       | 57.0      | 36.2      | 5.6       | 0.2        | 0.2        |            |            |            |            |            |
|                      | Year   | 0.2                         | 2.0       | 54.5      | 36.3      | 6.5       | 0.5        | 0.1        |            |            |            |            |            |
| Vachnadziani-Khareba | Cold   |                             | 5.1       | 63.0      | 21.6      | 9.0       | 1.1        | 0.2        |            |            |            |            |            |
|                      | Warm   |                             | 0.2       | 65.8      | 26.6      | 6.6       | 0.7        | 0.2        |            |            |            |            |            |
|                      | Year   |                             | 2.6       | 64.4      | 24.1      | 7.8       | 0.9        | 0.2        |            |            |            |            |            |
| Ruispiri             | Cold   | 0.4                         | 2.6       | 58.4      | 22.9      | 11.7      | 3.8        | 0.2        |            |            |            |            |            |
|                      | Warm   | 0.9                         | 0.5       | 49.0      | 37.9      | 9.5       | 2.0        | 0.2        |            |            |            |            |            |
|                      | Year   | 0.6                         | 1.6       | 53.7      | 30.4      | 10.6      | 2.9        | 0.2        |            |            |            |            |            |
| Dzveli Anaga         | Cold   | 0.4                         | 26.3      | 51.7      | 16.2      | 4.7       | 0.8        |            |            |            |            |            |            |
|                      | Warm   | 3.2                         | 11.2      | 64.1      | 19.0      | 2.0       | 0.6        |            |            |            |            |            |            |
|                      | Year   | 1.8                         | 18.7      | 57.9      | 17.6      | 3.4       | 0.7        |            |            |            |            |            |            |
| Bakurtsikhe          | Cold   | 0.2                         | 25.5      | 51.3      | 18.7      | 4.0       | 0.4        | 0.0        |            |            |            |            |            |
|                      | Warm   | 0.0                         | 13.1      | 63.6      | 17.3      | 5.3       | 0.5        | 0.2        |            |            |            |            |            |
|                      | Year   | 0.1                         | 19.3      | 57.4      | 18.0      | 4.7       | 0.5        | 0.1        |            |            |            |            |            |
| Zemo Kedi            | Cold   |                             |           | 6.2       | 52.6      | 27.5      | 10.1       | 3.1        | 0.5        |            |            |            |            |
|                      | Warm   |                             |           | 0.2       | 27.6      | 48.1      | 18.5       | 5.1        | 0.5        |            |            |            |            |
|                      | Year   |                             |           | 3.2       | 40.1      | 37.8      | 14.3       | 4.1        | 0.5        |            |            |            |            |
| Sagarejo             | Cold   |                             | 0.2       | 11.5      | 33.5      | 22.2      | 13.2       | 10.4       | 7.1        | 1.6        | 0.2        | 0.0        | 0.0        |
|                      | Warm   |                             | 0.0       | 0.4       | 21.1      | 30.8      | 24.0       | 14.6       | 4.7        | 2.9        | 0.5        | 0.4        | 0.5        |
|                      | Year   |                             | 0.1       | 5.9       | 27.3      | 26.5      | 18.6       | 12.5       | 5.9        | 2.3        | 0.4        | 0.2        | 0.3        |
| Khornabuji           | Cold   |                             |           | 26.1      | 38.6      | 21.3      | 7.4        | 4.8        | 1.5        | 0.4        |            |            |            |
|                      | Warm   |                             |           | 0.7       | 29.2      | 48.1      | 15.0       | 5.2        | 1.8        | 0.0        |            |            |            |
|                      | Year   |                             |           | 13.5      | 33.9      | 34.7      | 11.2       | 5.0        | 1.7        | 0.2        |            |            |            |
| Naendrovali          | Cold   |                             | 0.5       | 37.0      | 38.8      | 13.0      | 7.3        | 2.0        | 1.1        | 0.0        | 0.2        |            |            |
|                      | Warm   |                             | 0.0       | 8.9       | 52.6      | 24.2      | 9.5        | 2.7        | 1.8        | 0.2        | 0.0        |            |            |
|                      | Year   |                             | 0.3       | 22.9      | 45.8      | 18.6      | 8.4        | 2.4        | 1.5        | 0.1        | 0.1        |            |            |
| Kistauri             | Cold   |                             | 0.4       | 20.7      | 41.2      | 15.6      | 13.4       | 6.0        | 2.4        | 0.2        | 0.2        |            |            |
|                      | Warm   |                             | 0.0       | 4.9       | 45.5      | 34.1      | 10.6       | 4.0        | 0.9        | 0.0        | 0.0        |            |            |
|                      | Year   |                             | 0.2       | 12.8      | 43.4      | 24.8      | 12.0       | 5.0        | 1.6        | 0.1        | 0.1        |            |            |

In table 4 data about repetition of daily values of W in Kakheti in 2017-2019 according to Beaufort Wind Scale [<https://www.kakras.ru/interesn/wind.htm>; <https://www.spc.noaa.gov/faq/tornado/beaufort.html>] in three periods of year are presented.

The analysis of table 4 shows the following.

1 station - Tsn.: The greatest repetition values of W (65.0-67.9%) comes on Force 1 (Light Air) of BWS (Smoke drift indicates wind direction, still wind vanes). Repetition of greatest values of W (0.1-0.2%) comes on Force 5 (Fresh Breeze) of BWS (Small trees in leaf begin to sway).

7 stations - Kindz., Tel., San., Vachn., Ruisp., Dz. An., Bakur.: The greatest repetition values of W (49.0-66.8%) comes on Force 2 (Light Breeze) of BWS (Wind felt on face, leaves rustle, vanes begin to move). Repetition of greatest values of W for Tel. and Dz. An. (0.6-1.2%) comes on Force 5. Repetition of greatest values of W for Kindz., San., Vachn., Ruisp. and Bakur. (0.1-0.7%) comes on Force 6 (Strong Breeze) of BWS (Larger tree branches moving, whistling in wires).

3 stations - Z. Kedi., Sagar. and Khorn.: The greatest repetition values of W in cold period and in year (27.3-52.6%) comes on Force 3 (Gentle Breeze) of BWS (Leaves and small twigs constantly moving, light flags extended). The greatest repetition values of W in warm period (30.8-48.1%) comes on Force 4 (Moderate Breeze) of BWS (Dust, leaves, and loose paper lifted, small tree branches move).

Repetition of greatest values of W for Z. Kedi. (0.5%) comes on Force 7 (Near Gale; Whole trees moving, resistance felt walking against wind); for Sagar. (0.3-0.5%) – on Force 11 (Violent Storm; Seldom experienced on land, trees broken or uprooted, "considerable structural damage"); for Khorn. (0.2-0.4%) – on Force 8 (Gale; Twigs breaking off trees, generally impedes progress).

2 stations - Naendr. and Kist.: The greatest repetition values of W (38.8-52.6%) comes on Force 3. Repetition of greatest values of W (0.1-0.2%) comes on Force 9 (Strong Gale) of BWS (Slight structural damage occurs, slate blows off roofs).

Table 5-7. presents data about values of linear correlation coefficient R between meteorological stations on the max wind speed in Kakheti in 2017-2019 for three periods of year. In all - 77 pairs of stations. Critical value for R with  $\alpha \approx 0.35$  is 0.30 (upper level of negligible correlation).

In the correspondence with table 5 values of R between 13 station on mean annual values of W changes from 0.15 (negligible correlation, pair: Z. Kedi - Dz. An., distance – 30 km) to 0.83 (high correlation, pair: Ruisp. - Tel., distance – 17 km). Mean value of R is 0.45 (low correlation).

Values of R between 13 station on values of W in cold period (table 6) changes from 0.26 (negligible correlation) to 0.87 (high correlation). Pair the same as for annual data. Mean value of R is 0.54 (moderate correlation)

In warm period (table 7) values of R changes from 0.03 (negligible correlation, pair: Dz. An. – Tsn., distance - 9 km and Dz. An. – Sagar., distance – 59 km) to 0. 0.78 (high correlation, pair: Ruisp. - Tel.).

Table 5. Linear correlation between meteorological stations on the max wind speed in Kakheti in 2017-2019 (annual data).

| Year       | Tsn. | Kindz. | Tel.        | San. | Vachn. | Ruisp.      | Dz. An.     | Bakur. | Z. Kedi     | Sagar. | Khorn. | Naendr. | Kist. |
|------------|------|--------|-------------|------|--------|-------------|-------------|--------|-------------|--------|--------|---------|-------|
| Tsn.       | 1    | 0.57   | 0.37        | 0.60 | 0.54   | 0.32        | 0.22        | 0.36   | 0.37        | 0.25   | 0.34   | 0.36    | 0.41  |
| Kindz.     | 0.57 | 1      | 0.40        | 0.73 | 0.76   | 0.35        | 0.19        | 0.36   | 0.48        | 0.29   | 0.37   | 0.49    | 0.51  |
| Tel.       | 0.37 | 0.40   | 1           | 0.42 | 0.38   | <b>0.83</b> | 0.49        | 0.79   | 0.22        | 0.36   | 0.43   | 0.55    | 0.59  |
| San.       | 0.60 | 0.73   | 0.42        | 1    | 0.78   | 0.40        | 0.28        | 0.37   | 0.46        | 0.32   | 0.37   | 0.44    | 0.52  |
| Vachn.     | 0.54 | 0.76   | 0.38        | 0.78 | 1      | 0.41        | 0.23        | 0.38   | 0.58        | 0.39   | 0.47   | 0.55    | 0.58  |
| Ruisp.     | 0.32 | 0.35   | <b>0.83</b> | 0.40 | 0.41   | 1           | 0.46        | 0.76   | 0.29        | 0.44   | 0.51   | 0.58    | 0.65  |
| Dz. An.    | 0.22 | 0.19   | 0.49        | 0.28 | 0.23   | 0.46        | 1           | 0.45   | <b>0.15</b> | 0.21   | 0.31   | 0.30    | 0.35  |
| Bakur.     | 0.36 | 0.36   | 0.79        | 0.37 | 0.38   | 0.76        | 0.45        | 1      | 0.29        | 0.33   | 0.49   | 0.64    | 0.54  |
| Z. Kedi    | 0.37 | 0.48   | 0.22        | 0.46 | 0.58   | 0.29        | <b>0.15</b> | 0.29   | 1           | 0.36   | 0.55   | 0.48    | 0.42  |
| Sagar.     | 0.25 | 0.29   | 0.36        | 0.32 | 0.39   | 0.44        | 0.21        | 0.33   | 0.36        | 1      | 0.53   | 0.42    | 0.59  |
| Khorn.     | 0.34 | 0.37   | 0.43        | 0.37 | 0.47   | 0.51        | 0.31        | 0.49   | 0.55        | 0.53   | 1      | 0.66    | 0.58  |
| Naendr.    | 0.36 | 0.49   | 0.55        | 0.44 | 0.55   | 0.58        | 0.30        | 0.64   | 0.48        | 0.42   | 0.66   | 1       | 0.62  |
| Kist.      | 0.41 | 0.51   | 0.59        | 0.52 | 0.58   | 0.65        | 0.35        | 0.54   | 0.42        | 0.59   | 0.58   | 0.62    | 1     |
| Statistics |      |        |             |      |        |             |             |        |             |        |        |         |       |
| Min        |      | Max    |             | Mean |        | Range       |             | St Dev |             | Cv, %  |        | Median  |       |
| 0.15       |      | 0.83   |             | 0.45 |        | 0.68        |             | 0.15   |             | 33.2   |        | 0.43    |       |

Table 6. Linear correlation between meteorological stations on the max wind speed in Kakheti in 2017-2019 (cold season).

| Cold       | Tsn. | Kindz. | Tel.        | San.  | Vachn. | Ruisp.      | Dz. An.     | Bakur. | Z. Kedi     | Sagar. | Khorn. | Naendr. | Kist. |
|------------|------|--------|-------------|-------|--------|-------------|-------------|--------|-------------|--------|--------|---------|-------|
| Tsn.       | 1    | 0.57   | 0.36        | 0.63  | 0.57   | 0.32        | 0.39        | 0.35   | 0.47        | 0.37   | 0.45   | 0.40    | 0.46  |
| Kindz.     | 0.57 | 1      | 0.39        | 0.76  | 0.81   | 0.38        | 0.27        | 0.38   | 0.65        | 0.48   | 0.49   | 0.55    | 0.56  |
| Tel.       | 0.36 | 0.39   | 1           | 0.44  | 0.44   | <b>0.87</b> | 0.57        | 0.83   | 0.35        | 0.57   | 0.63   | 0.66    | 0.65  |
| San.       | 0.63 | 0.76   | 0.44        | 1     | 0.82   | 0.43        | 0.37        | 0.41   | 0.61        | 0.49   | 0.51   | 0.52    | 0.56  |
| Vachn.     | 0.57 | 0.81   | 0.44        | 0.82  | 1      | 0.47        | 0.34        | 0.44   | 0.69        | 0.54   | 0.52   | 0.56    | 0.60  |
| Ruisp.     | 0.32 | 0.38   | <b>0.87</b> | 0.43  | 0.47   | 1           | 0.58        | 0.80   | 0.37        | 0.63   | 0.64   | 0.66    | 0.70  |
| Dz. An.    | 0.39 | 0.27   | 0.57        | 0.37  | 0.34   | 0.58        | 1           | 0.53   | <b>0.26</b> | 0.39   | 0.52   | 0.42    | 0.45  |
| Bakur.     | 0.35 | 0.38   | 0.83        | 0.41  | 0.44   | 0.80        | 0.53        | 1      | 0.37        | 0.50   | 0.63   | 0.73    | 0.58  |
| Z. Kedi    | 0.47 | 0.65   | 0.35        | 0.61  | 0.69   | 0.37        | <b>0.26</b> | 0.37   | 1           | 0.45   | 0.54   | 0.53    | 0.49  |
| Sagar.     | 0.37 | 0.48   | 0.57        | 0.49  | 0.54   | 0.63        | 0.39        | 0.50   | 0.45        | 1      | 0.67   | 0.55    | 0.82  |
| Khorn.     | 0.45 | 0.49   | 0.63        | 0.51  | 0.52   | 0.64        | 0.52        | 0.63   | 0.54        | 0.67   | 1      | 0.69    | 0.71  |
| Naendr.    | 0.40 | 0.55   | 0.66        | 0.52  | 0.56   | 0.66        | 0.42        | 0.73   | 0.53        | 0.55   | 0.69   | 1       | 0.67  |
| Kist.      | 0.46 | 0.56   | 0.65        | 0.56  | 0.60   | 0.70        | 0.45        | 0.58   | 0.49        | 0.82   | 0.71   | 0.67    | 1     |
| Statistics |      |        |             |       |        |             |             |        |             |        |        |         |       |
|            | Min  | Max    | Mean        | Range | St Dev | Cv, %       | Median      |        |             |        |        |         |       |
|            | 0.26 | 0.87   | 0.54        | 0.62  | 0.14   | 26.5        | 0.53        |        |             |        |        |         |       |

Table 7. Linear correlation between meteorological stations on the max wind speed in Kakheti in 2017-2019 (warm season).

| Warm       | Tsn.        | Kindz. | Tel.        | San.  | Vachn. | Ruisp.      | Dz. An.     | Bakur. | Z. Kedi | Sagar.      | Khorn. | Naendr. | Kist. |
|------------|-------------|--------|-------------|-------|--------|-------------|-------------|--------|---------|-------------|--------|---------|-------|
| Tsn.       | 1           | 0.57   | 0.40        | 0.57  | 0.52   | 0.33        | <b>0.03</b> | 0.37   | 0.32    | 0.15        | 0.24   | 0.33    | 0.35  |
| Kindz.     | 0.57        | 1      | 0.41        | 0.70  | 0.71   | 0.32        | 0.09        | 0.34   | 0.36    | 0.12        | 0.25   | 0.46    | 0.44  |
| Tel.       | 0.40        | 0.41   | 1           | 0.39  | 0.30   | <b>0.78</b> | 0.39        | 0.77   | 0.14    | 0.18        | 0.26   | 0.46    | 0.52  |
| San.       | 0.57        | 0.70   | 0.39        | 1     | 0.73   | 0.36        | 0.16        | 0.32   | 0.33    | 0.14        | 0.20   | 0.36    | 0.47  |
| Vachn.     | 0.52        | 0.71   | 0.30        | 0.73  | 1      | 0.33        | 0.09        | 0.31   | 0.47    | 0.22        | 0.41   | 0.54    | 0.54  |
| Ruisp.     | 0.33        | 0.32   | <b>0.78</b> | 0.36  | 0.33   | 1           | 0.30        | 0.72   | 0.21    | 0.22        | 0.34   | 0.49    | 0.57  |
| Dz. An.    | <b>0.03</b> | 0.09   | 0.39        | 0.16  | 0.09   | 0.30        | 1           | 0.37   | 0.05    | <b>0.03</b> | 0.05   | 0.18    | 0.21  |
| Bakur.     | 0.37        | 0.34   | 0.77        | 0.32  | 0.31   | 0.72        | 0.37        | 1      | 0.21    | 0.15        | 0.33   | 0.55    | 0.50  |
| Z. Kedi    | 0.32        | 0.36   | 0.14        | 0.33  | 0.47   | 0.21        | 0.05        | 0.21   | 1       | 0.20        | 0.48   | 0.39    | 0.37  |
| Sagar.     | 0.15        | 0.12   | 0.18        | 0.14  | 0.22   | 0.22        | <b>0.03</b> | 0.15   | 0.20    | 1           | 0.32   | 0.26    | 0.31  |
| Khorn.     | 0.24        | 0.25   | 0.26        | 0.20  | 0.41   | 0.34        | 0.05        | 0.33   | 0.48    | 0.32        | 1      | 0.60    | 0.42  |
| Naendr.    | 0.33        | 0.46   | 0.46        | 0.36  | 0.54   | 0.49        | 0.18        | 0.55   | 0.39    | 0.26        | 0.60   | 1       | 0.59  |
| Kist.      | 0.35        | 0.44   | 0.52        | 0.47  | 0.54   | 0.57        | 0.21        | 0.50   | 0.37    | 0.31        | 0.42   | 0.59    | 1     |
| Statistics |             |        |             |       |        |             |             |        |         |             |        |         |       |
|            | Min         | Max    | Mean        | Range | St Dev | Cv, %       | Median      |        |         |             |        |         |       |
|            | 0.03        | 0.78   | 0.36        | 0.75  | 0.18   | 50.1        | 0.34        |        |         |             |        |         |       |

Number of pairs of stations with the significant value of R ( $\alpha \approx 0.35$ ) is following: Annual data (table 5) – 76, Cold season (table 6) – 67, Warm season (table 7) - 53.

Distribution of number of pairs of stations with values of R according to [26] is following.

Annual data: Negligible (or absence) correlation – 14.1% ( $\alpha \geq 0.35$ ), Low correlation – 51.3% ( $0.08 \leq \alpha < 0.35$ ), Moderate correlation ( $0.008 \leq \alpha < 0.08$ ) – 26.9%, High correlation ( $0.0004 \leq \alpha < 0.008$ ) – 7.7%.

Cold season: Negligible (or absence) correlation – 2.6%, Low correlation – 39.7%, Moderate correlation – 44.9%, High correlation – 12.8%.

Warm season: Negligible correlation (or absence) – 32.1%, Low correlation – 46.1%, Moderate correlation – 14.1%, High correlation – 7.7%.

As a whole level of linear correlation between meteorological stations on the max wind speed in Kakheti are low or moderate. The highest level of this correlation in cold half-year is observed

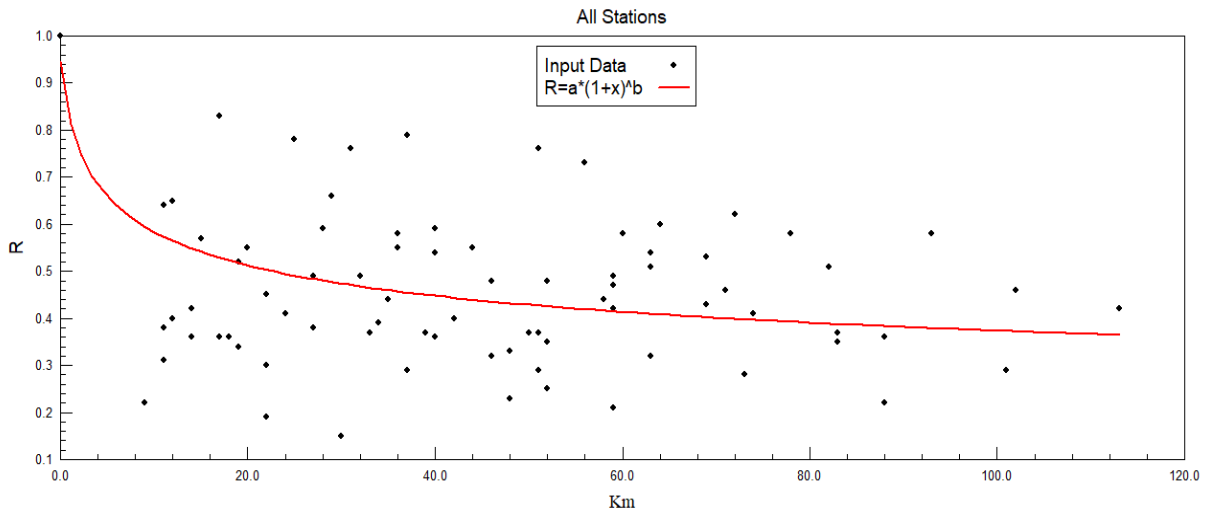


Fig. 4. Dependence of the correlation coefficient by the max wind speed on the distance between 13 meteorological stations in Kakheti (annual data).

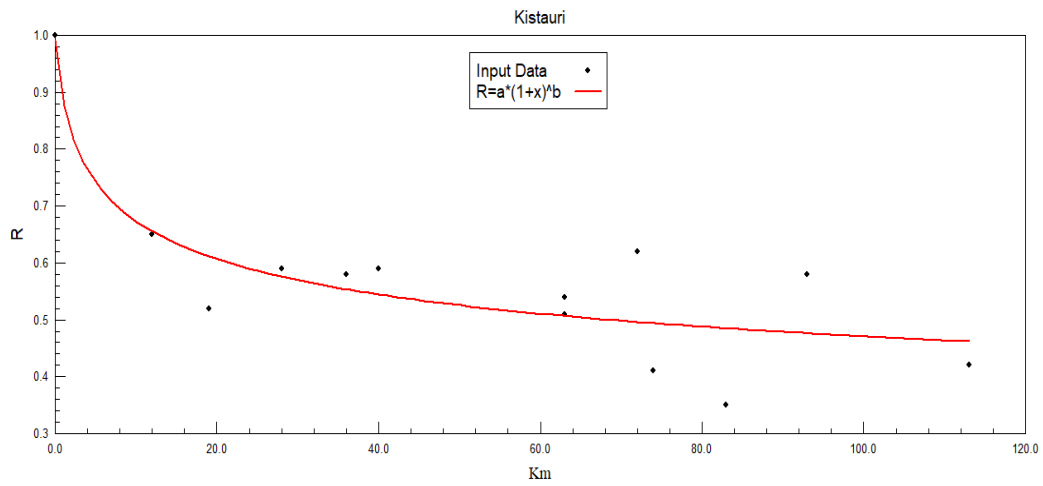


Fig. 5. Dependence of the correlation coefficient by the max wind speed on the distance from Kistauri to 12 meteorological stations in Kakheti (annual data).

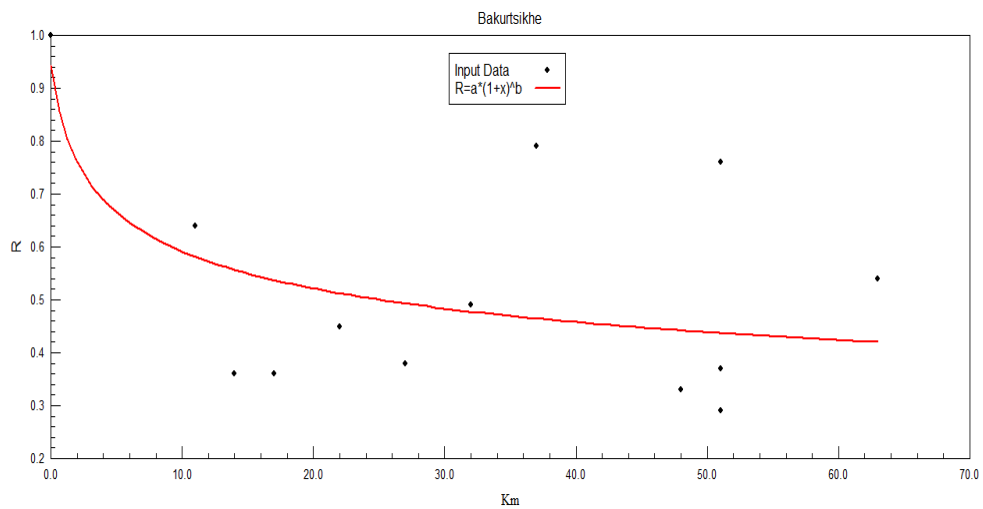


Fig. 6. Dependence of the correlation coefficient by the max wind speed on the distance from Bakurtsikhe to 12 meteorological stations in Kakheti (annual data).

In fig. 4 the example of curve of dependence of the correlation coefficient by the max wind speed on the distance between 13 meteorological stations in Kakheti according to annual data is presented. In fig. 5-6 the examples of curves of this dependence from Kistauri and Bakurtsikhe to 12 meteorological stations in Kakheti are presented.

As follows from fig. 4-6 these dependence have form of power function. Analogous dependence is observed for all seasons of year and separate stations. The values of the corresponding coefficients of the equation of regression in the table 8 are represented.

Table 8. Values of the coefficients of the equation of regression of dependence of the correlation coefficient by the max wind speed on the distance from separate meteorological station to 12 meteorological stations in Kakheti in 2017-2019 in three periods of year.

| Location   | Year  |        |                | Cold season |        |                | Warm season |        |                |
|------------|---|--------|----------------|-------------|--------|----------------|-------------|--------|----------------|
|            | Equation of Regression: $R = a \cdot (1+x)^b$ ; X – distance, km; $\alpha(R^2) \leq 0.06$ |        |                |             |        |                |             |        |                |
|            | a   | b      | R <sup>2</sup> | a           | b      | R <sup>2</sup> | a           | b      | R <sup>2</sup> |
| Tsn.       | 0.900   | -0.240 | 0.480          | 0.911       | -0.206 | 0.540          | 0.885       | -0.271 | 0.373          |
| Kindz.     | 0.948   | -0.204 | 0.372          | 0.930       | -0.159 | 0.299          | 0.963       | -0.250 | 0.383          |
| Tel.       | 0.986   | -0.198 | 0.460          | 0.963       | -0.149 | 0.339          | 0.993       | -0.244 | 0.478          |
| San.       | 0.946   | -0.184 | 0.443          | 0.911       | -0.134 | 0.337          | 0.975       | -0.244 | 0.474          |
| Vachn.     | 0.952   | -0.178 | 0.374          | 0.944       | -0.142 | 0.331          | 0.958       | -0.225 | 0.377          |
| Ruisp.     | 0.990   | -0.187 | 0.490          | 0.980       | -0.147 | 0.374          | 0.999       | -0.242 | 0.544          |
| Dz. An.    | 0.914   | -0.318 | 0.564          | 0.911       | -0.215 | 0.525          | 0.953       | -0.552 | 0.633          |
| Bakur.     | 0.943   | -0.195 | 0.367          | 0.930       | -0.152 | 0.281          | 0.958       | -0.245 | 0.403          |
| Z. Kedi    | 0.976   | -0.226 | 0.611          | 0.955       | -0.166 | 0.485          | 0.986       | -0.298 | 0.692          |
| Sagar.     | 0.995   | -0.251 | 0.727          | 1.005       | -0.160 | 0.570          | 0.997       | -0.426 | 0.880          |
| Khorn.     | 0.895   | -0.172 | 0.445          | 0.880       | -0.106 | 0.343          | 0.917       | -0.280 | 0.493          |
| Naendr.    | 0.945   | -0.172 | 0.506          | 0.942       | -0.135 | 0.452          | 0.954       | -0.220 | 0.526          |
| Kist.      | 0.991   | -0.161 | 0.780          | 0.987       | -0.126 | 0.581          | 0.991       | -0.209 | 0.743          |
| All Points | 0.947   | -0.201 | 0.447          | 0.933       | -0.149 | 0.363          | 0.959       | -0.270 | 0.464          |

Depending on the level of the coefficient of determination, it is accepted to divide design models into three groups: 1)  $0.8 < R^2 \leq 1$  - model of a good quality; 2)  $0.5 < R^2 \leq 0.8$  - model of acceptable quality; 3)  $0 < R^2 \leq 0.5$  - model of poor quality.

As it follows from fig. 4-6 and table 8 the quality models of dependence values of R from distance X for separation station is different. Model of a good quality – only for Sagarejo, in warm season; model of acceptable quality – 5 stations for annual data, 4 stations for cold season and 5 stations for warm season; model of poor quality – 8 stations for annual data, 9 stations for cold season and 7 stations for warm season.

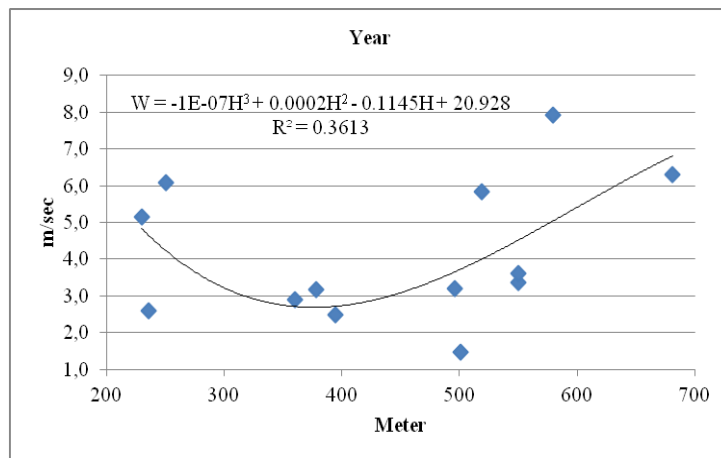


Fig. 7. Vertical distribution of mean annual max wind speed in Kakheti for all 13 stations ( $\alpha(R^2) = 0.03$ ).

In fig. 7 data about vertical distribution of mean annual max wind speed in Kakheti for all 13 stations is presented. As follows from this figure dependence of W from H has form of third power of polinomial and as a whole with an increase of altitude of locality wind speed grows.

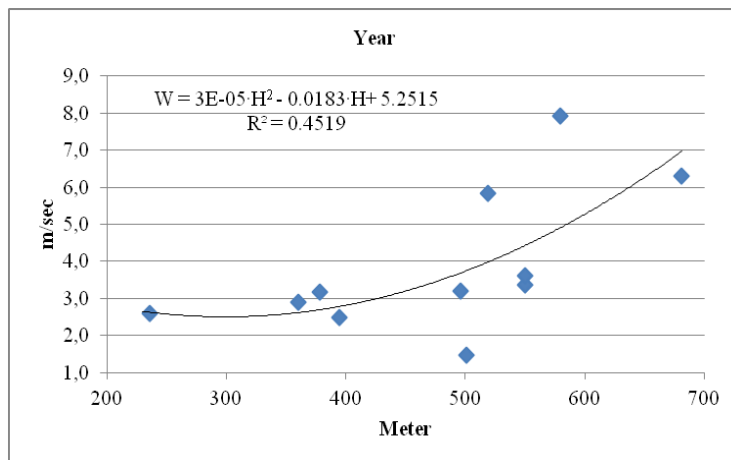


Fig. 8. Vertical distribution of mean annual max wind speed in Kakheti for 11 stations without Khornabuji and Naendrovali ( $\alpha(R^2) = 0.03$ ).

Table 9. Values of the coefficients of the equation of regression of dependence of mean half-year max wind speed in Kakheti with height stations

|   | All 13 stations                                 |        |          |   | 11 stations without Khornabuji and Naendrovali |        |          |
|---|---|--------|----------|---|--|--------|----------|
|   | $W = a \cdot H^3 + b \cdot H^2 + c \cdot H + d$ | $R^2$  | $\alpha$ |   | $W = a \cdot H^2 + b \cdot H + c$              | $R^2$  | $\alpha$ |
|   | Cold period                                     |        |          |   | Cold period                                    |        |          |
| a | -1E-07  | 0.3271 | 0.04     | a | 2E-05  | 0.4139 | 0.04     |
| b | 0.0002  |        |          | b | - 0.0125                                       |        |          |
| c | -0.0962   |        |          | c | 4.1908   |        |          |
| d | 17.726  |        |          |   |  |        |          |
|   | Warm period                                     |        |          |   | Warm period                                    |        |          |
| a | -1E-07  | 0.3873 | 0.025    | a | 4E-05  | 0.4806 | 0.02     |
| b | 0.0003  |        |          | b | - 0.,241                                       |        |          |
| c | -0.1325   |        |          | c | 6.098  |        |          |
| d | 24.095  |        |          |   |  |        |          |

However, it should be noted that at stations Khornabuji and Naendrovali, located on heights 251 and 230 m, the high speeds of wind are observed. This specifies the presence of the minimum in calculated curve of values of W in the range of hight of locality 300-400 m, with further increase value of W with an increase of H.

Without taking into account these stations the dependence W from H takes the form of the second power polynomial (Fig. 8). In this case, more or less a permanent increase in wind speed with an increase in altitude of locality is observed. Similar pattern is observed for the cold and warm seasons (table 9).

## Conclusion

The detailed statistical analysis of the daily maximum wind speed W for 13 points of Kakheti in the period from 1 January 2017 through 31 December of 2019 is carried out.

Distribution of W on the territory of Kakheti has the complex, heterogeneous nature, depending on area relief and its height above sea level. The analysis of correlation and regression connections between the

meteorological stations in terms of the values of wind speed showed that frequently the regime of wind has local special features and little it is connected with the adjacent locations. Therefore for the larger detailing of wind regime on the territory of Kakheti should be increased the number of observation points.

In the near future it is planned to draw the comparison of the wind regime in the days with the hail with the non hail days, developments the possible connection between the data about the extreme wind on the earth's surface with the data of the radar measurements of the wind speed on height 2-2.5 km.

## Acknowledgments

We would like to express our deepest appreciation to Georgian National Environmental Agency, who provided data about daily max wind speed in Kakheti region of Georgia.

## References

- [1] Klimat i klimaticheskie resursi Gruzii. Tr. ZAKNIGMI, vip. 44(50), L., Gidrometeoizdat, 1971, 384 s., (in Russian).
- [2] Svanidze G.G., Papinashvili L.K. (edit.). *Climat Tbilisi*. Sankt-Petersburg, Gidrometeoizdat, L., 1992, 230 p., (in Russian).
- [3] Elizbarashvili E. *Climate of Georgia*. Monograph, Institute of Hydrometeorology of GTU, ISBN 978-9941-0-9584-9, Tbilisi, 2017, 360 p., (in Georgian).
- [4] Tavartkiladze K., Begalishvili N., Kharchilava J., Mumladze D., Amiranashvili A., Vachnadze J., Shengelia I., Amiranashvili V. *Contemporary climate change in Georgia. Regime of some climate parameters and their variability*. Monograph, ISBN 99928-885-4-7, Tbilisi, 2006, 177 p., (in Georgian).
- [5] Svanidze G.G., Tsutskiridze Ia. A. (edit.). *Opasnie gidrometeorologicheskie protsessi na Kavkaze*. L., Gidrometeoizdat., 1980, 288 p., (in Russian).
- [6] Varazanashvili O., Tsereteli N., Amiranashvili A., Tsereteli E., Elizbarashvili E., Dolidze J., Qaldani L., Saluqvadze M., Adamia Sh., Arevadze N., Gventcadze A. *Vulnerability, Hazards and Multiple Risk Assessment for Georgia*. *Natural Hazards*, Vol. 64, Number 3, 2012, pp. 2021-2056, DOI: 10.1007/s11069-012-0374-3, <http://www.springerlink.com/content/9311p18582143662/fulltext.pdf>.
- [7] Amiranashvili A.G. *Increasing Public Awareness of Different Types of Geophysical Catastrophes, Possibilities of Their Initiation as a Result of Terrorist Activity, Methods of Protection and Fight with Their Negative Consequences. Engaging the Public to Fight Consequences of Terrorism and Disasters*. NATO Science for Peace and Security Series E: Human and Societal Dynamics, vol. 120. IOS Press, Amsterdam•Berlin•Tokyo•Washington, DC, ISSN 1874-6276, 2015, pp. 155-164. <http://www.nato.int/science>; <http://www.springer.com>; <http://www.iospress.nl>
- [8] Pipia M., Elizbarashvili E., Amiranashvili A., Beglarashvili N. *Dangerous Regions of Blizzard in Georgia*. *Annals of Agrarian Science*, ISSN 1512-1887, vol. 17, No 4, 2019, pp. 403 – 408.
- [9] Abshaev A.M., Abshaev M.T., Berekova M.V., Malkarova A.M. *Rukovodstvo po organizacii i provedeniu protivogradovih rabot*. ISBN 978-5-905770-54-8, Nalchik, Pechatni dvor, 2014, 500 s, (in Russian).
- [10] Amiranashvili A., Bliadze T., Chikhladze V. *Photochemical smog in Tbilisi*. Monograph, Trans. of Mikheil Nodia institute of Geophysics, ISSN 1512-1135, vol. 63, Tb., 2012, 160 p., (in Georgian).
- [11] Kukhalashvili V.G., Kordzakhia G.I., Gigauri N.G., Surmava A.A., Intskirveli L.N. *Numerical Modelling of Dust Propagation in the Atmosphere of Tbilisi City: The Case of Background Eastern Gentle Breeze*. *Journal of the Georgian Geophysical Society*, ISSN: 1512-1127, *Physics of Solid Earth, Atmosphere, Ocean and Space Plasma*, v. 23(1), 2020, pp. 46-50.
- [12] Kukhalashvili V.G., Gigauri N.G., Surmava A.A., Demetrashvili D.I., Intskirveli L.N. *Numerical Modelling of Dust Propagation in the Atmosphere of Tbilisi City: The Case of Background Eastern Fresh Breeze*. *Journal of the Georgian Geophysical Society*, ISSN: 1512-1127, *Physics of Solid Earth, Atmosphere, Ocean and Space Plasma*, v. 23(1), 2020, pp. 51–56.
- [13] Saakashvili N.M., Tabidze M.Sh., Tarkhan-Mouravi I.D., Amiranashvili A.G., Melikadze G.I., Chikhladze V.A. *To a Question about the Certification of the Health Resort and Tourist Resources of Georgia*. “Modern Problems of Using of Health Resort Resources”, Collection of Scientific Works of International Conference, Sairme, Georgia, June 10-13, 2010, ISBN 978-9941-0-2529-7, Tbilisi, 2010, pp. 175-180, (in Russian).
- [14] Amiranashvili A.G., Chikhladze V.A. Saakashvili N.M., Tabidze M.Sh., Tarkhan-Mouravi I.D. *Bioclimatic Characteristics of Recreational Zones – Important Component of the Passport of the Health*

- Resort – Tourist Potential of Georgia. Transactions of the Institute of Hydrometeorology at the Georgian Technical University, vol. 117, ISSN 1512-0902, 2011, pp. 89-92.
- [15] Amiranashvili A., Danelia R., Mirianashvili K., Nodia Kh., Khazaradze K., Khurodze T., Chikhladze V. On the Applicability of the Scale of Air Equivalent- Effective Temperature in the Conditions of Tbilisi City. Trans. of Mikheil Nodia Institute of Geophysics, ISSN 1512-1135, vol. 62, Tbilisi, 2010, pp. 216-220, (in Russian).
- [16] Amiranashvili A., Mirianashvili K., Fedorova N., Levit V., Fabiana Medeiros Carnaúba, Aliton Oliveira da Silva. Comparative analysis of air equivalent - effective temperature in some cities of Georgia and Brazil, Proc. of Int. Conf. “Environment and Global Warming”, Dedicated to the 100<sup>th</sup> Birthday Anniversary of Academician F. Davitaya, Collected Papers New Series, N 3(82), ISSN 2333-3347, Tbilisi, 2011, pp. 105-110.
- [17] Khazaradze K. R. Comparative Analysis of Mean-Daily Value of Air Equivalent-Effective Temperature in Tbilisi and Kojori. Journal of the Georgian Geophysical Society, Issue B. Physics of Atmosphere, Ocean and Space Plasma, v. 20B, 2017, pp. 65–72.
- [18] Amiranashvili A., Japaridze N., Kartvelishvili L., Megrelidze L., Khazaradze K. Statistical characteristics of the monthly mean values of air effective temperature on Missenard in the Autonomous Republic of Adjara and Kakheti (Georgia). Trans. of Mikheil Nodia institute of Geophysics, ISSN 1512-1135, vol. 69, Tb., 2018, pp. 125 – 144, (in Russian).
- [19] Amiranashvili A.G., Japaridze N.D., Kartvelishvili L.G., Khazaradze K.R., Matzarakis A., Povolotskaya N.P., Senik I.A. Tourism Climate Index of in the Some Regions of Georgia And North Caucasus. Journal of the Georgian Geophysical Society, Issue B. Physics of Atmosphere, Ocean and Space Plasma, v. 20B, 2017, pp. 43–64.
- [20] Amiranashvili A.G., Kartvelishvili L.G., Megrelidze L.D. Changeability of the Meteorological Parameters Associated with Some Simple Thermal Indices and Tourism Climate Index in Adjara and Kakheti (Georgia). Journal of the Georgian Geophysical Society, ISSN: 1512-1127, Physics of Solid Earth, Atmosphere, Ocean and Space Plasma, v. 21(2), Tbilisi, 2018, pp. 77-94.
- [21] Amiranashvili A.G. History of Active Effects on Atmospheric Processes in Georgia. In the book: Essays of the History of Weather Modification in the USSR and the Post-Soviet Territory, ISBN 978-5-86813-450-0, St. Petersburg, RSHMU, 2017, 352 pp., ill., pp. 234-254, (in Russian), <http://mig-journal.ru/toauthor?id=4644>.
- [22] Amiranashvili A., Chikhladze V., Dzodzuashvili U., Ghlonti N., Sauri I., Telia Sh., Tsintsadze T. Weather Modification in Georgia: Past, Present, Prospects for Development. International Scientific Conference “Natural Disasters in Georgia: Monitoring, Prevention, Mitigation”. Proceedings, ISBN 978-9941-13-899-7, Publish Hous of Iv. Javakhishvili Tbilisi State University, December 12-14, Tbilisi, 2019, pp. 216-222.
- [23] Amiranashvili A., Barekchian I., Dvalishvili K., Dzodzuashvili U., Lomtadze J., Osepashvili A., Sauri I., Tatishvili G., Telia Sh., Chikhladze V. Characteristics of Ground Means Action on Hail Process in Kakheti. Trans. of Mikheil Nodia institute of Geophysics, ISSN 1512-1135, vol. 66, Tb., 2016, pp. 39 – 52, (in Russian).
- [24] Avlokhashvili Kh., Banetashvili V., Gelovani G., Javakhishvili N., Kaishauri M., Mitin M., Samkharadze I., Tskhvediasvili G., Chargazia Kh., Khurtsidze G. Products of Meteorological Radar «METEOR 735CDP10». Trans. of Mikheil Nodia Institute of Geophysics, ISSN 1512-1135, vol. 66, Tb., 2016, pp. 60-65, (in Russian).
- [25] Kobisheva N., Narovlianski G. Climatological processing of the meteorological information, Leningrad, Gidrometeoizdat, 1978, 294 p., (in Russian).
- [26] Hinkle D. E., Wiersma W., Jurs S. G. Applied Statistics for the Behavioral Sciences. Boston, MA, Houghton Mifflin Company, 2003.

# კახეთში 2017-2019 წწ. ქარის დღე-ღამური მაქსიმალური სიჩქარის სტატისტიკური მახასიათებლები

ა. ამირანაშვილი, ვ. ჩიხლაძე, გ. გვასალია, დ. ლოლაძე

## რეზიუმე

წარმოდგერნილია ქარის მაქსიმალური დღე-ღამური სიჩქარის (W) სტატისტიკური ანალიზი კახეთის 13 პუნქტისათვის 2017 წლის 1 იანვრიდან 2019 წლის 31 დეკემბრამდე დროის პერიოდისათვის.

მიღებულია კერძოდ შემდეგი შედეგები: გამოთვლილია W-ს საშუალო თვიური და სეზონური (თბილი და ცივი ნახევარწელი, წლიური) მნიშვნელობები ყველა სადგურისთვის დაკვირვების მთელ პერიოდისათვის; ნაჩვენებია, რომ კახეთის ტერიტორიაზე W – ს საშუალოთვიური მნიშვნელობების განაწილებას აქვს არათანაბარი ხასიათი და იგი იცვლება 0.7 მ/წმ-დან (წნორი, ნოემბერი) 9.5 მ/წმ-დე (საგარეჯო, ივნისი); მოყვანილია კახეთის ტერიტორიაზე W –ს საშუალო წლიური მნიშვნელობების განაწილების რუკა; შესწავლილია W-ს დღე-ღამური მნიშვნელობების განმეორადობა კახეთის ყველა პუნქტისთვის ბოფორტის სკალის შესაბამისად; ნაჩვენებია, რომ კორელაციის წრფივი კოეფიციენტის R-ს მნიშვნელობები სადგურებს შორის W-ს ყველა დღე-ღამური მნიშვნელობებით შეადგენს საშუალოდ 0.45 და იცვლება 0.15-დან 0.83-დე, ცივ პერიოდისთვის 0.54 (იცვლება 0.26-დან 0.87-დე), თბილ პერიოდისათვის 0.36 (იცვლება 0.03-დან 0.78-დე); შესწავლილია კორელაციის წრფივი კოეფიციენტის დამოკიდებულება სადგურებს შორის W-ს მნიშვნელობებით მათ შორის მანძილისგან (სადგურებს შორის მანძილის ზრდასთან ერთად R –ს მნიშვნელობა მცირდება ხარისხობრივი ფუნქციის მიხედვით); შესწავლილია W-ს დამოკიდებულება სადგურის განლაგების სიმაღლეზე წლის განმავლობაში, წლის თბილ და ცივ ნახევარწლებისთვის.

## Статистические характеристики суточной максимальной скорости ветра в Кахетии и 2017-2019

А.Г. Амиранашвили, В.А. Чихладзе, Г.Д. Гвасалия, Д.А. Лоладзе

### Резюме

Представлен статистический анализ суточной максимальной скорости ветра (W) для 13 пунктов Кахетии в период с 1 января 2017 по 31 декабря 2019 гг.

В частности, получены следующие результаты: рассчитаны среднемесячные и сезонные (теплое и холодное полугодия, год) значения W для всех станций за весь период наблюдений; показано, что распределений среднемесячных значений W на территории Кахетии имеет неравномерный характер и меняется от 0.7 м/сек (Цнори, ноябрь) до 9.5 м/сек (Сагареджо, июнь); приводится карта распределения среднегодовых значений W на территории Кахетии; изучена повторяемость суточных значений W для всех пунктов Кахетии в соответствии со шкалой Бофорта; показано, что значения линейного коэффициента корреляции R между станциями по всем суточным значениям W в среднем составляет 0.45 и меняется от 0.15 до 0.83, для холодного полугодия – 0.54 (меняется от 0.26 до 0.87), для теплого полугодия – 0.36 (меняется от 0.03 до 0.78); изучена зависимость линейного коэффициента корреляции между станциями по значениям W от расстояния между ними (с ростом расстояния между станциями значение R убывает по степенному закону); изучена зависимость W от высоты расположения станций в среднем за год, в холодное и теплое полугодия.

# **International Scientific Conference „Natural Disasters in Georgia: Monitoring, Prevention, Mitigation“**

**<sup>1</sup>Nugzar Ya. Ghlonti,<sup>2</sup>Tengiz N. Tsintsadze, <sup>3</sup>Tamari V. Khakhutashvili**

*<sup>1</sup>M. Nodia Institute of Geophysics of I. Javakhishvili Tbilisi State University, Tbilisi, Georgia  
e-mail: Ghlonti60@yahoo.com*

*<sup>2</sup>Institute of Hydrometeorology of Technical University of Georgia, Tbilisi, Georgia  
e-mail: tengo\_hydro@live.ru*

*<sup>3</sup>N(N)LE Association for Science, Tbilisi, Georgia  
e-mail: tamar@4science.ge*

## **ABSTRACT**

*Information about the international scientific conference “Natural Disasters in Georgia: Monitoring, Prevention, Mitigation”, which was held on December 12-14, 2019 at Ivane Javakhishvili Tbilisi State University is presented.*

*The conference was dedicated to 175 and 120 anniversary of the organization in Georgia of regular magneto-meteorological and seismological observations.*

**Key words:** *Natural Disasters; Monitoring, Prevention, Mitigation.*

## **Introduction**

December 12-14, 2019 at Ivane Javakhishvili Tbilisi State University held an international scientific conference “Natural Disasters in Georgia: Monitoring, Prevention, Mitigation”.

The conference was dedicated to the 175<sup>th</sup> anniversary of organizing regular instrumental Geomagnetic and Meteorological observations in Georgia (1844) and the 120<sup>th</sup> anniversary of seismic observations (Tbilisi, 1899) with the help of K. Gauss, A. Humboldt and other great scientists.

It should be noted that the Tbilisi Magnetic-Meteorological Observatory was the cradle of exact science in Georgia. This Observatory was first work place of I. Stalin (from 1899 till the end of 1900). The institute of Geophysics (1933) and the institute of Hydrometeorology (1953) were established on the base of Tbilisi (Later of Dusheti) Observatory.

Georgia is located in the disaster region of natural disasters. In Georgia and its adjacent countries have similar problems in the fight against of natural disasters.

## **Goal of the Conference**

- Promoting the historical achievement of Georgia and its current scientific-technical potential related to the theme of the conference.
- Introducing the World Scientific, Governmental Structures, and the other interested organizations and individual persons with the current state of the problems related to the monitoring, prevention and mitigation of natural disasters in Georgia.

- Strengthen international scientific cooperation around the theme of conference.
- Identify the possibility of organizing a unified operational warning system on the hazardous natural phenomena.
- Identify opportunities for improvement of scientific and educational fields of secondary and higher education institutions in the topic of the conference.

## Conference Organizers

**Georgia:** TSU, Institute of Geophysics; GTU, Institute of Hydrometeorology; N(N)LE Association for Science.

## Conference Supporting Organizations

**Georgia:** LEPL State Military Scientific Technical Center "DELTA"; LEPL National Environmental Agency; TSU, Vakhushti Bagrationi Institute of Geography; LEPL Iakob Gogebashvili Telavi State University; BP Exploration Caspian Sea LTD –Georgia; G. Tsulukidze Mining Institute; Ministry of Internally Displaced Persons from Occupied Territories, Labour, Health and Social; LEPL Tbilisi State Medical University; Emergency Management Service of the Ministry of Internal Affairs of Georgia; Georgian Geophysical Association.

**Other Countries:** Institute of Geology and Geophysics, State Committee on Geology and Mineral Resources of Uzbekistan; Scientific Centre for Aerospace Research of the Earth, National Academy of Sciences of Ukraine; Institute of Helioclimatology, Germany.

## Scientific Committee and Editorial Board

**Tamaz Chelidze:** Academician, Chairman of the Scientific Committee, Editor-in-Chief; **Avtandil Amiranashvili:** secretary; **Demuri Demetrashvili;** **Zurab Kereselidze;** **Nodar Varamashvili,** - TSU, M. Nodia Institute of Geophysics, Georgia.

**Nana Bolashvili:** Co-Chairman of the Scientific Committee, - TSU, Vakhushti Bagrationi Institute of Geography, Georgia.

**Tengiz Tsintsadze:** Co-Chairman of the Scientific Committee; **Elizbar Elizbarashvili;** **Marika Tatishvili;** **Giorgi Meladze,** - GTU, Institute of Hydrometeorology, Georgia.

**Liana Kartvelishvili;** **Emil Tsereteli,** - National Environmental Agency, Georgia.

**Tamar Nadiradze;** **Magda Davitashvili,** - Iakob Gogebashvili Telavi State University, Georgia.

**Bezhan Asanidze** - BP Exploration Caspian Sea LTD – Georgia.

**Omar Lanchava** - G. Tsulukidze Mining Institute, Georgia.

**Ketevan Khazaradze** - Georgian State Teaching University of Physical Education and Sport, Georgia.

**Nino Japaridze** - Tbilisi State Medical University, Georgia.

**Bakhtier Nurtaev** - Institute of Geology and Geophysics, State Committee on Geology and Mineral Resources of Uzbekistan, Uzbekistan.

**Sergey Stankevich** - Scientific Centre for Aerospace Research of the Earth, National Academy of Sciences of Ukraine, Ukraine.

**Bakhram Nurtaev** - Institute of Helioclimatology, Germany.

## Organizing Committee

**Nugzar Ghlonti:** Chairman of Organizing Committee; **Manana Nikolaishvili:** Deputy Chairman of Organizing Committee; **Sophiko Matiashvili;** **Ekaterine Mepharidze;** **Irma Glonti;** **Inga Janelidze,** - TSU, M. Nodia Institute of Geophysics, Georgia

**Tamari Khakhutashvili:** Co - Chairman of Organizing Committee; **Nino Berianidze:** Coordinator - N(N)LE Association for Science, Georgia.

**Mikheil Pipia:** Deputy Chairman of Organizing Committee; **Narine Arutiniani,** - GTU, Institute of Hydrometeorology, Georgia.

**Rusudan Kakhishvili** - Office of the National Security Council, Georgia.

**Nodar Javakhishvili** - State Military Scientific Technical Center "DELTA", Georgia.

**Nino Taniashvili** - Georgian Geophysical Association

## **Conference Themes**

### **I. Monitoring (measurements, analysis, modeling, forecast)**

- Earthquake and related events;
- Hydrometeorological Disasters;
- Climate change and related disasters;
- Heliocosmic Disasters;
- Forest fires;
- Mathematical, empirical, laboratory modeling of natural disasters (and induction among them);
- Satellite and ground distant measurements;
- Geological networking measurements;
- Point Measurements;
- Assessment of social and economic losses caused by natural disasters

### **II. Prevention**

- Weather modification;
- Engineering protection from natural disasters;
- Early Notification Systems;

### **III. Mitigate results**

- Planning events for mitigating natural disasters results;
- Improvement of Emergency Response Services Activities;
- International cooperation;
- Improve the legislative basis.

## **Expected Results**

- Promotion of historical and modern achievements of Georgia on natural disaster survey issues
- Introducing a wide range of problems for the world. What is connected to monitoring, prevention and mitigation of natural disasters in the Black Sea and Caspian Sea areas.
- Extend International Cooperation for scientific and Practical usage of modern advances on monitoring, prevention and mitigation of natural disasters in the Black and Caspian Seas.
- Assessment of social and economic risk of natural disasters
- Identify the organization's common cause for prevention of natural disasters
- Identify opportunities for improvement educational and academic base of secondary and higher education of the issues related to natural disasters

The conference was opened by Chairman of the Scientific Committee, Editor-in-Chief, Academician T. Chelidze, who made a general review on the problems of natural disasters in Georgia and wished the conference participants fruitful work.

Co-Chairman of the Scientific Committee, Director of Institute of Hydrometeorology of Technical University of Georgia, T. Tsintsadze made a report about progress of hydrometeorological observations in Georgia for 175 Years.

Leading Specialist of M. Nodia Institute of Geophysics, TSU, L.Darakhvelidze, made detailed information about 120 years of seismic observations in Georgia.

Member of Organizing Committee, Leading Specialist of Office of the National Security Council of Georgia, R. Kakhishvili talked about development of National Disaster Risk Management System in Georgia.

A total of 61 oral and poster presentations were considered at the conference. The proceedings of this conference as a whole [1], as well as its individual works [2-62], are published and posted on the portal of the Institute of Geophysics, which are included in the international electronic library data base *DSpace*, indexed in *Google Scholar* and *Publish or Perish*.

At the end of the conference, a decision was made in which the achievements and shortcomings of the work in the field of natural disaster research in Georgia were examined. In particular, it was decided to constantly hold such a conference once every two years.

In December 14, 2020 acquaintance with the work of the Center of Active Impact on Natural Phenomena (LEPL State Military Scientific Technical Center "DELTA") was carried out.



Photos from Conference



175 YEAR OF THE ORGANIZATION OF REGULAR MAGNETO-METEOROLOGICAL OBSERVATIONS IN GEORGIA



Tbilisi Magneto-Meteorological Observatory



Plan of the Tbilisi Observatory (1866)



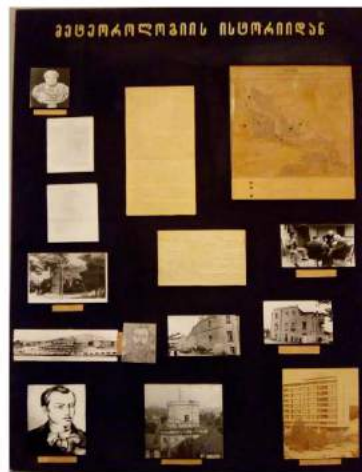
Dusheti Geomagnetic Observatory



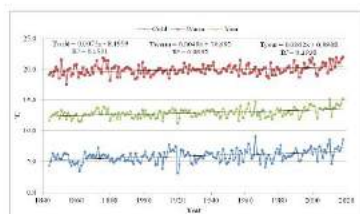
Directors of the Tbilisi Observatory



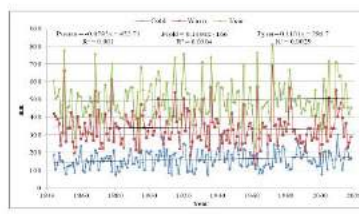
Some Instruments of the Observatory



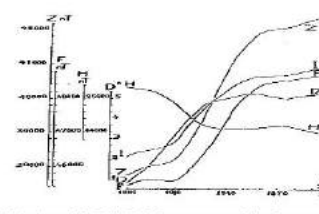
A Brief History of Meteorological and Magnetic Observations.



Trend of Air Temperature in Tbilisi in Three Period of Year in 1844-2018



Trend of Atmospheric Precipitation in Tbilisi in Three Period of Year in 1844-2018



Variations of F, Z, H, D, I Components of the Geomagnetic Field in 1880-2003

Poster about 175 year anniversary of the organization in Georgia of regular magneto-meteorological observations.

## References

- [1] International Scientific Conference “Natural Disasters in Georgia: Monitoring, Prevention, Mitigation”. Proceedings, ISBN 978-9941-13-899-7, Publish House of Iv. Javakhishvili Tbilisi State University, December 12-14, Tbilisi, 2019, 276 p., <http://dSPACE.gela.org.ge/handle/123456789/8613>; <http://dSPACE.gela.org.ge/handle/123456789/8614>
- [2] Gogua R. Dusheti (Tbilisi) Magnetic Observatory in the World Observatory Network. Int. Sc. Conf. “Natural Disasters in Georgia: Monitoring, Prevention, Mitigation”. Proc., Tbilisi, 2019, pp. 11-15, (in Georgian). <http://dSPACE.gela.org.ge/handle/123456789/8621>
- [3] Jimsheledze T., Melikadze G., Kobzev G., Matiashvili T. Probable Influence of the Earth’s Electromagnetic Impedance on PC3- PC5 Pulsation Spectrum During an Earthquake Preparation Process. Int. Sc. Conf. “Natural Disasters in Georgia: Monitoring, Prevention, Mitigation”. Proc., Tbilisi, 2019, pp. 16-18. <http://dSPACE.gela.org.ge/handle/123456789/8622>
- [4] Mepharidze E., Sborshchikovi A., Chelidze T., Zhukova N., Davitashvili I., Tepnadze D., Laliashvili L., Matcharashvili T. Temporal Analysis of Stick-Slip Records. Int. Sc. Conf. “Natural Disasters in Georgia: Monitoring, Prevention, Mitigation”. Proc., Tbilisi, 2019, pp. 19-22. <http://dSPACE.gela.org.ge/handle/123456789/8623>
- [5] Kereselidze Z., Melikadze G., Jimsheledze T. Evaluation of Electromagnetic Radiation Power in Connection with Seismic Activity in the Tskaltsminda-Ureki Geomagnetic Anomaly Area. Int. Sc. Conf. “Natural Disasters in Georgia: Monitoring, Prevention, Mitigation”. Proc., Tbilisi, 2019, pp. 23-26. <http://dSPACE.gela.org.ge/handle/123456789/8624>
- [6] Kiria T., Nikolaishvili M., Lomadze E. On One Effective Evaluation of 1989-1991 Data by Vertical Extensometer of the Underground Circulatory Laboratory in Tbilisi. Int. Sc. Conf. “Natural Disasters in Georgia: Monitoring, Prevention, Mitigation”. Proc., Tbilisi, 2019, pp. 27-31, (in Georgian). <http://dSPACE.gela.org.ge/handle/123456789/8625>
- [7] Kartvelishvili K., Berishvili G., Mebhagishvili N., Kiria T., Nikolaishvili M., Lomadze E. Study of Strong Local Magnetic Anomaly in Order to Create a Baseline Model of a Natural Magnetotherapy Resort in Atsana Region. Int. Sc. Conf. “Natural Disasters in Georgia: Monitoring, Prevention, Mitigation”. Proc., Tbilisi, 2019, pp. 32-35, (in Georgian). <http://dSPACE.gela.org.ge/handle/123456789/8626>
- [8] Nazaretyan S.N., Nazaretyan S.S., Mirzoyan L.B. Some Baseline Data for a Effective Response of Emergency Services in a Seismic Disaster in Southern Caucasus. Int. Sc. Conf. “Natural Disasters in Georgia: Monitoring, Prevention, Mitigation”. Proc., Tbilisi, 2019, pp. 36-39. <http://dSPACE.gela.org.ge/handle/123456789/8627>
- [9] Nazaretyan S.N., Mkhitaryan K.A., Nazaretyan S.S. Methodology for Preliminary Assessment of the Consequences of a Strong Earthquake in Armenia. Int. Sc. Conf. “Natural Disasters in Georgia: Monitoring, Prevention, Mitigation”. Proc., Tbilisi, 2019, pp. 40-42. <http://dSPACE.gela.org.ge/handle/123456789/8628>
- [10] Nurtaev Bakhram. Effect of Solar Forces on Earthquakes. Int. Sc. Conf. “Natural Disasters in Georgia: Monitoring, Prevention, Mitigation”. Proc., Tbilisi, 2019, pp. 43-44. <http://dSPACE.gela.org.ge/handle/123456789/8629>
- [11] Nurtaev B.S., Kurbanova D.U. Landslides Triggered by Distant Earthquakes in Central Asia. Int. Sc. Conf. “Natural Disasters in Georgia: Monitoring, Prevention, Mitigation”. Proc., Tbilisi, 2019, pp. 45-49. <http://dSPACE.gela.org.ge/handle/123456789/8630>
- [12] Odilavadze D., Ghlonti N., Tarkhan-Mouravi A. Storages in Seismically Active Territories. Int. Sc. Conf. “Natural Disasters in Georgia: Monitoring, Prevention, Mitigation”. Proc., Tbilisi, 2019, pp. 50-53, (in Georgian). <http://dSPACE.gela.org.ge/handle/123456789/8631>
- [13] Oragvelidze M., Gheonjian L., Paatashvili T. Laboratory Model of Self-Organized Criticality Parametric Modulation and the Results of Experiments for Applications in Seismology. Int. Sc. Conf. “Natural Disasters in Georgia: Monitoring, Prevention, Mitigation”. Proc., Tbilisi, 2019, pp. 54-57. <http://dSPACE.gela.org.ge/handle/123456789/8632>
- [14] Kherkheulidze G. Assessment of the Nature of Mudflow Hazards in the Lower Svaneti Region And Identifying Its Spreading Zones. Int. Sc. Conf. “Natural Disasters in Georgia: Monitoring, Prevention, Mitigation”. Proc., Tbilisi, 2019, pp. 58-62, (in Georgian). <http://dSPACE.gela.org.ge/handle/123456789/8633>
- [15] Kherkheulidze G. Initial Estimation of Mudflow Situation in the Ponds of Rivers and the Expected Trends of their Subsequent Development. Int. Sc. Conf. “Natural Disasters in Georgia: Monitoring, Prevention, Mitigation”. Proc., Tbilisi, 2019, pp. 63-66, (in Georgian). <http://dSPACE.gela.org.ge/handle/123456789/8634>

- [16] Tsintsadze T., Grigolia G., Gorgijanidze S., Tsintsadze N. Assessment of the River Enguri Run off Dynamics During Summer. Int. Sc. Conf. "Natural Disasters in Georgia: Monitoring, Prevention, Mitigation". Proc., Tbilisi, 2019, pp. 67-69, (in Georgian). <http://dspace.gela.org.ge/handle/123456789/8635>
- [17] Basilashvili Ts. Challenges of Expected Low Water Levels on the Rivers of East Georgia and the Ways of Overcoming them. Int. Sc. Conf. "Natural Disasters in Georgia: Monitoring, Prevention, Mitigation". Proc., Tbilisi, 2019, pp. 70-73, (in Georgian). <http://dspace.gela.org.ge/handle/123456789/8636>
- [18] Bliadze T., Gvasalia G., Kirkitadze D., Mekoshkishvili N. Changeability of the Atmospheric Precipitations Regime in Kakheti in 1956-2015. Int. Sc. Conf. "Natural Disasters in Georgia: Monitoring, Prevention, Mitigation". Proc., Tbilisi, 2019, pp. 74-77. <http://dspace.gela.org.ge/handle/123456789/8637>
- [19] Elizbarashvili M., Elizbarashvili E., Elizbarashvili Sh. Modeling of the Stochastic Process of Joint Implementation of Various Dangerous and Catastrophic Meteorological Phenomena. Int. Sc. Conf. "Natural Disasters in Georgia: Monitoring, Prevention, Mitigation". Proc., Tbilisi, 2019, pp. 78-81, (in Georgian). <http://dspace.gela.org.ge/handle/123456789/8638>
- [20] Kapanadze N., Mkurnalidze I. Tbilisi Air Temperature Fluctuations Against the Background of Global Climate Change. Int. Sc. Conf. "Natural Disasters in Georgia: Monitoring, Prevention, Mitigation". Proc., Tbilisi, 2019, pp. 82-85, (in Georgian). <http://dspace.gela.org.ge/handle/123456789/8639>
- [21] Amiranashvili A. Changeability of Air Temperature and Atmospheric Precipitations in Tbilisi for 175 Years. Int. Sc. Conf. "Natural Disasters in Georgia: Monitoring, Prevention, Mitigation". Proc., Tbilisi, 2019, pp. 86-90. <http://dspace.gela.org.ge/handle/123456789/8640>
- [22] Jamrishvili N., Tavidashvili Kh. Effect of Climate Change on the Freezing Level in Kakheti. Int. Sc. Conf. "Natural Disasters in Georgia: Monitoring, Prevention, Mitigation". Proc., Tbilisi, 2019, pp. 91-95. <http://dspace.gela.org.ge/handle/123456789/8641>
- [23] Meladze G., Meladze M. Impact of Global Climate Change on Agroclimate Features and Reoccurrence Droughts in Georgia (On the Example of Kakheti Region). Int. Sc. Conf. "Natural Disasters in Georgia: Monitoring, Prevention, Mitigation". Proc., Tbilisi, 2019, pp. 96-100, (in Georgian). <http://dspace.gela.org.ge/handle/123456789/8642>
- [24] Miqautadze D., Kvabziridze M. Assessing the Repeatability of Extreme Rainfalls in the Background of Revealed Climate Change of Kutaisi. Int. Sc. Conf. "Natural Disasters in Georgia: Monitoring, Prevention, Mitigation". Proc., Tbilisi, 2019, pp. 101-104, (in Georgian). <http://dspace.gela.org.ge/handle/123456789/8643>
- [25] Mkurnalidze I., Kapanadze N. Seasonal Distribution of Thunderstorms in Georgia. Int. Sc. Conf. "Natural Disasters in Georgia: Monitoring, Prevention, Mitigation". Proc., Tbilisi, 2019, pp. 105-108, (in Georgian). <http://dspace.gela.org.ge/handle/123456789/8644>
- [26] Nurtaev Bakhran. Predictive Analytics Application Experience for Climate Trends in Caucasus Mountain Region. Int. Sc. Conf. "Natural Disasters in Georgia: Monitoring, Prevention, Mitigation". Proc., Tbilisi, 2019, pp. 109-109. <http://dspace.gela.org.ge/handle/123456789/8645>
- [27] Pipia M., Beglarashvili N., Diasamidze L., Jincharadze G. Some Features of Blizzard in Samtskhe-Javakheti Region. Int. Sc. Conf. "Natural Disasters in Georgia: Monitoring, Prevention, Mitigation". Proc., Tbilisi, 2019, pp. 110-113, (in Georgian). <http://dspace.gela.org.ge/handle/123456789/8646>
- [28] Janelidze I., Pipia M. Hail Storms in Georgia in 2016-2018. Int. Sc. Conf. "Natural Disasters in Georgia: Monitoring, Prevention, Mitigation". Proc., Tbilisi, 2019, pp. 114-116. <http://dspace.gela.org.ge/handle/123456789/8647>
- [29] Tatishvili M., Khvedelidze Z., Samkharadze I., Palavandishvili A. Atmosphere Processes and Climate Parameters Variation in River Mtkvari Basin. Int. Sc. Conf. "Natural Disasters in Georgia: Monitoring, Prevention, Mitigation". Proc., Tbilisi, 2019, pp. 117-121. <http://dspace.gela.org.ge/handle/123456789/8648>
- [30] Kartvelishvili L., Megrelidze L., Kurdashvili L. Winter Tourism Development Trends in Georgia. Int. Sc. Conf. "Natural Disasters in Georgia: Monitoring, Prevention, Mitigation". Proc., Tbilisi, 2019, pp. 122-125. <http://dspace.gela.org.ge/handle/123456789/8649>
- [31] Jamrishvili N., Tavidashvili Kh. Estimation of the Critical Size of Hailstones in Clouds Non Prejudiced to Agriculture in Kakheti. Int. Sc. Conf. "Natural Disasters in Georgia: Monitoring, Prevention, Mitigation". Proc., Tbilisi, 2019, pp. 126-129. <http://dspace.gela.org.ge/handle/123456789/8650>
- [32] Shavliashvili L., Intskirveli L., Bakradze E., Kuchava G., Buachidze N., Mdivani S. Change of Heavy Metal Concentration in Surface Waters and Soils of East Georgia Considering the Anthropogenic Impact. Int. Sc. Conf. "Natural Disasters in Georgia: Monitoring, Prevention, Mitigation". Proc., Tbilisi, 2019, pp. 130-133, (in Georgian). <http://dspace.gela.org.ge/handle/123456789/8651>
- [33] Surmava A., Gigauri N., Kukhalashvili V., Intskirveli L., Mdivani S. Numerical Modeling of the Anthropogenic Dust Transfer by Means of Quasistatic and Non-Quasistatic Models. Int. Sc. Conf. "Natural

- Disasters in Georgia: Monitoring, Prevention, Mitigation”. Proc., Tbilisi, 2019, pp. 134-137. <http://dspace.gela.org.ge/handle/123456789/8652>
- [34] Davitashvili M., Margalitashvili D., Nadiradze T., Azikuri G. Noise Pollution Level in Telavi. Int. Sc. Conf. “Natural Disasters in Georgia: Monitoring, Prevention, Mitigation”. Proc., Tbilisi, 2019, pp. 138-140, (in Georgian). <http://dspace.gela.org.ge/handle/123456789/8654>
- [35] Demetrashvili D., Kvaratskhelia D. Pollution of the World Ocean (With Focusing on the Black Sea) by Oil Products and Marine Litter. Monitoring and Forecasting. Int. Sc. Conf. “Natural Disasters in Georgia: Monitoring, Prevention, Mitigation”. Proc., Tbilisi, 2019, pp. 141-144, (in Georgian). <http://dspace.gela.org.ge/handle/123456789/8655>
- [36] Matiashvili S. Overview of Radioecological Research in some Current Areas of Georgia. Int. Sc. Conf. “Natural Disasters in Georgia: Monitoring, Prevention, Mitigation”. Proc., Tbilisi, 2019, pp. 145-149, (in Georgian). <http://dspace.gela.org.ge/handle/123456789/8656>
- [37] Kekenadze E., Kharchilava J., Chkhaidze G., Senik I. Comparative Analysis of the Surface Ozone Concentration in Tbilisi and at Kislovodsk High Mountain Station. Int. Sc. Conf. “Natural Disasters in Georgia: Monitoring, Prevention, Mitigation”. Proc., Tbilisi, 2019, pp. 150-154. <http://dspace.gela.org.ge/handle/123456789/8657>
- [38] Gunia G. Aspects of Surface Monitoring of Environmentally “Dangerous” Meteorological Phenomena in Georgia. Int. Sc. Conf. “Natural Disasters in Georgia: Monitoring, Prevention, Mitigation”. Proc., Tbilisi, 2019, pp. 155-158, (in Georgian). <http://dspace.gela.org.ge/handle/123456789/8658>
- [39] Elizbarashvili E. Meteorological Observations at the Automatic Weather Station of Iakob Gogebashvili Telavi State University. Int. Sc. Conf. “Natural Disasters in Georgia: Monitoring, Prevention, Mitigation”. Proc., Tbilisi, 2019, pp. 159-162, (in Georgian). <http://dspace.gela.org.ge/handle/123456789/8661>
- [40] Gheonjian L., Paatashvili T., Oragvelidze M., Tsotskolauri P. Tbilisi State University Extremely Low Frequency Radiation Research Net (ELFTSU NET). Int. Sc. Conf. “Natural Disasters in Georgia: Monitoring, Prevention, Mitigation”. Proc., Tbilisi, 2019, pp. 163-166. <http://dspace.gela.org.ge/handle/123456789/8663>
- [41] Mitin M., Khvedelidze I. Radar Characteristics of Rain Cloud wich Caused Landslide into Akhaldaba and Catastrophic Flood in Tbilisi on June 13-14, 2015. Int. Sc. Conf. “Natural Disasters in Georgia: Monitoring, Prevention, Mitigation”. Proc., Tbilisi, 2019, pp. 167-171. <http://dspace.gela.org.ge/handle/123456789/8664>
- [42] Gvasalia G., Kekenadze E., Mekoshkishvili N., Mitin M. Radar Monitoring of Hail Processes in Eastern Georgia and its Neighboring Countries (Azerbaijan, Armenia). Int. Sc. Conf. “Natural Disasters in Georgia: Monitoring, Prevention, Mitigation”. Proc., Tbilisi, 2019, pp. 172-176. <http://dspace.gela.org.ge/handle/123456789/8665>
- [43] Javakhishvili N., Janelidze I. On the Prediction of Floods Caused by Rainfall in the Area of Action of the Meteorological Radar “METEOR 735CDP10”. Int. Sc. Conf. “Natural Disasters in Georgia: Monitoring, Prevention, Mitigation”. Proc., Tbilisi, 2019, pp. 177-181. <http://dspace.gela.org.ge/handle/123456789/8666>
- [44] Berianidze N., Javakhishvili N. Mtchedlishvili A. About the Possibility of using the “METEOR 735CDP10” Radar for Monitoring Volcanic Formations, Dust Storms and Smoke from Large Fires in Atmosphere in South Caucasus. Int. Sc. Conf. “Natural Disasters in Georgia: Monitoring, Prevention, Mitigation”. Proc., Tbilisi, 2019, pp. 182-186. <http://dspace.gela.org.ge/handle/123456789/8667>
- [45] Stankevich S.A., Titarenko O.V, Svideniuk M.O. Landslide Susceptibility Mapping Using Gis-Based Weight-of-Evidence Modelling in Central Georgian Regions. Int. Sc. Conf. “Natural Disasters in Georgia: Monitoring, Prevention, Mitigation”. Proc., Tbilisi, 2019, pp. 187-190. <http://dspace.gela.org.ge/handle/123456789/8668>
- [46] Bliadze T., Kirkkitadze D., Samkharadze I., Tsiklauri Kh. Statistical Characteristics of Angstrom Fire Index for Tbilisi. Int. Sc. Conf. “Natural Disasters in Georgia: Monitoring, Prevention, Mitigation”. Proc., Tbilisi, 2019, pp. 191-194. <http://dspace.gela.org.ge/handle/123456789/8669>
- [47] Adeishvili T., Berdzenishvili N. Some Cosmogenic Factors in People with Diabetes. Int. Sc. Conf. “Natural Disasters in Georgia: Monitoring, Prevention, Mitigation”. Proc., Tbilisi, 2019, pp. 195-200, (in Georgian). <http://dspace.gela.org.ge/handle/123456789/8670>
- [48] Japaridze N., Khazaradze K. Studies in the Field of the Influence of Natural and Anthropogenic Environmental Factors on Human Health in Georgia: Current Status and Planned Works. Int. Sc. Conf. “Natural Disasters in Georgia: Monitoring, Prevention, Mitigation”. Proc., Tbilisi, 2019, pp. 201-204. <http://dspace.gela.org.ge/handle/123456789/8671>

- [49] Japaridze N., Khazaradze K. Changeability of Mortality in Georgia in Different Seasons and Periods of Year into 1993-2017. Int. Sc. Conf. "Natural Disasters in Georgia: Monitoring, Prevention, Mitigation". Proc., Tbilisi, 2019, pp. 205-208. <http://dSPACE.gela.org.ge/handle/123456789/8672>
- [50] Telia Sh., Kveselava N., Sauri I., Chikhladze V., Dzodzuashvili U., Tsereteli A. Physical and Economic Efficiency of Anti-Hail Works in Kakheti for the Period 2015-2019. Int. Sc. Conf. "Natural Disasters in Georgia: Monitoring, Prevention, Mitigation". Proc., Tbilisi, 2019, pp. 209-211, (in Georgian). <http://dSPACE.gela.org.ge/handle/123456789/8673>
- [51] Beritashvili B., Burnazde A., Kveselava N., Tsereteli A. Carrying out Anti-Hail Works on the Territory of Kvemo Kartli - A Retrospective Analysis and the Prospect of their Resumption. Int. Sc. Conf. "Natural Disasters in Georgia: Monitoring, Prevention, Mitigation". Proc., Tbilisi, 2019, pp. 212-215, (in Georgian). <http://dSPACE.gela.org.ge/handle/123456789/8674>
- [52] Amiranashvili A., Chikhladze V., Dzodzuashvili U., Ghlonti N., Sauri I., Telia Sh., Tsintsadze T. Weather Modification in Georgia: Past, Present, Prospects for Development. Int. Sc. Conf. "Natural Disasters in Georgia: Monitoring, Prevention, Mitigation". Proc., Tbilisi, 2019, pp. 216-222. <http://dSPACE.gela.org.ge/handle/123456789/8675>
- [53] Alphenidze M., Gongadze M., Korsantia K., Mzarelua L. Black Sea Discrete Coastal Flows and Coast Protection. Int. Sc. Conf. "Natural Disasters in Georgia: Monitoring, Prevention, Mitigation". Proc., Tbilisi, 2019, pp. 223-227, (in Georgian). <http://dSPACE.gela.org.ge/handle/123456789/8676>
- [54] Odilavadze D., Tarkhan-Mouravi A., Varamashvili N., Arziani Z. Prevention of the Danger Triggered by an Earthquake of Exogenous and Endogenous Processes, using a Combination of Geophysical-Geoelectric Methods In Geotechnics. Int. Sc. Conf. "Natural Disasters in Georgia: Monitoring, Prevention, Mitigation". Proc., Tbilisi, 2019, pp. 228-232, (in Georgian). <http://dSPACE.gela.org.ge/handle/123456789/8677>
- [55] Tsereteli E., Gaprindashvili G., Gaprindashvili M., Bolashvili N. Geodynamic Hazard Risk Assessment and Management Methodological Aspects in Georgia. Int. Sc. Conf. "Natural Disasters in Georgia: Monitoring, Prevention, Mitigation". Proc., Tbilisi, 2019, pp. 233-236, (in Georgian). <http://dSPACE.gela.org.ge/handle/123456789/8678>
- [56] Kandelaki N., Iordanishvili I., Iremashvili I., Kupreishvili Sh., Iordanishvili K. Development of New Constructions Against Washing the Reservoirs Abrasive Shores. Int. Sc. Conf. "Natural Disasters in Georgia: Monitoring, Prevention, Mitigation". Proc., Tbilisi, 2019, pp. 237-243, (in Georgian). <http://dSPACE.gela.org.ge/handle/123456789/8679>
- [57] Lanchava O. Separation and Evaluation of Simultaneous Heat-Mass Exchange in Subway Tunnels. Int. Sc. Conf. "Natural Disasters in Georgia: Monitoring, Prevention, Mitigation". Proc., Tbilisi, 2019, pp. 244-247. <http://dSPACE.gela.org.ge/handle/123456789/8680>
- [58] Varamashvili N., Asanidze B., Jakhutashvili M. Ultrasonic Methods for Assessing the State of Hydrotechnic Concrete Structures. Int. Sc. Conf. "Natural Disasters in Georgia: Monitoring, Prevention, Mitigation". Proc., Tbilisi, 2019, pp. 248-251, (in Georgian). <http://dSPACE.gela.org.ge/handle/123456789/8681>
- [59] Gekkieva S. Modeling in the System of Ecological Monitoring of Reservoirs. Int. Sc. Conf. "Natural Disasters in Georgia: Monitoring, Prevention, Mitigation". Proc., Tbilisi, 2019, pp. 252-254. <http://dSPACE.gela.org.ge/handle/123456789/8682>
- [60] Gekkieva S. Evaluation of the Effect of the Redistribution of Precipitation by the Method of the Climatic Average. Int. Sc. Conf. "Natural Disasters in Georgia: Monitoring, Prevention, Mitigation". Proc., Tbilisi, 2019, pp. 255-259. <http://dSPACE.gela.org.ge/handle/123456789/8683>
- [61] Tavartkiladze K., Suknidze N. Extreme Temperature Regime in Georgia and the Impact of Global Warming on It. Int. Sc. Conf. "Natural Disasters in Georgia: Monitoring, Prevention, Mitigation". Proc., Tbilisi, 2019, pp. 260-266, (in Georgian). <http://dSPACE.gela.org.ge/handle/123456789/8684>
- [62] Porchkhidze A. Ecological Catastrophes Caused by Climate Global Warming and their Prevention Possibilities in Georgia. Int. Sc. Conf. "Natural Disasters in Georgia: Monitoring, Prevention, Mitigation". Proc., Tbilisi, 2019, pp. 267-270, (in Georgian). <http://dSPACE.gela.org.ge/handle/123456789/8685>

**საერთაშორისო სამეცნიერო კონფერენცია  
„ბუნებრივი კატასტროფები საქართველოში: მონიტორინგი,  
პრევენცია, შედეგების შერბილება“**

**ნ. ლლონტი, თ. ცინცაძე, თ. ხახუტაშვილი**

**რეზიუმე**

წარმოდგენილია ინფორმაცია საერთაშორისო სამეცნიერო კონფერენციაზე „ბუნებრივი კატასტროფები საქართველოში: მონიტორინგი, პრევენცია, შედეგების შერბილება“, რომელიც ჩატარდა ივანე ჯავახიშვილის სახელობის თბილისის სახელმწიფო უნივერსიტეტში 2019 წ. 12–14 დეკემბერს.

კონფერენციზ მიემდგვნა საქართველოში რეგულარული მაგნიტურ-მეტეოროლოგიური და სეისმური დაკვირვებების ორგანიზების 175 და 120 წლისთავს.

**Международная научная конференция  
“Природные катастрофы в Грузии: мониторинг, превенция,  
смягчение последствий”**

**Н.Я. Глонти, Т. Н. Цинцадзе, Т.В. Хакуташвили**

**Резюме**

Представлена информация о международной научной конференции “Природные катастрофы в Грузии: мониторинг, превенция, смягчение последствий”, которая прошла 12-14 декабря 2019 года в Тбилиском государственном университете имени Иванэ Джавахишвили.

Конференция была посвящена 175 и 120-летию организации в Грузии регулярных магнито-метеорологических и сейсмических наблюдений.

## **To the Memories of M. Alania (1935-2020)**

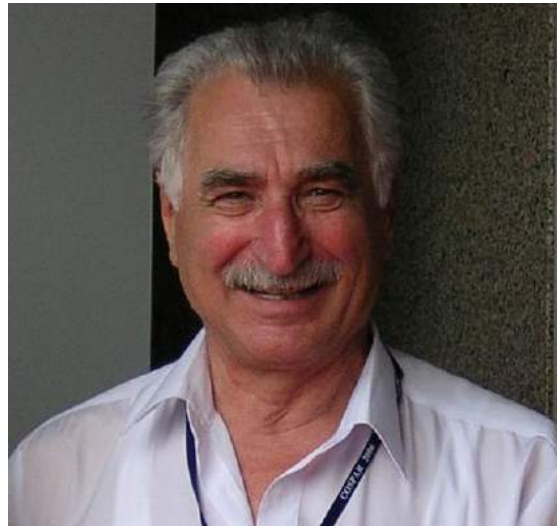
**Liana K. Darakhvelidze**

*M. Nodia Institute of Geophysics of I. Javakhishvili Tbilisi State University*

### **ABSTRACT**

*A brief biographical information about the doctor of physical and mathematical sciences, professor Michael Alania is presented.*

**Key words:** *cosmic rays intensity variations*



**Michael V. Alania**

Michael V. Alania, Professor, Doctor of Sciences in Physics and Mathematics birth on April 30, 1935 in Kvaloni, Chobi Reg., Georgia and died on May 18, 2020 in Tbilisi, Georgia. Professor Alania studied the near-Earth space on the basis of the researches on cosmic rays intensity variations.

#### **Education:**

- **1988** - Professor of Geophysics (from Highest attest Commission of USSR, Attestation PRN016443, Moscow, 18-03-1988, Protocol, N10 PC/6);
- **1982** - Doctor of Sciences in Physics and Mathematics (from the Institute of Geophysics of the Academy of Sciences of Ukraine, Kiev, and from Highest attest Commission of USSR;
- **1971** - Senior Scientist of Nuclear and Cosmic ray physics (from Georgian the Academy of Sciences and from the Highest attest Commission of USSR, Attestation MCH N037072, Moscow, **21-01-1971**);
- **1967** - Candidate of Sciences (PhD) in Physics and Mathematics (from Tbilisi state University and from the Highest attest Commission of USSR, Diploma MFM N007357, Moscow, **08-08-1967**);

- **1958** - Post graduated (MS- in Physics, teacher of Physics and Mathematics) from Tbilisi state University, Diploma H N662191, Tbilisi, 01-07-1958;
- **1953-1958** – Student, Tbilisi state University, Faculty of Physics;
- **1942-1953** –Pupil of Kvaloni School, Chobi Reg., Georgia.

#### **Career:**

- **2009– present**- Full Professor and Head of the Department of Physics and Numerical Analysis of the Institute of Mathematics and Physics (Sciences Faculty) of Siedlce University, Siedlce, Poland ([www.uph.edu.pl](http://www.uph.edu.pl));
- 1995- 2009 – Full Professor and Head of the Physics Department of the Institute of Mathematics and Physics (Sciences Faculty) of Podlasie University, Siedlce, Poland ([www.ap.siedlce.pl](http://www.ap.siedlce.pl));
- 1995-2005 - Director of the Institute of Mathematics and Physics (Sciences Faculty) of the Podlasie University, Siedlce, Poland;
- 1995-2005 – member of Senate of the Podlasie University, Siedlce, Poland;
- 1994-2009- Head of the Physics Department of the Institute of Mathematics and Physics (Sciences Faculty) of Podlasie University, Siedlce, Poland;
- 1993-1994- Professor of the Institute of Mathematics and Physics (Sciences Faculty) of Podlasie University, Siedlce, Poland;
- 1994 – 2020 - Member of the editorial board of the Journal of the Georgian Geophysical Society;
- 1993- ***I left Georgia for Poland***
- 1969-1993- Head of the Cosmic Ray Department of the Institute of Geophysics Georgian Academy of Sciences, Tbilisi , Georgia;
- 1971-1992- Invited Lecturer of the geophysics Department of Tbilisi State University;
- 1967-1969- Senior Scientific Worker of the Cosmic Ray Department of the Institute of Geophysics Georgian Academy of Sciences, Tbilisi , Georgia;
- 1962-1967- Scientific Worker of the Cosmic Ray Department of the Institute of Geophysics Georgian Academy of Sciences, Tbilisi , Georgia;
- 1958-1962- Junior Scientific Worker of the Cosmic Ray Department of the Institute of Geophysics Georgian Academy of Sciences, Tbilisi, Georgia;

#### **Supervisor of:**

- Supervisor of 13 PhD Dissertations; 9 PhD Dissertations in Georgia during 1982-1994 (Tbilisi University, Institute of Geophysics Georgian Academy of Sciences) and 4 PhD Dissertations in Poland during 2001-2010 (university of Podlasie);
- Supervisor of more than 30 MSc Thesis in Georgia during 1975- 1993 (Tbilisi University, Institute of Geophysics Georgian Academy of Sciences) and more than 35 MSc Thesis in Poland; 1995-2010 (University of Podlasie).
- Supervisor of current (2012-2015) Grant 13/09 of the Shota Rustaveli National Science Foundation , Tbilisi, Georgia (Ilia University);

#### **Membership in:**

- National Research Council of Cosmic Rays of the Academy of Sciences of the USSR (1970-1993) and Russia (1993 –2002);
- National Research Council of Solar-terrestrial physics of the Academy of Sciences of the USSR (1970-1993) and Russia (1993 –2002);
- Board of doctorate and doctor-habillate degrees of Institute of Geophysics Georgian Academy of Sciences (1975 – 2002);
- Chairman of National Research Council of Solar-terrestrial physics of the Georgian Academy of Science (1982 – 1996);
- International Organization COSPAR (Commission of Space Exploration), since 1993;
- European Academy of Science, since 2005;
- Polish Astroparticle Physics Network, since 2007.

### **Recognized and honored for consistent high performance and commitment:**

- 1970 - Award of the USSR Government for research activities,
- 1982 - Award of Georgian Academy of Science for research activities;
- 1983 - Award of Georgian Government for research activities;
- 1993 - Research grant of American Scientist' society;
- Awards of the Rector of the University of Podlasie (in 1995, 1998, 2000, 2004, 2006, 2008, and - University of Siedlce ( in 2010 and 2013);
- Team Award - University of Podlasie in 2002 and 2009;
- 2001 - Medal 'Achievements for Siedlce University';
- 2004 - Medal of the Minister of National Education and Sport of Poland;
- 2009 - Gold Medal for Long Service awarded by President of the Republic of Poland Lech Kaczyński.

**Publications (full updated list at: <http://alania.uph.edu.pl/>)** Author and coauthor of more than 280 papers and abstracts, and 3- monographs. Among them:

- In refereed journals during last 20 years (2001-2020) ~ 60 papers,
- Published in Conference Proceedings ~ 80 papers.

The memory of Mikheil Alania will forever remain in our hearts.

## **მ. ალანიას ხსოვნისათვის (1935-2020)**

**ლ. დარახველიძე**

**რეზიუმე**

წარმოდგენილია მოკლე ბიოგრაფიული ინფორმაცია, ფიზიკა-მათემატიკის მეცნიერებათა დოქტორის, პროფესორ მიხეილ ალანიას შესახებ.

## **Памяти М.В. Алания (1935-2020)**

**Л.К. Дарахвелидзе**

**Резюме**

Представлена краткая биографическая информация о докторе физико-математических наук, профессоре Михаиле Алания.

## Information for contributors

Papers intended for the Journal should be submitted in two copies to the Editor-in-Chief. Papers from countries that have a member on the Editorial Board should normally be submitted through that member. The address will be found on the inside front cover.

1. Papers should be written in the concise form. Occasionally long papers, particularly those of a review nature (not exceeding 16 printed pages), will be accepted. Short reports should be written in the most concise form not exceeding 6 printed pages. It is desirable to submit a copy of paper on a diskette.
2. A brief, concise abstract in English is required at the beginning of all papers in Russian and in Georgian at the end of them.
3. Line drawings should include all relevant details. All lettering, graph lines and points on graphs should be sufficiently large and bold to permit reproduction when the diagram has been reduced to a size suitable for inclusion in the Journal.
4. Each figure must be provided with an adequate caption.
5. Figure Captions and table headings should be provided on a separate sheet.
6. Page should be 20 x 28 cm. Large or long tables should be typed on continuing sheets.
7. References should be given in the standard form to be found in this Journal.
8. All copy (including tables, references and figure captions) must be double spaced with wide margins, and all pages must be numbered consecutively.
9. Both System of units in GGS and SI are permitted in manuscript
10. Each manuscript should include the components, which should be presented in the order following as follows:  
Title, name, affiliation and complete postal address of each author and dateline.  
The text should be divided into sections, each with a separate heading or numbered consecutively.  
Acknowledgements. Appendix. Reference.
11. The editors will supply the date of receipt of the manuscript.

## CONTENTS - სარჩევი

|  |         |
|--|---------|
| O.Sh. Varazanashvili, N.S. Tsereteli - Models for Area Seismic Source Definition and Parameterization for Georgia and the Surrounding Region<br>ო. ვარაზანაშვილი, ნ. წერეთელი - სეისმური კერების არეების მოდელების აგება და პარამეტრიზაცია საქართველოსა და გარემომცველი რეგიონისთვის   | 5 –19   |
| B. Nurtaev - General Relativity Theory and Earthquakes<br>ბ. - ფარდობითობის ზოგადი თეორია და მიწისძვრები   | 20-26   |
| G.T. Dalakishvili, G.G. Didebulidze, M.M. Todua - Formation of Sporadic E (Es) Layer by Homogeneous Horizontal Wind<br>გ. დალაქიშვილი, გ. დიდებულოძე, მ. თოდუა - სპორადული E (Es) ფენის ფორმირება ერთგვაროვანი ჰორიზონტალური ქარის მიერ  | 27-45   |
| V.G. Kukhalashvili, G.I. Kordzakhia, N.G. Gigauri, A.A. Surmava, L.N. Intskirveli - Numerical Modelling of Dust Propagation in the Atmosphere of Tbilisi City: The Case of Background Eastern Gentle Breeze<br>ვ. კუხალაშვილი, გ. კორძახია, ნ. გიგაური, ა. სურმავა, ლ. ინჭკირველი - ქ.თბილისის ატმოსფეროში მტვრის გავრცელების რიცხვითი მოდელირება: აღმოსავლეთის ფონური საშუალო სიქარის ქარის შემთხვევა | 46-50   |
| V.G. Kukhalashvili, N.G. Gigauri, A.A. Surmava, D.I. Demetrashvili, L.N. Intskirveli - Numerical Modelling of Dust Propagation in the Atmosphere of Tbilisi City: The Case of Background Eastern Fresh Breeze<br>ვ. კუხალაშვილი, ნ. გიგაური, ა. სურმავა, დ. დემეტრაშვილი, ლ. ინჭკირველი - ქ. თბილისის ატმოსფეროში მტვრის გავრცელების რიცხვითი მოდელირება: ფონური აღმოსავლეთის ძლიერი ქარის შემთხვევა   | 51-56   |
| A.G. Amiranashvili, D.D. Kirkitadze, E.N. Kekenadze - Pandemic of Coronavirus COVID-19 and Air Pollution in Tbilisi in Spring 2020<br>ა. ამირანაშვილი, დ. კირკიტაძე, ე. კეკენაძე - COVID-19 კორონავირუსის პანდემია და ჰაერის დაბინძურება თბილისში 2020 წლის გაზაფხულზე   | 57-72   |
| A.G. Amiranashvili, V.A. Chikhladze, G.D. Gvasalia, D.A. Loladze - Statistical Characteristics of the Daily Max of Wind Speed in Kakheti in 2017-2019<br>ა. ამირანაშვილი, ვ. ჩიხლაძე, გ. გვასალია, დ. ლოლაძე - კახეთში 2017-2019 წწ. ქარის დღე-ღამური მაქსიმალური სიქარის სტატისტიკური მახასიათებლები  | 73-86   |
| N.Ya. Ghlonti, T.N. Tsintsadze, T.V. Khakhutashvili - International Scientific Conference „Natural Disasters in Georgia: Monitoring, Prevention, Mitigation“<br>ნ. ლლონტი, თ. ცინცაძე, თ. ხახუტაშვილი - საერთაშორისო სამეცნიერო კონფერენცია „ბუნებრივი კატასტროფები საქართველოში: მონიტორინგი, პრევენცია, შედეგების შერბილება“   | 87-96   |
| L. K. Darakhvelidze - To the Memories of M. Alania (1935-2020)<br>ლ. დარახველიძე - მ. ალანიას ხსოვნისათვის (1935-2020)   | 97-99   |
| Information for contributors<br>ავტორთა საყურადღებო  | 100-102 |

საქართველოს გეოფიზიკური საზოგადოების ჟურნალი  
მყარი დედამიწის, ატმოსფეროს, ოკეანისა და კოსმოსური პლაზმის ფიზიკა

*ტომი 23, № 1*

ჟურნალი იბეჭდება საქართველოს გეოფიზიკური საზოგადოების პრეზიდიუმის დადგენილების  
საფუძველზე

ტირაჟი 40 ცალი

**JOURNAL OF THE GEORGIAN GEOPHYSICAL SOCIETY**

*Physics of Solid Earth, Atmosphere, Ocean and Space Plasma*

*Vol. 23, № 1*

Printed by the decision of the Georgian Geophysical Society Board

Circulation 40 copies

**ЖУРНАЛ ГРУЗИНСКОГО ГЕОФИЗИЧЕСКОГО ОБЩЕСТВА**

**Физика Твердой Земли, Атмосферы, Океана и Космической Плазмы**

*Том 23, № 1*

Журнал печатается по постановлению президиума Грузинского геофизического общества

Тираж 40 экз

**Tbilisi-თბილისი-Тбилиси**  
2020